



OpenAIR@RGU

The Open Access Institutional Repository at Robert Gordon University

<http://openair.rgu.ac.uk>

Citation Details

Citation for the version of the work held in 'OpenAIR@RGU':

EL-ZAROUK, K. M., 2007. Composite inorganic membranes for hydrogen reaction, separation and purification. Available from *OpenAIR@RGU*. [online]. Available from: <http://openair.rgu.ac.uk>

Copyright

Items in 'OpenAIR@RGU', Robert Gordon University Open Access Institutional Repository, are protected by copyright and intellectual property law. If you believe that any material held in 'OpenAIR@RGU' infringes copyright, please contact openair-help@rgu.ac.uk with details. The item will be removed from the repository while the claim is investigated.

**COMPOSITE INORGANIC MEMBRANES FOR
HYDROGEN REACTION, SEPARATION AND
PURIFICATION**

KHALED MOHAMED EI-ZAROUK

A thesis submitted in partial fulfilment of the

requirements of

The Robert Gordon University

for the degree of Doctor of Philosophy

JAN 2007

Dedicated to

My parents, my wife and whole my family

ABSTRACT

Silica-alumina composite membranes for hydrogen separation and high temperature chemical reactions were prepared using both conventional and modified dip-coating techniques. These were deposited on commercially available α -alumina macroporous support of 10 millimetre (mm) outer diameter, 7 mm inner diameter and average pore size of 6000 nanometre (nm) wash coated with Titania. The reactants of the coating technique were silicone elastomer and isopentane promoted by a catalyst. The catalyst (silicone curing agent) was added as a templating agent to control the eventual adhesion and densification of the elastomer sol.

In particular, the microporous membranes were prepared by creating suction in the bore side of the membrane and involved continuous stirring of the coating mixture during the process, and their pore characteristics were analysed. Then, the effects of thermal treatment on the gas transport and micro pore structure of the resulting membranes were investigated.

The pore size of the silica membrane prepared by conventional technique was in the range of approximately 8 to 11 nm while that prepared by modified dip-coating was in the range of about 3 to 4 nm. In addition, the membranes were segmented into five categories; silica membrane for hydrogen reaction, silica membrane for separation, silica membrane for purification, palladium (Pd)-impregnated membrane and silica on gamma – alumina (γ -alumina).

The hydrogen permeation of the silica membrane prepared for hydrogen reaction was of the order of 10^{-7} mol/m².s.pa, while the nitrogen permeance was of the order of 10^{-8} mol/m².s.pa. at pressure differential of 0.5-2.0 bar and temperature range of 323-473 Kelvin (K). The maximum hydrogen / nitrogen (H₂ / N₂) selectivity, determined from single-component permeances to H₂ and N₂ was approximately 3.58. These permeances were decreased for the silica membrane prepared for hydrogen separation when the dip coating, drying and calcination was applied 7 times instead of 3 times as in the case of the hydrogen reaction membrane.

The silica membrane for H₂ separation provides permeances of about 5.8×10^{-9} mole.meter⁻².second⁻¹.pascal⁻¹ (mol/m².s.pa) for H₂ and 9.4×10^{-10} mol/m².s.pa for N₂, with higher H₂/N₂ selectivity of about 8.

Higher mixed gas separation factors of H₂:N₂ > 400 and H₂ permeance of 4.1×10^{-9} mol/m².s.pa were achieved with silica membrane for H₂ purification prepared with the modified dip-coating using suction technique with silicone elastomer as precursor. This technique was especially effective in plugging the macroporous support which possessed a wide pore size distribution. The membrane permeated gases except propane (C₃H₈) by the activated diffusion mechanism at permeation temperature range of 298 - 573 K, and the activation energies are in the order of 10.6 - 13 kilojoules / mole (kJ/mol) and 26.1-28.7 kJ/mol for H₂ and N₂ respectively. The tests have demonstrated that this composite membrane has the capability to separate hydrogen from gas mixtures with almost complete H₂ selectivity and to produce high purity H₂ (up to 99.0 %) from a 50 / 50 % H₂/N₂ mixture stream.

A theoretical model for a propane dehydrogenation reaction scheme in tubular and annular membrane reactors is developed. This model is applied to three different membranes namely: a silica-alumina membrane, a silica-γ-alumina membrane and a Pd impregnated membrane. Results indicate that the Pd impregnated membrane provided very high theoretical conversions (82 % at 600°C) compared with the other two composite membranes.

TABLE OF CONTENTS

Chapter 1: INTRODUCTION	1
1.1. General Background	1
1.2. Motivation	3
1.3. Separation Technology	4
1.4. Membrane Reactors and Hydrogen Reaction	5
1.5. Hydrogen Separation and Purification	7
1.5.1. Dense palladium membranes	7
1.5.2. Silica membranes	8
1.6. Modelling and Simulation	11
1.7. Scope of the Research	12
1.8. Thesis Outline	13
Chapter 2: LITERATURE REVIEW	15
2.1. Introduction	15
2.2. Preparation Methods and Materials	15
2.2.1. Sol-gel method	15
2.2.2. Dip-coating process	17
2.2.3. Chemical vapour deposition	19
2.2.4. Electroless plating method	20
2.2.5. Magnetron sputtering method	22

2.3.	Membrane Reactor Applications	23
2.3.1.	Hydrogen reaction membranes	25
2.3.2.	Propane Dehydrogenation and Catalysts	27
2.4.	Hydrogen Separation and Purification membranes	31
2.5.	Modelling and Simulation	35
2.6.	Conclusions	39
Chapter 3: APPLICABLE THEORY		41
3.1.	Introduction	41
3.2.	General Background	41
3.2.1.	Porosity and permeability	41
3.2.2	Wettability	42
3.3.	Sol-Gel / Dip Coating Processes	43
3.4.	Modified dip-coating procedure	45
3.5.	Pore Size and Pore Size Distribution	48
3.5.1.	Gas adsorption	48
3.5.2.	Mercury porosimetry	50
3.6.	Separation of Gases and Transport Mechanisms	52
3.6.1.	Graham's law of diffusion	52
3.6.2.	Gas flow mechanisms in inorganic membranes	52
3.6.3.	Pure gas separation factor	60
3.6.4.	Binary mixture gas permeation	61

Chapter 4: EXPERIMENTAL APPARATUS AND PROCEDURE	63
4.1. Introduction	63
4.2. Preparation Equipments and Materials	63
4.2.1. Equipments	63
4.2.2. Materials	64
4.2.3. Porous support tubes	64
4.3. Preparation Methods and Procedure	65
4.3.1. Preparation of silica solution	65
4.3.2. Silica membrane for hydrogen reaction	65
4.3.3. Silica membrane for hydrogen separation	66
4.3.4. Silica membrane for hydrogen purification	67
4.3.5. Pd impregnated γ -alumina membrane	69
4.3.6. Silica on γ -alumina modified support	70
4.4. Flux Characterisation	70
4.4.1. Equipments and materials	70
4.4.2. Experimental rig and Feed supply	71
4.4.3. Membrane reactor and permeation cell	72
4.4.4. Gas analysis and chromatograph	76
4.5. Surface Characterisation	78
4.5.1. Scanning electron microscope (SEM)	78
4.5.2. Energy dispersive x-ray analysis (EDXA)	78

4.5.3. Accelerated surface area and porosimetry (ASAP 2010)	81
4.5.4. Mercury porosimetry (Autopore II 9220)	83
Chapter 5: RESULTS AND DISCUSSION	85
5.1. Introduction	85
5.2. Membrane Support Tube	85
5.2.1. Surface characterisation	85
5.2.2. Pure gas permeation tests	88
5.2.3. Mixed gas permeation	89
5.3. Silica Membrane for Hydrogen Reactions	90
5.3.1. Pore size and surface characterization	90
5.3.2. Pure gas permeation	93
5.3.3. Mixed gas permeation	100
5.3.4. Separation factor	101
5.3.5. Gas flow mechanism	103
5.4. Silica Membrane for Hydrogen Separation	105
5.4.1. Pore size and surface characterization	105
5.4.2. Pure gas permeation	108
5.4.3. Mixed gas permeation	112
5.4.4. Separation Factor	114
5.4.5. Gas flow mechanism	116
5.4.6. Membrane durability	117

5.5. Silica membrane for hydrogen purification	119
5.5.1. Pore size and surface characterization	119
5.5.2. Pure gas permeation	122
5.5.3. Mixed gas permeation	127
5.5.4. Separation factor	128
5.5.5. Gas flow mechanism	130
5.5.6. Ternary mixture separation	132
5.5.7. Membrane Stability and Durability	134
5.5.8. Membrane preparation reproducibility	136
5.6. Palladium Impregnated Silica Membrane	138
5.6.1. Pore size and surface characterization	138
5.6.2. Pure gas permeation	141
5.6.3. Separation factor	146
5.7. Silica γ -alumina membrane	148
5.7.1. Pore size and surface characterization	148
5.7.2. Pure gas permeation	151
5.7.3. Separation factor	155
5.8. Summary	156
Chapter 6: MODELLING AND SIMULATION	157
6.1. Introduction	157
6.2. Mathematical model	158

6.2.1. Mass balances	160
Reaction zone:	160
Permeation zone:	160
6.2.2. Energy balances	164
Annular configuration:	164
Reaction zone:	164
Permeation zone:	164
Tubular configuration: Reaction zone:	164
6.3. Outline of the study	165
6.3.1. Models	165
6.3.2. Solution strategy	166
6.3.3. Model comparison	166
6.4. Results and discussion	168
6.4.1. Catalyst performance	168
6.4.2. Feed flow rate	170
6.4.3. Feed composition	172
6.4.4. Sweep gas flow	174
6.4.5. Temperature Profiles	176
Chapter 7: CONCLUSIONS AND FUTURE WORK	178
7.1. Introduction	178
7.2. Silica Membrane for Hydrogen Reactions	178

7.3.	Silica Membrane for Hydrogen Separation	179
7.4.	Silica Membrane for Hydrogen Purification	180
7.5.	Palladium Impregnated Silica Membrane	181
7.6.	Silica γ -Alumina Membrane	182
7.7.	General Conclusion	183
7.8.	Modelling and simulation	184
7.9.	Summary of Conclusions	186
7.10.	Future work	187
	REFERENCES	188
	APPENDIX	206

LIST OF FIGURES

<u>Figure 2.1: Classification of membrane reactor</u>	<u>24</u>
<u>Figure 3.1: Scheme of sol-gel routes: Colloidal sol-gel route and polymeric gel route</u>	<u>44</u>
<u>Figure 3.2: Scheme of dip-coating deposition stages</u>	<u>45</u>
<u>Figure 3.3: (A), (B): Capillary tubes of various diameters</u>	<u>47</u>
<u>Figure 3.4: Mechanisms of transport through porous inorganic membranes</u>	<u>53</u>
<u>Figure 4.1: Schematic of membrane support tubes.</u>	<u>64</u>
<u>Figure 4.2: Schematic of dip coating process</u>	<u>66</u>
<u>Figure 4.3: Schematic of modified dip-coating process.</u>	<u>68</u>
<u>Figure 4.4: photo of dip-coating process for the preparation of Pd impregnated γ-alumina membrane.</u>	<u>69</u>
<u>Figure 4.5: Schematic of experimental rig for the flow diagram</u>	<u>71</u>
<u>Figure 4.6: Schematic of experimental rig for the Permeation cell</u>	<u>73</u>
<u>Figure 4.7: Schematic of membrane reactor assembly</u>	<u>75</u>
<u>Figure 4.8: A schematic layout of a gas chromatograph.</u>	<u>77</u>
<u>Figure 4.9: Calibrated product chromatograph.</u>	<u>77</u>
<u>Figure 4.10: Set up for Scanning Electron Microscope (SEM) and Energy Dispersive X-ray Analysis (EDXA).</u>	<u>80</u>
<u>Figure 4.11: Micromeritics ASAP 2010 Analyzer and calibration result.</u>	<u>82</u>
<u>Figure 4.12: Mercury Porosimetry Autopore II 9220</u>	<u>84</u>

<u>Figure 5.1: Pore size distribution of the support (mercury porosimetry).</u>	<u>86</u>
<u>Figure 5.2: SEM micrographs showing support Outer surface (A), Inner surface (B) and Cross section (C).</u>	<u>87</u>
<u>Figure 5.3: Pore size distribution of the silica membrane for hydrogen reaction applications.</u>	<u>91</u>
<u>Figure 5.4: SEM micrographs of the membrane for reaction applications A) Outer surface B) Inner surface and C) Cross section.</u>	<u>92</u>
<u>Figure 5.5: Hydrogen permeances of silica membrane for hydrogen reactions.</u>	<u>93</u>
<u>Figure 5.6: Nitrogen permeances of silica membrane for hydrogen reactions.</u>	<u>96</u>
<u>Figure 5.7: Propane permeances of silica membrane for hydrogen reactions.</u>	<u>97</u>
<u>Figure 5.8: Methane permeances of silica membrane for hydrogen reactions.</u>	<u>98</u>
<u>Figure 5.9: CO₂ permeances of silica membrane for hydrogen reactions.</u>	<u>100</u>
<u>Figure 5.10: Pure and Mixed gas separation factors</u>	<u>102</u>
<u>Figure 5.11: Gases permeance vs. molecular weight-1/2</u>	<u>103</u>
<u>Figure 5.12: Gases permeance vs. temperature-1/2</u>	<u>104</u>
<u>Figure 5.13: pore size distribution of the silica membrane for hydrogen separation applications</u>	<u>106</u>
<u>Figure 5.14: SEM micrographs of the separation membrane A) Outer surface B) Inner surface and C) Cross section.</u>	<u>107</u>
<u>Figure 5.15: Hydrogen permeances of silica membrane for hydrogen separation.</u>	<u>108</u>

<u>Figure 5.16: Nitrogen permeances of silica membrane for hydrogen separation.</u>	110
<u>Figure 5.17: Propane permeances of silica membrane for hydrogen separation.</u>	111
<u>Figure 5.18: Mixed gas separation factors of silica composite membrane for hydrogen separation.</u>	115
<u>Figure 5.19: Durability for hydrogen separation silica membrane.</u>	118
<u>Figure 5.20: Pore size distribution of the silica membrane for hydrogen purification applications. (Nitrogen Adsorption)</u>	120
<u>Figure 5.21: SEM micrographs of the purification membrane A) Outer surface B) Inner surface and C) Cross section.</u>	121
<u>Figure 5.22: Hydrogen permeances of silica membrane for hydrogen purification.</u>	122
<u>Figure 5.23: Nitrogen permeances of silica membrane for hydrogen purification.</u>	123
<u>Figure 5.24: Methane permeances of hydrogen purification silica membrane.</u>	124
<u>Figure 5.25: Propane permeance for hydrogen purification silica membrane.</u>	125
<u>Figure 5.26: CO₂ permeance data for hydrogen purification silica membrane.</u>	126

<u>Figure 5.27: Separation factors for hydrogen purification silica membrane using ternary gas mixture.</u>	<u>133</u>
<u>Figure 5.28: Membrane Stability for the hydrogen purification silica composite.</u>	<u>134</u>
<u>Figure 5.29: Membrane durability for the hydrogen purification silica composite.</u>	<u>135</u>
<u>Figure 5.30: Pore size distribution of the palladium impregnated membrane</u>	<u>139</u>
<u>Figure 5.31: SEM micrographs of the palladium A) Outer surface B) Inner surface and C) Cross section.</u>	<u>140</u>
<u>Figure 5.32: Hydrogen permeances of Pd impregnated membrane.</u>	<u>141</u>
<u>Figure 5.33: Nitrogen permeances of Pd impregnated membrane.</u>	<u>142</u>
<u>Figure 5.34: Argon permeances of Pd impregnated membrane.</u>	<u>143</u>
<u>Figure 5.35: Propane permeances of Pd impregnated membrane.</u>	<u>144</u>
<u>Figure 5.36: Methane permeances of Pd impregnated membrane.</u>	<u>145</u>
<u>Figure 5.37: Pore size distribution of the silica on γ-alumina membrane.</u>	<u>149</u>
<u>Figure 5.38: SEM micrographs of silica-γ-alumina membrane A) Outer surface B) Inner surface and C) Cross section.</u>	<u>150</u>
<u>Figure 5.39: Hydrogen permeances of silica - γ-alumina composite membrane.</u>	<u>151</u>
<u>Figure 5.40: Nitrogen permeances of silica - γ-alumina composite</u>	

<u>membrane.</u>	<u>152</u>
<u>Figure 5.41: Argon permeances of silica - γ-alumina composite</u>	
<u>membrane.</u>	<u>153</u>
<u>Figure 5.42: Propane permeance of silica - γ-alumina composite</u>	
<u>membrane.</u>	<u>154</u>
<u>Figure 6.1: Schematic of annular and tubular membrane reactor</u>	
<u>configurations.</u>	<u>159</u>
<u>Figure 6.2: Impact of feed flow rate on different configurations.</u>	<u>172</u>
<u>Figure 6.3: Impact of feed composition on the performance of</u>	
<u>different configurations.</u>	<u>173</u>
<u>Figure 6.4: Impact of sweep gas flow on propane conversion.</u>	<u>175</u>
<u>Figure 6.5: Reaction zone temperature profiles.</u>	<u>177</u>

LIST OF TABLES

Table 1.1: Summary of silica composite membranes for various reaction schemes...	6
Table 1.2: Summary of silica composite membranes for separation and purification applications.	10
Table 2.1: Classification of membrane reactors.....	23
Table 2.2: Summary of membrane reactor studied for propane dehydrogenation....	30
Table 5.1: Pure gas separation factors for the support at room temperature.....	86
Table 5.2: Pore size distributions of silica membrane for hydrogen reaction applications.	90
Table 5.3: Pure and mixed H ₂ and N ₂ permeances of silica membrane for reaction applications.	100
Table 5.4: Pure gas separation factors for different pairs of gases for silica membrane applicable for hydrogen reactions.	101
Table 5.5: Average pore size of the silica membrane for reaction applications evaluated from gas permeance.....	104
Table 5.6: Pore size distribution of the silica composite membrane prepared for hydrogen separation applications.....	105
Table 5.7: Pure and Mixed gas hydrogen permeances of silica composite membrane for hydrogen separation.	112
Table 5.8: Pure and mixed gas nitrogen permeances of silica composite membrane for hydrogen separation.	113
Table 5.9: Pure gas separation factors for separation membrane at different temperatures.....	114

Table 5.10: Activation energies and pre-exponential factors for hydrogen separation silica membrane.	116
Table 5.11: Pore size distribution of the silica composite membrane prepared for hydrogen purification.....	119
Table 5.12: Pure and mixed gas hydrogen permeances for the hydrogen purification silica membrane.	127
Table 5.13: Pure and mixed gas nitrogen permeances for the hydrogen purification silica membrane.	128
Table 5.14: Pure gas separation factors for the hydrogen purification silica.	129
Table 5.15: Activation energies and pre-exponential factor for permeation of different gases through hydrogen purification composite membrane ..	131
Table 5.16: Pure and ternary hydrogen permeances for hydrogen purification membrane.....	132
Table 5.17: Reproducibility test of the silica membrane for purification applications evaluated from gas permeance.....	137
Table 5.18: Pore size distribution of the palladium impregnated membrane.....	138
Table 5.19: Pure gas separation factors for different pairs of gases for Pd impregnated membrane.....	147
Table 5.20: Pore size distribution of silica on γ - alumina membrane.	148
Table 5.21: Pure gas separation factors for different pairs of gases for silica γ -alumina membrane.....	155

ACKNOWLEDGEMENTS

Praise be to Alla, most beneficent, most merciful

“I am most grateful to Allah, without his help this thesis would not bring to completion.”

I would like to express my heartfelt gratitude and appreciation to my supervisor Dr. Edward Gobina for his invaluable guidance, unlimited support and patience during my research. Further, this work would have not been definitely in a good shape had if I not had the critical comments and review of my ideas and proposal from Dr. Gobina. The author wishes to express his sincere thanks to my second supervisors Dr. Douglas Morrison for his help and support and Dr. .Kostas Rados for his comments regarding the modelling and simulation. Many thanks to Dr. Ali Siddiqui for his help in the physics related areas and Dr. Ramagopal Uppaluri, post doctoral research fellow for his valuable inputs regarding the polymath software. Thanks to Dr. W. E. Mason, Dr Sha Jihan and Mr. John Dickson for their help and support. Many thanks to Joe da Costa, David Forehand, Barry Mckenzie and Susanne Olsen for their support and friendship and to all the staff within the RGU in general and the School of Engineering in particular.

My sincere thanks to the technicians, Bill Walker, Technical services officer for sourcing and ordering of equipment, Milton Montgomery, TSO for building test rigs etc., and Steven Pirie, TSO for manufacture of equipment used etc., and Stand Buchan, TSO for assembling engineering equipment etc., and for there efforts to prepare the membrane reactor assembly. Many thanks to Iain Tough for his valuable assistance for preparing the SEM and EDXA results and Maureen Byres for her help. Thanks to Martin Johnstone and Allan Macpherson for their friendship and support.

The author thanks sincerely the Ministry of Libya Education for their sponsorship during his postgraduate studies. To end with, I am really grateful to my parents and family back home for their praying and continued support. I would also regard my wife for her constant support in difficult times, and her confidence to bring me back to the mood of research cannot be repaid back. Thanks to my children, Usama, Mohaned, Zaid and Duaa. Finally, all thanks to my friends for giving me a great environment all through the time of my stay in Aberdeen.

NOMENCLATURE

Chapter 3

ΔP	Pressure drop across the membrane, Pa
r, r_p	pore radius of the membrane, m
M, M_i, M_s	Molecular weight of the species, kg/kmol
T	Temperature of permeation
P_{avg}	Average pressure, Pa
μ, μ_s	Viscosity of the gas, kg/(m.s)
δ	Thickness of the membrane, m
N_A	Avagadro number
dq/dl	Surface concentration gradient
ΔH	Net effect of activation and adsorption energy, kJ/mol
R	Gas constant
Q_{st}	Isoteric heat of adsorption
E_m	Positive mobility energy, kJ/mol
E_a	Activation energy, kJ/mol
K	Knudsen permeability, mol.m/m ² .s.Pa
V	Viscous permeability, mol.m/m ² .s.Pa
D_0	Pre-exponential diffusion coefficient
K_0	Pre-exponential proportionality constant
J_i	Component flux, mol/m ² .s
α_{ij}	Separation factor for the mixed pair i,j
y_i	Composition of gas in the permeate stream

Chapter 4

q	Flow rate, ml/min
A	Membrane permeation area, m ²
Per	Permeance of the membrane, mol/m ² .s.Pa
Perm	Permeability of the membrane, mol.m/m ² .s.Pa

Chapter 6

A	Propane
B	Propylene
C	Hydrogen
D	Nitrogen
E	Argon
C_{ps_i}	Heat capacities of component i in the shell side, J/(kmol.K)
C_p^t	Heat capacity of gas in the tube per unit mass, J/kg.K
C_{pt_i}	Heat capacity of component i in the tube, J/kmol.K
d^s	Inner diameter of the shell, m

d^t	Inner diameter of the tube in the membrane reactor, m
d^{os}	Outer diameter of the shell, m
d^{ot}	Outer diameter of the tube, m
d_p	Diameter of the catalyst, m
F_i	Molar flow rate of components i in the reaction zone, kmol/s
G_i	Molar flow rate of component i in the permeation zone, kmol/s
J_i	Permeation flux of component i, kmol/m ²
K_0	Equilibrium constant, bar
k_0	Forward reaction rate constants, kmol/(m ³ .s)
L	Length of the membrane reactor, m
Per_i	Permeances for component i through the membrane, kmol/(m ² .s.bar)
P_i	Partial pressure of component i in the reaction zone, bar
P^R	Reaction zone pressure, bar
r_i	Reaction rate of component i, kmol/m ³ .s.
S^M	Perimeter of the membrane surface, m
S^P	Cross sectional area of the permeation zone, m ²
S^R	Cross sectional area of the reaction zone, m ²
S^s	Perimeter of the membrane reactor, m
T	Temperature of the reaction zone used in permeance expressions, K
T^o	Temperature of the oven
T^s	Temperature of the shell, K
T^t	Temperature of the tube, K
U^s	Heat transfer coefficient of the gas in the shell, W/(m ² .K)
U^t	Heat transfer coefficient of the gas in the tube, W/m ² .K
ΔH	Heat of reaction, J/(kmol)
ΔT	Temperature difference for heat transfer due to natural convection, K
M^t	Average molecular weight of the gas in the tube, kg/kmol
R	Gas constant, J/kmol.K
P_{A-C}	Partial pressure of A,B and C in reaction zone, bar
H_{A-E}^t	Enthalpy of components A – E in the tube, J
H_{A-E}^s	Enthalpy of components A – E in the shell, J

Chapter 1:

INTRODUCTION

1.1. General Background

Membranes can be used to separate different components (gas or liquid) based on its properties by allowing or preventing the passage of one or more components under the action of a driving force (Armor, 1989). For gas separation, the driving force for the diffusion of gas through the membrane is usually the pressure differential applied across the membrane (Hsieh, 1991). In recent years, interest in membranes made of unusual inorganic materials has increased. Inorganics membrane support tubes such as alumina and Vycor were first produced in the early seventies (Yoldas, 1975) and have now become commercially available with excellent pore size uniformity and good thermal and mechanical properties. These tubes have been used as a membrane in different applications in the food, pharmaceutical and electronic industries, for waste water treatment and in bioreactor applications (Hakuta, 1988). High temperature ceramic membranes are also finding applications in catalytic and reaction engineering (Armor, 1989).

Nowadays the majority of porous ceramic membrane supports available in the market are of the multilayer type consisting of a bottom macroporous layer, an intermediate layer and a top layer. Usually, the bottom layer is a few millimetres thick and possesses a macroporous structure with pore diameters between 1 and 10 micrometer (μm). The intermediate layer is usually about 10 – 100 μm thick with pore diameter ranging between 0.05 to 0.5 μm (Burggraff and Cot, 1996). The top layer actually serves the purpose of selective gas permeation with a thickness varying between 1 and 10 μm and pore diameters varying from 0.004 to 0.05 μm . The multilayer composite membranes possess excellent pore size uniformity and good thermal and mechanical properties (Burggraff and Cot, 1996).

The preparation of composite inorganic membranes is usually carried out by the deposition of a thin layer (to increase the permeance of the membrane) with a narrow

range of pore sizes on a porous support. The top layer has superior separation properties compared to the porous support which provides mechanical stability for the system in operation. Therefore, the permeability and selectivity of a membrane is strongly affected by the pore size and its distribution of the support, shrinkage of the thin layer and interaction between the support and the thin layer (Nair et al., 1997).

With respect to the pore size, Moaddeb and Koros (1995) studied the effects of the support pore size and its distribution on the final permeation behaviour of polymer thin layers. Based on their experimental observations, they have inferred that the use of large pore size supports could produce consistency problems. They have also concluded that the relative size of the precursors (used for deposition) and the pore size of the support are key factors in determining defect free deposition. According to authors, defect-free deposition is achievable when the pore size of the precursor is larger than or equal to the pore size of the support.

Referring to IUPAC classification of the pore size, there are three categories as given below (Rouquerol et al., 1994).

- Micropores, which have diameters less than 2 nm
- Mesopores, which have diameters between 2 nm and 50 nm
- Macropores, which have diameters greater than 50 nm

This classification is associated with the gas transport mechanisms in the pores of the membranes. For instance, if the membrane contains pores large enough to allow viscous flow, separation will not occur. However, when the membrane pores size is reduced such that it becomes smaller than the mean free path of the gas molecules (i.e. the average distance travelled between collisions for gas molecules), Knudsen diffusion mechanism becomes predominant. In this case low molecular weight gases are able to diffuse more rapidly than heavier ones, and separation occurs. Therefore, when pure Knudsen diffusion occurs, the ideal separation factor α_{12} of the light gas 1 and heavy gas 2 will be $\sqrt{M_2} / \sqrt{M_1}$, where M_1 and M_2 correspond to the molecular weights of gases 1 and 2 respectively (Sturchio et al., 1966).

Based on their pore structures, inorganic membranes can be classified into two categories: porous inorganic membranes and dense membranes. Porous membranes such as alumina and glass provide high hydrogen permeance, but relatively low selectivity. These combinations of high permeance and low selectivity are governed mainly by the Knudsen diffusion mechanism (Wu et al., 1994). Separation factors achieved by this mechanism are too low and are not satisfactory for membrane reactor industrial applications. On the other hand, dense membranes such as palladium and its alloys have hydrogen permeance values that are low compared with porous membranes, but excellent selectivity of hydrogen with respect to other components. Thus, it is always necessary to compromise between permeance and selectivity according to the desired applications.

1.2. Motivation

Many industrial processes such as crude oil processing and other chemical process performed using hydrogen as a raw material (Internet reference 1). The hydrogen mostly participates in reactions for chemical transformation or as a reducing agent. Hydrogen is also considered as the most promising fuels as future energy sources, (Uemiya et al., 1991). Therefore, it has been predicted that the future demand for hydrogen will be significantly higher than that currently supplied (Internet reference 2). Unfortunately, the production of pure hydrogen at a low process cost has been a particular challenge as it is generally observed that it is costly to produce or separate hydrogen from gas mixtures.

These upcoming technologies and transition to a hydrogen economy can significantly influence the total hydrogen demand for which newer methods of hydrogen purification and production need to be investigated and assessed. Hence, industrial gas processing using membranes can develop relatively cheaper technologies that can allow the production of relatively pure hydrogen. Motivation for the present work comes from the increasing demand for hydrogen due to the substantial increase in industrial processing especially petroleum refining and petrochemical production based on world economy growth.

1.3. Separation Technology

Industrial separation technologies for hydrogen removal from hydrogen rich streams constitute of cryogenic distillation, pressure swing adsorption (PSA), and membrane separation. Of these technologies, cryogenic distillation is considered as expensive due to very high heat demands for separation carried out at lower temperatures. Both pressure swing adsorption and membrane technology are presented as competent technologies to produce hydrogen (Internet reference 3). The basic disadvantage of PSA system is its inability to be cost effective for small scale operation. However, in this regard membrane technology offers the advantages of compactness and less maintenance cost (Internet reference 4).

PSA is based on the adsorption of gases onto special materials known as adsorbents. These adsorbents remove all non-hydrogen components such as carbon monoxide (CO), carbon dioxide (CO₂), methane (CH₄) and N₂ from an impure H₂ stream to produce pure H₂ (Garside, 1988). Once the adsorbents are near saturation, the impurities are purged, so regenerating their adsorbents for the next PSA cycle.

Membrane technology relates the separation of hydrogen based on its specific interaction with the membrane surface as opposed to other elements and by the application of a pressure differential across the membrane to drive the hydrogen to the enriched product stream (Baker, 2000). Both pressure swing adsorption and membrane technology offer ample opportunity for possible breakthrough in existing limitations. The separation behaviour of both of these technologies is significantly influenced by the specific interaction of hydrogen with respect to the surface of the adsorbent/membrane. Hence, advances in materials research can provide new horizons for both these technologies and extend their applications considerably. For industrial application using membrane technology, membrane stability at higher temperature (>100°C) coupled with higher hydrogen flux and selectivity are aspiring properties for different applications. In this regard, inorganic membranes offer the basic advantage of thermal and chemical stability, which is attractive for hydrogen reaction, separation, and purification applications.

1.4. Membrane Reactors and Hydrogen Reaction

A membrane reactor is an apparatus that constitutes a chemical reaction process supported with a membrane that can provide different functionality such as separation (Bernstein and Lund, 1993). In a membrane reactor, one of the components (usually H_2) is preferentially removed by membranes from the reactor chamber to shift the equilibrium to the product side.

Due to the limitations offered by the existing commercial process with conventional reactor in equilibrium conversion, different reactions such as hydrogenation (Itoh, 1987; Farris and Armor, 1993) and dehydrogenation (Zhao et al., 1990 and Champagnie et al., 1992) and H_2 recovery from process streams (Cicero and Jarr, 1985) has attracted a considerable research interest.

The driving forces behind the interest are the availability of high H_2 perm-selectivity membranes and capability of operating at high temperature for driving the equilibrium limited reaction towards higher conversion. Furthermore, it is reported that membranes could be used for the preparation of unsaturated hydrocarbon from low cost saturated hydrocarbons (Gorriz et al., 1992).

Many review publication (Soria, 1993; Armor, 1998 and Saracco, et al., 1999) addressing the development of the membrane reactor for catalytic reactions taking place at high temperature. Of these reactions, propane dehydrogenation to produce propylene is of commercial significance with the fact that propylene is the second largest petrochemical commodity available. Propylene is used in the production of poly-propylene which has applications and huge demand for the production of packaging materials and outdoor clothing (Munro, 1964).

Table 1.1 presents different reaction schemes experimentally studied using silica composite membranes. All these reactions involve H_2 participation in the reaction either for hydrogenation or dehydrogenation purposes.

Authors	Reaction system	H ₂ Permeance	Selectivity	Reaction temperature
Giessler et al., (2003)	Water gas shift	1.5×10^{-6} mol/m ² .s.pa	H ₂ /N ₂ 18	280 °C
Weyten et. al., (2000)	Propane dehydrogenation	1.4×10^{-7} mol/ m ² .s.Pa	H ₂ /C ₃ H ₈ 70	500 °C
Prabhu et al., (1999)	Dry methane reforming	1.8×10^{-8} mol/ m ² .s.Pa	H ₂ /CH ₄ 23000-27000	600 °C
Yildirim et al., (1997)	Propane dehydrogenation	0.52 cm ³ /cm ² .s.bar	H ₂ /N ₂ 6	450 °C
Ioannides and Gavalas, (1993)	Isobutane dehydrogenation	0.3 cm ³ /cm ² .min.atm	H ₂ /Hydrocarbon 80 – 300	350 °C

Table 1.1: Summary of silica composite membranes for various reaction schemes.

1.5. H₂ Separation and Purification

The successful application of membranes for H₂ separation and purification depends critically on the ability to produce relatively cheap H₂ perm-selective membranes with high selectivity. There are many membranes that have been proposed for H₂ separation and purification (Connor, 1962 and Philpott, 1985). When considering H₂ separation and purification, the most frequently used membranes are palladium and its alloys, and silica membranes, which offer promising capability for H₂ separation and purification (Morooka et al., 1996).

1.5.1. Dense palladium membranes

Since dense palladium membranes are basically selective only to H₂, there is no problem with the selectivity when defect-free membranes can be successfully prepared. On the other hand, the cost is directly proportional to the membrane thickness and since palladium is very expensive the most important issue is to fabricate very thin membranes without defects. Since 1980's, research interests have been focused on dense membrane fabrication deploying palladium and its alloys for fabricating defect-free thin composite membranes.

By coating tubes with a thin film up to 10 μm of palladium alloy, composite membranes have been developed in order to reduce the metal thickness, cost and to increase the permeation fluxes (Meunier and Manaud, 1992). Such membranes were used for H₂ separation and purification (Gryaznov et al., 1993 and Kikuchi, 1995) as well as membrane reactor applications (Uemiya et al., 1988).

Nevertheless, these composite membranes that were investigated and proposed for some industrial applications have limitations such as good durability (Collins and Way, 1993) and lack of complete selectivity to H₂ due to surface micro-defects. Hence these membranes could be difficult for industrial and commercial utilization for schemes such as production of pure H₂ from hydrocarbon reforming, purification of H₂ streams from CO in fuel cells (Mordkovich et al., 1992) (Ye et al., 1991).

1.5.2. Silica membranes

To date, almost all silica composite membranes have been prepared by the acid catalysed hydrolysis of tetraethoxysilane (TEOS) (Yan, 1994) using different preparation techniques such as sol-gel (Brinker et al., 1993) and chemical vapor deposition (CVD) of silica precursors (Tsapatsis and Gavalas, 1994). CVD is a time consuming and tedious procedure requiring expensive and complex system and the commercial production of membranes by this method is hindered (Jayaraman, 1995). Sol-gel modification of mesoporous membranes with polymeric silica has proven to be a very successful process for the preparation of microporous membranes (Kitao, 1990; Uhlhorn, 1992 and De Lange, 1995) and is usually recommended than any other process due to its simplicity.

The silica membranes usually prepared by deposition of top thin layer on the surface of intermediate layer(s) such as γ -alumina using different porous supports such as α -alumina (Morooka, et al., 1995) or Vycor glass (Lee and Oyama, 2002). The membrane thin layer can provide high permeance but the possibility of forming defects that decrease the membrane selectivity is high. Consequently, high quality support with narrow pore size distribution and homogeneous surface characteristics (such as wettability) is required to produce a thin layer and defect-free membranes (Tsai et al., 2000).

Table 1.2 summarises different silica composite membranes prepared by different experimental groups and proposed for H₂ separation and purification applications.

Author(s)	Support(s)	Intermediate layer(s)	Prep. method	H ₂ permeance	Selectivity	Temp.
Lee et. al. (2003)	stainless steel 500 nm	SiO ₂ 500 & 150 nm	CVD	10 ⁻⁸ mol/m ² .s.P a	H ₂ /N ₂ 112.22	250 °C
Hwang et. al. (2003)	α-Al ₂ O ₃ 1000 nm	γ-Al ₂ O ₃ 10 nm	CVD	10 ⁻⁷ – 10 ⁻⁸ mol/m ² .s.P a	H ₂ /N ₂ 4 – 64	300 – 600 °C
Lee and Oyama (2002)	Vycor glass 4 nm	-	CVD	10 ⁻⁸ mol/m ² .s.P a	H ₂ /CH ₄ 10 ⁴	600 °C
Diniz da Costa et. al. (2002)	α-Al ₂ O ₃ 500 – 1000	-	Sol-gel	2 – 3 x 10 ⁻⁹ mol/m ² .s.P a	H ₂ /CO ₂ 69 – 319	500 – 600 °C
Asaeda (2001)	α-Al ₂ O ₃ 1000nm	α-Al ₂ O ₃ 190 nm	Sol-gel	1.3 x 10 ⁻⁶ mol/m ² .s.P a	H ₂ /C ₃ H ₈ 6300	35 - 300 °C
Richard et. al. (2001)	α-Al ₂ O ₃ 140 nm	γ-Al ₂ O ₃ 3 nm	Sol-gel	2 x 10 ⁻⁶ mol/m ² .s.P a	H ₂ /N ₂ < Knudsen	20 – 200 °C
Schafer et. al. (2001)	α-Al ₂ O ₃ 6000 nm	1 st α-Al ₂ O ₃ 2000 nm 2 nd α-Al ₂ O ₃ 400 nm 3 rd α-Al ₂ O ₃ 120 nm 4 th γ-Al ₂ O ₃ 12 nm	Dip coating	20 m ³ /m ² .h.ba r	H ₂ /C ₃ H ₈ 30 - 75	450 – 500 °C
Nakao et. al. (2000)	Vycor glass 4 nm	-	CVD	10 ⁻⁷ – 10 ⁻⁸ mol/ m ² .s.Pa	H ₂ /N ₂ 100 - 900	50 - 30 °C
Prabhu and Oyama (2000)	Vycor glass 4 nm	-	CVD	1.8 x 10 ⁻⁸ mol/ m ² .s.Pa	H ₂ /CH ₄ 23000- 27000	200 - 700 °C
Hwang et. al. (1999)	α-Al ₂ O ₃ 1000 nm	1 st α-Al ₂ O ₃ 80 nm 2 nd γ-Al ₂ O ₃ 10 nm	CVD	6 x 10 ⁻⁹ mol/ m ² .s.Pa	H ₂ /N ₂ 160	600 °C
De Vos et. al. (1999)	α-Al ₂ O ₃ 160 nm	γ-Al ₂ O ₃ 5 nm	Dip coating	2 x 10 ⁻⁶ mol/ m ² .s.Pa	H ₂ /C ₃ H ₈ 250	300 °C
Kusakabe et. al. (1999)	α-Al ₂ O ₃ 110 - 180 nm	γ-Al ₂ O ₃ 5 - 10 nm	Sol-gel	1 x 10 ⁻⁷ mol/ m ² .s.Pa	H ₂ /N ₂ 100	200 °C
Sea et. al. (1998)	α-Al ₂ O ₃ 110 – 180 nm	-	CVD	5 x 10 ⁻⁷ mol/ ² .s.Pa	H ₂ /H ₂ O 3-5	400 °C
Nijmeijer et. al. (1998)	α-Al ₂ O ₃ 80 nm	γ-Al ₂ O ₃ 2.5 nm	CVD	4 x 10 ⁻⁷ mol/ m ² .s.Pa	H ₂ /N ₂ 40	250 °C

Author(s)	Support(s)	Intermediate layer(s)	Prep. method	H ₂ permeance	Selectivity	Temp.
De Vos et. al. (1998)	α -Al ₂ O ₃ 160 nm	γ -Al ₂ O ₃ 2.5 nm	Sol-gel	2×10^{-6} mol/ m ² .s.Pa	H ₂ /N ₂ 10	200 °C
So et. al. (1998)	α -Al ₂ O ₃ 80 nm	-	Sol-gel + CVD	2.5×10^{-8} mol/ m ² .s.Pa	H ₂ /N ₂ 10	400 °C
Sea et. al. (1996)	α -Al ₂ O ₃ 110 – 180 nm	γ -Al ₂ O ₃ 6 nm	CVD	3×10^{-7} mol/ m ² .s.Pa	H ₂ /N ₂ 100 - 1000	600 °C
Morooka et. al. (1996)	α -Al ₂ O ₃ 150 nm	-	CVD	10^{-8} mol/ m ² .s.Pa	H ₂ /N ₂ 600	600 °C
De Lange et. al. (1995)	α -Al ₂ O ₃ 160 nm	γ -Al ₂ O ₃ 2 – 2.5 nm	Sol-gel	10^{-6} mol/ m ² .s.Pa	H ₂ /CH ₄ 50 – 200	200 °C

Table 1.2: Summary of silica composite membranes for separation and purification applications.

1.6. Modelling and Simulation

In order to compare the performance of various membrane reactor configurations such as tubular membrane reactor, (TMR: where catalyst is placed inside the membrane tube) and annular membrane reactor (AMR: where catalyst is placed in the annular space between the shell and membrane tube), modelling is an attractive tool for comparative purposes.

Experimental research for propane dehydrogenation using membrane reactor has been carried out by a number of authors (Ziaka et al., 1993; Sheintuch and Dessau, 1996; Weyten et al., 1997; Yildirim et al., 1997 and Weyten et al., 2000). The authors performed membrane reactor experimental by placing the catalyst inside the membrane tube (TMR) and coating the support from the outside. Such a design works out very well to build a membrane reactor in a research laboratory, as it is easy to place catalyst in a tube and operate the membrane reactor.

However, most of the reaction engineering technology uses jacketed heat source that coiled around the stainless steel tube of the reactor. For the case of a tubular membrane reactor the heat reaches the tube crossing over various resistance such as the steel tube, gas film resistance in the shell side, resistance in the composite support and gas film resistance on the tube side. Since the gas film resistance in the shell is significant, it could seriously restrict the overall heat transfer from the jacket to the reaction zone thereby demanding the necessity for operating of the membrane reactor at higher oven temperatures to provide heat for the endothermic reaction that takes place in the membrane tube.

On the other hand, placing the catalyst on the shell side would offer both lower thermal resistance for the heat transfer and more catalyst weight per unit flow rate of the feed. In conclusion, a membrane reactor packed with catalyst in the shell side is characterised by a higher reactor volume and higher heat flux (Marigliano et al, 2001). Henceforth, operation of endothermic reactions by placing catalyst in the shell side makes the behaviour of the membrane reactor close to isothermal path (Marigliano et al, 2001).

The impact of various heats demanding sinks on conversion have not been studied till date for propane dehydrogenation in a membrane reactor. These sinks can be regarded as heat transfer coefficient of the shell, heat transfer coefficient of the tube, heat of reaction and enthalpy due to flux. Since the gas phase heat transfer coefficient in the tube is significantly low $2 - 5 \text{ watt} / \text{m}^2 \cdot \text{K}$ ($\text{W}/\text{m}^2 \cdot \text{K}$), equilibrium conversion with a tubular membrane reactor can be lower than the corresponding annular membrane reactor operated at the same conditions. Hence, profit margins evaluated using tubular membrane reactor configurations cannot be treated as acceptable values for the actual industrial implementation of membrane reactors.

1.7. Scope of the Research

The scope of this research incorporates the use non-conventional types of silica sols, yet commercially available, relatively cheap and effective in providing the desired membrane characteristics for producing high purity H_2 from a wide variety of gas mixtures. In this regard, silicone elastomer can be regarded as one of the competent materials that have not been widely studied for the preparation of silica composite membranes. Keeping in mind the motivation behind this project, the objectives and advantages of fabricating silica composite membranes for H_2 reaction, separation and purification may be summarized as follow.

1. Preparation and characterisation of different silica composite membranes using inexpensive alumina porous tubes as a support with wide range of pore size as an alternative to the multi-layer asymmetric supports. This will reduce the cost by eliminating the need for an extra intermediate layer(s) deposition which requires a highly complex, tedious and time consuming process.
2. Easy scale up of the sol-gel / dip-coating process using silicone elastomer precursor instead of CVD and TEOS due to elimination of complex equipment needed.

3. Silica composites have to be investigated and their performance has to be tested for high temperatures ($>100^{\circ}\text{C}$) as required for H_2 separation and purification applications.
4. Investigate the possibility of increasing membrane separation properties by impregnating the membrane with H_2 selective metals such as palladium.
5. To develop a mathematical model for the assessment of tubular and annular membrane reactor configurations for propane dehydrogenation by performing comparative analysis.

1.8. Thesis Outline

This thesis has been organized in the following chapters:

In the next chapter, a general overview of literature available for composite inorganic membranes and membrane reactors aimed for H_2 reaction, separation and purification applications is presented. The review can be classified into six sections namely: Preparation methods and materials, membrane reactor applications, catalysis and membrane reactor studies for propane dehydrogenation as model H_2 reaction scheme, silica membranes for H_2 separation and purification and simulation models for membrane reactors.

Chapter 3 presents the theory and experimental studies conducted for silica composite membranes. It assesses characteristics for H_2 reaction, separation and purification. Theory presented in this chapter relates the evaluation of membrane characteristics (permeance and selectivity) coupled with transport phenomena for single and binary gaseous systems

Chapter 4 presents experimental apparatus and procedure for the preparation, surface and flux characterisation of silica composites and noble metal impregnated composites for H_2 reaction, separation and purification. This chapter also summarises various equipment used for membrane preparation, and the chemicals that have been used for the preparation of the membrane composites.

Chapter 5 presents the results obtained from surface and flux characterization studies. Detailed surface characteristics of the silica composite membrane are presented for silica composite membranes prepared for hydrogen reaction applications. This chapter include also details of the hydrogen purification membrane tested for different single gases and equimolar mixture of hydrogen and nitrogen. Finally, section 6.4 presents results and discussion for the silica composites prepared for hydrogen purification applications (with high separation factor). This is followed by results and discussion for the silica composite membrane prepared for reaction applications in section 6.5. The results obtained for palladium impregnated γ -alumina membrane and silica γ -alumina membrane are presented in sections 6.6 and 6.7. Finally conclusions are summarised in section 6.8.

Chapter 6 presents a comparative mathematical simulation study for propane dehydrogenation in different operational schemes based on modelling and simulation for laboratory scale configurations. Operational performance of different configurations namely tubular reactor, annular reactor, tubular membrane reactor and annular membrane reactor are investigated in this chapter.

Chapter 7 presents the conclusions that have been drawn from the experimental and theoretical research conducted in this work. Opportunities for possible future research are summarised in section 7.4.

Chapter 2:

LITERATURE REVIEW

2.1. Introduction

This chapter highlights the features in the preparation methods that can be explored for further research and presents a general overview of the literature covering composite inorganic membranes and membrane reactor catalysis. These membranes aimed at hydrogen reaction, separation and purification employing different types of supports and various fabrication methods with certain modifications. Some modifications are suggested to offer higher hydrogen permeance and selectivity in various applications.

2.2. Preparation Methods and Materials

Inorganic composite membranes can be prepared by a variety of methods, the choice of which depends on such factors as the facilities available on site, required thickness, shape, etc. The most important criteria for the selection of these methods are low cost and/or short preparation time and good membrane performance with the desired properties (permeability, selectivity and stability).

By far the most commonly used methods for preparation of silica membranes are sol-gel, dip-coating and CVD. For metal membranes such as palladium / palladium alloy composite membranes, popular methods used are electroless plating and chemical vapor deposition. The magnetron sputtering method has also been used.

2.2.1. Sol-gel method

The sol-gel method has been widely used to obtain silica polymeric sols which allow the preparation of silica membranes with superior quality (Kitao et al., 1990 ;

Uhlhorn et al., 1992). Other research groups working with the sol-gel process have prepared silica composite membranes with narrow pore sizes and high performance in terms of permeance and selectivity. By use of polymeric sols, De Lange et al., (1995^b) deposited a silica layer upon mesoporous γ -alumina intermediate layer with 5nm pore size. Such top layer (pore size <1nm) enabled molecular sieve-like separation factors in order of 50-200 for H₂/CH₄, well above the Knudsen value of 2.8. The authors concluded that extreme care is demanded by the process in order to control the pore size of the sol effectively.

Other molecular sieving silica membranes were prepared by Raman and Brinker (1995) using hybrid organic – inorganic polymers. The membranes material prepared by polymerization of TEOS and methyltriethoxysilane (MTES) which deposited on alumina support (support details not provided). This approach for the synthesis of molecular sieving silica membranes was tested for CO₂/CH₄ separation with CO₂ permeability value of 2.5×10^{-7} mol/m².s.pa and separation factor higher than 70 was reported.

A modified novel sol-gel dip coating derived silica membranes were obtained by Tsai et al., (2000). The authors prepared dual layer asymmetric silica membranes with improved membrane performance by deposited surface template silica intermediate layer on an asymmetric membrane whose skin layer is γ -alumina with 5 nm pore size. This procedure had resulted in an asymmetric membrane that provided a gradual change in pore diameter from 5 nm (γ -alumina support layer) to 1-1.2 nm and then to 0.3 – 0.4nm silica top layer whose thickness is about 30 nm. The membrane provided a separation factor of about 200 – 600 for CO₂/CH₄. In order to obtain a thin top layer as a selective membrane, Tsai et al., (2000) showed that the quality of the support determines to a high degree, the performance of the membrane top layer. Large pore support surface would cause defects and cracking of the membranes due to stress development on unequal film coating.

Other good results in the area of sol-gel derived silica membranes were obtained by Verweii and coworkers. In these investigations, deposition of 30 nm thickness silica membranes was accomplished via a sol prepared from hydrolysis of TEOS upon a flat support made of α -alumina disk covered with two γ -alumina layer of about 3-

5 μ m thickness (De Vos and Verweij, 1998). Due to low silica film thickness, high H₂ permeance 2×10^{-6} mol/m².s.pa and a H₂/CH₄ separation factor of 500 at 300 °C was reported. The authors conclude that the sol-gel modification provides good selectivity and permeability as opposed to CVD method where there is an attendant loss of permeability, though the selectivity is enhanced. They found that most of the membrane defects arising in the sol-gel derived membranes originated from dust particles present in the environment in which the membranes are produced.

Nair et al., (1996) prepared polymeric sols by hydrolysis and condensation of TEOS in ethanol with HNO₃ as catalyst. The membrane was prepared by dip coating of a γ -alumina intermediate layer in silica sol for four second (4s) using α -alumina support. For the membrane, γ -Al₂O₃ was used as the selective sorption layer in order to separate propylene and propane whose kinetic diameters are very close. A maximum separation factor of about 1.8 was obtained for propane/propylene mixture at 325 °C for the composite membrane. At higher temperatures, therefore the separation factor was decreased to 1.2.

Although, the sol-gel method has some advantages such as simplicity, low cost and pore size control flexibility (Brinker et al., 1993), it suffers from lack of reproducibility (Prabhu and Oyama, 2000). However, the size of the micropores can be more successfully controlled by sol-gel compared with the chemical vapor deposition (Sea et al., 1997).

2.2.2. Dip-coating process

The technology of dip coating inorganic sols to make stable films was pioneered in Germany and became widely known after World War II (Schroeder, 1969).

In general, the repeated coating procedure assists in the reduction of the membrane defects resulting in an increase the membrane selectivity, but at the expense of permeation. As the number of coating steps increases, the membrane flux decrease because of the increase in the layer thickness. According to Larbot et al., (1987), high flux needs membrane thickness from 1 to 10 microns and high selectivity needs narrow pore size distribution. In the case where the membrane thickness is

increased, the possibility of membrane cracks arising after thermal treatment could increase. To avoid this problem and to keep the membrane as durable as possible, the thickness of the membrane layer should be optimised. The important parameters that control the membrane thickness are sol concentration, coating time and the number of coating steps as well as the pore size of the support (Burggraaf and Cot, 1996).

Using dip-coating technique (Lee et al., 2003) prepared silica composite membrane on porous stainless steel support having a pore size of 500nm and 1mm wall thickness by hydrolysis of TEOS. In this process, the macroporous stainless steel substrate pores are reduced by different colloidal silica sols. A sub-micron nickel powder is used in order to reduce pore size and surface roughness of the support as a first stage, then the support was modified again by introducing intermediate layers of 150 nm and 50 nm silica sol. By repeating dipping – drying – calcinations process for four times the selective top layer was produced from the silica sol. This membrane exhibited an H₂ permeance of 1.0×10^{-8} mol/m².s.Pa and an H₂/N₂ selectivity of 112.22 at 250 °C.

Da Costa et al., (2002) reported the use of a two – step catalysed hydrolysis approach for the preparation of molecular sieve silica membranes with TEOS. The α -alumina support with an average pore size of 500 – 1000 nm was coated first by dip coating in diluted sols before a series of silica layers deposit to produce the final top layer. The composite membrane offered a hydrogen permeance of $2 - 3 \times 10^{-9}$ mol/m².s.Pa and Helium (He)/CO₂ selectivity of about 69 – 319 at 500 – 600 °C.

Commercial alumina tubes of asymmetric structure were used by Schafer et al., (2001) for the deposition of silica using the sol-gel / dip coating technique. For this purpose, the commercial membrane used is an ultra filtration membrane with the skin layer being γ -alumina (pore size = 6 nm). The silica layer is deposited on the γ -alumina layer of the ceramic support using a silica polymer sol. The composite provided a hydrogen permeance of about $2 - 3 \times 10^{-6}$ mol/m².s.Pa with H₂/C₃H₈ selectivity in the range of 20 – 55 over the temperature range of 150 – 550 °C.

Identical selectivity results (20 – 50) for H₂ and He with respect to propane and isobutane were obtained by De Vos et al., (1999). The authors prepared silica

membranes by repeated dip coating of an asymmetric support with TEOS. The asymmetric support consisted of a γ -alumina top layer with 5 nm pore size on the top of α -alumina discs with pore size of 160nm. These membranes offered high gas permeance ($1 \times 10^{-5} \text{ mol/m}^2 \cdot \text{s} \cdot \text{Pa}$) for small molecules like H_2 and He.

Nair et al., (1997) prepared a polymeric sol by acid catalyzed hydrolysis and condensation of TEOS and deposited on a flat supports of 150 nm α -alumina to produce silica membranes. These membranes were produced after dipping the support into a boehmite sol for 10s to create γ -alumina with 4nm as intermediate layer and then dipped in silica sol for 10s as well. Hydrogen permeance of the composite indicated activated diffusion with hydrogen permeance of $10^{-7} \text{ mol/m}^2 \cdot \text{s} \cdot \text{Pa}$ and activation energy of 17 kJ/mol at 303 – 460 K. At 303 K, the membrane propane permeance was about 2 times higher than N_2 and Ar. Further, He/ N_2 selectivity of about 1000 and helium permeance with the same value of the hydrogen permeance of $10^{-7} \text{ mol/m}^2 \cdot \text{s} \cdot \text{Pa}$ were measured in the temperature range of 303 – 460 K using the composite membrane.

2.2.3. Chemical vapour deposition

CVD method was used extensively for deposition of thin films of silica membranes and in the case of palladium deposition. In this method, a chemical reaction involving a metal complex in the gas phase is initiated at a controlled temperature and the metal produced by this reaction deposits as a thin layer onto the desired support. Such reactants as organometallic compounds are commonly used due to their high volatility. The deposition of the thin layer usually takes place at high temperature which can be reached using different sources such as resistive heating.

Using CVD, Gavalas et al., (1989) and Tsapatsis et al., (1991) produced a highly hydrogen selective silica membrane with activated diffusion mechanism. The authors were able to deposit silica inside the surface of a vycor glass support. A palladium membrane was prepared by Xomeritakis and Lin (1996) through pore size reduction of γ -alumina layer (pore size = 4nm) with the CVD method. This membrane inferred hydrogen permeance higher than $10^{-7} \text{ mol/m}^2 \cdot \text{s} \cdot \text{Pa}$.

CVD using different silica sources such as TEOS has been followed by Sea et al., (1997). The hydrogen permeance of the membrane was measured to be in the order of 10^{-7} mol/m².s.Pa at 600°C and was not significantly dependent on type of silica source. For these membranes, H₂/N₂ selectivity evaluated from the permeation of single gas was approximately 100. The component permeances were also observed to be similar when a 50/50 mixture of H₂ and N₂ was fed to the system. The authors concluded that the CVD method in general is much easier and simpler than sol-gel. In the mean time, they found that silica membranes produced by CVD are not useful for the separation of large molecules than hydrogen.

A microporous silica membrane on porous vycor glass tube (with 4 nm pore size) was prepared by Nakao et al., (2000) using CVD. The composite membrane obtained was categorized as molecular sieve membranes with He/N₂ permselectivity of 950 at 40 °C. The helium permeance was found to be limited because of the Vycor glass pore size that offer flow resistance. Kusakabe et al., (1999) and Prabhu and Oyama, (2000) concluded that the CVD method is suitable for controlling both pore size and surface modification, but require high capital investment and suffer from difficulties in uniformity of deposits on complex shapes. In addition, this technique needs the development of a complex experimental setup consisting of heating element and control system to regulate the vapour generation and condensation process (Jayaraman et al., 1995). In other words, there is requirement to develop procedures that can present silica composite membranes prepared by simple and cost effective process.

2.2.4. Electroless plating method

Several studies have focused on the development of palladium based membranes using this method (Itoh et al., 1987; Shu et al., 1991; Govind and Atnoor, 1991; Yeung and Varama, 1995). Electroless plating is performed by controlled autocatalysed reduction of metal stable metallic salt complexes on a suitable support. In the case of palladium, complexes such as palladium salt solution may be used to deposit thin film in the presence of a reducing agent, typically hydrazine (Uemiya et al., 1988).

A composite palladium ceramic membrane was prepared by Uemiya et al., (1990) for the study of aromatization of propane in a membrane reactor. In their work, the authors deposited an 8.6 μm thick palladium film on the outer surface of a porous alumina tube. One year later, Uemiya and co-workers used electroless plating to deposit palladium films ranging from 13-20 μm on the outside surface of porous glass tubes with 0.3 μm pores (Uemiya et al., 1991^{a,b}). They report an infinite hydrogen selectivity, which means defect free deposition was carried out. These membranes were tested in a membrane reactor for steam reforming of methane and water gas shift reactions.

Electroless plating technique to prepare a Pd composite membrane was also developed by Kikuchi et al., (1991). Compared to commercially available palladium membranes with thickness of 150 μm , their membrane exhibited a higher permeance to hydrogen and had a high H_2 selectivity. Shu, et al., (1991) deployed stainless steel support to prepare palladium-silver (Pd-Ag) composite membrane applying electroless plating. However, no permeation results were given. It has been demonstrated that this method can produce a uniform metallic deposition on complex shaped support with simple equipment. Collins et al., (1996) deposited thin palladium films on the inner surface of a tubular porous ceramic support using electroless plating. The thickness of the deposited palladium film was about 12 μm on a porous support of 200 nm pore size.

It can be concluded from different research groups (Govind and Atnoor, 1991; Shu et al., 1993 and Li et al, 1996) that electroless plating technique offers some advantages such as simplicity, low cost and capability for providing uniform dense coating on different kind of supports (i.e. vycor glass and stainless steel) with uniform and non-uniform shapes. The main drawback of this method is that sequential deposition is required for preparing Pd alloy film. Furthermore, Xomeritakis and Lin, (1996) reported that it is difficult to control film thickness above 3 microns that has uniform and high film quality and good adhesion property.

2.2.5. Magnetron sputtering method

This is another method that can be used to prepare metal membranes. By this method, thin film metal membranes can be produced on almost any type of supports. During magnetron sputtering, metal particles like palladium are sputtered to the clean support in a vacuum chamber at low pressure (10^{-7} Torr) using electric field. To vary the thickness of the deposited films different coating times can be applied. The distance between the target and the support should be maintained constant during deposition in order to produce uniform membranes. The deposition temperature can be controlled with a resistance substrate heater. The advantages of this method are flexibility to synthesize alloys, easily controllable process parameters and ultra and uniform thickness. The disadvantages of the method are high cost and its low efficiency. According to Hara et al., (2000) it is not easy to prepare defects-free thin membranes on supports, using sputtering method.

Athayde et al., (1994) prepared ultrathin Pd / Ag alloy films with about 50 nm thickness on polymeric supports by the sputter deposition in order to increase the selectivity of polymer membrane without reducing the permeability. Since these polymer / metal composites are not stable at high temperature due to the thermal stability limitation of the support, Jayaraman, (1995) used a ceramic support and prepared a palladium films (<500nm) after applying a γ -alumina thin layer on disc α -alumina porous tube. A pure palladium (99.9 %) target of 100 mm thickness was used as the sputtering source. The prepared membrane was tested for hydrogen / nitrogen separation and different parameters such as support type, sputtering temperature and film thickness also investigated. Itoh et al., (2000) combined sputtering and electroplating technique for palladium composite membrane preparation for hydrogen separation. The sputtering process was used in order to provide an electro-conductivity on the top of the outer surface of the alumina layer using radio frequency sputtering equipment. They found that it is possible to fill the support pores to an extent even in the sputtering process. The membrane exhibited a separation factor of hydrogen to nitrogen of about 1640 at 350°C.

2.3. Membrane Reactor Applications

There has been an intense, worldwide effort on the concept of membrane reactors (combining reaction and separation in one unit operation) for the last several decades as presented in many review articles (Hsieh, 1991; Shu et al., 1991; Saracco and Specchia, 1994). This is because of many advantages such as compact process equipment; lower energy requirement and reduced production of undesired compounds. One of the most important objectives of membrane reactor research has been to achieve a conversion enhancement over the thermodynamic equilibrium. By selectively removing of one or more of the reaction products through the membrane tube, it is possible to shift the equilibrium towards the product side, and overcome the thermodynamic limitations of the reaction. Thus, higher conversion can be attained at lower temperatures thereby avoiding intense catalyst deactivation and undesired side reaction.

Several membrane reactor configurations have been proposed and studied (Zaman 1994) and some of these configurations can be classified as shown in Table 2.1 and schematically presented in Figure 2.1 (Dittmeyer et al., 2001).

Catalytic Membrane Reactor (CMR)	Selective removal of products from the reaction zone. (one product permeate through the membrane)
Catalytic Non-permselective Membrane Reactor (CNMR)	Non selective removal of products from the reaction zone. (all components permeate through the membrane at comparable rates)
Packed Bed Catalytic Reactor IMCR (PBCR)	The membrane is inert and acts as a diffusing element and reaction takes place on a catalyst bed.
Packed Bed Catalytic Membrane Reactor CMR (PBCMR)	The membrane acts as a catalyst and a diffusing element. In addition to the catalytic membrane, a packed bed catalyst is used to increase the reaction rates

Table 2.1: Classification of membrane reactors.

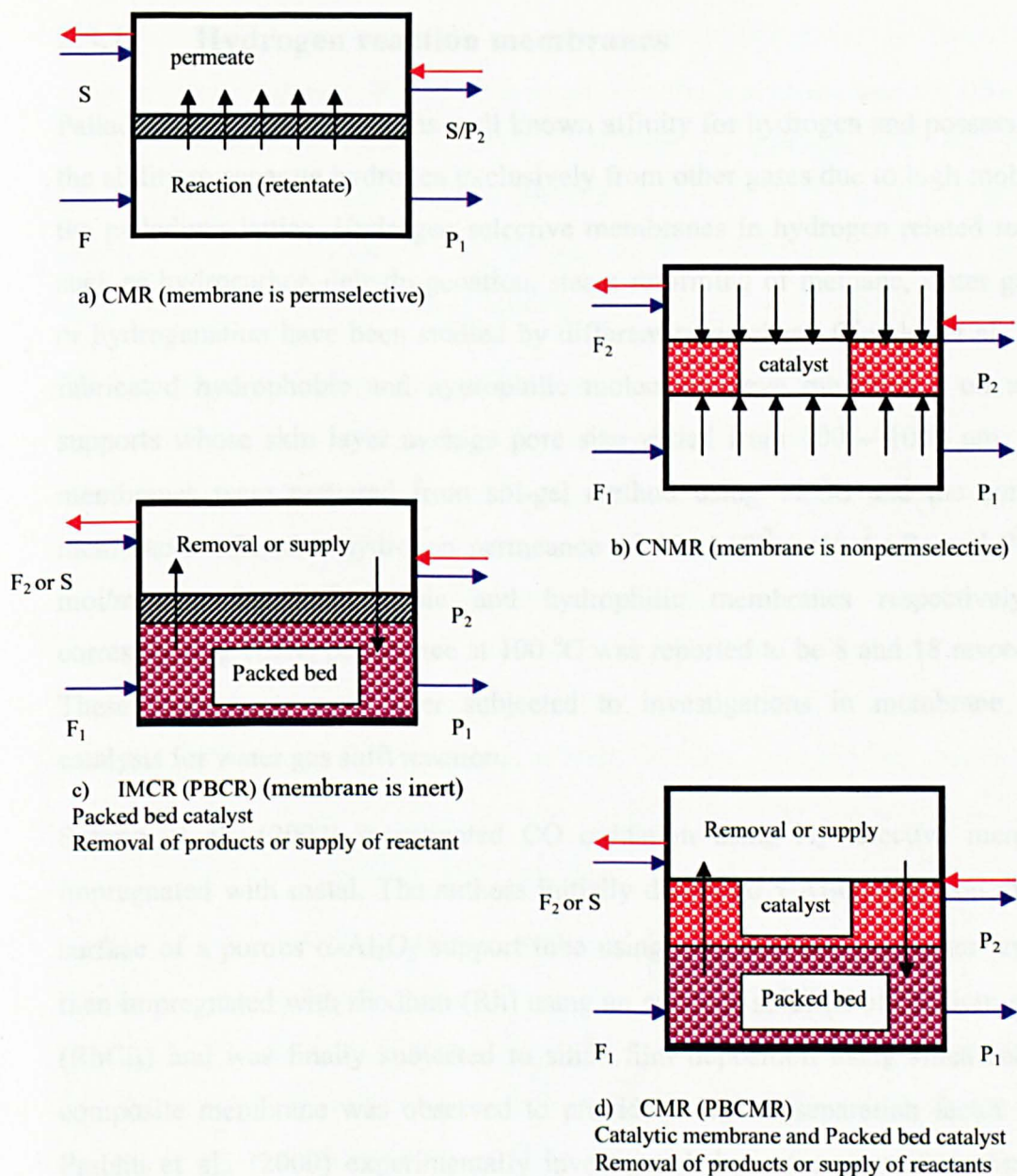


Figure 2.1: Classification of membrane reactor (Dittmeyer et al, 2001).

2.3.1. Hydrogen reaction membranes

Palladium is remarkable for its well known affinity for hydrogen and possesses both the ability to separate hydrogen exclusively from other gases due to high mobility in the palladium lattice. Hydrogen selective membranes in hydrogen related reactions such as hydrocarbon dehydrogenation, steam reforming of methane, water gas shift or hydrogenation have been studied by different researchers. Giessler et al., (2003) fabricated hydrophobic and hydrophilic molecular sieve membranes on alumina supports whose skin layer average pore size varied from 500 – 1000 nm. These membranes were prepared from sol-gel method using TEOS and the composite membranes offered a hydrogen permeance of $15 \times 10^{-7} \text{ mol/m}^2 \cdot \text{s} \cdot \text{Pa}$ and $7 \times 10^{-9} \text{ mol/m}^2 \cdot \text{s} \cdot \text{Pa}$ for hydrophobic and hydrophilic membranes respectively. The corresponding H_2/N_2 permeance at 100 °C was reported to be 8 and 18 respectively. These membranes were later subjected to investigations in membrane reactor catalysis for water gas shift reaction.

Sotowa et al., (2002) investigated CO oxidation using H_2 selective membranes impregnated with metal. The authors initially deposited $\gamma\text{-Al}_2\text{O}_3$ layer on the outer surface of a porous $\alpha\text{-Al}_2\text{O}_3$ support tube using boehmite sol. The outer layer was then impregnated with rhodium (Rh) using an aqueous solution of rhodium chloride (RhCl_3) and was finally subjected to silica film deposition using silica sols. This composite membrane was observed to provide a H_2/CO separation factor of 100. Prabhu et al., (2000) experimentally investigated dry reforming of methane in a membrane reactor with 1% rhodium-alumina ($\text{Rh}/\text{Al}_2\text{O}_3$) / Silica-Vycor glass (Nanosil) membrane reactor. The membrane observed to exhibit 100 % selectivity of hydrogen with respect to other components in the reaction scheme.

Lee et al., (1995) prepared Pd impregnated membranes using an asymmetric porous support whose skin layer pore size is 80 nm. The support was first deposited with Pd impregnated on γ -alumina employing sol-gel technique. Subsequently, palladium acetate solution was used to soak the material further. The composite was then dried at 293 K and 373 K respectively for 3 hours. Finally, CVD method with deposition at 453 K under vacuum application was carried out which yielded the composite membrane that had about 0.52 wt % Pd on its surface. The gas separation

characteristics of the palladium membrane before and after modification were summarised as follows. The sol-gel prepared γ -alumina membrane exhibited H_2/N_2 separation factor of about 3.6 at 400 °C. Therefore, the reduction of the pore size due to the deposition of γ -alumina is confirmed. However, the palladium supported γ -alumina membrane exhibited a H_2/N_2 separation factor of about 5 – 6 at the same temperature which is higher than that achieved using Knudsen diffusion (3.74).

Yildirim et al., (1997) prepared Pd impregnated composite porous membranes for membrane reactor studies directed towards the propane dehydrogenation reaction scheme. The membrane used for Pd impregnation was either γ -alumina or silica (both with an average pore size of about 4 nm). Therefore, two palladium impregnated membranes were fabricated using palladium chloride ($PdCl_2$) solutions employing impregnated method. The amount of Pd deposited in both the cases was estimated to about 0.45 wt % using weight gain method. The Pd impregnated composite membranes exhibited good performance during membrane studies. At 517 °C for example, propane conversion was evaluated to be 47 % which is higher than the corresponding equilibrium value (40 %).

Vitulli et. al., (1995) prepared platinum (Pt) impregnated silica composite membranes for the hydrogenation of toluene. The silica sol used was a commercial sol (LUDOX) consisting of 40 % silica. Slip-casting was used as the method for the fabrication of the silica membrane on an alumina support. The membrane permeance and selectivity were agreed with Knudsen values.

It can be concluded that, the desirable properties of the membrane would be high permeance and acceptable values of H_2/N_2 selectivity (higher than Knudsen value). This is due to the fact that lower hydrogen permeance cannot increase conversions significantly using membrane reactor because if the permeance is low, the membrane will not be able to remove sufficient hydrogen from the reaction zone at high reaction rate. Further enhancement of separation potential without lowering H_2 permeance value is also of concern in literature. This is targeted to be achieved by noble metals impregnation (Pd) membranes. There has been lack of literature for the utilisation of other types of silica polymer sols that can be as effective as TEOS in providing required characteristics for hydrogen reaction applications.

2.3.2. Propane Dehydrogenation and Catalysts

Dehydrogenation of propane is a thermodynamic limited reaction and highly endothermic, therefore heat supply is required through the reaction. The reaction is usually carried out in the reaction conditions of high temperature (873 K) and atmospheric pressure (Stitt et al., 2001) in order to obtain conversion of commercial significance. In membrane reactor idea, as the reaction proceeds, the continuous removal of the product (usually hydrogen) from the reversible reaction system can allow the conversion to exceed thermodynamic limitations Bitter (1988). Based on this idea, much attention has been paid to the application of membrane reactors in dehydrogenation reactions (Zaspalis et al., 1991 and Gobina et al., 1995^{a, b}). Propane dehydrogenation via selective removal of hydrogen is one of the typical applications of a membrane reactor. A number of researchers have studied this reaction using various types of membrane materials and catalysts.

Schafer et. al., (2003) dehydrogenated propane in a low flux silica membrane (H_2 permeance of $2.6 \text{ m}^3/\text{m}^2 \cdot \text{h} \cdot \text{bar}$ with a selectivity of 13 for H_2/N_2 and 25 for H_2/C_3H_8) and a high flux silica membrane (H_2 permeance of $10.0 \text{ m}^3/\text{m}^2 \cdot \text{h} \cdot \text{bar}$) with a selectivity of 12 for H_2/N_2 and 17 for H_2/C_3H_8). They investigated the performance of two different types of catalysts, chromia / alumina (Cr_2O_3 / Al_2O_3) and platinum-tin / alumina ($Pt-Sn / Al_2O_3$) at temperatures ranging between 500 to 535 °C. The authors found that the propane conversion in the membrane reactor is 12% higher than in the conventional fixed bed.

Chang et al., (2002) studied propane dehydrogenation with $Pt-K-Sn / \gamma-Al_2O_3$ catalyst coupled to an electroless plated Pd-alumina composite membrane. In their study, propane conversion was reported to be above the equilibrium value between the temperatures of 350 to 500 °C. At 500 °C, propane conversion was evaluated to be about 52 % (equilibrium value of about 18 % at this temperature). Furthermore, the selectivity of propane dehydrogenation reaction was evaluated to be more than 90 % at 550 °C.

Propane dehydrogenation was also studied by Quicker et. al. (2000) using commercial $Pt-Sn / alumina$ catalyst and electroless plated Pd-steel and Pd-alumina membranes. Both membrane reactor systems were reported to provide higher

conversions than conventional packed bed catalytic reactor systems. Propylene yield is observed to be 26.1 % using Pd-alumina membrane and was evaluated to be about 4 % higher than that achieved using a packed bed reactor system at 500 °C. The hydrogen yield is observed to be 34 % for Pd-alumina membrane reactor and 39 % for Pd-steel membrane reactor. For both membrane reactors, propylene selectivity was observed to be slightly low due to the formation of by products.

Weyten et al., (2000) studied membrane catalysis for propane dehydrogenation using palladium – silver and silica-alumina composite membranes. Higher propylene yield was evaluated for Pd-Ag membrane compared to the silica composite membrane. The yield was observed to decrease with an increase in weight hour space velocity (WHSV) and feed flow rate. For both membranes reactor systems (Pd-Ag & silica), selectivity achieved for the membrane reactor was evaluated to be higher than that of the conventional packed bed reactor under the same conditions. The catalyst used by the authors is the chromia / alumina ($\text{Cr}_2\text{O}_3 / \gamma\text{-Al}_2\text{O}_3$) catalyst with surface area of about 80 - 90 m^2/g . At 500 °C, the deactivation of the catalyst was relatively slow and propane conversion gradually decreases after 7 hours. After 30 hours, propane conversion decreased to about half the original value. This was attributed to coke formation on the catalyst surface. Catalyst regeneration of the deactivated catalyst was performed by passing 96 % N_2 and 4 % O_2 at 500 °C for about 12 hours, followed by passage of pure H_2 for 1 hour for reactivation.

Yildirim et. al., (1997) studied propane dehydrogenation reaction using different membrane types, dense Pd-Ag membrane, silica modified metal impregnated membrane and metal sputtered porous membranes. They employed two types of commercial catalysts (0.5 wt % Pd - alumina and 0.5 wt % Pt - alumina cylindrical pellets with 3.4 mm diameter and 3.6 mm long) for their membrane reactor studies. The catalyst pellets were packed into a membrane tube and the surface area obtained was about 24.7 cm^2/g of catalyst. The authors concluded that the Pd-Ag membrane provided best values of propane conversion and was observed to be 4 times higher than the equilibrium conversion at 400 °C.

Weyten et. al., (1997) investigated propane dehydrogenation using silica composite alumina membrane with hydrogen permeance of $15 - 135 \times 10^{-9} \text{ mol}/\text{m}^2 \cdot \text{s} \cdot \text{Pa}$. at temperatures above 500 °C. The membrane was loaded with chromia-alumina

catalyst and nitrogen was used as sweep gas. Pure propane is fed to the tube side of the membrane reactor. The propane conversion was evaluated to be about 23.8 % at WHSV of 0.16/h at 500 °C, which is higher than the corresponding equilibrium conversion. The selectivity of propane dehydrogenation reaction scheme was evaluated to be about 89 %. However, propylene yield decreased from a value of 50 to 20 at higher values of WHSV (0.75/h). Three different commercial catalysts namely chromia / alumina ($\text{Cr}_2\text{O}_3 / \text{Al}_2\text{O}_3$), ($\text{Cr}_2\text{O}_3 / \text{Al}_2\text{O}_3$) containing a potassium (K) promoter and ($\text{Cr}_2\text{O}_3 / \text{Al}_2\text{O}_3$) containing cesium (Cs) and zirconium (Zr) have been used and tested for this reaction and the support material for all these catalysts is $\gamma\text{-Al}_2\text{O}_3$. At 600 °C, coke formation is significant and it caused serious catalyst deactivation. At WHSV of 0.25/h (mass [g] of feed gas per hour per gram of catalyst), the equilibrium conversion at 500 °C was about 18 % using membrane reactor, which is identical with the value of equilibrium conversion at the same temperature using conventional reactor.

Sheintuch and Dessau (1996) studied propane dehydrogenation using commercial palladium-silver (25 % Ag) membrane tubes and palladium-ruthenium (2 % Ru) membranes tubes loaded with 0.52 wt % platinum catalyst. During their investigation, the shell side was swept by nitrogen or nitrogen-hydrogen gas mixture. Propylene yields of about 70 % at 550 °C (23 % at equilibrium) were reported using the membrane reactor system. However, propylene yield was observed to decrease with time for experimental runs taken using Pd-Ag membrane at 525 °C. This was attributed to both membrane deactivation and catalyst deactivation.

Collins et al., (1996) investigated the membrane reactor performance at space velocities similar to those used in conventional reactor using silica composite membranes prepared from polymeric silica sols. The silica layer was deposited on the inner surface of the ceramic support tube by dip-coating process. The composite membrane was then dried and calcined at 873 K. The composite membrane was observed to have H_2 permeance of $5 - 10 \times 10^{-7} \text{ mol/m}^2 \cdot \text{s} \cdot \text{Pa}$ for a corresponding H_2/N_2 selectivity of about 10 – 19 at 773 K. This combination of permeability and selectivity was evaluated to be lower than that available for palladium composite membrane. The authors concluded that the selectivity of the silica based membrane

needs to be improved without reducing the hydrogen permeance and the problem of the Pd based membrane stability is a serious limitation.

Ziaka et. al., (1993) studied membrane reactor for propane dehydrogenation using 5 % Pt - γ Al₂O₃ catalyst loaded in commercial multilayered composite porous alumina tubes. These tubes consisted of three layers with nominal pore diameters of 40 angstrom (Å), 2000 Å and 8000Å, supported on a macroporous layer with pore diameter of 15 μ m. Permeances of hydrogen, propane, propylene and argon of the commercial composite membrane were found to be constant over a wide range of transmembrane pressure. Therefore, the flow mechanism was confirmed to be dominated by Knudsen mechanism. The feed reaction mixture contained hydrogen in order to reduce coking effect. During the experiments, the tube pressure was maintained at 2-3 pound square inch (psi) while the shell pressure was varied between 0-1 psi for a gas residence time of about 2 seconds. For a feed mixture of propane to hydrogen with 4:1 molar ratio, the propylene yield was observed to be 26 % (with 90 % selectivity) at 560°C.

Table 2.2 summarises experimental membrane reactor and catalysis studies performed for propane dehydrogenation.

Membrane	Catalyst	Temp. °C	Reference	Performance
Al ₂ O ₃	5 % Pt - γ Al ₂ O ₃	560	Ziaka et. al. (1993)	26 % Conversion
Pd - Ag tube	0.52 % Pt	530	Sheintuch and Dessau (1996)	70% conversion
Dense Pd - Ag Silica porous Sputtered Pd - porous	0.5 wt % Pt / Al ₂ O ₃ 0.5 wt. % Pd / Al ₂ O ₃	400	Yildirim et. al. (1997)	Four fold increase in conversion with Pd-Ag
SiO ₂ / Al ₂ O ₃	Cr ₂ O ₃ / Al ₂ O ₃ Cr ₂ O ₃ - K / Al ₂ O ₃ Cr ₂ O ₃ - Cs-Zr / Al ₂ O ₃	450	Weyten et. al. (1997).	34 % higher conversion from reactor
Pd - Stainless steel Pd - Al ₂ O ₃	Pt - Al ₂ O ₃	400	Quicker et. al. (2000)	Propylene yield 26.1
Pd - Al ₂ O ₃	Pt - Sn - K / Al ₂ O ₃	500	Chang et. al. (2002)	52 % conversion

Table 2.2: Summary of membrane reactor studied for propane dehydrogenation.

2.4. Hydrogen Separation and Purification membranes

Preparation of membranes for hydrogen separation and purification purposes is one of the key techniques for efficient hydrogen production. Different membranes such as silica and palladium and its alloy composites have been prepared and extensively studied. Hwang et al., (2003) used two different alumina tubes to fabricate silica composites. One was made of α -alumina with an average pore size of 100 nm where as the other was a three layer composite with a γ -alumina final layer of 10 nm average pore size. The chemical vapour deposition method was applied to prepare the silica composite membrane with tetraethoxysilane as silica source. The membrane prepared using γ -alumina exhibited a H_2/N_2 selectivity of about 7.5 – 63.7 at 600 °C and 3.8 for the membrane deposited on α -alumina support. Both membranes were studied for hydrogen separation from $H_2 - H_2O - HI$ gaseous mixture. After one day exposure to the $H_2 - H_2O - HI$ mixture, it was shown that the H_2 permeance remained the same.

An α -alumina support tube with 200 nm pore size was used by Rouessac et al., (2003) to fabricated silica composite membrane with deposition on the inner surface using plasma enhanced CVD. The membrane was reported to provide good thermal stability at up to 500 °C under inert atmosphere. While surface characterization is performed, the researchers did not perform flux characterisation studies. Silica membrane prepared with TEOS using a support of α -alumina with pore size of 1000 nm, high H_2 permeance of about $1.3 \times 10^{-6} \text{ mol/m}^2 \cdot \text{s} \cdot \text{Pa}$ at 300 °C was reported by Asaeda and Yamasaki (2001). The membrane was prepared by deposition a silica layer using of hot coating technique by the sol-gel method. The thickness of the separation layer is about 1 μm . The composite provided permeance ratios of 150 for H_2/CH_4 , 1100 for H_2/C_2H_6 and 6300 for H_2/C_3H_8 at the same temperature.

Porous Vycor glass support was used by Prabhu and Oyama (2000) to modify the support surface using high temperature CVD with TEOS. These membranes termed as nanosil provided hydrogen permeance of $1.5 \times 10^{-8} \text{ mol/m}^2 \cdot \text{s} \cdot \text{Pa}$ and high hydrogen selectivities (100%) with respect to CH_4 , CO , CO_2 and H_2O at 600 °C. Another silica membrane referred as nanosil with high hydrogen selectivity was prepared by Lee and Oyama (2002) on a porous vycor galss support (4 nm pore size)

using CVD as the preparation method. The membrane was fabricated by deposition of thin silica layer from TEOS at 873K in an argon stream. The composite membrane exhibited a permeance of 10^{-8} mol/m².s.Pa for the small gas molecules such as hydrogen at 873 K with a corresponding H₂/CH₄ selectivity of 10000. However, the hydrogen permeance of this membrane was limited due to the low gas permeance of the Vycor support itself at high temperatures.

Hwang et al., (1999) prepared silica membranes using two supports of different size (100 nm and 10 nm). The hydrogen permeance is evaluated to be 6×10^{-9} mol/m².s.Pa and H₂/N₂ selectivity of about 160 for the 10 nm composite membrane at 600°C. Kusakabe et al., (1999) prepared porous silica membranes using sol-gel technique on a tube whose skin layer is γ -alumina using sols prepared from TEOS. The composite membrane exhibited a hydrogen permeance of 10^{-7} mol/m².s.Pa and H₂/N₂ selectivity of about 100.

Silica layer deposited from silicon tetra-acetate as precursor on the top of mesoporous γ -alumina layer was carried out by Nijmeijer et al., (1998) using low – temperature chemical vapor infiltration. For this composite membrane, H₂/N₂ membrane selectivity higher than 40 and a hydrogen permeance of about 4×10^{-7} mol/m².s.Pa at 250 °C were reported. At higher temperature (400 °C), the similar hydrogen permeance (4×10^{-7} mol/m².s.Pa) was reported by Sea et al., (1998). The authors prepared their membrane using α -alumina porous tubular support with pore size of 110 – 180 nm following CVD method. The silica composite membrane prepared exhibited hydrogen / nitrogen separation factor close to Knudsen diffusion mechanism (3.74).

Morooka et al., (1996) produced silica composite membranes for hydrogen separation at high temperature by plugging 150 nm sized pores of the α -alumina support using TEOS as silica source following CVD process. The membrane separation characteristics were studied over a temperature of about 600 °C and good H₂/N₂ selectivities (100 - 600) and hydrogen permeance (about 10^{-8} mol/m².s.Pa) were reported. However, hydrogen permeance is reported to have decreased after operation for one day.

Sea et al., (1996) used TEOS for hydrogen selective silica composite membrane preparation for the application of hydrogen recovery at elevated temperature from a gaseous mixture containing steam. The composite membrane is prepared by depositing silica in two different pore size tubes using CVD method. These include macroporous α -alumina support (110-180 nm) and a mesoporous γ -alumina intermediate layer coated on the α -alumina tube (pore size = 160 nm). The silica membrane that produced in γ -alumina intermediate layer which coated on the α -alumina support resulted in hydrogen permeance of 3×10^{-7} mol/m².s.Pa at 600 °C. The membrane that was produced directly on α -alumina support offered a hydrogen permeance of 3×10^{-8} mol/m².s.Pa which is one order of magnitude lower than that of a membrane produced on the porous support with γ -alumina surface. For these membranes, very high selectivity for hydrogen with respect to nitrogen (H_2/N_2 100 – 1000) was reported and the activation energy of hydrogen permeation was evaluated to be 11 – 14 kJ/mol.

Jiang et al., (1995) prepared a silica modified membrane with H_2 permeance (4×10^{-8} mol/m².s.Pa) with H_2/N_2 selectivity at 600 °C as high as 1000. Prior to the silica deposition, the authors initially introduced temporary carbon barriers onto the porous structure of a vycor glass support (160nm pore size). Later, silica was deposited using CVD with $SiCl_4$ and H_2O and finally the carbon barriers are removed by oxidation.

De Lange et. al., (1995^{a,b,c}) prepared microporous silica membranes using sol-gel/dip-coating method. The authors initially deposited 7 – 10 μ m thick γ - Al_2O_3 layer on an α -alumina porous support (pore size of 160 nm) using bohemite sol. Later, silica is deposited by the acid catalysed hydrolysis of TEOS in ethanol. The permeation mechanism of H_2 and CO_2 was reported to be activated with activation energy of 13-15 and 5-6 kJ/mol for H_2 and CO_2 respectively. Since the deposited silica layer was of low thickness (due to γ - Al_2O_3 layer deposited initially), good permeance were reported (in order of 10^{-7} mol/m².s.Pa) and separation factors for H_2/CH_4 was evaluated to be 40 at 200 °C.

Chemical vapor deposition was carried out by Wu et. al., (1994) for preparing silica composite membranes on 4 nm pore size γ -alumina tubular supports. The H_2

permeance reported was 2×10^{-6} mol/m².s.Pa for a corresponding H₂/N₂ selectivity of 12.6 – 72 at 600 °C. Membranes with high H₂/N₂ selectivity of about 500 – 1000 were reported by Gavalas et. al. (1989, 1991, 1992, and 1993). The authors narrowed surface pores of a vycor glass tube with amorphous silica by CVD method. Hydrogen permeance was reported for the membrane to be 10^{-8} mol/m².s.Pa at 600 °C. They reported that the composite membranes exhibited good mechanical stability when silica was deposited inside the pores of the support skin layer. However, when silica was deposited on the outer surface of a porous skin layer, thermal stresses led to the formation of cracks.

2.5. Modelling and Simulation

Modelling and simulation can be considered as an important tool for various parametric studies allowing flexibility to determine values suited for specific applications. Many simulation models have been developed for the analysis of membrane reactor configurations. Most of these models are concerned with equilibrium-limited reactions since these systems have been mostly studied experimentally and confirmed that membrane reactor is effective to provide higher conversion than the conventional packed bed reactor.

A design guide has been developed and presented for the study of catalytic membrane reactor (Moon and Park, 2000). For dehydrogenation reactions, the most commonly used model is one dimensional axial model that accounts for the variation of system variables (flow rates, pressure etc) with respect to the length of the membrane reactor (Gokhale et. al., 1995). However, many simplistic assumptions have been considered. Such conditions include isothermal and isobaric assumptions. Whilst radial dispersion effects can be neglected for a combination of porous membranes and catalysts with higher dimensions, negating the effects of heat balances would have a serious limitation in the calculation procedures, thus overestimating the conversion.

To date, several publications have considered the development of models for gaseous hydrocarbon hydrogenation, dehydrogenation and decomposition reactions using membrane reactors. Barbieri et. al., (2002) developed a non-isothermal one dimensional mathematical model for microporous membrane reactors for CO₂ hydrogenation to produce methanol using zeolite membranes. The model considers assumptions such as plug flow, isobaric conditions on both sides (reaction and permeation) and the gas flux assumed as a linear function of the gases partial pressure. Their model involved also the enthalpy variation due to the mixing gases in the permeation side as well as the conductive heat transfer. The effect of temperature range between 150 to 300 °C at different operating pressure (1 – 100 bar) and gas permeation on the conversion, selectivity and yield were analyzed for traditional reactor and membrane reactor. The authors found that, the conversion difference between the traditional reactor and membrane reactor is higher at low temperature.

This was attributed to the higher methanol partial pressure on the reaction side. They also showed that the membrane reactor performance depends on many factors such as membrane properties, kinetics, flow conditions and heat exchange.

The catalytic decomposition of hydrogen iodide (HI) using silica membrane exhibited a selectivity of 650 for hydrogen was investigated theoretically by Hwang and Onuki (2001) in a membrane reactor for the hydrogen production. For this case, the authors chose isothermal operation, constant pressure, constant permselectivity and no reaction in the permeation zone assumptions. They evaluate the effect of the H_2 /HI selectivity on membrane reactor performance and conversion. Chan et. al., (2000) theoretically studied the H_2S decomposition in a membrane reactor. A mathematical model assuming plug flow and non-isothermal was developed. H_2S in the feed side was diluted with an inert gas and a sweep gas was introduced to the permeate side. In their approach, the conversion of the reactant was quantified in terms of Reynolds numbers in the tube and shell.

Prabhu et al., (2000) developed a one dimensional mathematical model to simulate methane reforming reaction for the study of three reactor systems including fixed bed reactor, partially selective (Vycor glass membrane) membrane reactor and a totally selective (Nanosil) membrane reactor. The authors have used annular membrane reactor configuration (the catalyst bed held in the shell side) for their analysis. Results from simulation analysis have indicated that there was a good agreement between the model and experimental results for all three reactor systems.

Koukou et al., (1997) developed a mathematical model for a non-isothermal packed bed membrane reactor consisting of a set of partial differential equations coupled with the appropriate initial and boundary conditions. The chosen reaction scheme was cyclohexane dehydrogenation that was assumed to have been carried out in a packed bed reactor enclosed with a microporous composite membrane that is selective towards hydrogen. Results from simulation analysis were concluded by noting that the assumption of isothermal conditions or the absent of certain thermal phenomena that take place in the membrane reactor system would involve significant overestimation of temperature predicted and hence membrane conversion.

Hermann et al., (1997) developed a one dimensional simulation model for ethylbenzene dehydrogenation reaction using palladium membrane reactor. The authors have considered different mass transport mechanisms in different layers of the composite membrane. The results obtained indicate that the benefits of the membrane with respect to ethylbenzene conversion and styrene selectivity depend on the catalyst activity. At 620⁰C the model predicted about 30% increase of ethylbenzene conversion can be achieved under isothermal conditions and high retentate pressure. They also observed that the increase of conversion in the membrane reactor is not accompanied by a significant loss of styrene selectivity.

Dehydrogenation of methyle-cyclohexane to toluene was simulated by Assabumrungrat and White (1996) using alumina composite membrane and pt / Al₂O₃ catalyst. The maximum conversion that the membrane reactor can achieved using various membrane diameters was studied. They conclude that the smaller the reactor diameter, the less catalyst is required for a given conversion. In the mean time, total conversion can be enhanced using larger diameter reactors.

Gobina et al., (1995) developed a two dimensional model accounting for radial and axial gradients in a catalytic membrane reactor. The reaction scheme investigated was ethane dehydrogenation. The two dimensional model consisting of partial differential equations was solved using orthogonal collocation method to obtain concentration profiles as a function of system variables namely contact time, reactor length and radius. The simulation analysis provided good insight in to the modelling approach. Radial concentration profiles have indicated that radial dispersion is insignificant and an axial model consisting of ordinary differential equations is sufficient enough to analyze the performance of the membrane reactor for a dehydrogenation reaction.

Gokhale et al., (1995) studied the effect of reactant permeation rate, membrane selectivity for hydrogen, feed composition and reactant space times on the conversion. The model consisting of mass balance was performed for an isothermal dehydrogenation of isobutane in a co-current flow using tubular membrane reactor. A one dimensional model was used for their simulation analysis. The authors have quantified their simulation results with respect to two dimensionless numbers namely Damkohler number (the ratio of maximum reaction rate to inlet reactant flow rate)

and permeation number (the ratio of maximum reactant permeation rate to inlet reactant flow rate). Becker et al., (1993) formulated a two dimensional model for ethylbenzene dehydrogenation in a catalytic membrane reactor. The mathematical model was used to simulate a tubular membrane reactor in which the catalyst was placed in the tube. The simulation study has presented an analysis of coupled mass transfer with chemical reaction in the membrane reactor.

Itoh, (1990) used palladium membrane to study the concept of bifunctional membrane reactor by coupling dehydrogenation and oxidation reactions under isothermal and adiabatic conditions. The reaction occurs on the two sides of the palladium membrane separately but simultaneously. Under an isothermal condition, the dehydrogenation reaction taking place in a catalyst packed bed was enhanced owing to continuous removal of the hydrogen that was produced in the reaction zone and permeated through the membrane. It was concluded that the amount of hydrogen removable was remarkably increased by the subsequent oxidation of hydrogen on the palladium surface of the permeation side. In addition to such effects, it was shown by the adiabatic model that transfer of heat by oxidation to the dehydrogenation side across the membrane can lead to further enhancement of dehydrogenation.

The dehydrogenation of cyclohexane in a porous Vycor glass tube using Pd-Al₂O₃ and Pt-Al₂O₃ was simulated by Itoh et al., (1985). They investigated the effects of different parameters such as pore size, pore volume and membrane thickness on the conversion. They found that the rate of gas permeation through porous Vycor glass depends mainly on thickness of the membrane and pore size. The authors have found that there is an optimum relationship between the rates of reaction and permeation and to the selectivity for which the conversion is at a maximum. In the theoretical study, higher conversion (58%) than that achieved for equilibrium conditions (28%) was obtained at temperature of 483K. Itoh et al., (1984) reported simulation results of membrane that exhibit Knudsen diffusion transport mechanism for hydrogen iodide (HI) decomposition using membrane reactor. They concluded that the hydrogen yield can be increased twice compared to the equilibrium yield. They found that under the given permeation and reaction rates, there is a maximum conversion due to the permeation of both products and reactant.

2.6. Conclusions

A number of experimental investigations have been made for the preparation and characterisation of porous silica membranes for hydrogen reaction, separation and purification. In these publications, sol-gel and chemical vapor deposition are the main methods that have been employed to prepare composites. Mainly TEOS had been used as the source of the silica membrane material and the hydrogen permeance varied from 10^{-6} to 10^{-9} mol/m².s.Pa for a corresponding H₂/N₂ selectivity varying from 10 to 1000.

The most striking advantage of the chemical vapour deposition method is that it can provide a membrane with a deposition carried out only once opposed to the sol-gel process (number of deposition). However, it should also be noted that the investment for CVD is very high when compared to sol-gel method. This is due to the fact that for CVD much equipment is desired and complex process is involved to carry out the deposition process.

Almost all the researchers mentioned above have used expensive membrane supports of asymmetric nature (several layers) and present a skin layer with lower pore size such as γ -alumina as intermediate layer for silica film deposition. Even though these supports may provide good membrane properties, the cost of the asymmetric membrane with lower pore size (3-10 nm) of the skin layer would be higher than a support of higher pore size and symmetric nature.

The propane dehydrogenation reaction usually demands operation at high temperature and low pressure which enhance equilibrium conversion. However, both these conditions cause catalyst deactivation and coking problem and hence regeneration of catalytic bed is inevitable. In this regard, catalyst regeneration is reported to be not economic (Schafer et al., 2003). Therefore, a number of alternative procedures have been suggested of which membrane assisted reactor system is promising. In such a system, selective removal of hydrogen from the reaction zone via the hydrogen selective membrane would enable enhancing conversions above equilibrium. Therefore, if a membrane reactor system is employed, lower temperature can still provide good equilibrium conversion and reduce coking problem.

Membrane reactor for propane dehydrogenation involved the utilisation of different types of catalysts (such as Pt - alumina, Pd – alumina and chromia – alumina) and membranes (Pd-Ag dense membrane, Pd-Ruthenium dense membrane and silica composite membranes). The operation of membrane reactor system for experimental runs was conducted within the temperature range of 450 – 600 °C.

Improvements in catalyst performance (stability and activity for prolonged catalysis) coupled with improvements in membrane technology (thermal, chemical stability as well as consistent performance of inorganic composites at higher temperatures) are required to stabilize membrane reactor technology for industrial propylene production processes. Such improvements have significant impact on the cost reduction of propylene produced per unit propane fed to the industrial process system.

Modelling of membrane reactors with different reaction schemes has achieved good attention and provided design rules for catalytic membrane reactors. In general, these models represent one-dimensional model involving the variation of flow rates and pressure with respect to the membrane reactor length for isothermal and isobaric conditions. In addition, the development of a mathematical model for the simulation of catalytic membrane reactor with simultaneous heat and mass balances was also reported and various operating conditions such as adiabatic and non-adiabatic were studied.

The conversion attainable with a tubular membrane reactor (the catalyst backed in the membrane tube) can be lower than the corresponding annular membrane reactor (the catalyst backed in the shell space) operated at the same conditions. This is attributed to the lower value of the gas film heat transfer coefficient ($2 - 5 \text{ W/m}^2\cdot\text{K}$) that would involve significant gas film resistance in the case of a tubular membrane reactor.

Chapter 3:

APPLICABLE THEORY

3.1. Introduction

This chapter presents relevant theory applicable to the experimental investigations performed in this work for the development of silica composite membranes towards hydrogen reaction, separation and purification. The theory in general relates to the properties, preparation and characterization of membranes coupled with transport phenomena for pure and binary mixture gaseous systems.

3.2. General Background

3.2.1. Porosity and permeability

There are two essential properties for the flow of fluids through any porous media such as membranes. The first is porosity (ϕ), which is defined as the ratio of the pore volume (V_p) to the bulk volume (V_b) and is commonly expressed as a percentage fraction.

$$\phi = \frac{V_p}{V_b} \times 100 \quad \text{Eq. (3.1)}$$

The value of porosity is usually distinguished as being either absolute (total) or effective. The absolute porosity can be defined as the ratio of total of pore volume to bulk volume regardless of whether or not all of the pores are interconnected. The effective porosity is the ratio of the interconnected pore volume to the total bulk volume. It is commonly less than the absolute porosity (Collins, 1961).

Secondly, the membrane must have continuity of pore spaces to permit fluids to flow. This is called permeability, which can be defined as a property of the porous

media which measures the ability to pass a fluid through its interconnected pore network (De Wiest, 1969).

The permeability can be obtained by measuring the gas flow rate through a membrane under a total gas pressure gradient using the following equation:

$$Perm = \frac{ql}{A \Delta P} \quad \text{Eq. (3.2)}$$

Where: $Perm$ = permeability of the porous medium, (mol.m /m².s. pa)

q = molar flow rate, (mol/s)

l = thickness, m

A = area of porous medium, m²

ΔP = pressure gradient across the membrane, pas

Permeance is another common term used in membrane technology which can be calculated according to the following equation:

$$Per = \frac{q}{A\Delta P} \quad \text{Eq. (3.3)}$$

where: Per is permeance (mol/m².s.pa)

3.2.2. Wettability

Wettability (sometimes called energy of adhesion) is a measure of the capacity of a fluid to coat a solid surface for a wetting fluid; the contact angle is less than 90°. If the fluid spreads over the solid surface and preferentially wets the solid, then the fluid is termed as wetting phase and the contact angle approaches zero. In the case of non-wetting phase there is little or no affinity for the solid and the contact angle exceeds 90°. The rise or depression of liquids in fine bore tubes is a result of surface tension and wetting preference and is called capillary rise (or capillary depression).

3.3. Sol-Gel / Dip Coating Processes

Basically sol-gel is a process that involves the conversion of a colloidal or polymeric solution, called a sol to a gel. Usually, sols can be obtained by controlled acid hydrolysis of metal alkoxides or metal salts to form particulate or polymer sols. The gelation of these sols occurs by condensation reactions (Brinker and Scherer, 1990). These condensation reactions produce molecules with large molecular weight, which form a gel when they combine together. The morphology of the gel formed during the condensation of the sol has a direct relationship on the final properties of the gel (Sperling, 1992). Depending on the reaction conditions of the sol, the sol-gel process can be divided into two routes namely, the colloidal suspension route and the gel route as shown in Figure 3.1. In the colloidal suspension route a faster hydrolysis rate is obtained by adding excess water to the precursor. However, in the polymeric gel route, the hydrolysis rate is kept low by adding successively small amounts of water. As far as silica precursor is concerned, both colloidal and polymeric gel routes can be realized due to their versatile controllability.

In dip coating, the support is dipped into the solution containing the material that needs to be deposited for a considerable amount of time. The dip coating process comprises five different steps in sequence (Scriven, 1988), namely immersion, start-up, deposition, drainage and evaporation. The initial stages of dip coating occurs due to the capillary pressure on the support surface which causes the fluid consisting of the silica polymeric sols to be drawn into the porous support. However, during the final stages of the dip coating (when the support is withdrawn from the sol), further deposition occurs by the evaporation of the sol entrained in the support pores. This would lead to gelation. Finally, in drying step, the gel network would collapse by the prevalent capillary forces. The thickness of the coating is achieved using dip coating process is a function of withdrawal speed and the sol viscosity. Typical coating thickness can be varied from few nm up to 60 μm using dip coating technique (Hsieh, 1996). Figure 3.2 illustrates the dip coating process.

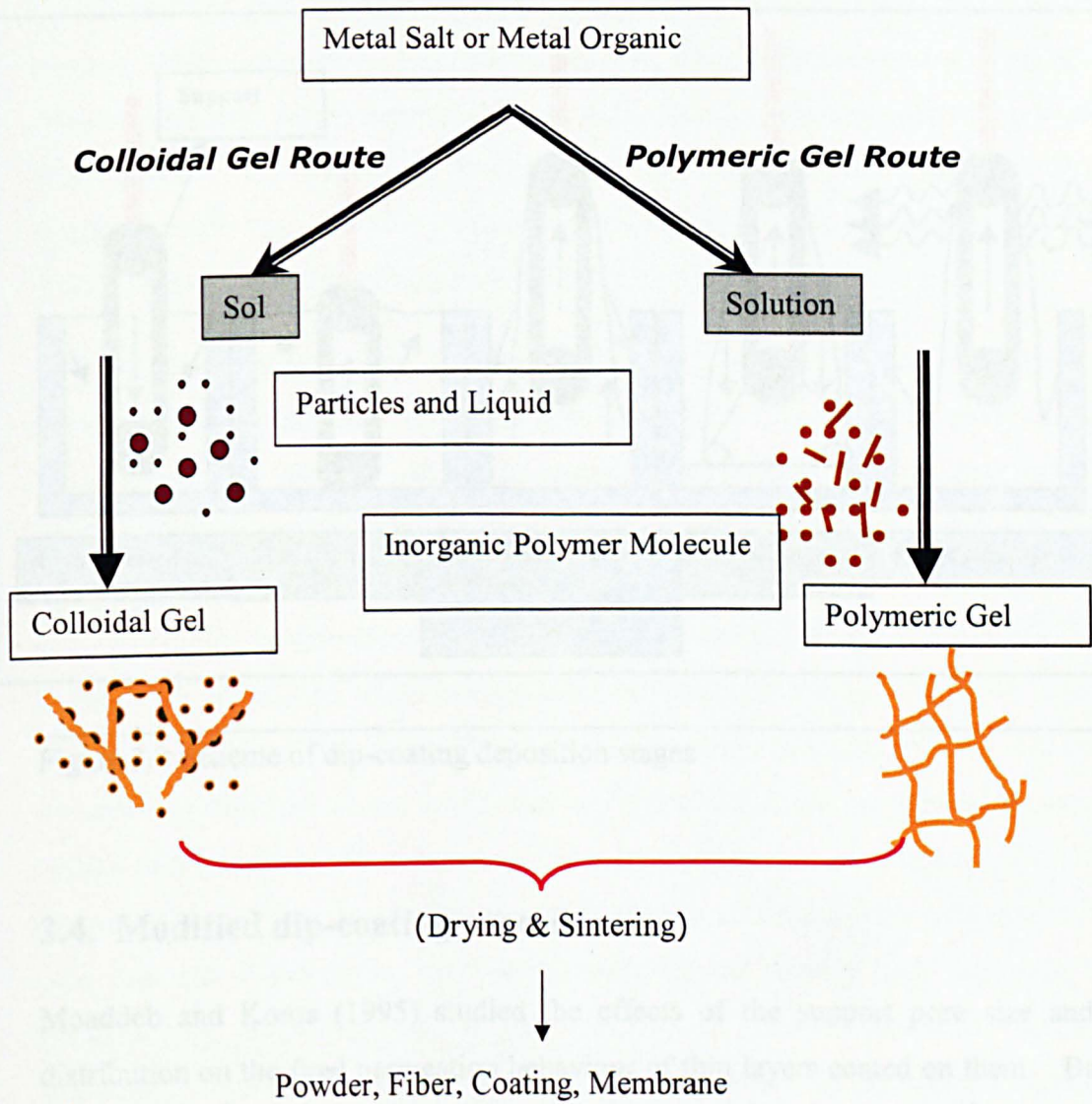


Figure 3.1 Scheme of sol-gel routes: Colloidal sol-gel route and polymeric gel route (Bhave, 1991)

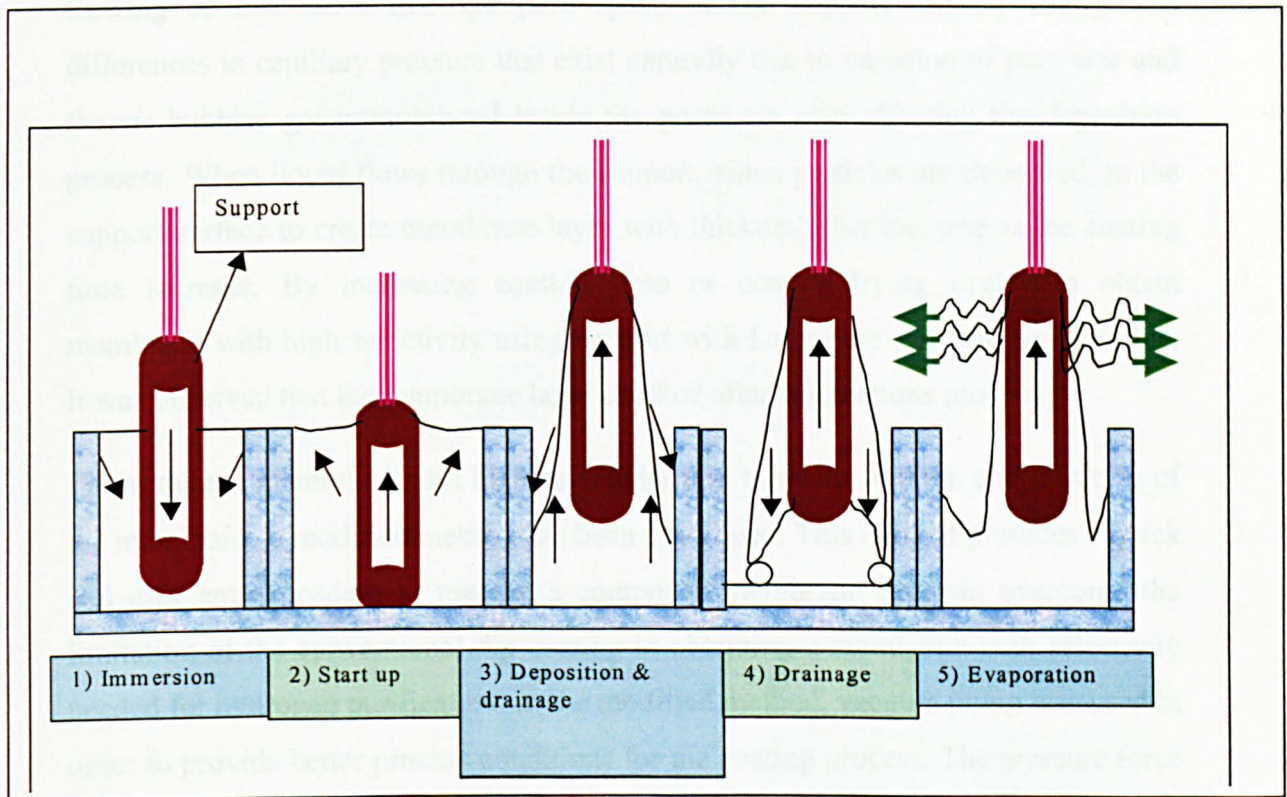


Figure 3.2 Scheme of dip-coating deposition stages

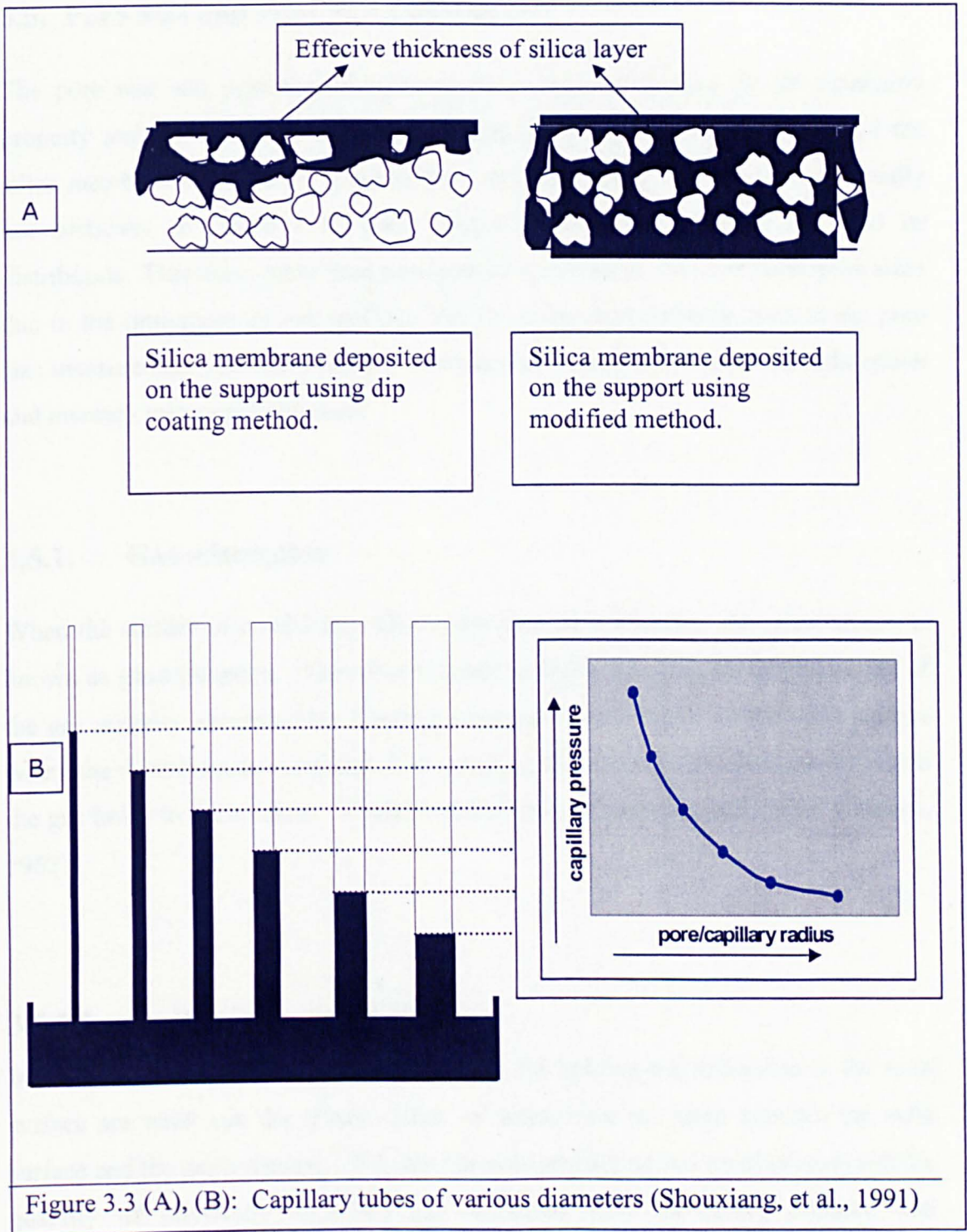
3.4. Modified dip-coating procedure

Moaddeb and Koros (1995) studied the effects of the support pore size and its distribution on the final permeation behaviour of thin layers coated on them. Based on their experimental observations, they have inferred that the use of large pore size supports could produce consistency problems. They have also concluded that the relative size of the precursors (used for deposition) and the pore size of the support are key factors in determining defect free deposition. According to them, defect free deposition is achievable when the pore size of the precursor is larger or of the same magnitude as the diameter of the pores of the support.

Under conventional dip coating technique in atmospheric condition, the preparation of silica composite membranes with high separation factor using support having large pores can not be achieved. In the dip coating process a capillary pressure drop

between the support pores and the liquid (silica solution in this case) control the flowing of this silica into the pore space of the support (Hsieh, 1996). The differences in capillary pressure that exist naturally due to variation of pore size and the air bubbles get immobilized inside the pores are also affecting the deposition process. When liquid flows through the support, silica particles are deposited on the support surface to create membrane layer with thickness that increase as the coating time increase. By increasing coating time or coating-drying cycles to obtain membrane with high selectivity using support with large pore size was not possible. It was observed that the membrane layer cracked after calcinations process.

To produce a membrane with high selectivity and to avoid fracture and cracking of the membrane, a modified method has been developed. This method provides a quick and efficient procedure to prepare a composite membrane that can overcome the limitation of the conventional dip coating in obtaining a membrane with selectivity needed for hydrogen purification. In the modified method, vacuum pump was used in order to provide better process conditions for the coating process. The pressure force in the form of suction allow the solution to penetrate through the pores leaving behind the silica particles that fill the pores and cover the support surface thereby overcoming capillary forces and removing immobilized air bubbles in the porous texture of the support. With this procedure, the coating time, the number of coating-drying-calcination steps needed for conventional dip coating and the preparation time were reduced. Furthermore, the membranes prepared provide high selectivity and produce pure hydrogen from a wide variety of gaseous mixtures containing hydrogen. The details with respect to the fabrication of the composite membrane with high separation factors for H_2/N_2 are presented below.



3.5. Pore Size and Pore Size Distribution

The pore size and pore size distribution has a major influence on the separation property and the behaviour of the membrane. To characterize the support and the silica membranes with wide range of pore sizes using one method alone is usually not sufficient to obtain a complete picture with respect to pore size and its distribution. Therefore, more than one method is needed to measure these pore sizes due to the limitations of any method. The most common methods used in the pore size measurement and characterization of the membranes are nitrogen gas adsorption and mercury injection techniques.

3.5.1. Gas adsorption

When the surface of a solid has affinity towards gas molecules, the phenomenon is known as gas adsorption. This phenomenon basically involves the determination of the gas quantity necessary for forming a monomolecular layer on the solid surface where the measurement is desired. Conceptually, there are two mechanisms by which the gas holds to the surface. These are physical and chemical adsorption (Osipow, 1962).

3.5.1.1. Physical adsorption:

In physical adsorption, the forces responsible for holding the molecules to the solid surface are weak van der Waals' forces of interaction that exist between the solid surface and the gas molecule. Usually physical adsorption is a rapid process and the quantity of physically adsorbed gas increases with increasing pressure and decreasing temperature.

3.5.1.2. Chemical adsorption:

During chemical adsorption or chemisorption, the adsorbed molecules get attached to the solid surface by fairly strong interaction between the gas molecule and solid

surface than that prevalent in physical adsorption. During chemical adsorption, the gas quantity adsorbed decreases as the temperature is decreased. Consequently the most adsorption measurements are carried out at low temperatures to ensure least chances exist for chemisorption to take place (Young and Crowell, 1962).

3.5.1.3. Nitrogen gas adsorption

The working principle behind nitrogen adsorption method is that the deviation in the atomic forces on the surface of a clean, evacuated solid attracts gas molecules. When these molecules collide with the surface, they either bounce off or adsorb to it. The time taken by the gas to adsorb on the surface depends on the molecular surface interaction during collision, physical and chemical nature of the sample, gas and temperature of the sample (Ruthven, 1984).

When molecules leave the bulk of the gas to adsorb onto the sample surface, the average number of gas molecules decrease and therefore the pressure decreases which is measured by a pressure transducer in the instrument. Therefore, based on the adsorption isotherm the Accelerated Surface Area and Porosimetry (ASAP) analysis instrument can provide pore size distribution ranging from 1.7 to 300 nanometer. In addition to the pore size, the equipment automatically calculates and provides Brunauer, Emmett and Teller (BET) surface area (Hsieh, 1996).

3.5.1.4. Surface area

The BET theory which is widely used for determining the surface area of solids is based on the determination of the amount of the adsorptive gas required to cover the external and the accessible internal pore surfaces of a solid with a complete monolayer of adsorbate. This monolayer capacity can be calculated from the adsorption isotherm by means of BET equation shown below (Everett and Ottewill, 1969):

$$\frac{P}{V(P_s - P)} = \frac{1}{V_m C} + \left(\frac{C-1}{V_m C} \right) \frac{P}{P_s} \quad \text{Eq. (3.4)}$$

Where:

C = dimensional constant related to the heat of adsorption.

P_s = saturation pressure of the gas.

V_m = volume of gas required to form a monolayer.

V = volume of gas adsorbed at pressure p .

From the plot of data for $\frac{P}{V(P_s - P)}$ versus $\frac{P}{P_s}$, the values of V_m and C may be obtained from the intercept and slop of which are $\frac{1}{V_m C}$ and $\frac{C-1}{V_m C}$ respectively.

The gases used as adsorptives have to be only physically adsorbed by weak bounds at the surface of the solid (Van der-Waals forces) and can be desorbed by a decrease of pressure at the same temperature. The most common gas is nitrogen at its boiling temperature (77.3 K). When very small surface area (below $1\text{m}^2/\text{g}$ need to be measured krypton at 77.3 K is recommended instead of nitrogen (Everett and Ottewill, 1969).

3.5.2. Mercury porosimetry

Compared to nitrogen gas adsorption, mercury porosimetry is based on simpler principle, is much faster and can produce a full pore size distribution data in less time. The other advantage of this method is that it can cover a very wide range of pore diameters, up to $360\ \mu\text{m}$, depending on the pressure used (Dullien, 1992). Since very high pressures are needed for pores in the nanometer range, Micromeritics Autopore II 9220 porosimeter which capable of intruding mercury with intrusion

pressures (by increasing pressure) up to about 414 Mega Pascal has been used for quantifying the pore size and pore size distributions.

Mercury porosimetry uses the capillary law governing liquid penetration into small pores. This law, in the case of a non-wetting phase is expressed by the Washburn equation (Eq. 3.5) (Dullien, 1992):

$$P = \frac{2\sigma \cos \theta}{r} \quad \text{Eq. (3.5)}$$

Where r is the pore radius in microns, σ the surface tension of mercury and θ is the contact angle of mercury in the membrane.

The volume of mercury penetrating the pores is measured directly as a function of applied pressure. This pressure-volume data serves as a unique characterization of pore structure. Due to the practical limitations on the maximum pressure than can be applied, the minimum pore size that can be measured using mercury porosimetry is in the range of 5 nm (Ruthven, 1984).

3.6. Separation of Gases and Transport Mechanisms

The concept of separating gases using membranes had been researched for more than 160 years. The first publication related to gas separation membrane is attributed to Mitchell and Graham (Osada and Nakagawa, 1992). Mitchell observed that natural rubber balloons filled with hydrogen gas descended after some time delay. He attributed this feature to the phenomenon of gas diffusion through the balloon wall. Later, Graham repeated Mitchell's experiments with films of natural rubber and made the first quantitative measurement of gas permeation rate.

3.6.1. Graham's law of diffusion

Thomas Graham in 1829 investigated the relative rates of diffusion of gases and discovered the quantitative law describing the permeation rates. He later postulated a statement termed as Graham's Law of diffusion: "the rate of diffusion of a gas is inversely proportional to the square root of the molecular weight or density of the gases."(Sturchio et al, 1966)

When gases are kept in a porous container, they have a tendency to diffuse out of the container due to diffusion phenomena. The kinetic energy of a molecule undergoing diffusion is proportional to the mass of the molecule and square of the velocity of the molecule. Therefore, if two different molecules have the same kinetic energy but different mass, the lighter molecule will move faster than the heavier molecule. Due to this reason, lighter molecules will diffuse more rapidly than heavier ones. In this regard, the controlled pore size and surface properties of the material primarily achieve diffusion. The same principle occurs in porous inorganic membranes.

3.6.2. Gas flow mechanisms in inorganic membranes

The transport of gases through porous membrane materials can occur by different mechanisms. These are viscous diffusion, Knudsen diffusion, surface diffusion, capillary condensation and molecular sieving (Hsieh, 1996). Figure 3.4 presents a schematic of the main different separation mechanisms.

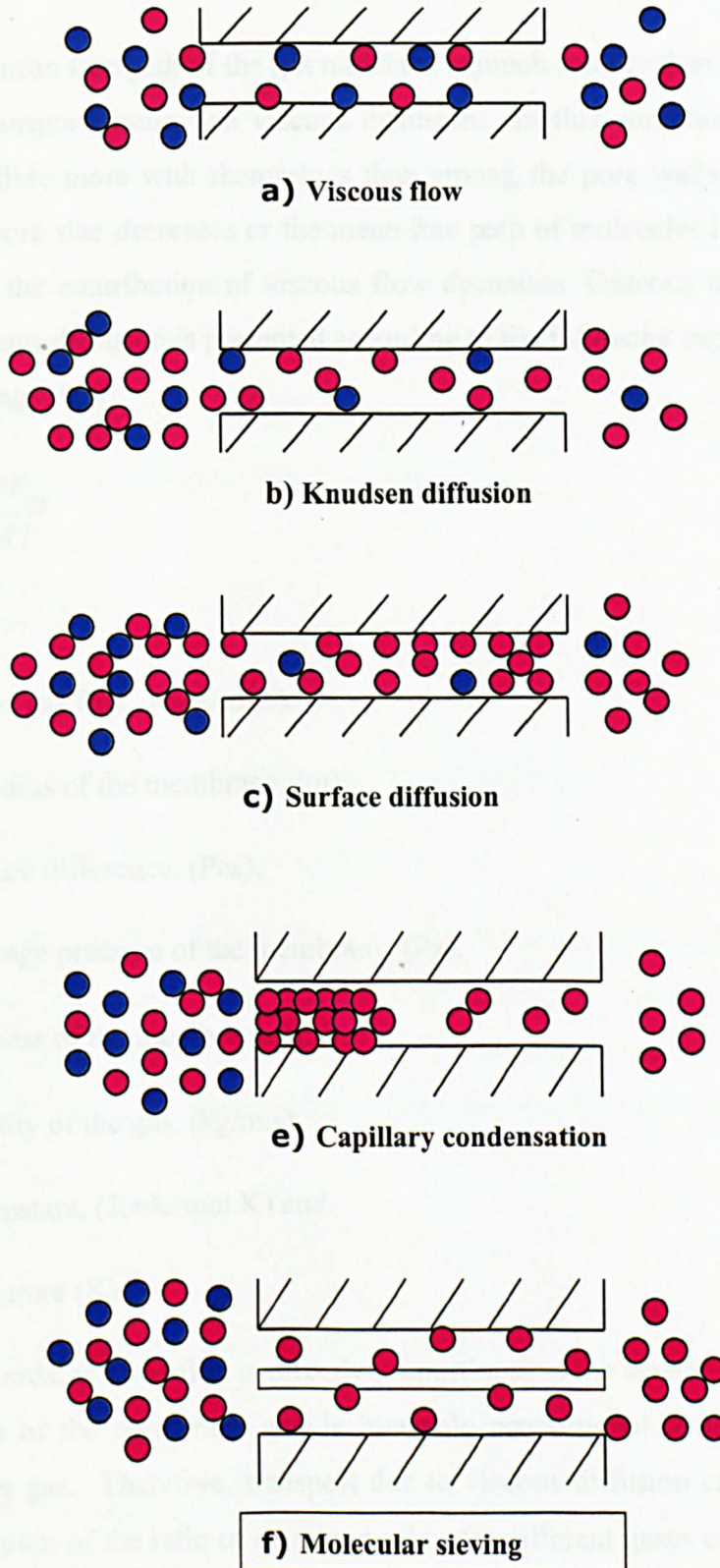


Figure 3.4: Mechanisms of transport through porous inorganic membranes (Hsieh, 1996)

3.6.2.1. Viscous diffusion

When the mean free path of the gas molecule is much smaller than the pore diameter, gaseous transport occurs via viscous diffusion. In this condition, the permeating species collide more with themselves than among the pore walls. In other words, when the pore size decreases or the mean free path of molecules increases (pressure decreases) the contribution of viscous flow decreases. Gaseous transport occurring due to viscous diffusion is presented according to the following expression (Beuscher and Gooding, 1998):

$$J_v = \frac{r_p^2 \Delta P P_{avg}}{8\delta\mu RT} \quad \text{Eq. (3.6)}$$

where:

J_v = viscous gas flux, (mol/m².s),

r_p = pore radius of the membrane, (m),

ΔP = pressure difference, (Pas),

P_{avg} = Average pressure of the membrane, (Pa),

δ = Thickness of the membrane, (m),

μ = Viscosity of the gas, (kg/m.s),

R = Gas constant, (Joule/mol.K) and

T = temperature (K).

In other words, viscous flux is directly proportional to the square of the average pore radius (r_p) of the membrane and is inversely proportional to the viscosity of the permeating gas. Therefore, transport due to viscous diffusion can be identified by the calculation of the ratio of membrane flux for different gases expressed as (Hsieh, 1996).

$$\frac{J_i}{J_j} = \frac{\mu_j}{\mu_i} \quad \text{Eq. (3.7)}$$

3.6.2.2. Knudsen diffusion

Knudsen flow occurs in the membrane pores when the mean free path of the gas molecule is large compared with the pore diameter. In this condition the gas molecule collision with the walls of the pores dominates the gas transport mechanism. In order to achieve pure Knudsen diffusion, the gas temperature must be high enough to avoid surface flow mechanism (>300 °C) and the pressure of the gas should be low enough (Mulder, 1996).

Gaseous flux that exists due to Knudsen diffusion is presented according to the following expression (Pandey and Chauhan, 2001):

$$J_K = \frac{8r_p \Delta P}{3\delta \sqrt{2\pi MRT}} \quad \text{Eq.(3.8)}$$

Where:

J_K = Knudsen gas flux through the membrane, (mol/m².s),

M = Molecular weight of the gas, (kg/mol),

Knudsen diffusive flux is directly proportional to the average pore radius of the membrane r_p and inversely proportional to the square root of the molar mass M of the permeating gas. Therefore, transport due to Knudsen diffusion can be identified by evaluating the ratio of membrane flux for different gases related as:

$$\frac{J_i}{J_j} = \sqrt{\frac{M_j}{M_i}} \quad \text{Eq. (3.9)}$$

J_i = flux permeating component i through the membrane, (mol/m².s)

J_j = flux permeating component j through the membrane, (mol/m².s)

M_i = Molecular weight of component i, (kg/mol)

M_j = Molecular weight of component j, (kg/mol)

Coupled Knudsen and viscous diffusion

Gas transport in porous membranes follows different mechanisms which can share the flow. In practical scenarios, two or more mechanisms can exist in one membrane and the contribution of each mechanism will be controlled by pore size and pore size distribution, gas molecular weight and the operated conditions (Beuscher and Gooding, 1998). For instance, viscous flow is a characteristic of materials with relatively large pores (i.e. > 50 nm), but for mesoporous range (2 – 50 nm), Knudsen flow is predominating. In the case where the flow follows a combination of both viscous and Knudsen diffusion mechanisms, the total flux is obtained by coupling equations 3.6 and 3.8 expressed as:

$$J_{tot} = \frac{8r_p \Delta P}{3\delta\sqrt{2\pi MRT}} + \frac{r_p^2 \Delta P P_{avg}}{8\delta\mu RT} \quad \text{Eq. (3. 10)}$$

The above equation can be expressed in terms of total permeability (perm) as:

$$Perm = \frac{J_{tot}\delta}{\Delta P} = K + VP_{avg} \quad \text{Eq. (3. 11)}$$

Where K and V represent Knudsen and Viscous permeability constant expressed as:

$$K = \frac{8r_p}{3\sqrt{2\pi MRT}} \quad \text{Eq. (3. 12)}$$

$$V = \frac{r_p^2}{8\mu RT} \quad \text{Eq. (3. 13)}$$

By plotting the permeability versus average pressure (P_{avg}) should result in straight line, the intercept and slop of which are (K) and (V) respectively. Based on these values, the approximate pore size of the membrane can be estimated using both the mechanisms applying the following equations (Burggraaf and Cot, 1996):

$$r_p = \frac{3\sqrt{2\pi MRT}}{8K} \quad \text{Eq. (3. 14)}$$

$$r_p = \sqrt{8\mu RTV} \quad \text{Eq. (3. 15)}$$

3.6.2.3. Surface diffusion

During surface diffusion, molecules interact, adsorb and diffuse in the membrane surface. A difference in surface occupation will occur if there is a pressure gradient. The transport gradient driving the surface flow is termed as the surface concentration gradient. The quantity (and hence concentration) of the species adsorbed on the membrane surface is dependent on the pressure, temperature and nature of the surface (Gilliland et al., 1974). The flux due to surface flow of permeating species is presented using the following expression (Bhave, 1991):

$$J_s = -A\rho_{app}D_s\mu_s \frac{dq}{dl} \quad \text{Eq. (3.16)}$$

Where A is the surface area, ρ_{app} is the apparent density (kg/mol), D_s is the surface diffusion coefficient (m^2/s), μ_s is the reciprocal tortuosity and the term dq/dl referred to the surface concentration gradient (mol/kg.m). It can be noted from the above equation that surface flux is directly proportional to the term dq/dl . When surface diffusion occurs, it is assumed generally that strongly adsorbed molecules are less mobile than weakly adsorbed molecules.

Surface diffusion can be easily identified with different gaseous species such as CO_2 by the deviation of the gaseous flux from Knudsen and viscous diffusion mechanisms. When surface diffusion prevails, a gas with a higher molecular weight (i.e. $\text{CO}_2 = 44$) can have a higher flux than a lighter one (i.e. $\text{N}_2 = 28$). Furthermore, it is very common that surface flux decreases with increasing temperature. The reason for this is due to the decrease in surface concentration at higher temperature due to lower adsorption capability of the membrane.

3.6.2.4. Capillary condensation

Capillary condensation usually occurs at low temperatures and high pressures. Under these conditions, certain permeating species strongly adhere at the pores of the membrane surface and pore blocking takes place. This is due to the condensation of one of the components due to strong capillary forces. The pore blocking with

permeating species is termed as capillary condensation. The transport of different species would then be controlled by the altered pore size of the membrane and surface concentration of the permeating species. Very high separation factors can be achieved with capillary condensation (Uhlhorn, et al. 1992).

3.6.2.5. Molecular sieving and Activated diffusion

Molecular sieving mechanism occur when the pore diameter of the membrane exactly allows a smaller molecule to pass through and a bigger molecule to be retained. Molecular sieving occurs with very small pore sizes ($r_p < 1$ nm). The membrane surface would work as a sieve to perform the separation and achieve higher separation factors in addition to that achieved with Knudsen and surface diffusion mechanism (Diniz da Costa et al., 2002).

The membrane flux is derived from fick's first law as (Bennett and Myers, 1962):

$$J = -D \frac{dc}{dx} \quad \text{Eq. (3.17)}$$

Where D is the gas diffusion coefficient, c is the concentration of molecules and x the coordinate along the permeate direction.

When the membrane flux increase with temperature the transport of the gas through the membrane named activated (de Lange et al, 1995^b). The temperature dependence of diffusivity is expressed as:

$$D = D_0 \exp\left(\frac{E_m}{RT}\right) \quad \text{Eq. (3.18)}$$

Where D_0 is the diffusion constant and E_m is the positive mobility energy and corresponds to the energy barrier between two adjacent sorption sites.

The concentrations of molecules on both sides of the membrane surface can be derived from equilibrium gas-membrane adsorption data. Such data is usually defined using Henry's law for lower concentrations.

$$c = KP \quad \text{Eq. (3.19)}$$

Where K is proportionality constant dependent on temperature expressed as (Diniz da Costa et al, 2000):

$$K = K_0 \exp\left(\frac{Q_{st}}{RT}\right) \quad \text{Eq. (3.20)}$$

Where Q_{st} is the heat of adsorption (J/mol), K_0 is a temperature independent proportionality. The final flux equation for membrane flux due to activated / adsorption diffusion presented by coupling the above set of equations to give the following expression:

$$J = -D_0 K_0 \exp\left(\frac{Q_{st} - E_m}{RT}\right) \frac{\Delta P}{\delta} \quad \text{Eq. (3.21)}$$

In the above equation, a new temperature independent proportionality constant is defined as $J_0 = D_0 K_0$ and effective activation energy for permeance:

$$E_a = E_m - Q_{st} \quad \text{Eq. (3.22)}$$

E_a is termed as effective activation energy. Therefore, positive values of E_a would exist when mobility energy E_m is higher than Q_{st} and negative values of E_a would exist for the opposite case. When the measured membrane flux corresponds to positive E_a then the process is termed as activated diffusion. On the other hand, if E_a is negative, then the process is called as adsorptive diffusion.

however, when the length of mean free path of gas molecules is still low, the membrane pore size becomes similar to the size to the diffusing molecule. Under these conditions, gas transport will follow activated diffusion mechanism. on the other hand, transport due to surface diffusion becomes predominant at pore radius values lower than 3nm, if the material exhibits a high surface area and if the gas molecules have specific adsorptive tendency on the membrane surface. Flux arising due to activated diffusion of permeated species can be expressed by the following equation:

$$J \frac{\delta}{\Delta P} = \frac{-D_0 K_0 \delta}{\Delta P} \exp\left(\frac{-E_a}{RT}\right) \quad \text{Eq. (3.23)}$$

The above equation is simplified to obtain the membrane permeability equation due to activated diffusion:

$$Perm = Perm_0 \exp\left(\frac{-E_a}{RT}\right) \quad \text{Eq. (3.24)}$$

This equation is used to obtain the activation energy of different permeating species across the composite membrane. A plot of natural logarithm of membrane permeability obtained from experimental study against $1/T$ yields the exponential of the y-intercept would provide pre-exponential factor P_0 . Similarly, the slope of the plot would provide the value of $-E_a/R$. Based on the sign of E_a the process is either termed activated diffusion (+ve) or absorptive diffusion (-ve).

3.6.3. Pure gas separation factor

The ratio of membrane permeance at same permeation pressure for different pure gases is termed as the pure gas separation factor. The pure gas separation factor achieved for inorganic composite membranes with the dominance of one of the above mechanisms is explained as follows. Dominance of Knudsen diffusion mechanism in the gaseous transport would allow the separation of lighter gases from heavier gases based on the difference in the molecular weight of the gases. Prominent example for consideration for silica composite membrane is the separation of hydrogen from propane, propylene and nitrogen, which are all heavier than hydrogen. Dominance of viscous diffusion mechanism would not offer significant values of separation factor due to insignificant differences in the values of gas viscosity. Separation factor achieved due to surface diffusion would be dominant at low temperatures and at high temperatures would be lowered. The presence of separation factors due to capillary condensation is neglected for high temperature inorganic membrane reaction and separation applications due to irrelevance in process conditions (low pressure and high temperature as opposed to high pressure and low temperature).

3.6.4. Binary mixture gas permeation

While pure gas permeation is effective in describing the mechanism of transport of gaseous molecules through the composite, it is not effective in providing the actual separation factor. Basic draw back in pure gas permeation is the lack of the presence of other components permeating through the membrane simultaneously.

When two or more components are fed to a membrane system, the component flux is obtained as a fraction of the total flux as

$$J_i = Jy_i \quad \text{Eq. (3.25)}$$

Where y_i refers to the composition of species i in the permeate stream.

The separation factor α for a binary mixture is expressed as

$$\alpha_{ji} = \left(\frac{y_i}{y_j} \right) \frac{x_j}{x_i} \quad \text{Eq. (3.26)}$$

It is very common in inorganic membrane literature that the pure gas separation factors are not the same as the mixed gas. This is because of different types of interactions that exist in a binary mixture and membrane material. Mixed gas separation factor higher than the corresponding pure gas separation factor evaluated as the ratio of corresponding flux of different gases have been reported (Hassan et al, 1995). For such a case, the more strongly interacting gas is supposed to saturate the surface and reduce the transport of the weakly interacting gases (Hassan et al., 1995). Gases that have strong adsorptive capability thereby preferentially occupy adsorption sites on the membrane surface that would prevent adsorption and surface diffusion of weakly adsorbed gas molecules. However in this case, the mixed gas separation factor would decrease and approach the pure gas separation factor when the temperature of the gas is increased. This is due to the fact that gas adsorption in porous media decreases drastically with an increase in the temperature due to the reduction in competitive adsorption effect at higher temperature for the strongly adsorbed gas.

The effect of concentration polarization in gas separation is low or can be neglected (Nobel and Stern, 1995). The back diffusion can effect on the actual separation factor especially when the flow rate through the membrane is high, which increase the permeate pressure due to the presence of large pores. This phenomenon occurs also if the permeate gas concentration in permeate side is higher than the feed side.

The pressure ratio effect on the actual separation factor can be represented by the following equation.

$$\alpha = 1 + \frac{(1 - P_r)(\alpha^* - 1)}{1 + P_r(1 - y)(\alpha^* - 1)} \quad \text{Eq. (3.27)}$$

Where P_r (pressure ratio) is defined as permeates pressure / feed pressure. It is clear from the above equation that the ratio pressure (P_r) should be low (i.e. ≈ 0).

Chapter 4:

EXPERIMENTAL APPARATUS AND PROCEDURE

4.1. Introduction

This chapter presents experimental materials, apparatus and procedure for the preparation, surface and flux characterisation of different silica composite membranes. The different membranes prepared in this work are silica membranes for hydrogen reaction, separation and purification and noble metal (Pd) impregnated γ -alumina membranes. The silica composite membranes are prepared using silicone elastomer as the silica precursor using dip coating technique with suitable modification (suction technique).

The next section summarises various equipment and materials used for membrane preparation. A detailed experimental procedure involved with the membrane fabrication followed by experimental rig also presented.

4.2. Preparation Equipments and Materials

4.2.1. Equipments

1. Magnetic stirrers with magnets pellets (Techne, MS1).
2. Test tube of 1000ml volume and perspex dip coating tank.
3. Vacuum pump (Edards, ECB1) for fluid circulation in suction technique.
4. Drier (Carbolite) 1 - 300 °C, type PF120(201).
5. Programmable furnace (Carbolite) 5 – 1050 °C, type RWF 11/23.
6. Scale (Sartorius, BL1500).
7. Class 100 clean room for membrane preparation.

4.2.2. Materials

1. 2-Methyl butane or Iso pentane (Fisher Scientific).
2. Silicone elastomer (Farnell).
3. Silicone curing agent (Farnell).
4. Acetone (Sigma Aldrich).
5. Aluminium monohydrate (Farnell).
6. PdCl₂ 99.9 % purity (Sigma Aldrich).

4.2.3. Porous support tubes

A porous α - alumina tube with a wash coat of titania in order to provide good catalytic properties (Figure 4.1) supplied by C.T.I. SA, France is used as the support to prepare various silica inorganic composites. The support had an outer diameter of 10 mm diameter and an inner diameter of 7 mm diameter and is about 368 mm long. The ends of the membrane are glazed in order to be leak proof when graphite seals are used for membranes test experimentation. The average pore size of the alumina support is about 6 μm , which does not modified significantly with the titania wash.

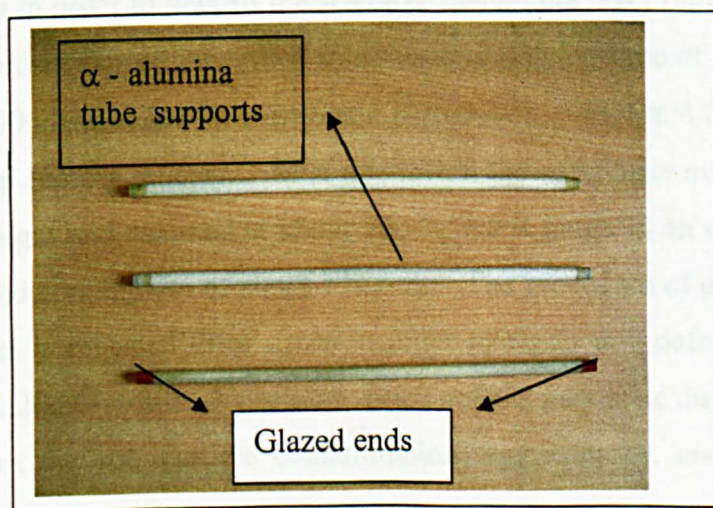


Figure 4.1: Schematic of membrane support tubes.

4.3. Preparation Methods and Procedure

4.3.1. Preparation of silica solution

The membrane material used in this work was Dow Corning's Sylgard 184 silicon elastomer. Sylgard 184 is a combination of silanes $(-\text{Si}-)_n$ and siloxanes $(-\text{Si}-\text{O}-\text{Si}-)_n$ with alkyl group substituting some of hydrogen atoms. The preparation of silica solution is based on the condensation reaction between silicone elastomer (solute) and 2-methyl butane (solvent) in the presence of silicone 184 curing agent. The solution is prepared by initially mixing 900 ml of 2-methylbutane $\{\text{CH}_3\text{CH}_2\text{CH}(\text{CH}_3)_2\}$ with 100 ml of silicone elastomer into a clean test tube of 1000ml volume. The mixture was shaken until the silicone was well dispersed into the 2-methyl butane (colourless solution obtained) using magnetic stirring. Later, 10 ml of 184 curing agent was added to the mixture after obtaining a homogenous solution. The curing agent is added to carry out the curing process for obtaining the desired solution for the surface modification of the porous ceramic support.

4.3.2. Silica membrane for hydrogen reaction

The fabrication of porous silica composite inorganic membrane is performed by initially cleaned the support with acetone and dried at 65 °C over night in oven to remove any contaminants or dusts. Before dip coating, the porous support is sealed at its ends in order to deposit the selective membrane layer on the outer surface. The support is then dipped into silica solution for a dipping time of about 5 minutes using a class 100 clean room for membrane preparation. Figure 4.2 presents a schematic for the dip coating process. After deposition the composite membrane is dried at 65 °C over night and calcined at about 300 °C for 4 hours in an electric furnace with a heating and cooling rate of about 1 °C/min. The procedure of dip coating, drying and calcination is repeated three times in order to repair any defects in the surface that would result due to poor deposition. Such defects may arise due to the presence of air bubbles in the sol, particle contamination, aggregations, and irregularities in the support surface itself.

4.3.3. Silica membrane for hydrogen separation

The silica membrane for hydrogen separation is prepared similar to that described for reaction applications. In this case however, the number of dip coating steps has been increased to 7 times and the procedure of dip coating, drying and calcination is repeated to obtain a defect free composite membrane. With the previous procedure methods it is not possible to produce a membrane with high selectivity which can be used for hydrogen separation and purification. Therefore other methods are applied to improve the membranes selectivity. One of these methods refers to rotation coating where in the support is rotated using rota machine for certain time duration while deposition takes place. The idea behind the rotation of the support is to decrease the amount of the silica penetrated inside the pores for producing a high permeable membrane with high selectivity. Due to the wide pore size of the support, this attempt was unsuccessful.

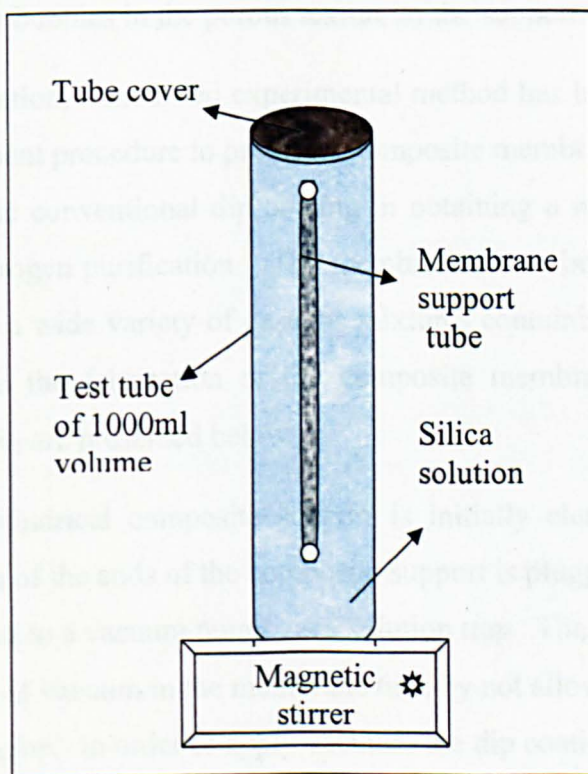


Figure 4.2: Schematic of dip coating process

4.3.4. Silica membrane for hydrogen purification

Conventional technique applied for the preparation of defect free composite membranes involve sol-gel and dip coating process under atmospheric conditions. Under these conditions, the formation of a defect free silica composite membranes with high separation factor, low membrane thickness and minimum coating-drying cycles is not possible. This is due to the presence of large pores and air bubbles in the porous matrix of the support on which silica layer deposition takes place. The presence of different capillary forces is also affect the deposition process due to natural pressure difference that exist due to mass transport on porous texture of the support. Further, air bubbles get immobilized in the porous structure with the absence of any forced convection within the support structure that can be typically achieved by the application of vacuum.

On the other hand, application of vacuum or a pressure force of lower order at one end of the membrane could provide better process conditions for the coating process. The pressure force in the form of a suction or vacuum could allow the dip coating solution to penetrate the porous structure thereby overcoming capillary forces and removing immobilized air bubbles in the porous texture of the support.

In this investigation, a modified experimental method has been developed provides a quick and efficient procedure to prepare a composite membrane that can overcome the limitation of the conventional dip coating in obtaining a membrane with selectivity needed for hydrogen purification. The membranes have been tested to produce pure hydrogen from a wide variety of gaseous mixtures containing hydrogen. The details with respect to the fabrication of the composite membrane with high separation factors for H_2/N_2 are presented below.

The porous cylindrical composite support is initially cleaned and dried at 65 °C overnight. One of the ends of the composite support is plugged with a seal. The other end is connected to a vacuum pump via a solution trap. The solution trap would allow the application of vacuum in the membrane tube by not allowing silica sol to block the tubing of the pump. In order to apply vacuum, the dip coating tank in which silica sol is prepared is kept air tight with the composite support placed in the sol. Once the silica sol is ready, vacuum is applied for about 10 - 15 minutes. When the vacuum is applied, silica particles would plug the membrane pore space due to plugging of the

pores by a cross flow created by the suction pressure. After the application of vacuum, the composite membrane is dried at 40 °C overnight. The procedure of dip-coating under vacuum conditions is repeated once again in order to reduce the surface defects. Finally the membrane is calcined at 280 °C for 4 hours at a heating and cooling rate of 1.5°C/min. Figure 4.3 presents a schematic for the deposition technique used for the preparation of dense silica membrane.

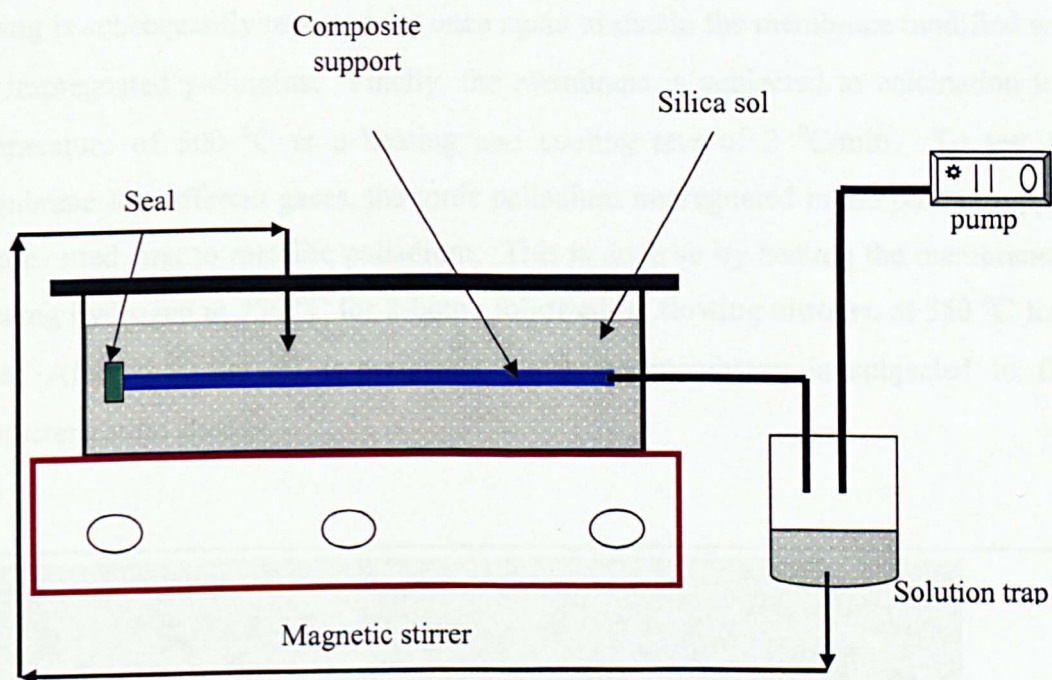


Figure 4.3: Schematic of dip-coating process for the preparation of silica composite membranes for hydrogen purification

4.3.5. Pd impregnated γ -alumina membrane

The preparation procedure for the Pd impregnated γ -alumina membrane is as follows. Initially 60 g of boehmite sol (alumina monohydrate) powder is dissolved in 0.7 litre water with nitric acid and left stirring for about 2 hours at 70 °C. Then 0.20 g of PdCl₂ is added to this solution and mixed for 1 hour Figure 4.4. The resulting greyish solution is transferred to a low height dip-coating tank and vacuum force is applied for 10 minutes to suck the solution into the pores of the support. The membrane is then taken out and dried at 120 °C overnight. This procedure of vacuum suction and drying is subsequently repeated for once again to obtain the membrane modified with Pd impregnated γ -alumina. Finally, the membrane is subjected to calcination to a temperature of 500 °C at a heating and cooling rate of 2 °C/min. To test the membrane for different gases, the ionic palladium impregnated in the porous support is converted first to metallic palladium. This is done so by heating the membrane in flowing hydrogen at 350 °C for 2 hours followed by flowing nitrogen at 350 °C for 1 hour. After this, the Pd impregnated γ -alumina membrane is subjected to flux characterization studies.

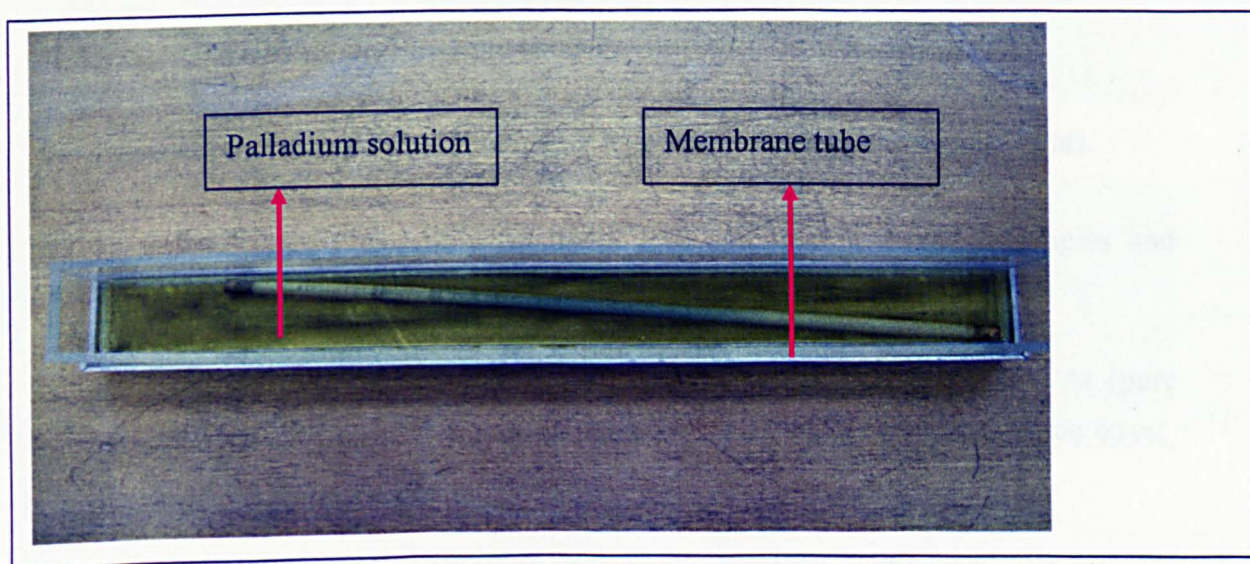


Figure 4.4: photo of dip-coating process for the preparation of Pd impregnated γ -alumina membrane.

4.3.6. Silica on γ -alumina modified support

The preparation procedure for silica on γ -alumina membrane is different to that presented for Pd impregnated γ -alumina membrane. The support is initially cleaned and then subjected to the deposition of γ -alumina by dissolving 60 g of boehmite powder into 0.7litre water with nitric acid and stirring for about 3 hour at 70 °C to get boehmite sol. The membrane is transferred into the boehmite sol and sucked in the sol to modify the pores of the membrane. The membrane is then dried at 120 °C overnight and calcined at 500 °C with a heating and cooling rate of 2 °C/min. The procedure for γ -alumina deposition consisting of dipping, drying and calcining is repeated once again and after the calcination, the membrane is subjected to silica deposition one time only by applying dip coating the support into silica solution. The membrane is then dried overnight at 40 °C and calcined at 400 °C with a heating and cooling rate of 1 °C/min. After calcination, the composite membrane termed as silica on γ -alumina membrane is subjected to surface and flux characterization studies.

4.4. Flux Characterisation

4.4.1. Equipments and materials

1. Permeation cell and digital flow meter 0 – 1000 ml/min (Varian instrument).
2. Membrane reactor assembly (made in lab) equipped with thermocouples and heating tape (HEF-445-090Q, Fisher).
3. H₂ (high purity 99.995%, P=175bar), N₂ (pure 99.99%, P=230bar) , Ar (pure 99.995%, P=230bar), C₃H₈ (pure 99.99%, P=7.5bar), CO₂ (pure 99.995%, P=50bar). (All supplied by BOC Gases).
4. H₂/N₂ 50: 50 gas mixture (P=200bar) and ternary mixture of H₂, CO₂ and CH₄.
5. For GC, pure H₂ used as a carrier gas and gas mixture of known compositions of CO, CO₂, O₂, N₂, CH₄ used for calibration, was supplied in 10L cylinders by BOC with a certificate of analysis.

4.4.2. Experimental rig and Feed supply

Figure 4.5 presents a schematic of the experimental rig for the flow diagram. As shown, nitrogen and hydrogen flow rates are adjusted and controlled by using a mass flow controller to mix and generate an equimolar mixture. This mixture is directly fed to the membrane reactor shell at desired transmembrane pressure differences (0.5 – 2.0 bar). When the membrane reactor shell is filled with the equimolar mixture, the retentate valve is opened slightly so as to purge the retentate stream for analysis using gas chromatograph (GC Varian model 3800). The mixed gas permeation rate is evaluated by measuring the permeate flow rate using a digital flow meter (Varian) for the case without sweep. Based on these compositions, the mole fractions of hydrogen in the retentate and permeate stream respectively are evaluated for the calculation of hydrogen flux and separation factor. Hence, binary gas experimentation generates the hydrogen flux and separation factors at different transmembrane pressures (0.5 – 2.0 bar) and temperatures (25 – 250 °C).

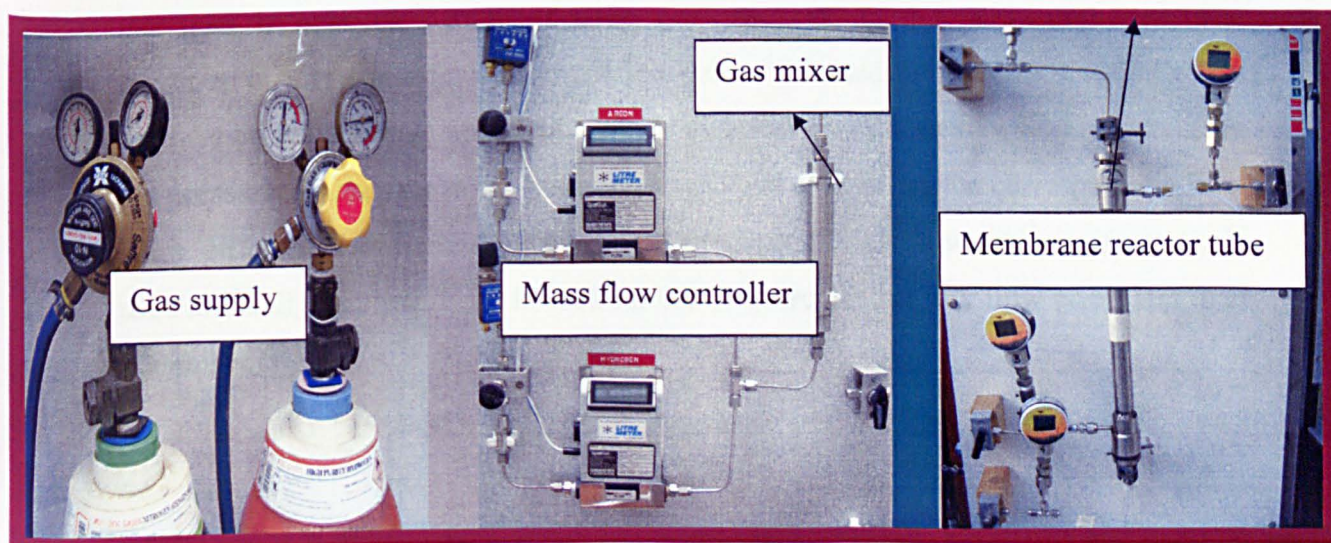


Figure 4.5: Schematic of experimental rig for the flow diagram

4.4.3. Membrane reactor and permeation cell

Gas permeation experiments are carried out using a permeation cell and membrane reactor assembly. The permeation cell is used to measure gas permeances at room temperature for the assessment of possible defects in between various steps of dip-coating. Once a composite membrane is ready for high temperature experimentation, it is inserted into a high temperature membrane reactor assembly. The following section presents a description of permeation cell and membrane reactor assembly.

A schematic of the room temperature permeation cell is presented in Figure 4.6. The permeation cell consists of two stainless steel slabs separated by a tube of bigger diameter to create an annular space to inject the gas. The composite membrane is fixed at either ends of the tube using stainless steel clamps and the outer tube is placed in between the stainless steel slabs. Metal bolts are used to seal the permeation cell. One end of the central tube connected to the membrane is sealed and the other end of the tube is left open in order to connect to a flow meter. The stainless steel slabs has got other provisions for gas inlet (for left slab), pressure gauge (right slab) and purge tap (right slab). In order to conduct permeation experiments at room temperature, the gas inlet is connected to the desired gas after sealing the permeation cell. The presence of any leaks in the permeation cell is detected using soap solution. Gas permeation experiments are conducted for different single gases by slowly increasing the pressure differential in the permeation cell and measuring the corresponding flow using different flow meters. For the measurement of high flow rates, a gap meter is used and a digital flow meter is used for the measurement of low flow rates (less than 1000ml/min).

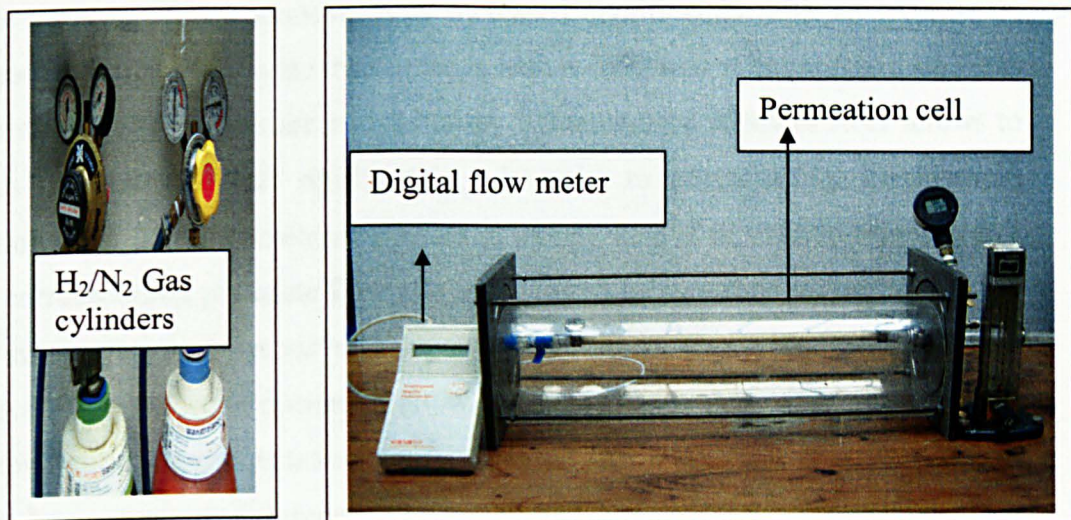


Figure 4.6: Schematic of experimental rig for the Permeation cell

Figure 4.7 presents schematic of membrane reactor assembly developed in the laboratory for high temperature permeation measurements. The assembly consists of a stainless steel tube (outer diameter 27 mm and inner diameter of 18 mm) in which composite membrane (outer diameter 10 mm and inner diameter 7 mm) is placed for high temperature permeation experiments. During operation, the membrane reactor assembly is sealed by SS O-rings and moulded graphite seals. Of these, one of the stainless steel O-ring is welded to the stainless steel reactor assembly where as the other is left for removal and placement in order to operate the membrane reactor in different configuration (annular and tubular).

The moulded graphite seals offer compressibility in order to provide a leak proof seal when the reactor assembly is tightened using stainless steel screws. The stainless steel tube is wound with a heating tape that can heat the membrane reactor to a maximum temperature of about 450 - 500 °C. Type K thermocouples inserted on strategic locations along the stainless steel tube to provide the temperatures values during experimentation.

The gas permeation measurement at higher temperature is performed as follows. The membrane reactor assembly is tightened by placing the composite membrane first. The assembly is initially tested for leak proof capability by sending nitrogen gas at different pressures in the shell and measuring the corresponding flow rates in the

permeate stream. If the permeate flow increased significantly with an increase in shell pressure for the composite membrane, a leak is indicated at the seal and stainless steel interface. These leaks are eliminated by tightening the stainless steel screws to compress the graphite seals significantly. In order to generate high temperature permeation data, the composite membrane is slowly heated to desired temperatures and the corresponding permeate flow rate is measured using a flow meter. When not using a sweep gas, the inlet valve at the sweep is closed; when using sweep gas, the inlet valve of the sweep is opened to allow the desired flow rate of the sweep. Thus high temperature experimentation would provide the membrane flux at different transmembrane pressure differences (0.5 – 2.0 bar) and different temperatures (25 – 600 °C).

From the measurements, the membrane flux is evaluated as the following function of flow rate:

$$J = \left(\frac{q}{22.4} \right) \left(\frac{1}{1000 \times 60A} \right) \quad \text{Eq. (4.1)}$$

Where q is the flow rate measured in (ml/min) and A is the membrane surface area (m^2).

The membrane permeance is evaluated using the following equation by dividing the flux on the transmembrane pressure as:

$$Per = \frac{J}{\Delta P} \quad \text{Eq. (4.2)}$$

The composite membrane permeability can also be evaluated as a function of the thickness of the separation layer.

$$Perm = per \times \delta \quad \text{Eq. (4.3)}$$

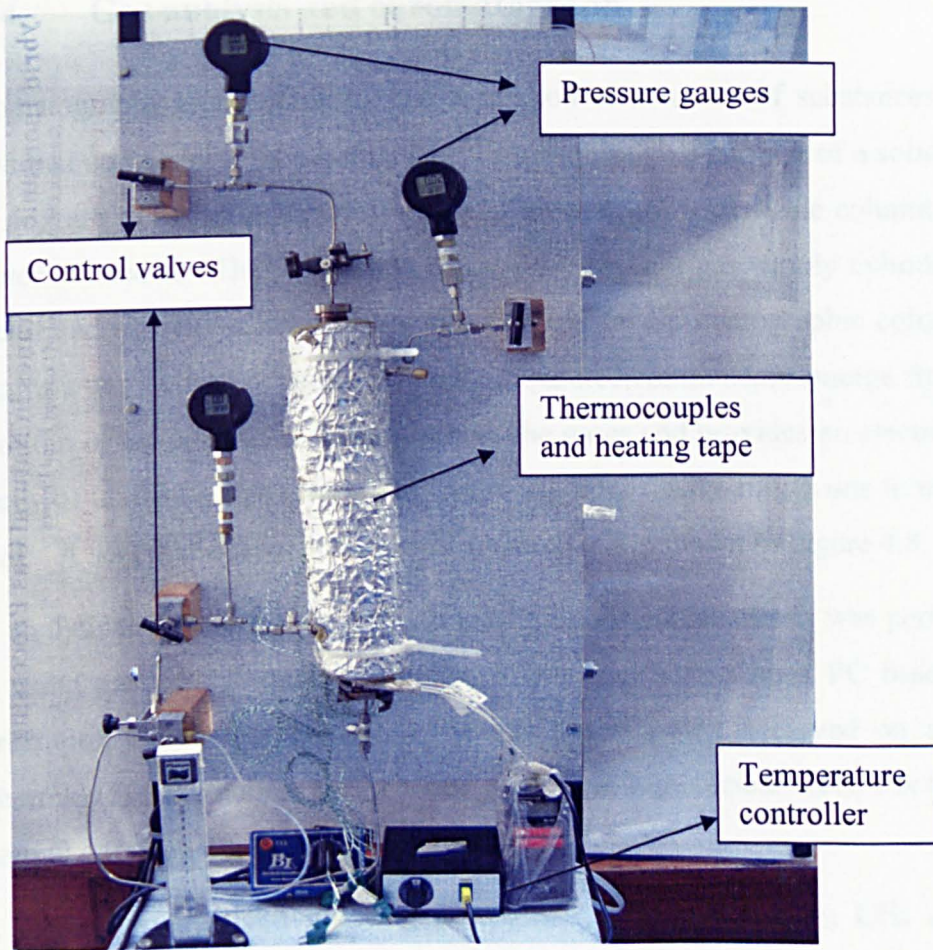


Figure 4.7: Schematic of membrane reactor assembly

4.4.4. Gas analysis and chromatograph

Chromatography is a method for the separation of mixtures of substances into their individual components by causing them to pass through a column of a solid or liquid. The mixture to be separated must put onto the start (or top) of the column and so an injector is needed. The gas mobile phase flows from a gas supply cylinder past the injector and carries the injected mixture through the chromatographic column, which contains a gas stationary phase. When the separated components emerge from the end or bottom of the column, a detector senses the gases and provides an electrical signal, directly or indirectly to a read out device or recorder finally allows one to measure the signal. A schematic layout of a gas chromatograph is shown in Figure 4.8.

The analytical system for the evaluation of gaseous compositions was performed on-line using gas chromatography (Varian 3800) interfaced with a PC based GC star Workstation for data analysis. The gas analysis was achieved on a 2m long isothermal (50⁰C) stainless steel column packed with molecular sieve 13x mesh using a thermal conductivity detector (TCD).

The calibration involved injecting pure gases such as H₂, CO₂, CH₄ and O₂ for qualitative analysis, i.e. to obtain the retention times of each of the gases used. The gas chromatograph was calibrated before any subsequent samples are run against it using certified reference standards. One example of the peaks for the gas product is shown in Figure 4.9.

The carrier gas used in this work is hydrogen and hence, hydrogen is not traced in the detector system. However, other gases such as N₂, CH₄, CO₂ are traced using the detector and the hydrogen composition is calculated based on the compositions of these gases.

If the mixture contains hydrogen as a major component, strange results can be obtained when a helium gas used as a carrier gas (Cowper and DeRose, 1983). This is because the hydrogen gives a relatively small response in helium. At low concentrations the signal is in the same direction as that for all other components, and as the concentration increases, the peak inverts at its maximum, eventually becoming strongly negative. Also the many advantages of hydrogen over helium as a carrier gas are well understood and include increased speed of analysis, increased separation efficiency and increased sensitivity.

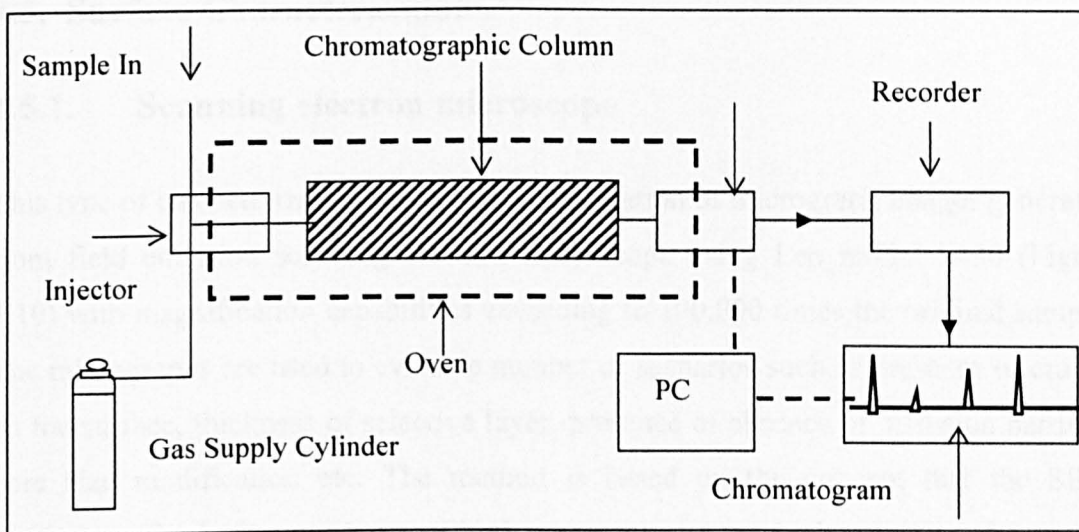


Figure 4.8: A schematic layout of a gas chromatograph.

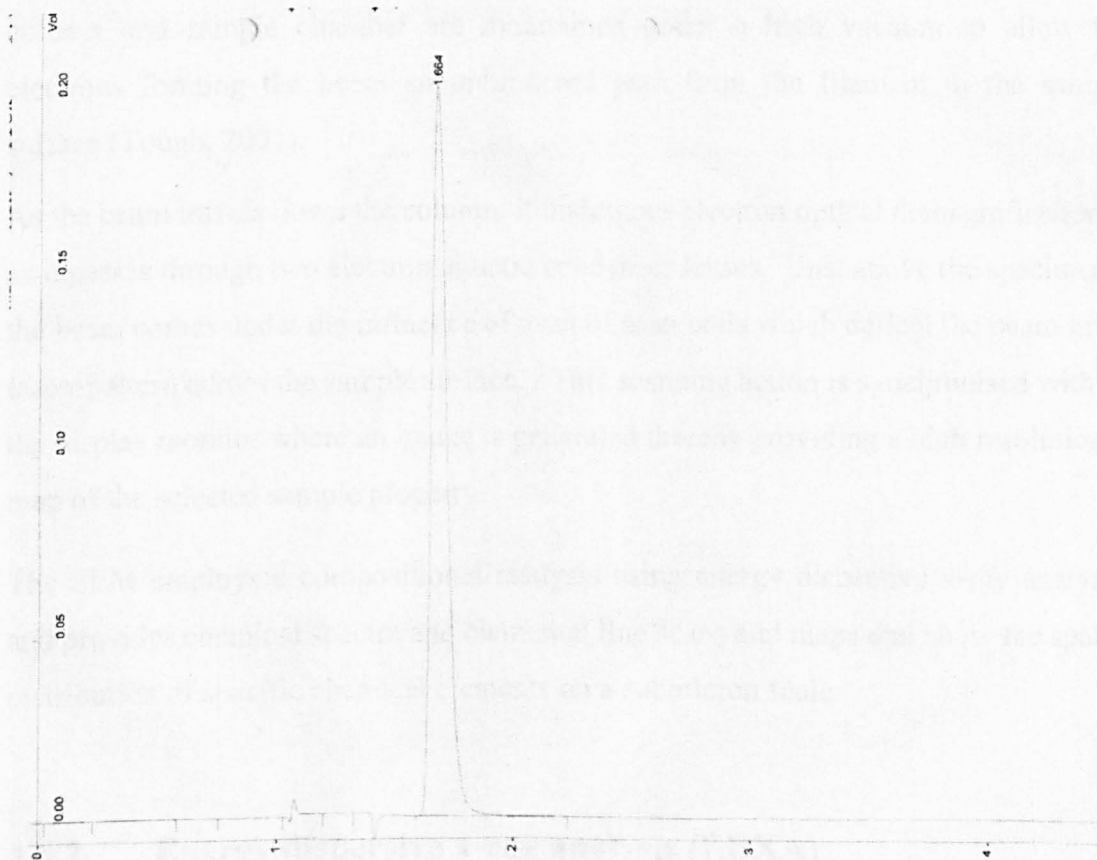


Figure 4.9: Calibrated product chromatograph.

4.5. Surface Characterisation

4.5.1. Scanning electron microscope

This type of characterization refers to the observation of micrograph images generated from field emission scanning electron microscope using Leo model S430 (Figure 4.10) with magnification capabilities exceeding to 100,000 times the original sample. The micrographs are used to evaluate number of scenarios such as presence of cracks on the surface, thickness of selective layer, presence or absence of diffusion barriers, pore size modification etc. The method is based on the concept that the SEM generates a finely focused beam of high energy electrons which are scanned over the membrane sample under inspection. The beam originates from the heating of tungsten wire filament housed in an electron gun at the top of the microscope column. The beam electrons are accelerated towards the specimen by means of an applied accelerating voltage between the filament assembly and an anode plate. The SEM column and sample chamber are maintained under a high vacuum to allow the electrons forming the beam an unhindered path from the filament to the sample surface (Tough, 2001).

As the beam travels down the column, it undergoes electron optical demagnification as it passes through two electromagnetic condenser lenses. Just above the specimen the beam comes under the influence of a set of scan coils which deflect the beam in a raster pattern across the sample surface. This scanning action is synchronised with the display monitor where an image is generated thereby providing a high resolution map of the selected sample property.

The SEM employs a compositional analysis using energy dispersive x-ray analysis, and provides chemical spectra and elemental line scans and maps that show the spatial distribution of specific chemical elements on a submicron scale.

4.5.2. Energy dispersive x-ray analysis (EDXA)

This type of surface characterization relates to the evaluation of elemental composition of the membrane / support surface using energy dispersive X-ray analysis (EDXA). The X-ray detector is connected to S430 SEM microscope to obtain

elemental composition from a single sample. The elemental characterization is significant to visualize whether the inner surface of the membrane is modified or not in the due course of deposition to evaluate the extent of surface modification with silica or other materials used for membrane support modification.

As the scanning electron microscope uses a high energy electron beam to illuminate a specimen, one of the by-products is the generation of x-ray as primary beam electrons interact with specimen electrons. The production of x-rays occurs in two basic ways. As an electron in the primary beam enters the volume of a specimen atom, it can be scattered in various ways.

Primary electrons may slow down by interaction with forces present within the volume of an atom resulting in the electron giving up energy. This energy loss can be accomplished by the emission of x-ray radiation. This type of radiation is known as braking radiation and is observed as a continuous spectrum which is regarded as background radiation for EDXA spectrometers.

Scattering also occurs due to collisions between primary electrons and electrons within specimen atoms. The consequent rearrangement of electrons within electron shells, as atoms strive to reach their lowest energy states, results in the release of energy in the form of x-ray photons. As the energy of these photons is related to the energy between electron shells, the x-ray photons are characteristic of the element present in the specimen. By collecting and analysing these x-rays, qualitative and quantitative information about the component elements of a specimen may be obtained (Tough, 2002).

System resolution calibration is carried out using cobalt (Co) standard for different dead times of 10%, 20%, 30%, 40% and 50%. Gain calibration is carried out before each analysis session (or every 3 hours). This routine corrects for any gain changes in the spectrometer. This ensures that previously recorded standard spectra can still be used at later dates without the need to record new data for every analysis session.

4.5.2. Accelerated surface area and morphology (ASAP 2010)

The nitrogen gas adsorption-desorption was measured using a fully automated

ASAP 2010. The ASAP 2010 is a fully automated nitrogen gas adsorption-desorption

measuring instrument. It is a fully automated nitrogen gas adsorption-desorption

measuring instrument. It is a fully automated nitrogen gas adsorption-desorption

measuring instrument. It is a fully automated nitrogen gas adsorption-desorption

measuring instrument. It is a fully automated nitrogen gas adsorption-desorption

measuring instrument. It is a fully automated nitrogen gas adsorption-desorption

measuring instrument. It is a fully automated nitrogen gas adsorption-desorption

measuring instrument. It is a fully automated nitrogen gas adsorption-desorption

measuring instrument. It is a fully automated nitrogen gas adsorption-desorption

measuring instrument. It is a fully automated nitrogen gas adsorption-desorption

measuring instrument. It is a fully automated nitrogen gas adsorption-desorption

measuring instrument. It is a fully automated nitrogen gas adsorption-desorption

measuring instrument. It is a fully automated nitrogen gas adsorption-desorption

measuring instrument. It is a fully automated nitrogen gas adsorption-desorption

measuring instrument. It is a fully automated nitrogen gas adsorption-desorption

measuring instrument. It is a fully automated nitrogen gas adsorption-desorption

measuring instrument. It is a fully automated nitrogen gas adsorption-desorption

measuring instrument. It is a fully automated nitrogen gas adsorption-desorption

measuring instrument. It is a fully automated nitrogen gas adsorption-desorption

measuring instrument. It is a fully automated nitrogen gas adsorption-desorption

measuring instrument. It is a fully automated nitrogen gas adsorption-desorption

measuring instrument. It is a fully automated nitrogen gas adsorption-desorption

measuring instrument. It is a fully automated nitrogen gas adsorption-desorption

measuring instrument. It is a fully automated nitrogen gas adsorption-desorption

measuring instrument. It is a fully automated nitrogen gas adsorption-desorption

measuring instrument. It is a fully automated nitrogen gas adsorption-desorption

measuring instrument. It is a fully automated nitrogen gas adsorption-desorption

measuring instrument. It is a fully automated nitrogen gas adsorption-desorption

measuring instrument. It is a fully automated nitrogen gas adsorption-desorption

measuring instrument. It is a fully automated nitrogen gas adsorption-desorption

measuring instrument. It is a fully automated nitrogen gas adsorption-desorption

measuring instrument. It is a fully automated nitrogen gas adsorption-desorption

measuring instrument. It is a fully automated nitrogen gas adsorption-desorption

measuring instrument. It is a fully automated nitrogen gas adsorption-desorption

measuring instrument. It is a fully automated nitrogen gas adsorption-desorption

measuring instrument. It is a fully automated nitrogen gas adsorption-desorption

measuring instrument. It is a fully automated nitrogen gas adsorption-desorption

measuring instrument. It is a fully automated nitrogen gas adsorption-desorption

measuring instrument. It is a fully automated nitrogen gas adsorption-desorption

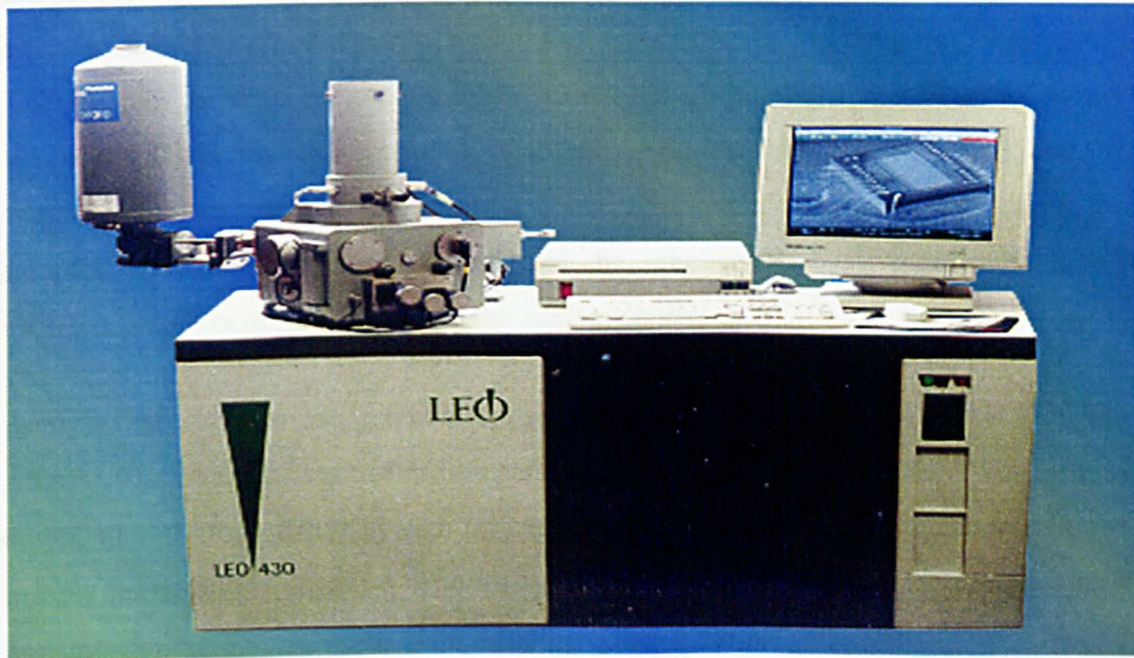


Figure 4.10: Set up for Scanning Electron Microscope (SEM) and Energy Dispersive X-ray Analysis (EDXA).

4.5.3. Accelerated surface area and porosimetry (ASAP 2010)

The nitrogen gas adsorption isotherms were measured using a fully automated apparatus (Micromeritics Accelerated Surface Area and Porosimetry Analyser, model 2010). The ASAP2010 shown in Figure 4.11 measures the pore size and surface area based on adsorption and desorption of gas on the surface and in the pores of the solid. The samples need to be analysed were degassed by heating the sample to certain temperature depends on the material type with degassing time of about 15hrs, and the sample was held under vacuum until the start of the analysis. After degassing, the samples were cooled under vacuum and the tubes were back filled with liquid nitrogen before being transferred to the analysis ports.

Analyses of samples are directed through the Windows operating system by the ASAP 2010 interface controller unit, allowing for automatic analysis. The system equipped with one vacuum system for sample analysis and another vacuum system for sample preparation (degas). The vacuum systems have separate cold traps which prevents contaminating vapor from entering either system. The analysis vacuum and degas vacuum are separate to allows the analysis and degas to proceeds simultaneously.

The ASAP has been calibrated before any pore size characterisation using silica-alumina sample (Reference material). The silica alumina sample has a pore size of 9.8 nm and surface area of 214 cm³/g. As can be seen form figure (4.11) that the pore size obtained is in good agreement with the values provided with the reference material.

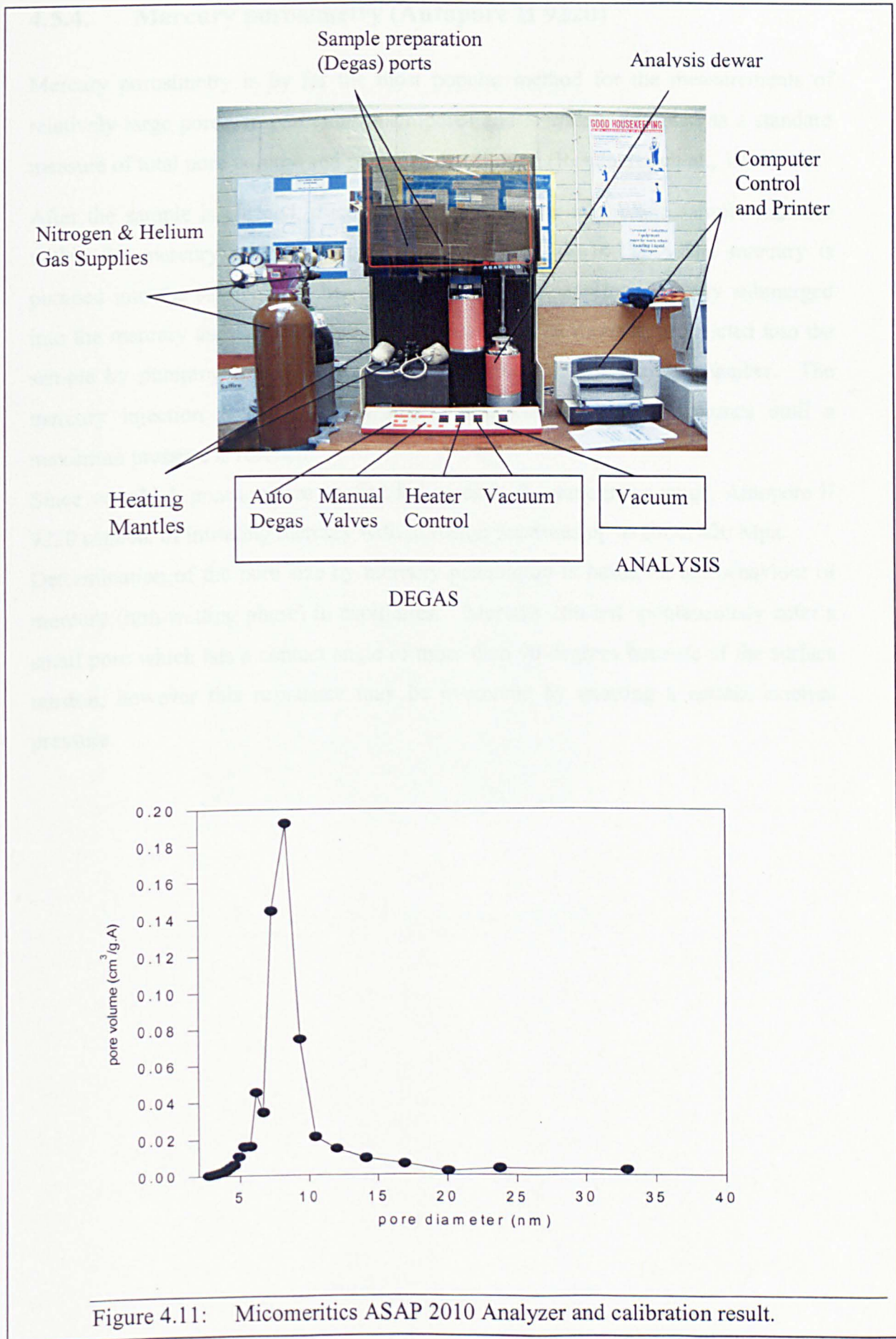


Figure 4.11: Micromeritics ASAP 2010 Analyzer and calibration result.

4.5.4. Mercury porosimetry (Autopore II 9220)

Mercury porosimetry is by far the most popular method for the measurements of relatively large pores, in particular macropores and is widely accepted as a standard measure of total pore volume and pore size distribution (Rouquerol et. al., 1994).

After the sample is cleaned, dried, it is placed into the membrane sample chamber within the mercury injection apparatus shown in Figure 4.12. The mercury is pumped into the sample chamber until the membrane sample is entirely submerged into the mercury and the reference mark is reached. The mercury is injected into the sample by pumping a measured additional volume into the sample chamber. The mercury injection is continued in small increments of known volumes until a maximum pressure is reached.

Since very high pressures are needed for pores in the nanometer range, Autopore II 9220 capable of intruding mercury with intrusion pressures up to about 420 Mpa.

Determination of the pore size by mercury penetration is based on the behaviour of mercury (non-wetting phase) in capillaries. Mercury can not spontaneously enter a small pore which has a contact angle of more than 90 degrees because of the surface tension, however this resistance may be overcome by exerting a certain external pressure.

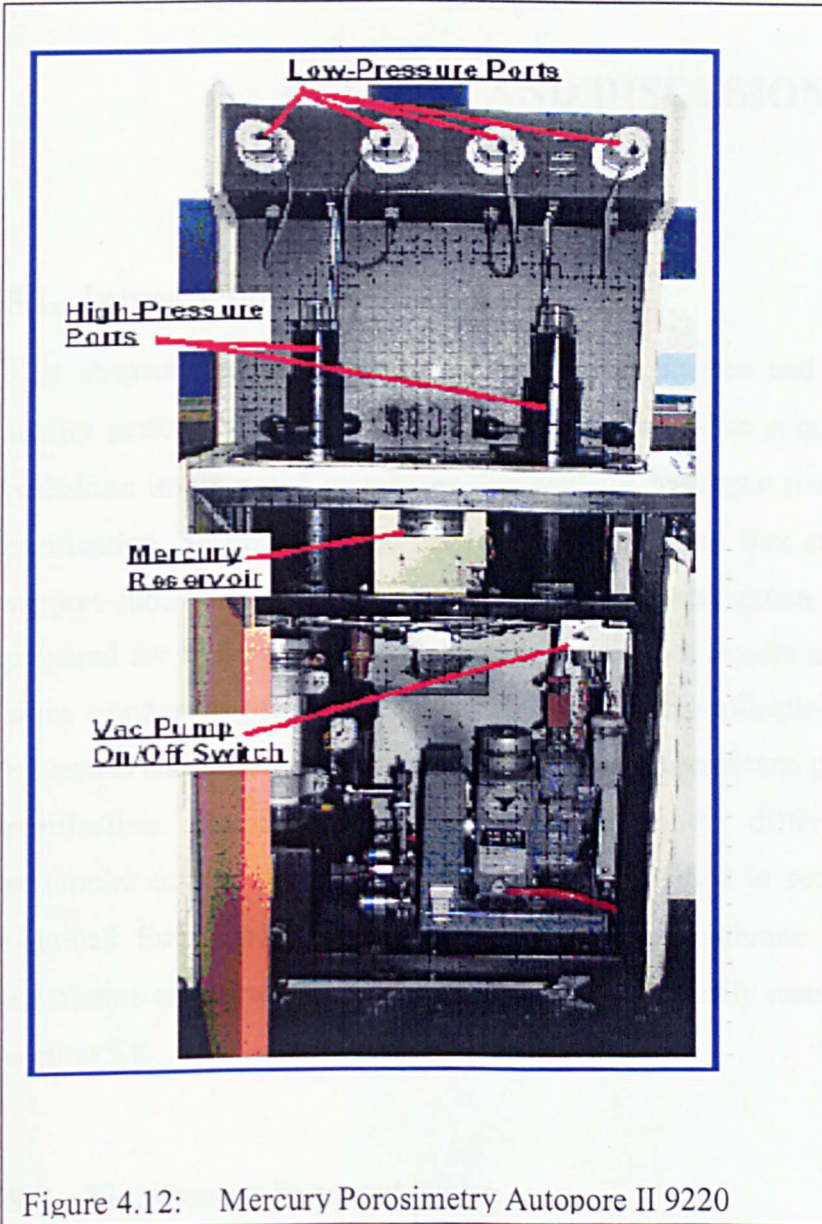


Figure 4.12: Mercury Porosimetry Autopore II 9220

Chapter 5:

RESULTS AND DISCUSSION

5.1. Introduction

This chapter presents the results obtained from surface and flux characterisation studies performed for the α -alumina support tube, silica composite membrane and palladium impregnated membrane prepared for hydrogen reaction, separation and purification. Sections 5.2 and 5.3 present surface and flux characterization of the support tube followed by surface and flux characterization of silica membranes prepared for hydrogen reaction. Section 5.4 presents results and discussion for the silica composites prepared for hydrogen separation applications. This is followed by results and discussion for the silica composite membrane prepared for hydrogen purification. The membrane permeance results for different pure gases and equimolar mixture of hydrogen and nitrogen detailed in section 5.5. The results obtained for palladium impregnated γ -alumina membrane and silica γ -alumina membrane are presented in sections 5.6 and 5.7. Finally results are summarised in section 5.8.

5.2. Membrane Support Tube

5.2.1. Surface characterisation

The average pore size of the α -alumina support provided by the manufacturer is about 6000 nm. It can be seen from Figure 5.1 that the pore size distribution of the porous support obtained from the mercury porosimetry analysis (Micromeritics Autopore II 9220) shows a dominant peak at about 6 μm which is in good agreement with the value provided by the company. Unfortunately, the use of mercury porosimetry is limited to the evaluation of pore volumes or pore size distributions only (Satterfield, 1991). Therefore, the surface area of the investigated

support was evaluated from the nitrogen adsorption method and the results presented in Appendix (5).

Energy Dispersive X-ray Analysis (EDXA) of the support provided the following elemental composition: Ti - 91.673 %, Al - 5.010 %, Si - 2.1938, P - 0.76 % and Ca - % 0.3632.

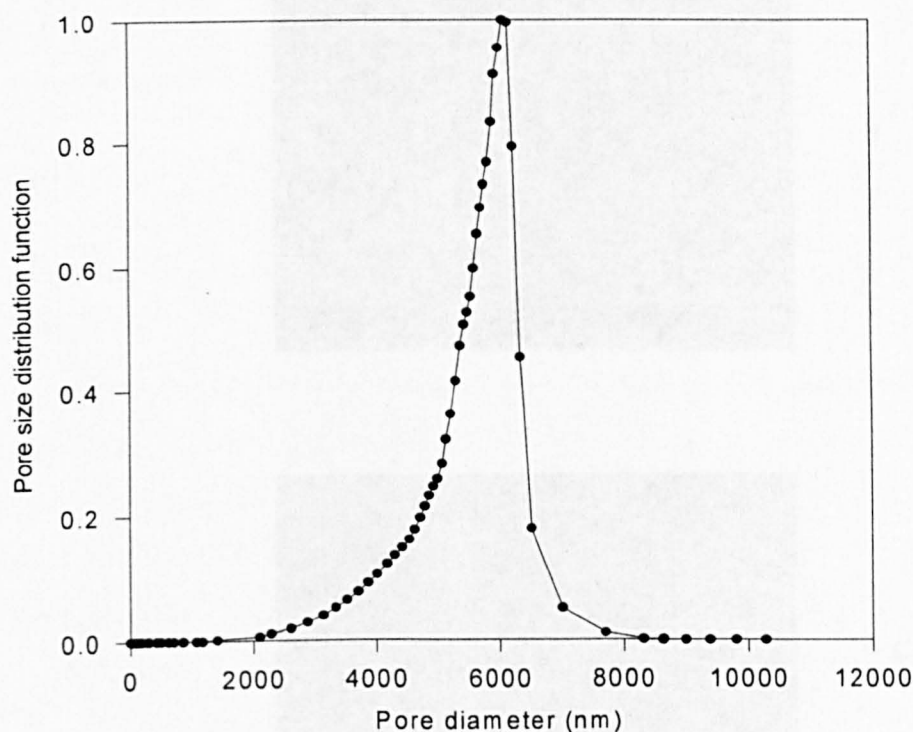
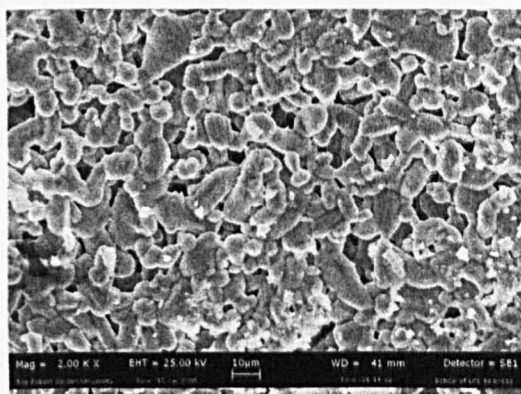
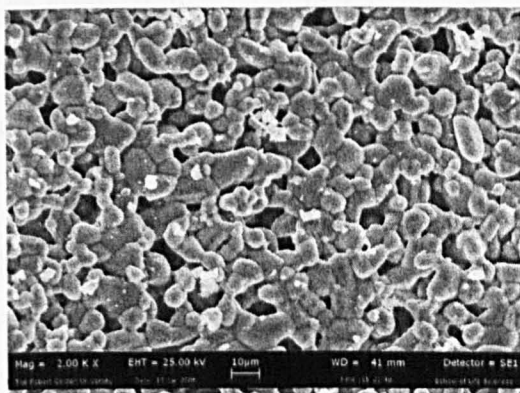


Figure 5.1:: Pore size distribution of the support (mercury porosimetry).

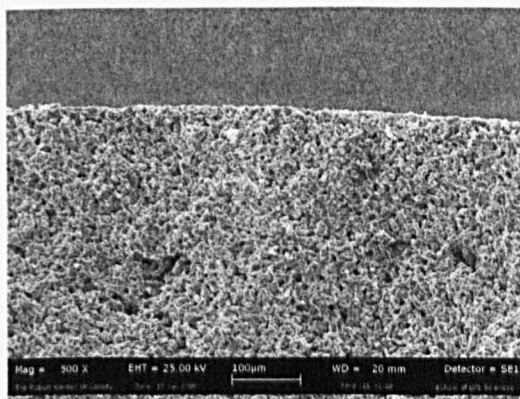
Figure 5.2 shows a scanning electron microscopic (SEM) photographs for the surface and cross-section of the support. It is clear from Figure 5.2 (A) that some pores higher than 6000 nm are present on the surface. Figure 5.2 (B) confirms that the support is single layer in nature with no differences in pore texture across the thickness of the membrane as shown on inner and the outer surfaces.



A



B



C

Figure 5.2: SEM micrographs showing support Outer surface (A), Inner surface (B) and Cross section (C).

5.2.2. Pure gas permeation tests

The permeation test through the porous support tube using pure gas (i.e. H₂, N₂, Ar and C₃H₈) has been determined experimentally as a function of pressure difference (up to 2 bar) by measuring the flow through the membrane support at room temperature (22-28 °C). The tubular support was mounted in a gas flow cell where the gas flowed into the annulus with the pressure set using a pressure controller. The flow rate through the support was measured using a digital flow meter. The hydrogen permeance varied from 5×10^{-6} to 8×10^{-6} mol/m².s.Pa. The permeance values for nitrogen, argon and propane obtained were $4.5 - 7 \times 10^{-6}$, $4.6 - 7.3 \times 10^{-6}$, $4.17 - 5.65 \times 10^{-6}$ mol /m².s.Pa respectively for a transmembrane pressure difference of 0.5 - 2 bar. The selectivity was calculated by taking the ratio of the permeance of the individual gases. It is apparent from the results that the permeance of hydrogen is greater than that of nitrogen and argon which in turn is greater than propane.

Table 5.1 presents the pure gas separation factors evaluated from pure gas permeances for the support at room temperature. The separation factor for H₂/N₂ varied from 1.12 – 1.17, whereas the separation factor for H₂/Ar and H₂/C₃H₈ varied from 1.09 – 1.15 and 1.2 – 1.5 respectively for a transmembrane pressure difference of 0.5 – 2.0 bar. It is apparent that the separation factors for the support are close to one which indicates that no separation occurs. It can be concluded that, the permeation of pure gases through the alumina support is dominated mainly by the viscous mechanism. This is because the permeation of fluids at values of pore size greater than 50 nm is governed mainly by viscous diffusion (Tsuru et al., 2000).

Average Pressure (Pa)	Separation factor H ₂ /N ₂	Separation factor H ₂ /Ar	Separation factor H ₂ /C ₃ H ₈
125000	1.17	1.15	1.50
150000	1.12	1.10	1.33
175000	1.10	1.09	1.23
200000	1.12	1.11	1.22

Table 5.1: Pure gas separation factors for the support at room temperature.

Based on the measurement of the flow rate of a gas through the support and the principles presented in section 3.6.2, the approximate average pore size of the support can be evaluated. According to Hsieh, 1996, the gas used in this method is pure, nonadsorbable and noncondensable. He also stated that, there are some indications that this method is influenced by the gas type. For instance, the nitrogen yield different pore size compared with helium.

The average pore diameter of the support is about 5561 nm using hydrogen, 7419 nm with nitrogen, 8479 nm using argon and finally 7011 nm with propane, all using pure gases. The pore sizes obtained using different gases are not similar as expected because of the difference in gas properties and gas-surface interactions and adsorption effects. It can be noted that these values are in the range of the pore size values obtained using the mercury porosimetry.

5.2.3. Mixed gas permeation

A permeation test experiment is conducted for mixed gas (H_2/N_2 50/50) in the permeation cell for the alumina support. It was found that permeate and feed compositions are exactly similar concentration. In other words, the support provided no separation for a mixed gas. This can be attributed once again to the fact that permeation of mixed gas mixture is also based on viscous diffusion.

In conclusion, surface and flux characterisations have both positively confirmed that the support offered very low resistance (i.e. high flow rates). The flow mechanism of pure and mixed gas permeation is governed mainly by viscous diffusion.

5.3. Silica Membrane for Hydrogen Reactions

5.3.1. Pore size and surface characterization

The determination of wide range of pore size of the support (6000 nm) and coated membrane (few nm) is not straightforward. The main reason for this is the overwhelmingly small pore volume of the thin, fine pore membrane layer compared to those of the support layer of the structure (Hsieh, 1996). The pore size of the silica membrane prepared for hydrogen reaction applications obtained from nitrogen adsorption are presented in Table 5.2. The results indicate that small pores were developed on the support and pores reduction was achieved to the extent that the percentage contribution of pores with an average pores varying from 1.86 nm – 11.64 nm is significant compared to higher pore size. Therefore, the support pore size distribution varies within the range shown in Figure 5.3. The percentage contribution of pore volume by larger pores (77.32 – 127 nm) is low. Other results obtained from ASAP 2010 are BET surface area which is 229.2 m²/g and total pore volume of 0.162 cm³/g.

pore diameter nm	BJH desorption pore volume cm ³ /g	% Contribution of pore volume
127.46	0.003898	1.917656
77.32	0.003465	1.704638
44.74	0.00637	3.133778
30.4	0.006229	3.064412
21.2	0.009272	4.561443
17.12	0.004929	2.424866
13.92	0.009324	4.587025
11.64	0.016501	8.117814
10.52	0.00364	1.790731
8.44	0.01663	8.181277
6.92	0.009673	4.758719
5.86	0.013185	6.486479
4.94	0.013398	6.591266
4.24	0.013141	6.464832
3.66	0.013146	6.467292
3.2	0.012908	6.350206
2.8	0.012328	6.06487
2.46	0.011777	5.7938
2.16	0.011317	5.567499
1.86	0.012138	5.971398

Table 5.2: Pore size distributions of silica membrane for hydrogen reaction applications.

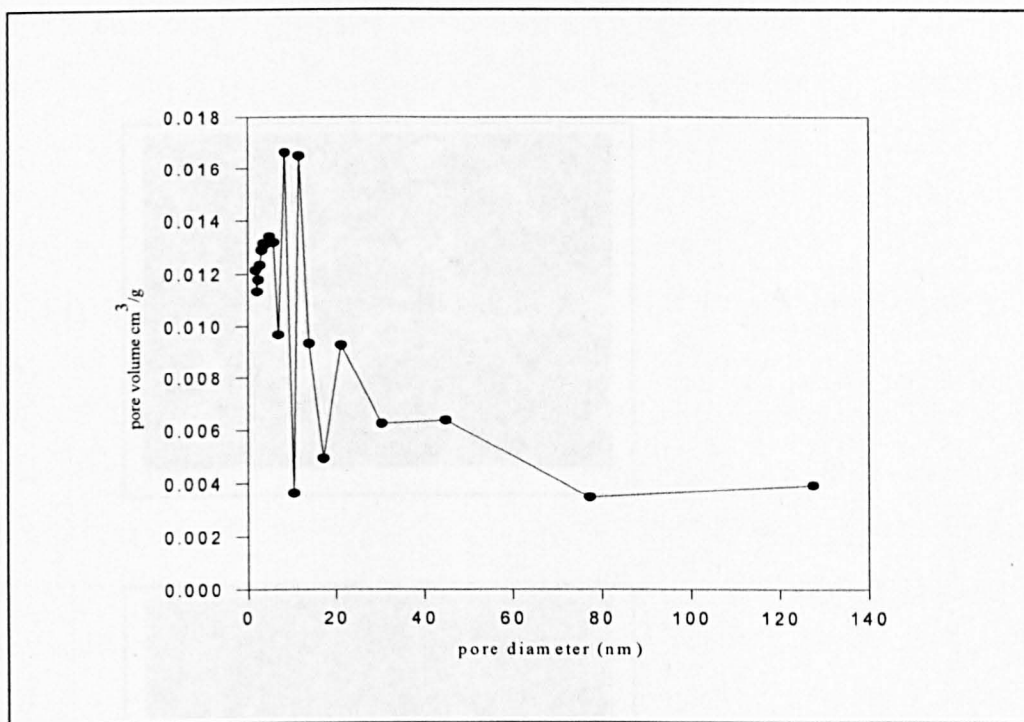
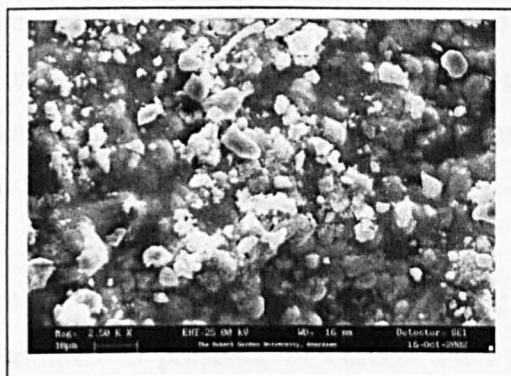
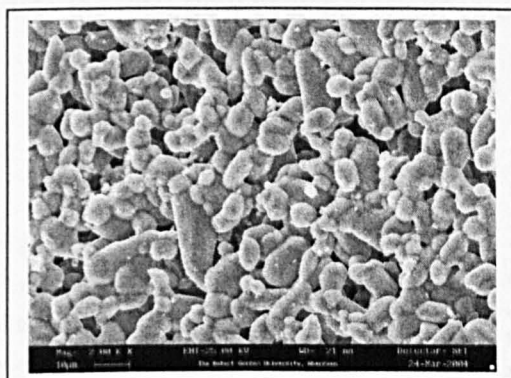


Figure 5.3: Pore size distribution of the silica membrane for hydrogen reaction applications.

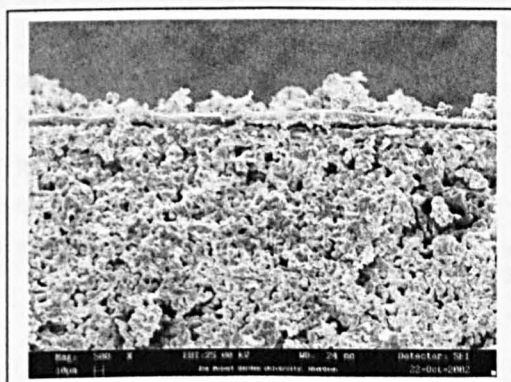
Morphology of the modified membrane was obtained through a combined SEM and EDXA analysis to examine the location and structure of the silica layer. Since the material of the modifier (silica) was different from the support (alumina), the combination of SEM and EDXA provided information on the thickness and the location of the modified layer. Theoretically, the modification could occur within and/or on the top of the existing support pores. The SEM image of the outer surface of the modified membrane demonstrated a non uniform layer with pinholes and/or cracks as shown in Figure 5.4 (A). It is clear from the inner surface in Figure 5.4 (B) that the silica layer deposited on the top surface of the membrane support has only a little penetration of the silica inside the pores. Figure 5.4 (C) shows the image of the cross section of the modified membrane with layer thickness of about 10 -20 μ m. Furthermore, EDX analysis of the top membrane surface showed insignificant silica content in addition to the base alumina. A silica content of 50.1 % was detected on the surface with 20.5 % Al, and 29.0 % Ti as well as 0.06 % P, 0.34 % Ca.



A



B



C

Figure 5.4: SEM micrographs of the membrane for reaction applications A) Outer surface B) Inner surface and C) Cross section.

5.3.2. Pure gas permeation

Figure 5.5 presents the hydrogen permeance of silica membrane fabricated for hydrogen reaction applications. Permeation measurements for pure gas were made with hydrogen, nitrogen, propane, methane and carbon dioxide at different temperatures and pressures. As shown, the hydrogen permeance decreases with temperature, and the hydrogen permeance values varied from $1 \times 10^{-7} - 9.79 \times 10^{-8}$ mol/m².s.Pa at a pressure differential range of 0.5 - 2.0 bar and for a temperature variation from 323 - 473 K.

The slight increase in the hydrogen permeance along with the pressure differential increase is attributed to presence of defects such as cracks and/or pinholes that increase the contribution of viscous flow (Nishiyama et al., 2003). The contribution of viscous flow to the total flow becomes significant at a higher pressure (Wu et al, 1993).

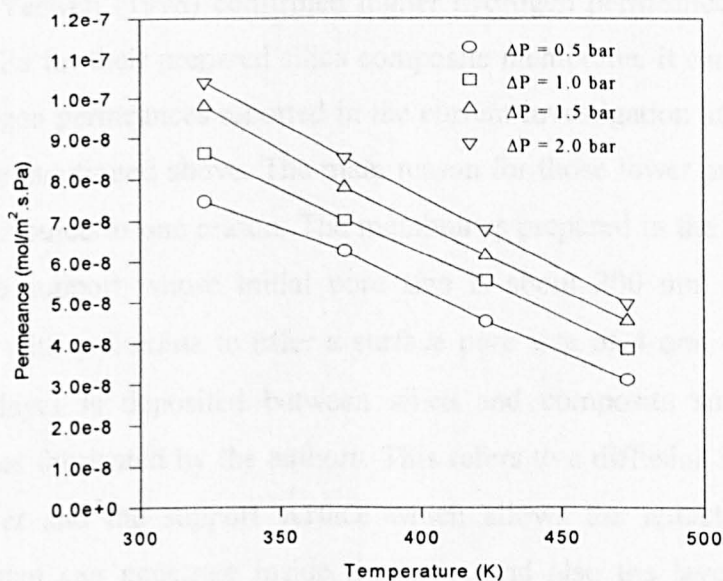


Figure 5.5: Hydrogen permeances of silica membrane for hydrogen reactions.

With respect to theory, if the hydrogen permeance is assumed to be due to the Knudsen mechanism only as a first approximation, the hydrogen permeance will not change with pressure (pressure independent), and will decrease with temperature. Therefore, it can be concluded from the results that the transport mechanism of this membrane is mainly due to Knudsen phenomena with contribution of viscous which can be observed from the pressure dependency. However, a separation factor for hydrogen with respect to other gases higher to that achieved by Knudsen mechanism can not be obtained if the Knudsen mechanism only prevails. So, in this case separation factor lower than Knudsen values are expected due to the contribution of viscous flow mechanism.

The permeances result can be compared with silica membrane prepared using TEOS. De Lange et. al. (1995^b) reported that the silica composite membranes prepared by them have hydrogen permeances in the range of 2×10^{-6} to 6×10^{-7} mol/m².s.Pa for a temperature variation of about 25 to 200 °C. These membrane permeances are independent with pressure differentials up to 5 bar. Similarly, De Vos and Verweij (1998) confirmed higher hydrogen permeance of about 2×10^{-6} mol/m².s.Pa for their prepared silica composite membrane. It can be concluded that the hydrogen permeances reported in the current investigation are two orders lower than those mentioned above. The main reason for those lower permeances reported can be attributed to one reason. The membranes prepared in the literature refer to a composite support whose initial pore size is about 200 nm, but which is later modified with γ -alumina to offer a surface pore size of 4 nm. In other words, γ -alumina layer is deposited between silica and composite support layer in the membranes fabricated by the authors. This refers to a diffusion barrier between the silica layer and the support surface which allows the reduction of fresh silica solution that can penetrate inside the pores and also the layer thickness on the membrane surface can be lowered.

Hence, it is concluded that the preparation method of γ -alumina membrane affected only the small pore size range (i.e. 30-200 nm). Since a diffusion barrier is not available, higher amount of silica has to be deposited in order to obtain a membrane with acceptable selectivity but the gas flow rate is reduced resulting in lower permeances. It is also important to note here that the support utilised in this

investigation has a higher pore size (6000 nm) as opposed to those used in literature (200 nm). From an economic point of view, the fabrication of asymmetric membranes with lower pore size on the surface would be expensive. This is due to the fact that three to four layers of different pore sizes need to be fabricated in order to reduce the surface pore size from 6000 nm to 500 – 1000 nm gradually. On the other hand, the utilisation of a symmetric support with 200 nm can be expensive when compared to the 6000 nm. This is because alumina support fabrication with higher pore size can be carried out at a cheaper cost due to reduced raw materials. Therefore, with respect to the obtained results, we can conclude that the lower order of hydrogen permeances can be argued with two reasons namely utilisation of cheap support and lower experimental costs. The lower experimental costs are due to the deposition of silica layer only (as opposed to deposition of silica and γ -alumina layers for the case of 200 nm).

Figure 5.6 presents the nitrogen permeances for silica membrane fabricated for hydrogen reaction applications. Once again, a permeance decrease with temperature which refers to the behaviour of viscous and/or Knudsen mechanism and pressure independency is clearer for nitrogen permeation as opposed to that presented earlier for hydrogen permeance especially at higher pressure. It could be due to the effect of both molecular weight and/or mean free path of nitrogen. The membrane exhibited nitrogen permeance range between 1.3×10^{-8} – 2.9×10^{-8} mol/m².s.Pa at 0.5 – 2 bar pressure differential with temperature variation from 25 – 200 °C. For comparison, values presented by De Vos and Verweij (1998) are analyzed. The authors provided values, which varied from 1.2 – 2.7×10^{-8} mol/m².s.Pa over the temperature range of 25 – 200 °C. Therefore, the values obtained in this work can be analysed to be close with values reported by Verweij. The H₂/N₂ selectivity of this membrane will be lower than their selectivity according to the hydrogen permeance difference.

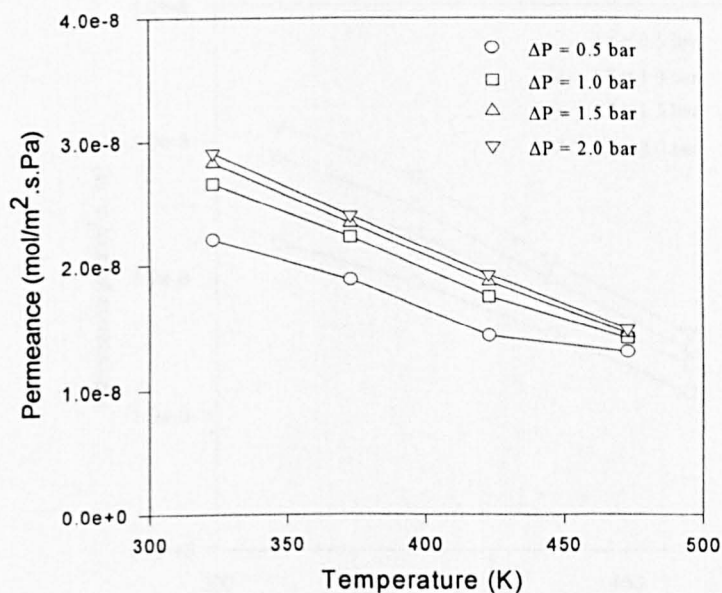


Figure 5.6: Nitrogen permeances of silica membrane for hydrogen reactions.

As represented in Figure 5.7, the dependence on both the temperature and pressure for propane permeation has similar behaviour as permeance values decreases with increasing temperature. The propane permeances are varying from 1.1×10^{-8} – 3.1×10^{-8} mol/m².s.Pa at 0.5 - 2.0 bar pressure differential for a temperature variation from 25 – 200 °C. It is accepted that the permeance of gas molecules is affected by adsorption of gas molecules on the membrane pore surface. The permeation of adsorbing gases such as propane showed higher permeance than nitrogen. Schafer et al., (2001) reported propane permeance of about 1×10^{-8} mol/m².s.Pa which did not vary significantly with temperature. Therefore, the permeance value obtained in this work is in the same order of magnitude; however, higher selectivities are reported by the authors, which could refer to higher hydrogen permeances.

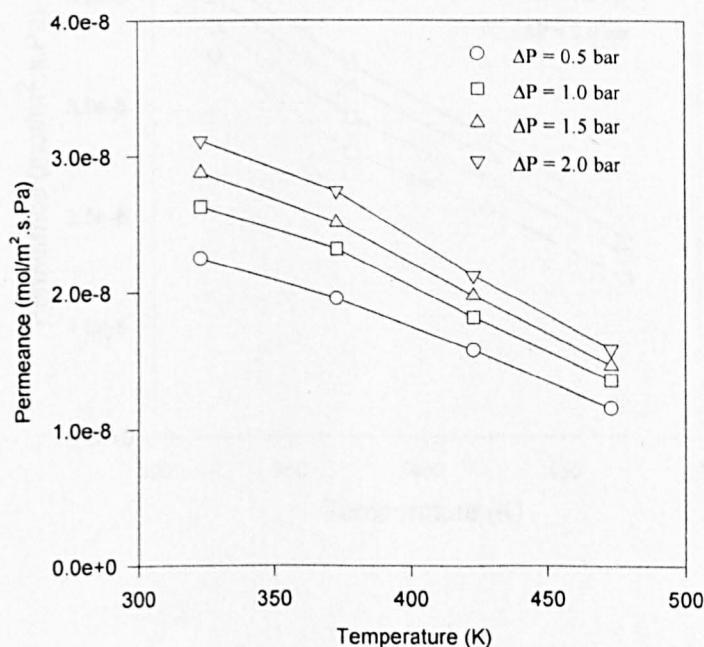


Figure 5.7: Propane permeances of silica membrane for hydrogen reactions.

Different gases have been used to test the membrane for additional investigation and understanding of the membrane behaviour in relation to gas transport. Figure 5.8 presents methane permeances for silica membrane fabricated for hydrogen reaction applications. As expected, a membrane has higher permeances than nitrogen which reflect the molecular weight differences between both gases. The methane permeance range obtained was $1.4 \times 10^{-8} - 4.2 \times 10^{-8} \text{ mol/m}^2 \cdot \text{s} \cdot \text{Pa}$ at the same pressure differential and a temperature variation from $50 - 200 \text{ }^\circ\text{C}$. These permeances are compared with those presented by De Lange et al., (1995^b). The authors reported methane permeance to vary from $2.7 \times 10^{-8} - 3.6 \times 10^{-8} \text{ mol/m}^2 \cdot \text{s} \cdot \text{Pa}$ for a temperature variation from $25 - 200 \text{ }^\circ\text{C}$.

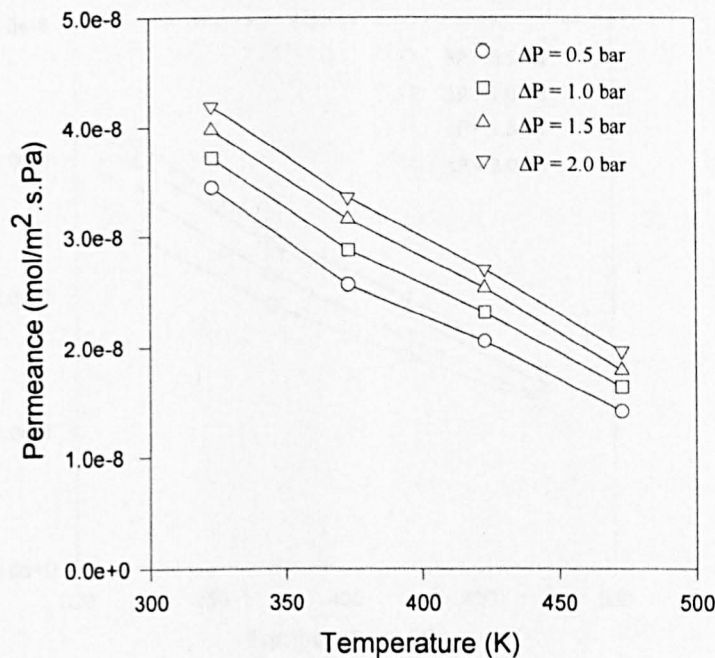


Figure 5.8: Methane permeances of silica membrane for hydrogen reactions.

The permeances of CO₂ are in the range of 1.1×10^{-8} to 3.1×10^{-8} mol/m².s.Pa at 0.5-2.0 bar pressure differential for a temperature variation from 50 – 200 °C as shown in Figure 5.9. As it can be seen, there is a characteristic decrease of permeance with increasing molecular weight as expected for Knudsen flow. Considering that the molecular weight of CO₂ is similar to the molecular weight of propane, the permeance of both gases are very close which could also reflect the similarity in their adsorption characteristics on silica. These permeances are compared with those presented by De Lange et al., (1995^b). The authors reported carbon dioxide permeance to vary from 25×10^{-8} – 30×10^{-8} mol/m².s.Pa for a temperature variation from 25 – 200 °C. These values are in the order of magnitude higher than the values obtained in this work.

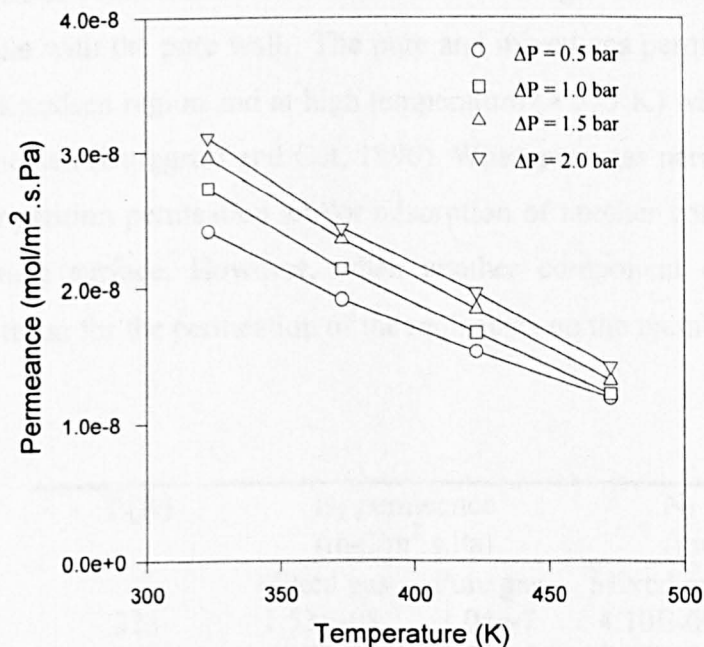


Figure 5.9: CO₂ permeances of silica membrane for hydrogen reactions.

5.3.3. Mixed gas permeation

Mixed gas permeation experiments were conducted to obtain more information about the gas transport mechanism and to compare the results with those obtained using pure gases. Table 5.3 presents mixed and pure gas permeances of both H₂ and N₂ at a transmembrane pressure differential of about 2 bars. When an equimolar mixture of H₂ and N₂ was fed into the feed side, each permeance of both H₂ and N₂ became lower than the corresponding pure gas permeance at temperature range of 323 – 473 K. However, the percent difference between the mixed gas and the pure gas permeance values decreased as the temperature increased for both hydrogen and nitrogen.

This is consistent with the results obtained by Tsai et al., (2000) for the case of micropores silica membranes. Hassan (1995) also reported situations where the mixed gas permeance is lower than the pure gas permeance.

This sort of behaviour could be attributed to the gas molecules interact and the gas molecule with the pore wall. The pure and mixed gas permeances are similar only in the Knudsen region and at high temperature (> 573 K) where this interaction can be neglected (Burggraff and Cot, 1996). When pure gas permeation occurs, there is no competition permeation and/or adsorption of another component present on the membrane surface. However, when another component exists, there would be competition for the permeation of the molecules on the membrane surface.

T (K)	H ₂ permeance (mol/m ² .s.Pa)		N ₂ permeance (mol/m ² .s.Pa)	
	Mixed gas	Pure gas	Mixed gas	Pure gas
323	1.53E-08	1.04e-7	4.10E-09	2.91e-8
373	2.15E-08	8.51e-8	5.63E-09	2.40e-8
423	2.60E-08	6.76e-8	5.65E-09	1.92e-8
473	2.71E-08	4.97e-8	5.39E-09	1.48e-8

Table 5.3: Pure and mixed H₂ and N₂ permeances of silica membrane for reaction applications.

5.3.4. Separation factor

The separation factor for pure gas permeation test is the ratio of hydrogen permeance to other gases permeance under the same transmembrane pressure and temperature. The results are presented in Table 5.4. These results showed that the separation factors are slightly lower than the values achievable due to Knudsen mechanism. In other words, a separation factor higher than Knudsen is not achievable due to the presence of defects that reduces the separation factor and increases the contribution of another flow mechanism such as viscous flow through the bigger pores. It is clear that all gases have separation factors, which relates to the main contribution of separation by the Knudsen mechanism. The possible increase in the gas separation factors can be achieved by more dip coating. This can be achieved by an increase in the number of coating-drying-calcination cycles. Such a membrane will result in lower permeance.

Gases pair	ΔP				
	T (K)	0.5	1	1.5	2
H_2/N_2 (3.741 ^a)	323	3.37	3.25	3.46	3.58
	373	3.32	3.13	3.33	3.54
	423	3.16	3.18	3.30	3.52
	473	2.39	2.73	3.14	3.36
H_2/C_3H_8 (4.69 ^a)	323	3.32	3.28	3.40	3.35
	373	3.21	3.01	3.10	3.11
	423	2.89	3.06	3.11	3.19
	473	2.70	2.85	3.11	3.14
H_2/CO_2 (4.69 ^a)	323	3.09	3.16	3.30	3.36
	373	3.26	3.28	3.30	3.50
	423	2.95	3.31	3.33	3.46
	473	2.60	3.16	3.44	3.49
H_2/CH_4 (2.828 ^a)	323	2.16	2.32	2.46	2.48
	373	2.44	2.43	2.46	2.53
	423	2.21	2.39	2.42	2.50
	473	2.19	2.35	2.54	2.53

^a Knudsen separation factor.

Table 5.4: Pure gas separation factors for different pairs of gases for silica membrane applicable for hydrogen reactions.

Figure 5.10 presents a comparison between pure gas and mixed gas separation factors for the H_2 and N_2 system. As shown, the pure gas separation factor decreased from 3.57 to 3.36 for a temperature variation of 323 - 473 K and 2 bar pressure drop. However, for gas mixture, the separation factor increased from 3.73 to 6.88 at the same condition. This is because the mean free path is longer at a higher temperature for a given pressure drop (Wu et al., 1993). In other words, the mixed gas separation factor is higher than that of pure gas. It is very common in the inorganic membrane literature that the mixed gas separation factors are larger than the pure gas values (Rao and Sircar, 1993).

In summary, higher separation factors are not achieved for this membrane support by conventional dip coating due to the high pore size which needs to be reduced owing to the fact that higher separation factors lead to lower membrane permeances. The combination of higher permeances coupled with higher separation factors is hard to implement. The membrane separation factor could be increased by more coating steps or plugging the pore with other procedure, but with permeance loss. The maximum selectivity of about 3.58 was achieved for hydrogen / nitrogen, which is 95.7 % of the theoretical Knudsen value (3.74) (Keizer et al., 1988).

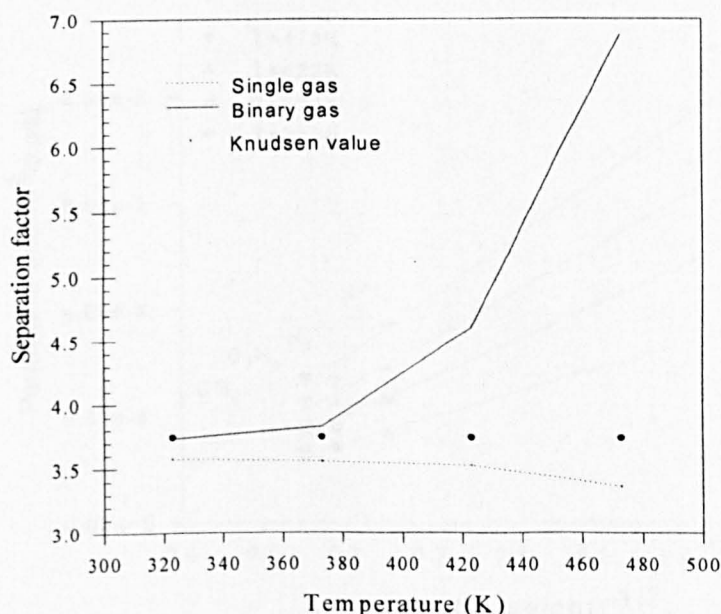


Figure 5.10: Pure and Mixed gas separation factors

5.3.5. Gas flow mechanism

According to Knudsen mechanism all gases with lower molecular weight offer higher permeances than higher molecular weight and vice versa. In other words, the hydrogen gas ($M = 2$) has permeance higher than the nitrogen ($M = 28$), and nitrogen higher than argon ($M = 40$). This is only true for non adsorbable gases or at low pressure and high temperature ($> 300\text{ }^{\circ}\text{C}$) where the surface diffusion can be negligible for adsorbable gases. The gas permeance obtained was plotted versus the inverse square root of molecular weight of the gases at different temperatures. The results shown in Figure 5.11 indicates that gas transport occurred mainly by Knudsen mechanism with good linear dependence and R^2 in the range between 0.994 – 0.997.

The gases permeances data was also plotted versus the inverse square root of the temperature and the linear regression fits are presented in Figure 5.12. The results again show good fits with R^2 ranges of 0.970 to 0.999 following the behaviour expected from Knudsen mechanism.

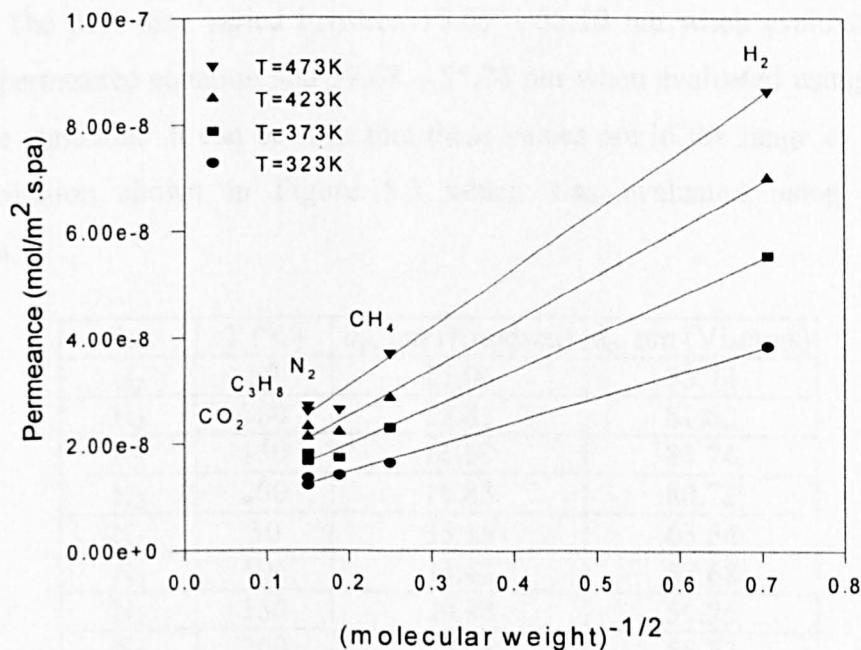


Figure 5.11: Gases permeance vs. molecular weight^{-1/2}

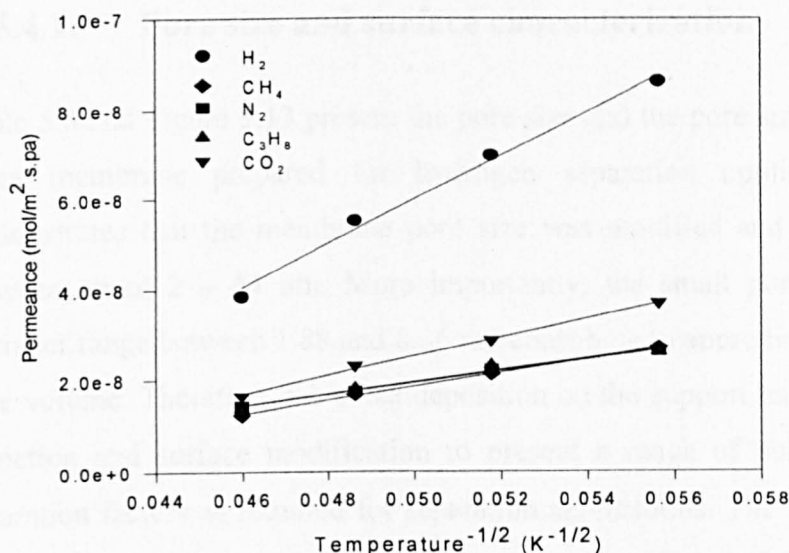


Figure 5.12: Gas permeance vs. temperature^{-1/2}

The approximate average pore size of the silica membrane prepared for reaction applications is calculated and shown in Table 5.5 for hydrogen and nitrogen pure gases. The values shown below are evaluated using the theory presented in Chapter 3 for a combined Knudsen and viscous flow mechanism for the overall permeation of gases. The pore size varied between 15.06 – 35.19 nm when evaluated using Knudsen permeance equation and 57.68 – 85.74 nm when evaluated using viscous permeance equation. It can be seen that these values are in the range of the pore size distribution shown in Figure 5.3 which was evaluated using nitrogen adsorption.

Gas	T (°C)	d _p , nm (Knudsen)	d _p , nm (Viscous)
H ₂	50	15.06	85.74
H ₂	100	15.81	81.62
H ₂	150	16.67	83.74
H ₂	200	16.83	80.72
N ₂	50	35.19	63.54
N ₂	100	34.43	57.68
N ₂	150	30.98	59.25
N ₂	200	35.06	58.73

Table 5.5: Average pore size of the silica membrane for reaction applications evaluated from gas permeance.

5.4. Silica Membrane for Hydrogen Separation

5.4.1. Pore size and surface characterization

Table 5.6 and Figure 5.13 present the pore size and the pore size distribution of the silica membrane prepared for hydrogen separation applications. The table demonstrates that the membrane pore size was modified and reduced to a range between about 2 – 64 nm. More importantly, the small pores with an average diameter range between 1.88 and 8.36 nm contribute to approximately $\frac{3}{4}$ of the total pore volume. Therefore, the silica deposition on the support has provided pore size reduction and surface modification to present a range of pores that could offer separation factors as required for separation applications. The BET surface area of the silica composite membrane for hydrogen separation is 265.09 m²/g and the pore volume is 0.203 cm³/g.

pore diameter (nm)	BJH desorption pore volume Cm ³ /g	% Contribution to total pore volume
63.9	0.00307	1.886109
41.48	0.00509	3.127131
28.66	0.005707	3.506196
21.28	0.005959	3.661017
16.82	0.005776	3.548587
13.88	0.005861	3.600809
11.78	0.005862	3.601423
10.48	0.003909	2.401563
8.36	0.01478	9.080353
6.88	0.008558	5.257758
5.82	0.01196	7.347837
4.92	0.01165	7.157383
4.22	0.0117	7.188101
3.64	0.01148	7.05294
3.18	0.011212	6.88829
2.78	0.010708	6.578648
2.42	0.01184	7.274112
2.12	0.00833	5.117682
1.88	0.009317	5.724063

Table 5.6: Pore size distribution of the silica composite membrane prepared for hydrogen separation applications.

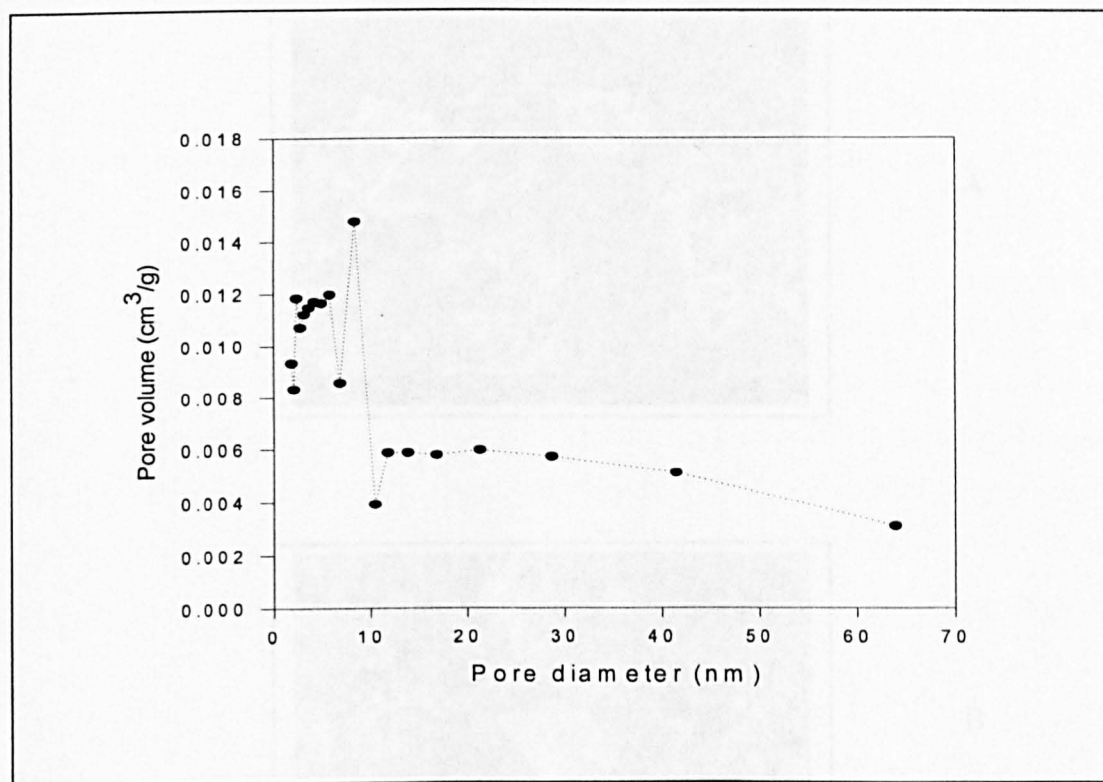
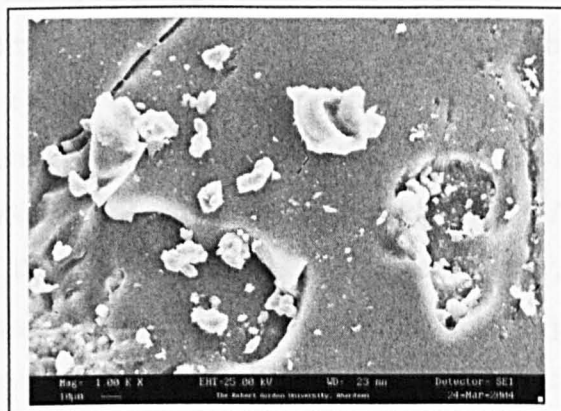
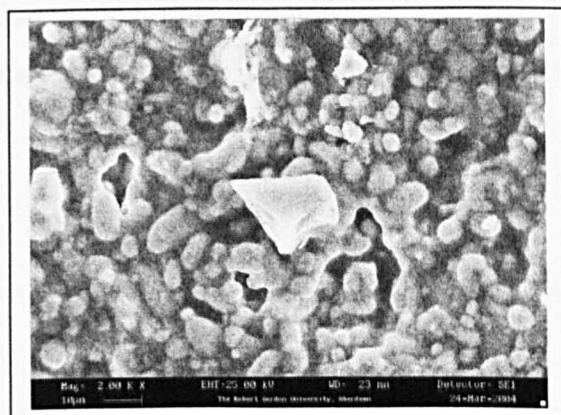


Figure 5.13: pore size distribution of the silica membrane for hydrogen separation applications

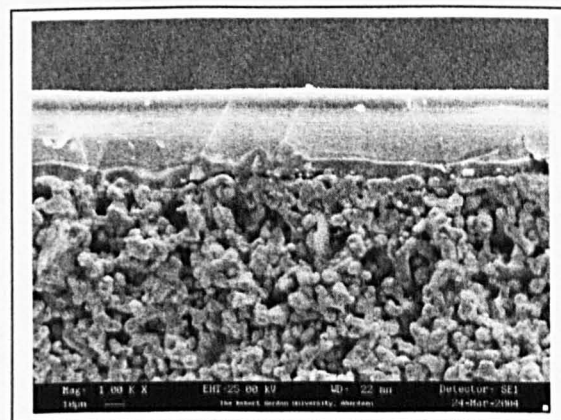
The SEM micrographs in Figure 5.14 shows the outer surface (A), inner surface (B) and cross section (C) for the silica composite membrane prepared for hydrogen separation. The outer surface of the membrane is deposited with a layer of silica and the inner surface of the membrane is modified due to the silica that penetrated through the pore spaces. The cross section of the membrane is where the deposition of silica layer is visible. The thickness of the silica layer is evaluated to about 30-40 microns based on the scale presented in the cross section micrograph. EDX analysis of the silica membrane for outer and inner surface provided different results. The EDX analysis of outer surface of the membrane related to 98 % Si, 0.2 % Cl and 1.8 % Ti and the EDX analysis of the inner surface of the membrane relates to 31.5 % Al, 29.9 % Si and 38.5 % Ti. This signifies that the inner surface of the composite membrane is modified with silica (the silica sol penetrates inside pore space of the support).



A



B



C

Figure 5.14: SEM micrographs of the separation membrane A) Outer surface B) Inner surface and C) Cross section.

5.4.2. Pure gas permeation

Figure 5.15 presents hydrogen permeance as a function of temperature at various transmembrane pressure differentials (0.5 to 2.0 bar). The hydrogen permeance varied from 4.2×10^{-10} (at room temperature) to 5.8×10^{-9} mol/m².s.Pa at the highest temperature of permeation (543 K). It is apparent from the figure that the hydrogen permeance increases with temperatures. A number of major characteristics of the behaviour can be mentioned. Firstly, the permeance profile had a sharp increase below 350 K after which the slope of permeance profile curve increase slowly until a value of 450 K. Secondly, at temperatures above 450 K, the slope of permeance profile curve increased exponentially. Such behaviour is good for hydrogen separation applications with the fact that higher hydrogen permeances at higher temperatures could provide significant increase in separation factor. It can be seen that the hydrogen permeances of silica membrane for hydrogen

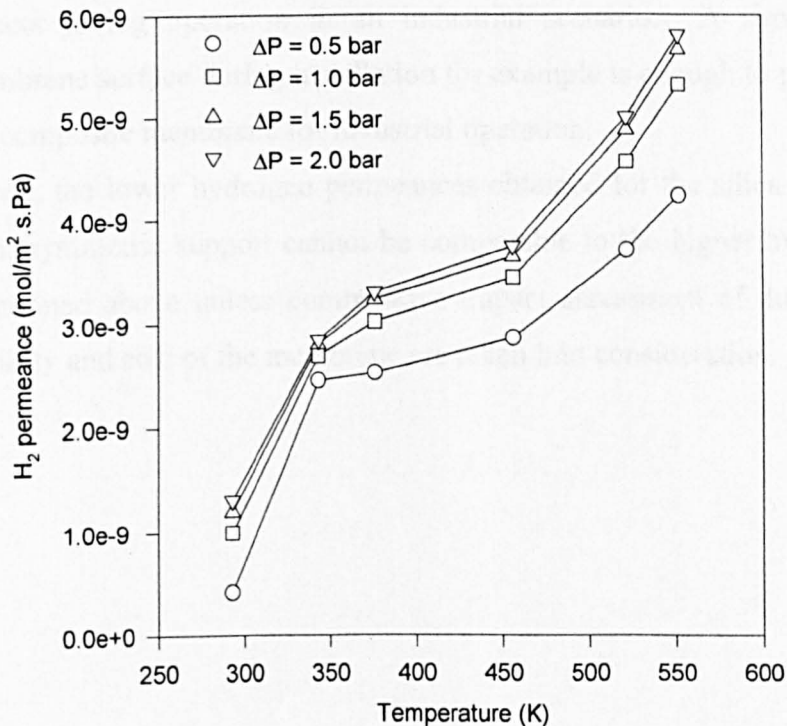


Figure 5.15: Hydrogen permeances of silica membrane for hydrogen separation.

separation are lower than the permeances obtained with the silica membrane for hydrogen reaction and that reported by De Lange et. al., (1995^b) and De Vos and Verweij, 1998). However, it has to be noted that both have fabricated thin silica films on an asymmetric support.

De Vos and Verweij, (1998) reported that the thickness of their silica layer is about 30 nm. Similarly, a thin silica membrane is deposited on a γ -alumina membrane. In the present case, silica composite membranes are prepared which could increase the thickness of silica layer due to the increase coating number and penetration of silica sol inside the pores and hence reduce the membrane permeance with the advantage of separation factor increase.

It can be further discussed here that the stability and durability of the separation layer at higher temperatures is important as much as the fabrication of thin silica membranes. Temperature cycling can have significant effect on the membrane durability and properties. Furthermore, the fabrication of a thin layer is convenient to express higher hydrogen flux. However, a 30nm layer is easily susceptible for defects during operation in an industrial scenario. A simple scratch on the membrane surface during installation for example is enough to permanently damage the composite membrane for industrial operation.

Hence, the lower hydrogen permeances obtained for the silica composite prepared from symmetric support cannot be comparable to the higher hydrogen permeances mentioned above unless comparative impact assessment of durability, mechanical stability and cost of the membrane are taken into consideration.

Figure 5.16 presents nitrogen permeance obtained at various temperatures and pressure differentials. Nitrogen permeance is varied from 5.5×10^{-10} to 9.4×10^{-10} mol / m².s.Pa for the range of temperature and pressures differentials studied. For comparison, values presented by De Vos and Verweij, (1998) are analyzed. The authors provided a values which varied from $0.12 - 0.27 \times 10^{-7}$ mol/m².s.Pa for a temperature variation of 25 – 200 °C. The values obtained in this work are lower than those presented due to the fact that silica composite membranes are prepared on a symmetric support. The permeation profiles of hydrogen and nitrogen are different regarding the impact of temperature on the permeance. While nitrogen permeation profiles increased slightly for different temperature, the same is not true for hydrogen permeance. Hydrogen permeance profiles increases sharply with temperature.

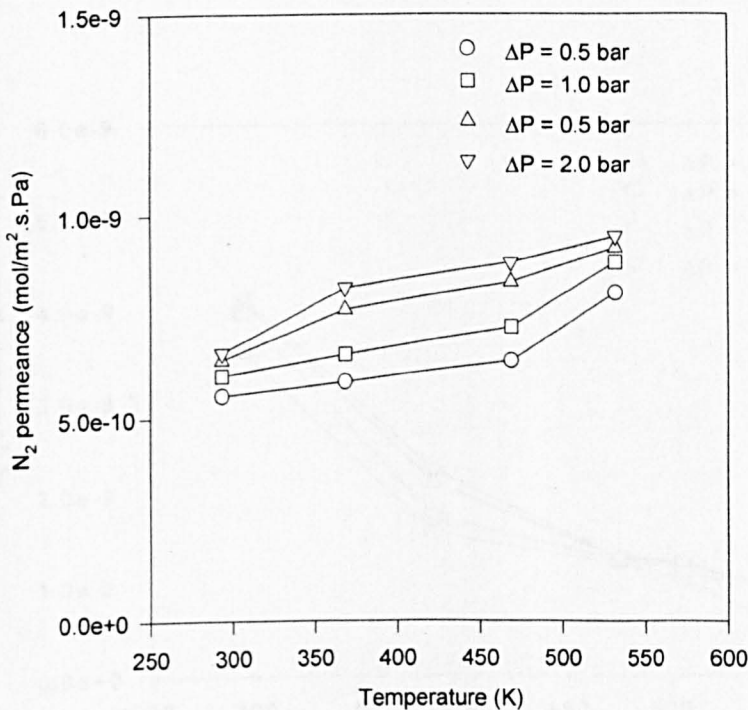


Figure 5.16: Nitrogen permeances of silica membrane for hydrogen separation.

Figure 5.17 illustrates propane permeance at various temperatures and pressure. Unlike hydrogen and nitrogen, propane permeances decreased with increasing temperature. Such behaviour for silica membrane has been reported (Munoz-Aguado and Gregorkiewitz, 1996). This can be explained due to the fact that propane permeation could be as a result of surface diffusion where the heat of adsorption is higher than the mobility energy as will be explained later. The higher permeance of propane indicates that the gas permeation was enhanced by the surface diffusion mechanism, which depends on the adsorption capacity on the membrane pore. The membrane exhibits propane permeance varied from 4.7×10^{-10} to 4.14×10^{-9} mol/m².s.Pa for a temperature variation from 298 to 550 K. These values are lower than the values reported by Schafer et al., (2001). The authors reported propane permeance of about 1×10^{-8} mol/m².s.Pa which did not vary significantly with temperature. These high permeances are not at all desired for a reaction like propane dehydrogenation applications with the fact that higher propane permeation refers to loss of reactant from the feed system.

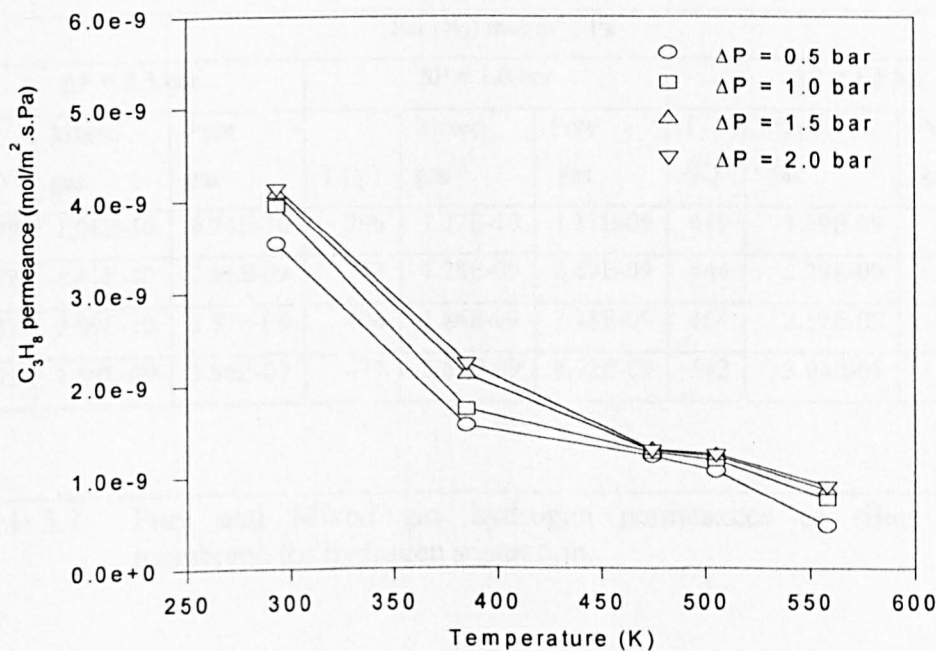


Figure 5.17: Propane permeances of silica membrane for hydrogen separation.

5.4.3. Mixed gas permeation

Table 5.7 summarises hydrogen permeance during the mixed gas permeation at different temperatures and pressure differentials for the silica composite membrane. These data are evaluated as the product of hydrogen mole fraction in the product (obtained from the gas chromatograph) with the total permeance of the system (obtained from the flow rate). For comparative purposes, corresponding hydrogen permeance is also presented. It can be seen that the mixed gas hydrogen permeance, is lower than the pure gas permeance. In other words, the permeation rate of hydrogen is affected by the presence of nitrogen.

The mixed gas activation energy for hydrogen permeation is evaluated using the theory presented (chapter 3) and the values are 10.77, 8.52 and 5.07 kJ/mol at $\Delta P = 0.5, 1.0$ and 1.5 bar respectively. Corresponding pure gas activation energy for hydrogen is observed to vary from 5.19 – 5.78 kJ/mol. Hence, it can be concluded that the mixed gas activation energy as well as the separation factor are higher than the pure gas activation energy.

Per (H ₂) mol/m ² .s.Pa								
$\Delta P = 0.5$ bar			$\Delta P = 1.0$ bar			$\Delta P = 1.5$ bar		
T (K)	Mixed gas	Pure gas	T (K)	Mixed gas	Pure gas	T (K)	Mixed gas	Pure gas
299	1.06E-10	6.74E-10	296	7.37E-10	1.11E-09	419	1.59E-09	3.46E-09
388	6.41E-10	2.56E-09	343	1.28E-09	2.69E-09	444	2.39E-09	3.59E-09
433	9.09E-10	2.77E-09	404	1.84E-09	3.18E-09	464	2.59E-09	3.79E-09
533	1.59E-09	3.96E-09	477	2.66E-09	3.72E-09	542	3.08E-09	5.46E-09

Table 5.7: Pure and Mixed gas hydrogen permeances of silica composite membrane for hydrogen separation.

Table 5.8 presents the nitrogen permeance for mixed gas experiment compared with pure gas permeation data at different temperature and pressure differentials. It can be seen that the mixed gas permeance is lower than the pure gas permeance at all the temperatures and pressure differentials tested for the composite membrane. Hence, it can be concluded that the presence of hydrogen in the system has the effect of decreasing the nitrogen flow rate.

Having observed the significant influence of hydrogen/nitrogen system for the hydrogen separation silica membrane, the activation energies of the composite membrane are evaluated for nitrogen permeation. The activation energy of the nitrogen varied between is 4.2 – 7.6 kJ/mol at pressure differential range between 0.5 to 1.5 bar. These values are lower than the corresponding pure gas activation energy for nitrogen (2.1 – 1.39 kJ/mol).

Per (N ₂) mol/m ² .s.Pa								
ΔP = 0.5 bar			ΔP = 1.0 bar			ΔP = 1.5 bar		
T (K)	Mixed gas	Pure gas	T (K)	Mixed gas	Pure gas	T (K)	Mixed Gas	Pure gas
299	2.12E-11	5.72E-10	296	6.88E-11	6.06E-10	419	1.03E-10	8.00E-10
388	5.42E-11	6.15E-10	343	8.36E-11	6.35E-10	444	1.79E-10	8.22E-10
433	4.36E-11	6.35E-10	477	4.16E-11	7.42E-10	464	2.38E-10	8.34E-10
533	1.27E-11	8.40E-10	519	5.14E-11	8.42E-10	542	3.59E-10	9.18E-10

Table 5.8: Pure and mixed gas nitrogen permeances of silica composite membrane for hydrogen separation.

5.4.4. Separation Factor

Table 5.9 summarises pure gas separation factors for nitrogen and propane gases with respect to hydrogen. It can be seen that H_2/N_2 selectivity varied from about 4 – 8 which is higher than Knudsen value. The respective Knudsen separation factor for this pair of gases is 3.74. It can be observed that both pressure and temperature have significant effect on the separation factor. For instance, at lower temperature, the selectivity for H_2/C_3H_8 gases is lower than Knudsen separation factor, which could indicate that the surface diffusion transport mechanism has a contribution as C_3H_8 is absorbable gas. In the mean time, when the temperature increases the selectivity increased and reached a value higher than Knudsen at higher temperature.

Gases pair	ΔP				
	T (K)	0.5	1	1.5	2
H_2/N_2 (3.741 ^a)	368	7.84	4.49	4.07	3.87
	472	7.3	5.15	4.73	4.6
	532	5.22	5.43	5.52	5.5
H_2/C_3H_8 (4.69 ^a)	368	1.3	1.37	1.26	1.23
	472	2.59	2.83	2.73	2.7
	532	5.16	4.95	4.87	4.82

^a Knudsen separation factor.

Table 5.9: Pure gas separation factors for separation membrane at different temperatures.

Figure 5.18 presents the variation of mixed gas separation factor evaluated from the composition of permeate and retentate stream. It can be seen from the figure that the separation factor increases with an increase in the temperature of the permeation at 0.5 and 1.0 bar. At pressure differentials of 1.5 bar, the S.F factor decreased with temperature to a lower value of 8.6 which is higher than Knudsen value.

Uhlhorn et al., (1989), reported for a H_2/N_2 mixture a decreased separation factor from 9 at pressure of 0.5 bar to separation factor value of 5 at 2.0 bar.

The reduction of separation factor was attributed to the decrease of surface diffusion contribution to the total permeation with increasing pressure due to saturation of the adsorption. At high pressure, the possibility of back diffusion phenomena can also reduce the separation factor. The separation factors are varied from 5 – 29, 11 – 52 and 9 – 16 at 0.5, 1.0 and 1.5 bar pressure differentials respectively. Corresponding pure gas separation factors are evaluated to vary to a maximum value of 8 at pressure of 0.5 bar. It can be concluded that the pure gas separation factor is much lower than the separation factor for mixed gas.

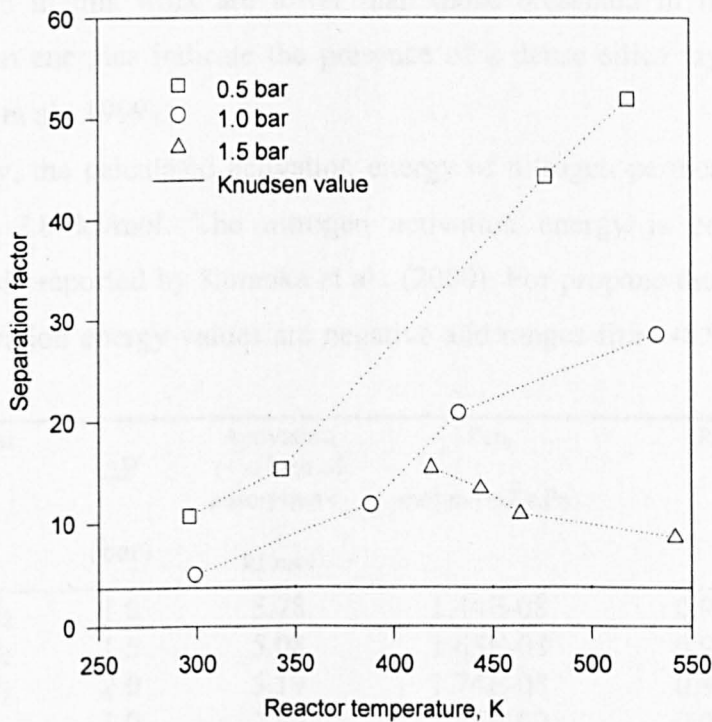


Figure 5.18: Mixed gas separation factors of silica composite membrane for hydrogen separation.

5.4.5. Gas flow mechanism

It is clear from the permeation and the separation factor results obtained that the flow mechanism of this membrane is a combination of surface diffusion mechanism for C_3H_8 and activated diffusion for other gases. Based on the equations provided in chapter 3, the activation energy and pre-exponential factor are evaluated for different gases at different pressures. The results of these calculations are summarised in Table 5.10. The table also presents the correlation coefficient (r^2) value which is a measure of the fitness of the straight line.

The activation energy for hydrogen is observed to vary between 5.19 – 5.78 kJ/mol. Corresponding values presented are 7.6 – 8 kJ/mol (De Vos and Verweij, (1998) and 13 – 15 kJ/mol (De Lange et al., (1995^b). Hence, the activation energy values measured in this work are lower than those presented in literature. The higher activation energies indicate the presence of a dense silica layer in the membrane (Hwang et al., 1999).

Similarly, the calculated activation energy of nitrogen permeation varied between 2.39 to 2.8 kJ/mol. The nitrogen activation energy is comparable with that previously reported by Kuraoka et al., (2000). For propane the results are different, the activation energy values are negative and ranges from -8.9 to -4.2. This shows

Gas	ΔP (bar)	Activation (+) / heat of adsorption (-) kJ/mol	Per_0 mol.m/(m ² .s.Pa)	R^2
H ₂	1.0	5.78	1.44E-08	0.996
H ₂	1.5	5.08	1.65E-08	0.993
H ₂	2.0	5.19	1.74E-08	0.996
N ₂	1.0	2.80	1.75E-09	0.996
N ₂	1.5	2.68	1.55E-09	0.997
N ₂	2.0	2.39	1.44E-09	0.997
C ₃ H ₈	1.0	-4.2	1.64E-10	0.995
C ₃ H ₈	1.5	-7.4	1.38E-10	0.997
C ₃ H ₈	2.0	-8.9	1.36E-10	0.979

Table 5.10: Activation energies and pre-exponential factors for hydrogen separation silica membrane.

that the activation energy is lower than the heat of adsorption and the apparent activation energy calculated is negative for propane. The pressure has impact on the activation energy of the gas permeating the membrane, which leads to change in separation factor. For instance, when the activation energy increases with pressure for hydrogen and decreases for nitrogen this would lead to increase the permeation of nitrogen and reduce the hydrogen therefore the S.F will decrease with pressure. This is due to the change of the transport mechanism contribution with pressure, which is controlled by the gas mean free path. In conclusion, the membrane performance depends on the transport mechanism contribution, the gas used and the interaction between the gas and the membrane material.

5.4.6. Membrane durability

For industrial applications of the membranes, not only a thin layer and separation properties are important, but also the durability of these membranes under test conditions. The hydrogen and nitrogen permeance under 1 bar and room temperature are shown in Figure 5.19 for six consecutive tests performed within 23 days of the initial run. It can be seen that the hydrogen permeance is more varied than nitrogen permeance which could be due to many reasons such as hydrogen molecular weight, and hydrogen membrane interaction. In general the silica membrane for hydrogen separation is fairly durable and stable to the extent of the testing period. This is the most important feature that has to be stressed for the industrial application of silica membranes.

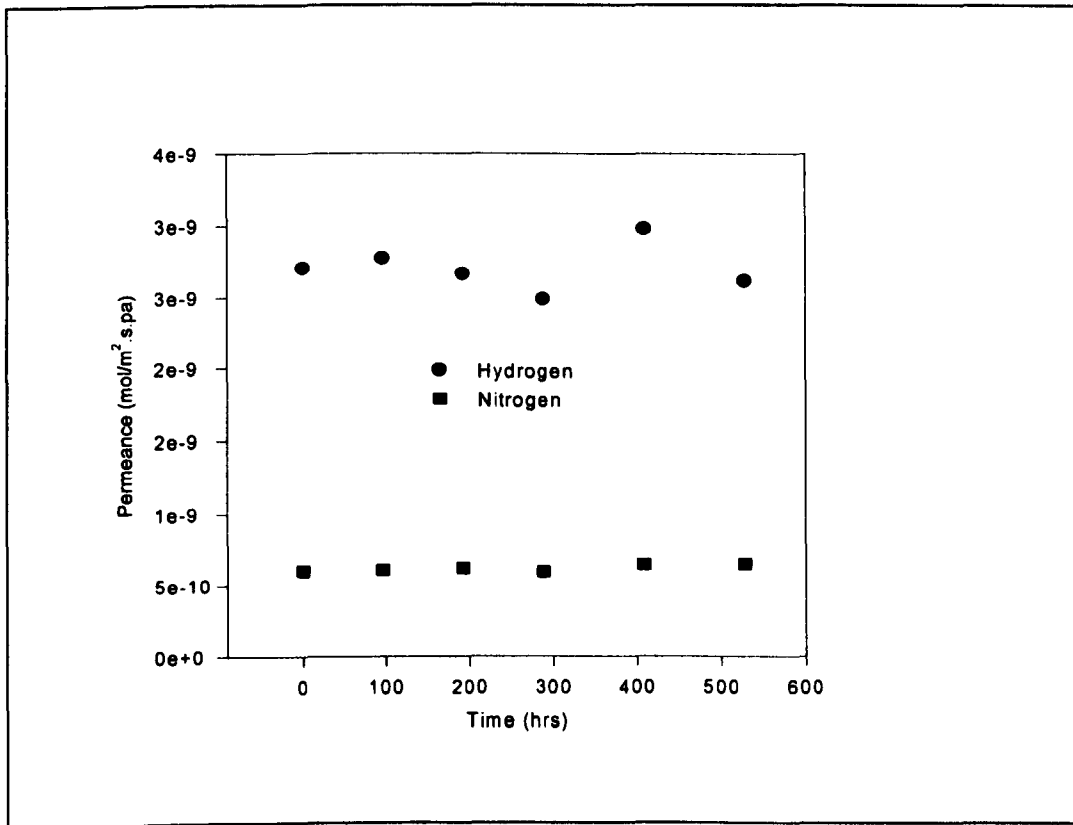


Figure 5.19: Durability for hydrogen separation silica membrane.

5.5. Silica membrane for hydrogen purification

5.5.1. Pore size and surface characterization

Table 5.11 presents the pore size of silica composite membrane prepared for hydrogen purification. The obtained results are in good agreement with the prepositions expected for this type of membrane. It is apparent from the table that the pores with an average diameter of ≥ 11.2 nm contribute insignificantly to the total pore volume. The major contributors to the total pore volume are the pores with an average diameter of ≤ 9.4 nm. This indicates that the membrane underwent significant reduction in pore size. Of note is that the small pores with an average diameter had the highest contribution to the total pore volume at 16.7 %. Therefore, it can be concluded that significant reduction in pore size has occurred in the silica membrane prepared for hydrogen purification. In other words, higher separation factors can be expected based on this pore size distribution.

pore diameter (nm)	BJH desorption pore volume cm^3/g	% Contribution to total pore volume
66.2800	0.003488	1.635348
42.9400	0.005634	2.641499
28.4200	0.007983	3.742827
21.7200	0.006194	2.904055
17.7000	0.007067	3.31336
14.8000	0.007553	3.541221
12.7000	0.007950	3.727355
11.2200	0.007000	3.281947
9.4400	0.015113	7.085724
7.7200	0.017621	8.261599
6.5200	0.017109	8.021548
5.6400	0.017870	8.378343
4.9400	0.018455	8.65262
4.3800	0.019678	9.226023
3.9200	0.020034	9.392933
3.4800	0.034509	16.17953
1.7000	0.000030	0.014065

Table 5.11: Pore size distribution of the silica composite membrane prepared for hydrogen purification.

Other results obtained from ASAP analysis are as follows. The BET surface area of the composite membrane is about $275.62 \text{ m}^2/\text{g}$ which is higher than the BET surface area of both membranes prepared for reaction and separation. Therefore, this result confirms that the surface underwent significant pore size modification. The BJH desorption total volume is about $0.2132 \text{ cm}^3/\text{g}$.

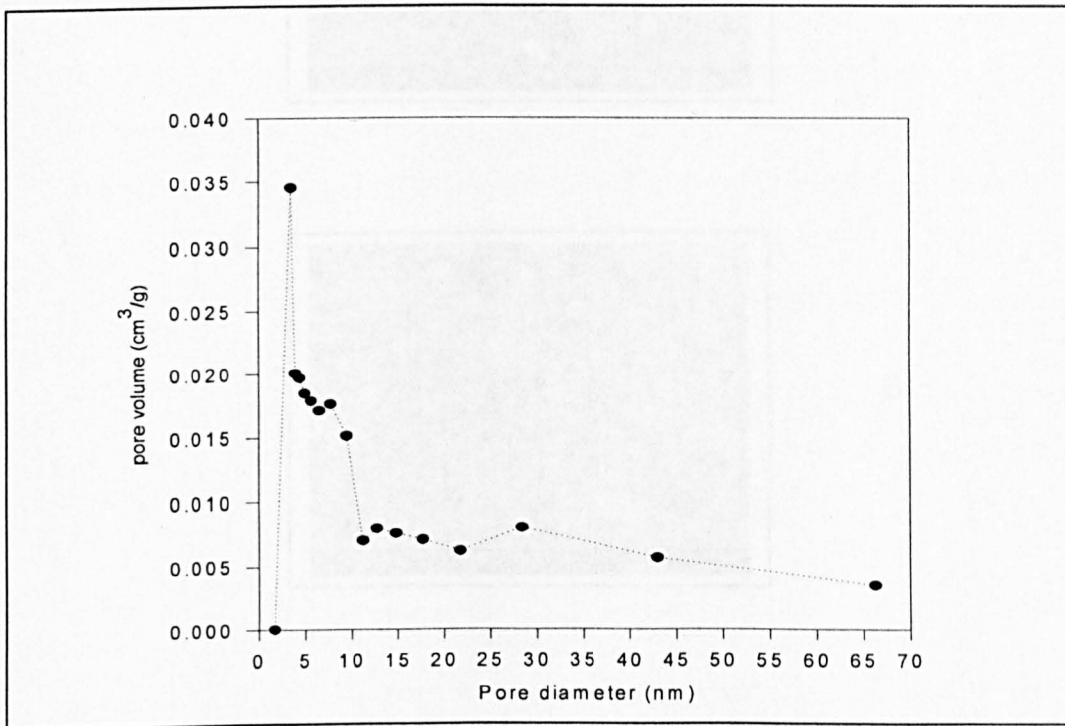
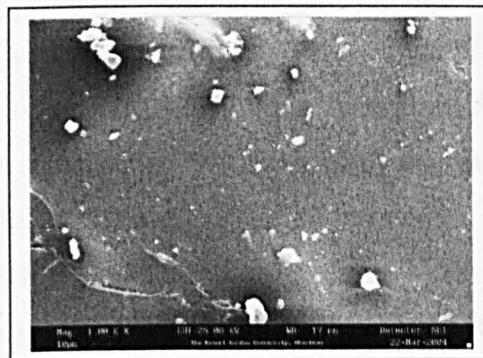


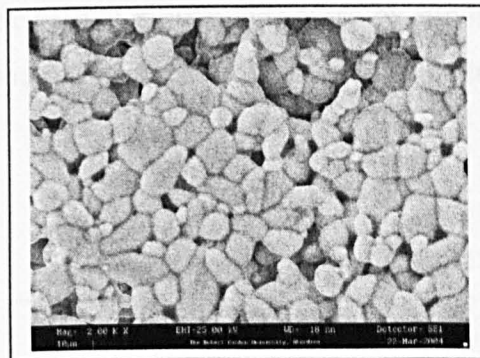
Figure 5.20: Pore size distribution of the silica membrane for hydrogen purification applications. (Nitrogen Adsorption)

Figure 5.21 presents the SEM micrographs of the purification membrane for outer surface (A), inner surface (B) and cross section (C). It can be seen that the outer surface underwent surface modification with silica with deposition fully covers the porous support and no crack appears in the thick membrane. The thickness of the silica film measured from the cross section micrograph is about 40 - 50 microns based on the scale presented for the micrograph.

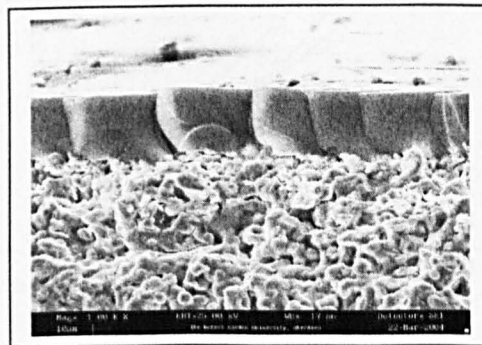
The EDX analysis of the outer and inner surface provided conclusions similar to that observed from micrographs. The EDX analysis of the outer surface provided 92.6 % Si, 7.0 % Ti and 0.4 % Cl. The EDX analysis of the inner surface provided 96 % Ti, 1.0 % Al and 3.0 % Si.



A



B



C

Figure 5.21: SEM micrographs of the purification membrane A) Outer surface B) Inner surface and C) Cross section.

5.5.2. Pure gas permeation

Figure 5.22 shows the temperature dependence of the pure gas permeance of hydrogen at different transmembrane pressure difference for the hydrogen purification silica membrane. The hydrogen permeance increases with increasing temperature due to an activated diffusion mechanism in the small pores of the silica layer. The membrane exhibits a hydrogen permeance varied from 3.86×10^{-10} (at room temperature) to 4.1×10^{-9} mol/m².s.Pa (at 238 °C). Sea et al., (1996) reported a hydrogen permeance of about 1.1×10^{-9} mol/m².s.Pa for a membrane at 200 °C formed with TEOS in α -alumina tube. In other words, it can be concluded that the membrane prepared using silicon elastomer by modified dip coating technique to plug the membrane macropores provides similar hydrogen permeance performance

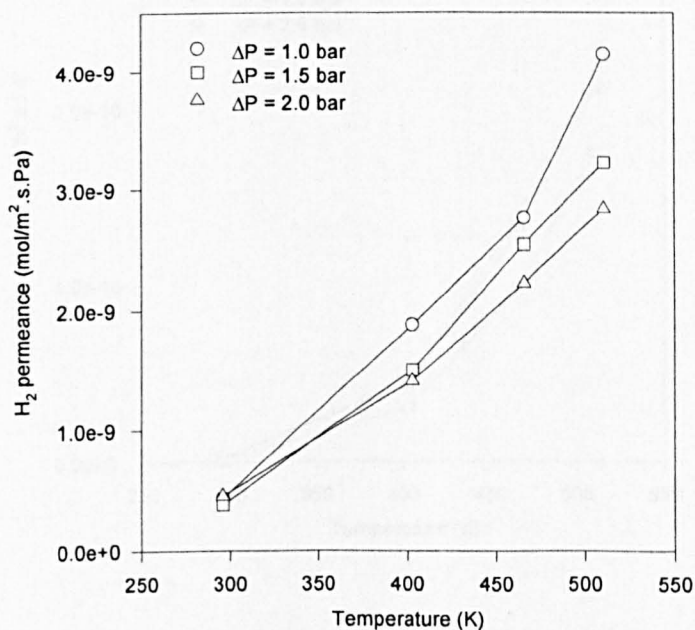


Figure 5.22: Hydrogen permeances of silica membrane for hydrogen purification.

as that developed by Sea et al., (1996) using chemical vapor deposition.

The influence of pressure and temperature on nitrogen permeance is shown in Figure 5.23 for the hydrogen purification silica membrane. Nitrogen permeance is lower than hydrogen permeance and varied from 1.3×10^{-12} (at 25 °C) to 1.6×10^{-10} mol/m².s.Pa (at 238 °C). For comparative purpose, again it was shown by Sea et al., (1996) that nitrogen permeance is about 4×10^{-10} mol/m².s.Pa for a membrane at 200 °C. The impact of transmembrane pressure on the performance of nitrogen permeance of hydrogen purification silica membrane at different temperature is minor. The nitrogen permeance is observed to be increased slightly with pressure as the temperature increased. In other words, the impact of temperature is stronger than the impact of pressure on nitrogen permeances.

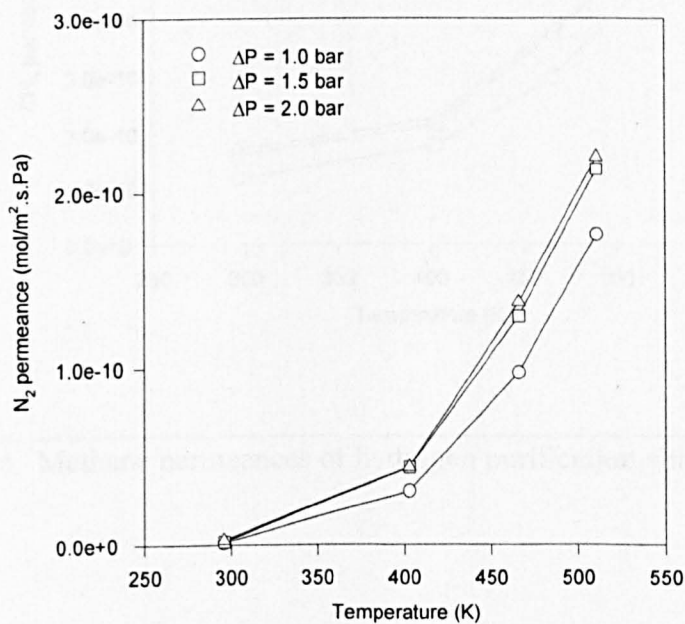


Figure 5.23: Nitrogen permeances of silica membrane for hydrogen purification.

Figure 5.24 presents methane permeance as a function of temperature and transmembrane pressure difference for the hydrogen purification membrane. The permeance of methane varied from 1.18×10^{-10} (at room temperature) to 5.17×10^{-10} mol/m².s.Pa (at 238 °C). It can be explained from the figure that the permeation of methane is influenced with temperature especially at higher temperature.

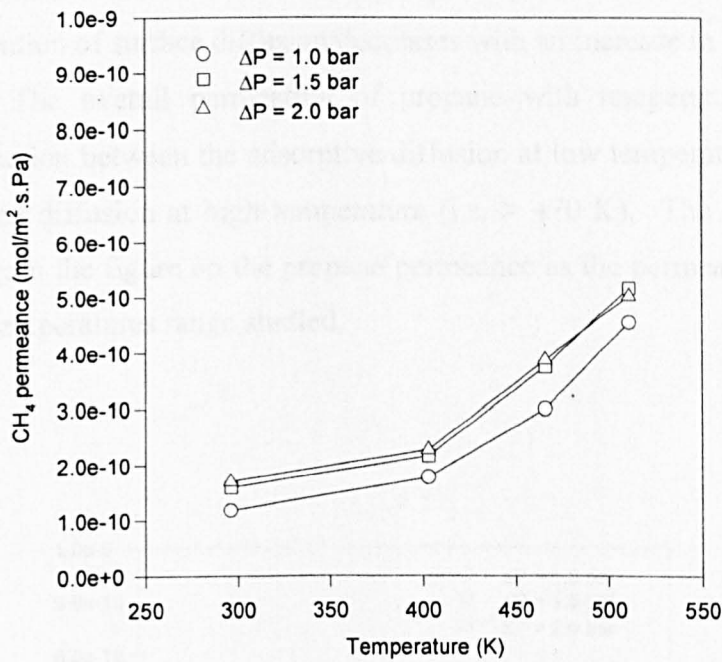


Figure 5.24: Methane permeances of hydrogen purification silica membrane.

Figure 5.25 presents propane permeance as a function of temperature and transmembrane pressure difference for the hydrogen purification membrane. It can be seen that the permeation of propane has completely different profile compared with the other gases (i.e. H_2 , N_2 and CH_4). The permeation decreased with temperature up to 470 K where the permeation starts to increase. The propane permeation obtained is 6.2×10^{-10} mol/m².s.Pa (at room temperature) and 6.4×10^{-10} mol/m².s.Pa (at 238 °C). Therefore, the propane permeation reduction at lower temperature could be due to the adsorption phenomena, which indicates that the contribution of surface diffusion decreases with an increase in temperature (Schafer, 2001). The overall permeation of propane with temperature could be due to combination between the adsorptive diffusion at low temperature (i.e. < 470 K) and activated diffusion at high temperature (i.e. > 470 K). The impact of pressure is clear from the figure on the propane permeance as the permeation profiles matched at the temperatures range studied.

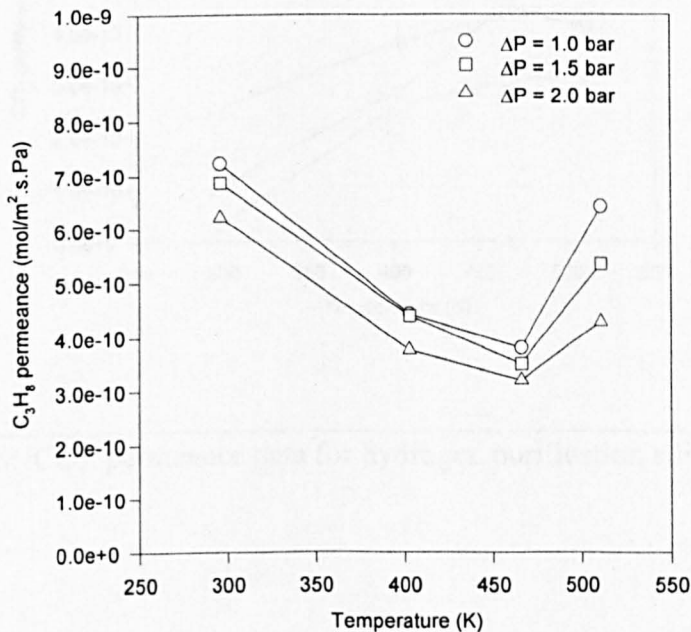


Figure 5.25: Propane permeance for hydrogen purification silica membrane.

The silica membrane performance for hydrogen purification has been tested using other gases such as CO₂. Figure 5.26 presents CO₂ permeance as a function of temperature and transmembrane pressure difference. The permeation of CO₂ increased with temperature with values varied from 4.2×10^{-12} mol/m².s.Pa (at room temperature) to 6.2×10^{-10} mol/m².s.Pa (at 238 °C). At low to moderate temperature, the permeation profiles of CO₂ increased to higher values at higher permeation pressure. Carbon dioxide permeation shows similar behaviour as activated transport for membranes characterized by a hydrogen activation energy higher than around 10 kJ/mol (De Lange et al., 1995^b). De Vos et al., (1998), reported an opposite behaviour for CO₂ permeance as it decreased with temperature.

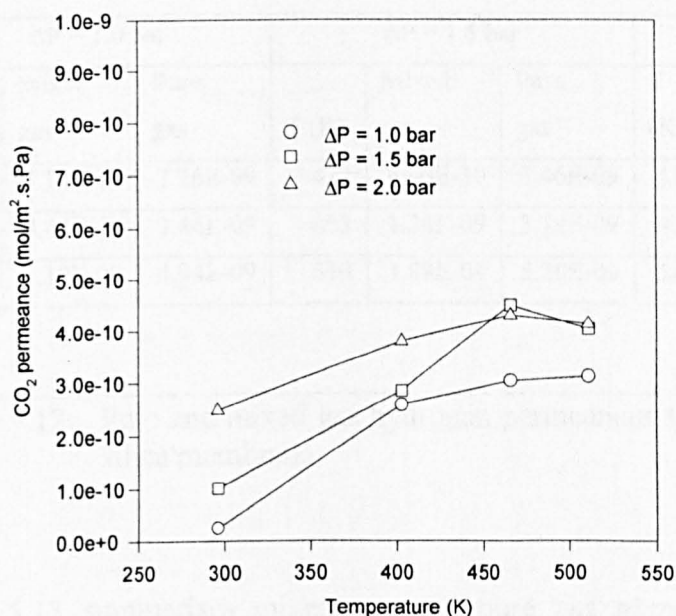


Figure 5.26: CO₂ permeance data for hydrogen purification silica membrane.

5.5.3. Mixed gas permeation

Permeance results as a function of temperature are presented in Tables 5.12 and 5.13. Table 5.12 summarises mixed gas as well as pure gas hydrogen permeances for the hydrogen purification membrane. It can be seen from the table that the mixed gas hydrogen permeances are lower than the pure gas hydrogen permeances at different transmembrane pressure differentials. Hence, it can be explained that the permeation rate of hydrogen is affected by the presence of nitrogen as compete gas under these conditions. In this regard, this statement (i.e the mixed gas permeance is lower than the pure gas permeance) has been reported in literature (Hassan et al., 1995).

Per (H ₂) mol/m ² .s.Pa								
ΔP = 1.0 bar			ΔP = 1.5 bar			ΔP = 2.0 bar		
T (K)	Mixed gas	Pure gas	T (K)	Mixed gas	Pure gas	T (K)	Mixed gas	Pure gas
422	7.14E-10	3.26E-09	422	9.90E-10	3.46E-09	422	1.11E-09	3.55E-09
452	8.42E-10	3.44E-09	463	1.24E-09	3.79E-09	472	1.30E-09	4.05E-09
533	1.19E-09	4.94E-09	539	1.89E-09	5.26E-09	547	1.72E-09	5.80E-09

Table 5.12: Pure and mixed gas hydrogen permeances for the hydrogen purification silica membrane.

Table 5.13 summarises mixed gas and pure gas nitrogen. Again the nitrogen permeance in mixed gas is lower than the pure gas nitrogen permeance at different transmembrane pressure differentials. Hence, it can be explained that the permeation rate of nitrogen is strongly affected by the presence of hydrogen as compete gas under these conditions. It can be concluded that the presence of hydrogen in the system would decrease the nitrogen flow rate due to the activity of hydrogen with temperature.

Per (N ₂) mol/m ² .s.Pa								
ΔP = 1.0 bar			ΔP = 1.5 bar			ΔP = 2.0 bar		
T (K)	Mixed gas	Pure gas	T (K)	Mixed gas	Pure gas	T (K)	Mixed gas	Pure gas
422	8.92E-13	6.88E-10	422	3.12E-12	8.00E-10	422	3.79E-12	8.51E-10
452	1.81E-12	7.15E-10	463	4.32E-12	8.34E-10	472	5.07E-12	8.82E-10
533	5.63E-12	8.82E-10	539	8.40E-12	9.29E-10	547	9.31E-12	9.67E-10

Table 5.13: Pure and mixed gas nitrogen permeances for the hydrogen purification silica membrane.

5.5.4. Separation factor

Table 5.14 summarises the pure gas separation factors for different pairs of gases expressed as a function of temperature and pressure. The H₂/N₂ separation factor varied from (12.84 - 62.22) for various temperature and pressure effects. For H₂/N₂ the high temperature separation factor is much above the corresponding Knudsen separation factor (3.74). The separation factor at a selected temperature increases as the pressure decreases.

The separation factor for H₂/C₃H₈ can be observed to be below and above a Knudsen value (4.69) at this range of temperature (100 - 250 °C). This reflects the presence of surface diffusion phenomena for propane permeation as presented earlier. The maximum separation factor obtained at temperature (200 °C) is 7.29 which is higher than the corresponding Knudsen separation factor (4.69). Similarly the H₂/CO₂ separation factor varied from 2.74 to 6.64 for a corresponding Knudsen separation factor of 4.69. It can be expected that the separation factor can achieve higher values at a higher temperature of 400 °C. H₂/CH₄ separation factor is varied from 5.64 to 10.57 which is higher than the corresponding Knudsen separation factor (2.83).

ΔP (bar)	T (K)	H_2/N_2^a (3.74)	$H_2/C_3H_8^a$ (4.69)	H_2/CH_4^a (2.83)	H_2/CO_2^a (4.69)
1	403	62.22	4.27	10.57	3.67
	466	28.28	7.29	9.21	4.56
	511	23.52	6.48	9.15	6.64
1.5	403	34.30	3.42	6.93	3.02
	466	19.74	7.28	6.79	4.51
	511	15.10	6.06	6.26	5.36
2	403	32.31	3.76	6.22	2.74
	466	16.20	6.96	5.75	3.89
	511	12.84	6.67	5.64	4.61

^a Knudsen separation factor

Table 5.14: Pure gas separation factors for the hydrogen purification silica.

The membrane has been tested using a membrane reactor assembly for their separation capability at different temperatures using 50 % H_2 / 50 % N_2 mixture. The mixed gas separation factors observed to vary from 1260 - 757, 1361 - 567 and 1556 - 436 (product purities of 99.92 - 99.86 %, 99.92 - 99.82 %, 99.93 - 99.97 %) respectively with a temperature variation from 25 - 300 °C at 1.0, 1.5 and 2.0 bar pressure differentials respectively. Corresponding hydrogen permeances are observed to be 7.14×10^{-10} - 1.19×10^{-9} , 9.9×10^{-10} - 1.89×10^{-9} , 1.11×10^{-9} - 1.72×10^{-9} mol/m².s.Pa at different pressure differentials 1.0, 1.5 and 2.0 bar respectively. Corresponding pure gas separation factors are evaluated to vary from 12 - 62 at the highest temperature investigated (280 °C). It can be concluded that the pure gas separation factor is much lower than the observed separation factors for mixed gas permeation. Furthermore, it can be observed from these values that the separation factor decreased with an increase in the temperature and pressure.

5.5.5. Gas flow mechanism

These results show that the transport of gases through the membrane is activated as the permeance increased with the temperature except for propane permeation. The activation energy is an important parameter that can be used parallel to the permeance and selectivity to evaluate the membrane quality. For instance, the activation energy for hydrogen permeance gives a good correlation with the separation factor and is used as a measure of quality (Burggraaf, 1996). The hydrogen activation energy of high quality membranes is not less than 10 kJ/mol (De Lange, 1995).

Table 5.17 summarises the activation energies for the permeation of different gases through silica purification membrane. The activation energy for pure hydrogen permeation system has a value of 13 kJ/mol to 10.6 kJ/mol for a variation in trans-membrane pressure from 1.0 bar to 2.0 bar. Typical results of the activation energy for hydrogen permeance for high quality silica membranes were reported by Sea et al., (1996), Wu et al., (1994) and De Lange et al., (1995^a) are 11-14, 11 and 15 kJ/mol respectively. It was thus concluded that the activation energy values obtained in this work (10.6 - 13) are close to that reported and categorized as high quality membranes.

The activation energy for nitrogen varied from 26.1 - 28.7 kJ/mol which is higher than hydrogen for a same variation in pressure differentials. This means that the nitrogen is more affected from the membrane densification than hydrogen due to the kinetic diameter difference. Therefore, even small differences in the kinetic diameters of the gas molecules result in large divergences in the values of the activation energy. Large differences in the activation energy of diffusion provide even larger differences in the permeability coefficients as the permeability coefficient is an exponential function of the activation energy (Shelekhin et al., 1995).

Activation energies for propane permeation through hydrogen purification membrane are observed to be negative. This can be attributed to the adsorption energy onto the surface exceeding the energy of diffusion through the pores. This

can explain the negative activation energy observed for propane which has a higher heat of adsorption than the other gases (De Lange et al., 1995^b). The activation energy of CO₂ decreased from 4.2 to 2.8 kJ/mol for a pressure differential variation from 1.0 to 2.0 bars.

The mixed gas hydrogen activation energy is evaluated to vary from 6.78 – 12.26 kJ/mol as opposed to the pure gas activation energies evaluated to vary from 10.6 – 13 kJ/mol. Hence, it can be observed that the activation energy of hydrogen is lower with the presence of nitrogen. The dependency of the hydrogen permeation of temperature in the case of mixed gas is less strong; this results in a decrease of the activation energies for hydrogen permeation from 10.6 to 13 kJ/mol.

The activation energy for nitrogen (i.e. in H₂/N₂ mixture) is evaluated to vary from 13.88 – 19.47 kJ/mol as opposed to the pure nitrogen gas activation energy which is varied from 26.1 – 28.7 kJ/mol.

Table 5.15 also summarises the pre-exponential factors for the permeation of different gases at different transmembrane pressure differentials (1.0 to 2.0 bar). It can be observed from the table that the pre-exponential factor value decreased for all gases as the pressure increases. Similar variation in activation energy is observed to account for the corresponding variations in permeation profiles.

Gas	E _{ac} (kJ/mol)			Per ₀ (mol/m ² .s.Pa)		
	ΔP = 1.0 bar	ΔP = 1.5 bar	ΔP = 2.0 bar	Per ₀	Per ₀	Per ₀
H ₂	13.00	12.50	10.6	7.13E-08	4.73E-08	3.97E-08
N ₂	28.7	28.4	26.1	1.18E-07	1.12E-07	1.11E-07
C ₃ H ₈	-15.8	-14.6	-10.7	3.76E-07	3.27E-08	1.18E-08
CH ₄	18.6	16.5	16	3.61E-08	2.47E-08	2.24E-08
CO ₂	4.2	3.1	2.8	1.54E-09	1.25E-09	1.19E-09

Table 5.15: Activation energies and pre-exponential factor for permeation of different gases through hydrogen purification composite membrane

5.5.6. Ternary mixture separation

Since high purity hydrogen (up to 99.9 %) is obtained in this work using mixed gas (i.e. H₂/N₂ mixture) permeation, the hydrogen purification membrane is also evaluated for its performance for a ternary gas mixture to investigate the ability of the membrane to produce high purity hydrogen with different gas compositions. The gas mixture consisting of 49 % hydrogen, 20 % methane and 31 % CO₂ and the corresponding ternary separation factors varied from 534 – 1873 at 60 – 300 °C (hydrogen purity of 99.82 – 99.94 %) at a transmembrane pressure differential of about 1.0 bar.

Table 5.16 illustrates the pure gas and ternary gas mixture hydrogen permeances for the hydrogen purification silica membrane. The operation temperature of the membrane shall not exceed a value of about 300 °C.

$\Delta P = 1.0$ bar				$\Delta P = 1.5$ bar			
T (K)	Ternary mixture	T (K)	Pure gas	T (K)	Ternary mixture	T (K)	Pure gas
353	6.02E-09	296	2.75E-09	298	1.04E-09	296	1.20E-09
383	7.59E-09	403	3.07E-09	370	1.60E-09	403	3.38E-09
403	1.15E-08	466	3.18E-09	428	2.44E-09	466	3.79E-09
453	2.25E-08	511	3.44E-09	463	6.88E-09	511	4.72E-09

Table 5.16: Pure and ternary hydrogen permeances for hydrogen purification membrane.

Figure 5.27 summarises the separation factors obtained at 1.0 and 1.5 bar pressure differentials across the hydrogen purification silica membranes. It can be clearly seen that the separation factors are very high (534 – 1873) for a transmembrane pressure differential of about 1.0 bar. This result indicates that the modified membrane could be effectively employed in the separation of hydrogen from different gas mixtures. At pressure of 1 bar the separation factor increases as a function of temperature, because the temperature dependency of the hydrogen permeance is higher than that of the methane and carbon dioxide permeances.

It can be seen also that the influence of an increased feed pressure from 1.0 to 1.5 bar, results in a decrease of the separation factors from about 21 – 12 at a transmembrane pressure differential of about 1.5 bar. This can be explained by the fact that the sorption capacity of methane and carbon dioxide will increase stronger as a function of pressure compared to hydrogen under the present experimental conditions.

Consequently, the concentration of hydrogen will decrease stronger in the feed side compared to methane and carbon dioxide leading to lower hydrogen selectivity.

The activation energy of hydrogen is varied from 18 – 11.1 kJ/mol. These values are high compared with the values obtained from the pure gas permeation data (9 – 14 kJ/mol). A significant increase in activation energy can be linked with the presence of other components in the permeating system. This is similar to the results obtained for mixed gas permeation.

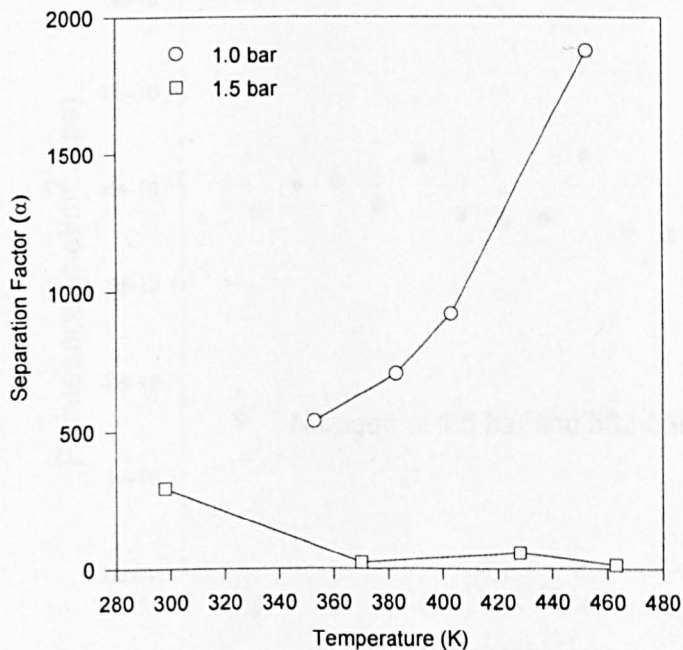


Figure 5.27: Separation factors for hydrogen purification silica membrane using ternary gas mixture.

5.5.7. Membrane Stability and Durability

The thermal stability of a membrane is important in terms of practical applications. Thus, the stability of the membrane prepared for hydrogen purification application was tested using nitrogen gas flowing under 1.5 bar and average temperatures of 565 K for nine consecutive tests performed within 37 days of the initial run. Figure 5.28 shows changes in nitrogen permeance between 3.47×10^{-10} to 4.33×10^{-10} . Figure 5.29 also shows the durability of the membrane using two different gases (H_2 & N_2) at temperature of 296 and 511K. It is clear from Figure 5.29 that the permeance was more affected at high temperature. This indicates that the membrane is less durable at high temperature and also depends on the gas used. For instance, the membrane is more durable with nitrogen than hydrogen at the same temperature.

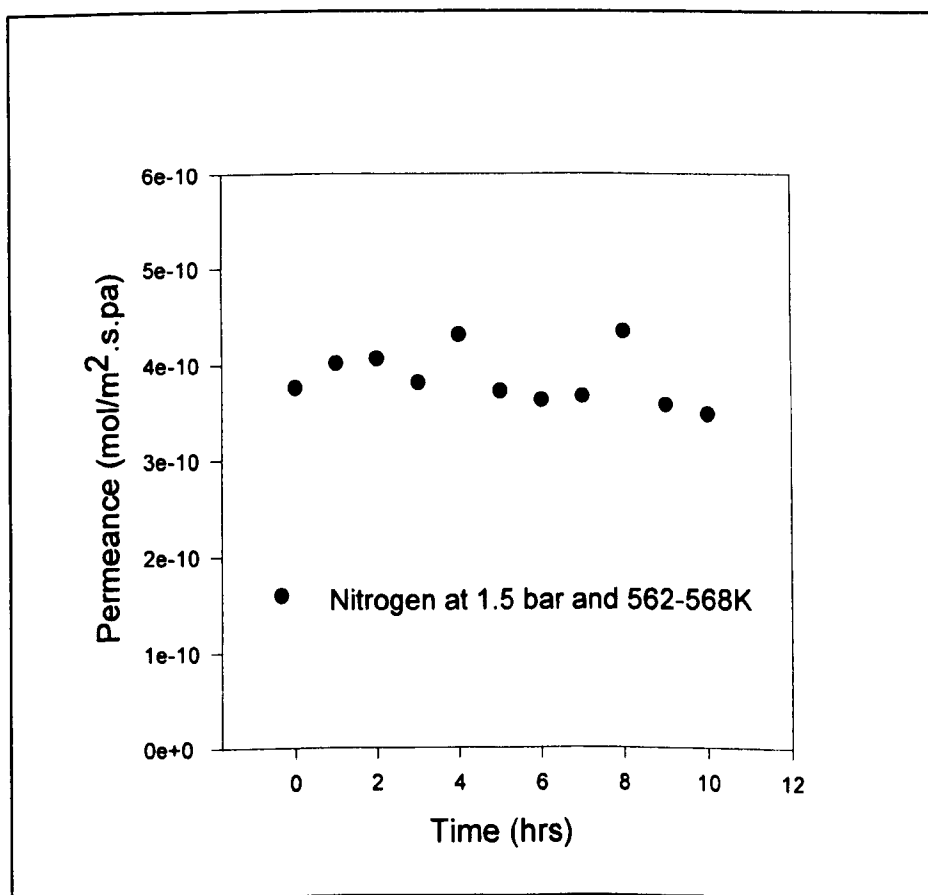


Figure 5.28: Membrane Stability for the hydrogen purification silica composite.

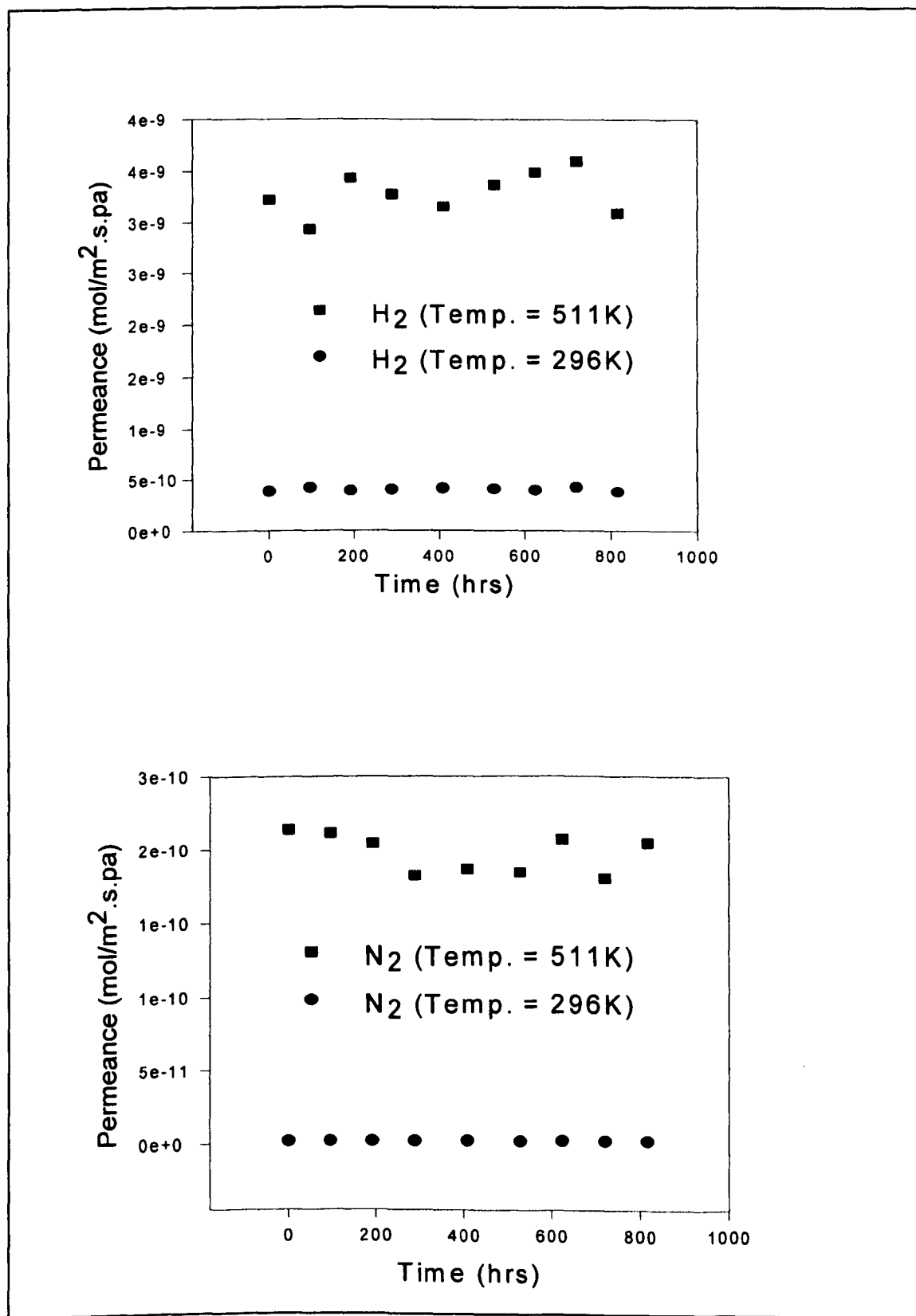


Figure 5.29: membrane durability for the hydrogen purification silica composite.

5.5.8. Membrane preparation reproducibility

Both the reproducibility of the membrane preparation and following gas permeation tests have been tested by preparing two membranes using the same experimental procedure. Although, inconsistent performance in gas permeances and selectivity values was noticed between two membranes (1 & 2) nominally identical membranes, the behaviour of these membranes during extended temperature–time tests were similar. The permeances and selectivity values differences occurs for many reasons. For instance, the sensitivity of these membranes to defects due to the manual preparation procedure and gas molecules adsorbing in the micropores of the silica layer.

Table 5.17 presents the results of pure gas permeances and selectivity using hydrogen and nitrogen gases. The results seem to show poor reproducibility of measurement, which is manifested in a clear difference between two consequently taken permeance and selectivity measurements.

In conclusion, it seems that it is not possible to re-produce membranes using this experimental procedure and therefore more developed procedure needs to be obtained to improve the reproducibility.

Hydrogen permeance (Membeame 1)			
Temperature K	$\Delta P = 0.5$ bar	$\Delta P = 1.0$ bar	$\Delta P = 1.5$ bar
403	1.88E-09	1.5E-09	1.41E-09
466	2.76E-09	2.54E-09	2.22E-09
511	4.15E-09	3.23E-09	2.84E-09
Hydrogen permeance (Membeame 2)			
Temperature K	$\Delta P = 0.5$ bar	$\Delta P = 1.0$ bar	$\Delta P = 1.5$ bar
403	3.75E-09	3.59E-09	1.41E-09
466	4.76E-09	4.47E-09	2.22E-09
511	5.15E-09	4.87E-09	2.84E-09
Nitrogen permeance (Membeame 1)			
Temperature K	$\Delta P = 0.5$ bar	$\Delta P = 1.0$ bar	$\Delta P = 1.5$ bar
403	3.02E-11	4.36E-11	4.37E-11
466	9.74E-11	1.29E-10	1.37E-10
511	1.76E-10	2.14E-10	2.21E-10
Nitrogen permeance (Membeame 2)			
Temperature K	$\Delta P = 0.5$ bar	$\Delta P = 1.0$ bar	$\Delta P = 1.5$ bar
403	5.63E-11	6.36E-11	3.99E-11
466	8.33E-11	9.51E-11	8.25E-11
511	1.99E-10	2.69E-10	1.84E-10

Separation Factor (Membrane 1)

Gases pair	T (K)	0.5	1	1.5
	H ₂ /N ₂ (3.741 ^a)	403	62.25	34.40
466		28.34	19.69	16.20
511		23.58	15.09	12.85

Separation Factor (Membrane 2)

Gases pair	T (K)	0.5	1	1.5
	H ₂ /N ₂ (3.741 ^a)	403	66.61	56.45
466		57.14	47.00	26.91
511		25.88	18.10	15.43

Table 5.17: Reproducibility test of the silica membrane for purification applications evaluated from gas permeance.

5.6. Palladium Impregnated Silica Membrane

5.6.1. Pore size and surface characterization

Table 5.18 and Figure 5.30 present the pore size and pore size distribution in the palladium impregnated silica membrane. The obtained results show the pore sizes range from 1.88 to 63.90 nm and the pores with an average diameter of 8.36nm shows the highest contribution to the total pore volume. It is obvious from the table that the pores with relatively larger diameter ($d_p \geq 10.48$ nm) did not contribute to the total pore volume significantly. This implies that the membrane underwent a noticeable reduction in pore size. For example, the percentage contribution to total pore volume of pores with an average diameter of 63.9 nm is 1.89 % in comparison to the pores with an average diameter of 5.82 nm at 7.35 %. Therefore, it can be concluded that significant reduction in pore size has occurred in the palladium impregnated silica membrane.

Other results obtained from ASAP analysis are as follows. The BET surface area of the composite sample is about 255.87 m²/g and the pore volume is about 0.19 cm³/g.

pore diameter (nm)	BJH desorption pore volume cm ³ /g	% Contribution to total pore volume
63.9	0.00307	1.886236
41.48	0.00509	3.127342
28.66	0.005707	3.506433
21.28	0.005959	3.661264
16.82	0.005776	3.548827
13.88	0.005861	3.601052
11.78	0.005862	3.601666
10.48	0.003909	2.401725
8.36	0.014776	9.078509
6.88	0.008558	5.258113
5.82	0.01196	7.348333
4.92	0.011648	7.156637
4.22	0.011698	7.187358
3.64	0.011476	7.050959
3.18	0.011212	6.888755
2.78	0.010708	6.579093
2.42	0.011841	7.275218
2.12	0.00833	5.118028
1.88	0.009317	5.72445

Table 5.18: Pore size distribution of the palladium impregnated membrane.

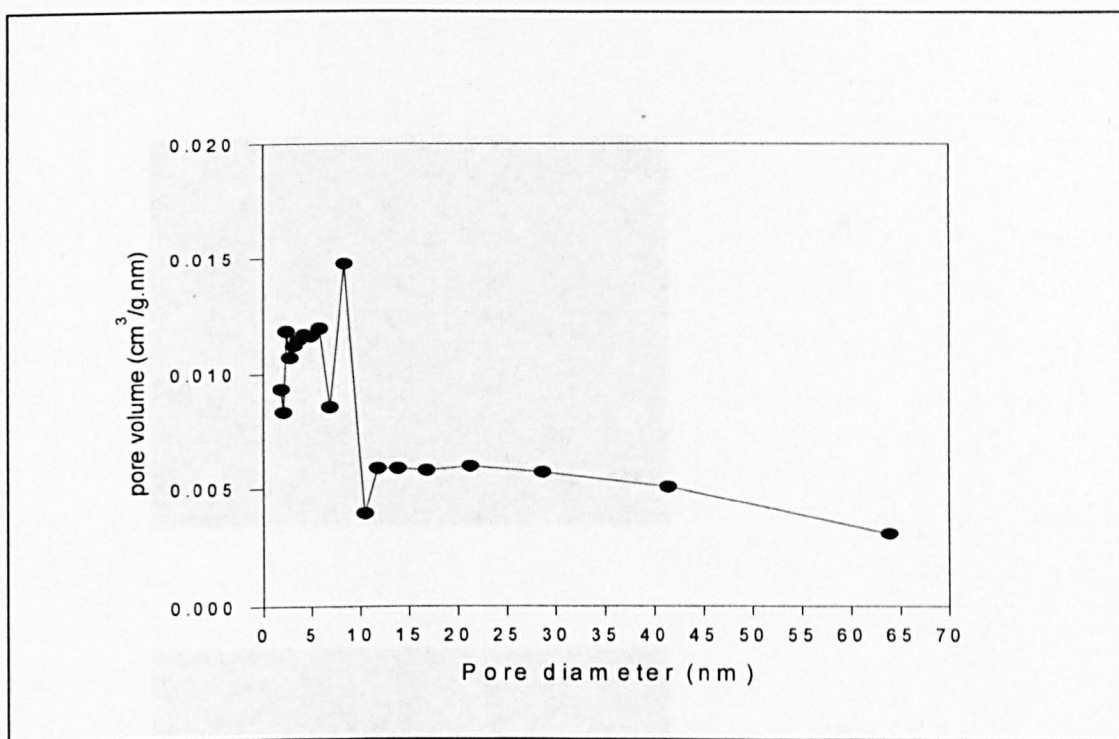
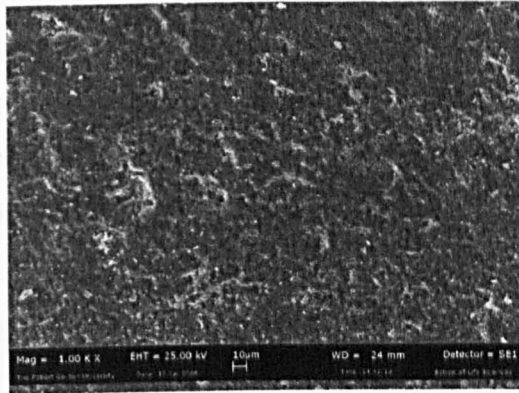
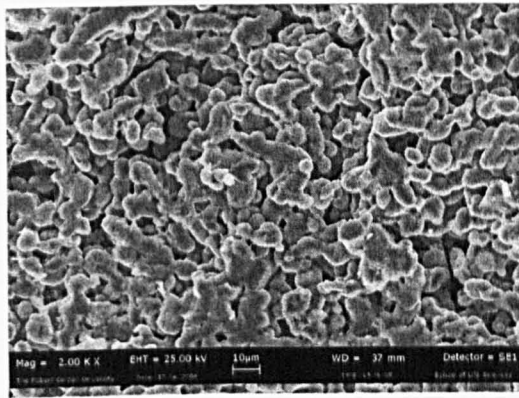


Figure 5.30: Pore size distribution of the palladium impregnated membrane

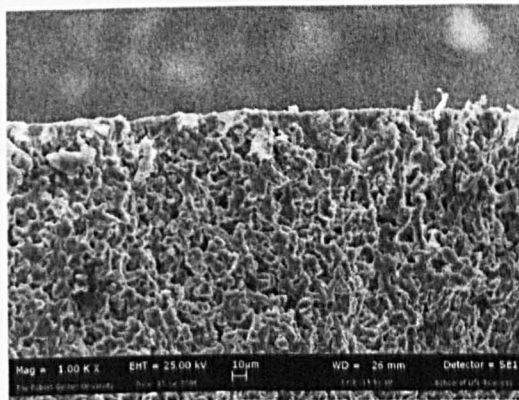
Figure 5.31 show the top surface and the cross section of Pd impregnated silica membrane obtained by SEM. No crack or cleavage can be seen on the surface of the palladium modified alumina membrane, which indicated that the addition of palladium did not destroy the uniform membrane. From the cross section of the membrane, it can be seen that the modified layer is on the top of the tube and the thickness of the membrane is about 2 - 3 μm . As the average pore size of the membrane support is much larger than that of the membrane, intermediate layer like is formed between the support and the top layer of the membrane during the repeated dipping, drying and calcinations process as observed from cross section. The EDXA of the membrane surface provided 93.3 % Si, 2.6% Al and 4.1% Ti.



A



B



C

Figure 5.31: SEM micrographs of the palladium A) Outer surface B) Inner surface and C) Cross section.

5.6.2. Pure gas permeation

Figure 5.32 presents the hydrogen permeation through palladium impregnated γ -alumina membrane at different transmembrane pressure differentials (0.5 – 2.0 bar) and at different temperatures (300 – 800 K). The permeance of hydrogen through the composite membrane showed a complicated dependence on temperature. Below 600 K, the hydrogen permeance decreased as temperature increased whereas above 600 K these permeances increased with temperature. The hydrogen permeance varied from a value of about 2.6×10^{-6} mol/m².s.Pa to a value of about 2.2×10^{-6} mol/m².s.Pa at 300 K with a pressure differential variation from 0.5 to 2.0 bar. When the transport rates decrease as function of temperature the gas transport mechanisms are Knudsen and surface diffusion (De Lang, 1995^b). According to this statement, the membrane transport mechanism can be explained to be combination between surface diffusion below 600 K and activated diffusion above this temperature.

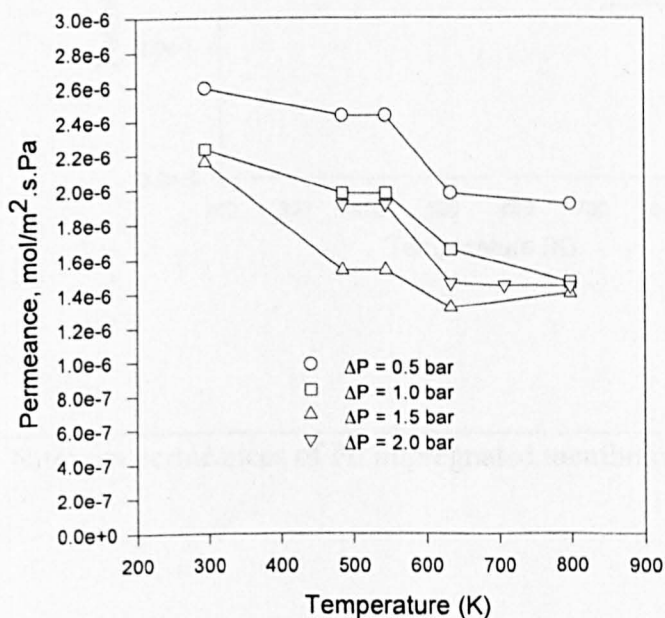


Figure 5.32: Hydrogen permeances of Pd impregnated membrane.

Unlike the distinct permeation profiles showed for hydrogen gas, the permeances of nitrogen through the impregnated membrane are not significantly dependent on the pressure differentials (0.5 – 2.0 bar) as shown in figure 5.33. In this membrane, there is a decrease of permeance with increasing permeation temperature up to about 600K and the permeance was nearly constant with increasing pressure difference. It means that contribution of surface diffusion decreased at higher than 600K and the contribution of activated increases. This variation in the gaseous transport can provide a complex transport mechanism. The nitrogen permeances obtained is in the range of about $5e^{-7}$ mol/m².s.Pa – $3e^{-7}$ mol/m².s.Pa.

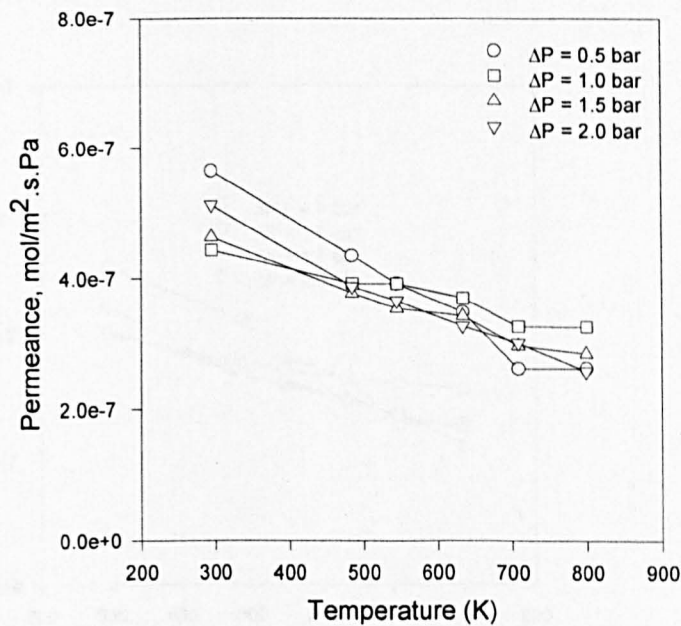


Figure 5.33: Nitrogen permeances of Pd impregnated membrane.

The permeances of argon are observed to follow similar profiles as those obtained for nitrogen permeation with values slightly lower than those obtained using nitrogen gas. The influence of pressure and temperature on argon permeance is shown in Figure 5.34 for the palladium impregnated silica membrane. The impact of transmembrane pressure on the performance of argon permeance of this membrane at different temperature is minor. The argon permeance is observed to be decreased slightly with pressure as the temperature increased. In other words, the impact of temperature is stronger than the impact of pressure on argon permeances which is varied from 2.2×10^{-7} to 5.09×10^{-7} mol/m².s.Pa.

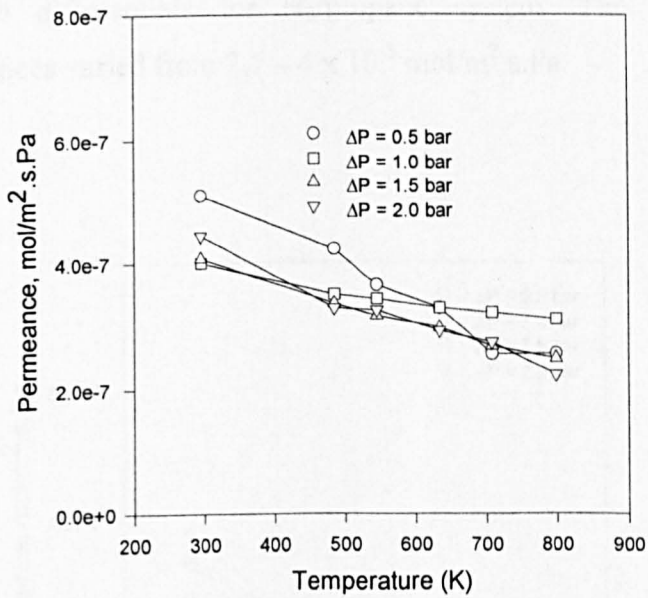


Figure 5.34: Argon permeances of Pd impregnated membrane.

Figure 5.35 presents the permeance profile of propane at different transmembrane pressure differentials (0.5 – 2.0 bar) and temperatures (300 – 800 K). In contrast to the permeation profiles of non-hydrocarbon gases (argon, nitrogen) and hydrogen, the permeation profiles of propane are observed to increase with pressure differential. Therefore, an increase in pressure differential across the membrane is observed to provide an increase in propane permeation. For the case of all other gases studied an increase in transmembrane pressure is observed to decrease the corresponding permeances. This phenomenon can be explained to the strong impact of heat of adsorption and surface diffusion effects for propane gas. It can be further noted that the propane gas permeance is distinctively lower at a transmembrane pressure differential at 0.5 bar and the permeation profiles matched closely at transmembrane pressure differentials at 1.0– 2.0 bar. Therefore, the conclusion, which can be drawn that distinct separation factors can be achieved at different pressure differentials for H₂/propane system. The observed values of gas permeances varied from $2.7 - 4 \times 10^{-8}$ mol/m².s.Pa.

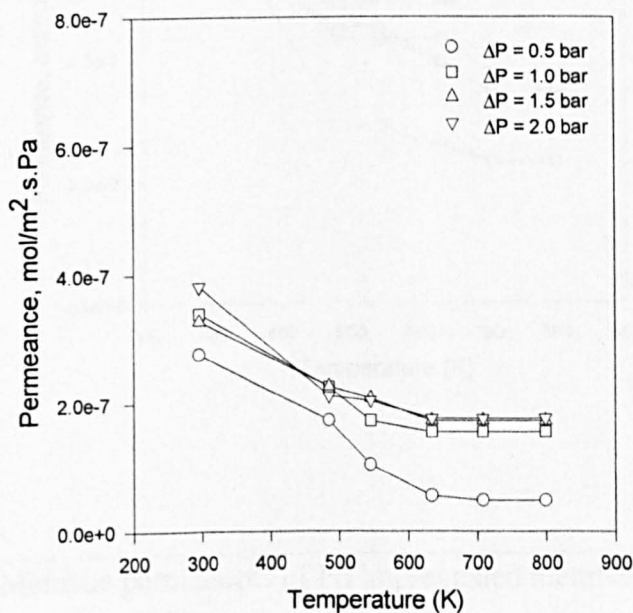


Figure 5.35: Propane permeances of Pd impregnated membrane.

Figure 5.36 presents the permeance of methane gas at different transmembrane pressure differentials and different temperatures. The methane permeance increases with pressure differentials and decreases with temperature. The gas permeance has been observed to have distinct profile at lower pressure differential (0.5 bar). The permeance increased predominantly to higher values at higher pressure differentials (1.0 – 2.0 bar). This confirms the specific interaction of the composite membrane towards propane and methane (and probably to other hydrocarbon gases) to offer distinct permeation profiles at lower pressure differentials due to lower surface diffusion effects. The permeation values are observed to vary from $3 - 7 \times 10^{-7}$ mol/m².s.Pa.

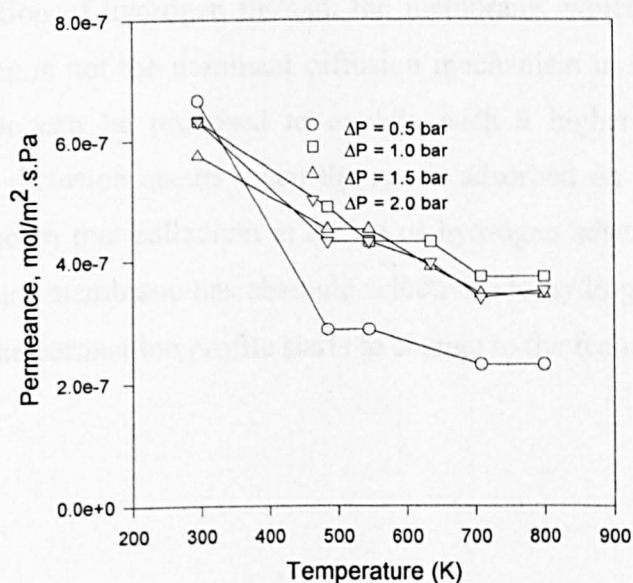


Figure 5.36: Methane permeances of Pd impregnated membrane.

5.6.3. Separation factor

The separation factor represents the quality of separation of a membrane. The variation of the pure gas separation factor obtained using the Pd impregnated membrane of H_2/N_2 , H_2/Ar , H_2/C_3H_8 and H_2/CH_4 with temperature and pressure are shown in Table 5.19. It can be seen from the table that the pure gas separation factors are higher than the values achieved using Knudsen diffusion mechanism. Furthermore, the separation factors for the pair H_2/C_3H_8 were significantly higher at high temperatures and lower pressures, which have decreased as the temperature decreases. In other words, the permeation of all gases through the composite membrane could be dominated with surface flow mechanism at lower temperature, but as the temperature increases the contribution of activated mechanism is increased.

These results show that dispersed palladium in the pores increase the selective permeation of hydrogen through the membrane, which indicate that the Knudsen diffusion is not the dominant diffusion mechanism in this membrane. The surface diffusion can be proposed to explain such a higher separation factor. Usually surface diffusion occurs when the gas is adsorbed on the membrane surface. It is well known that palladium is a kind of hydrogen adsorption material, and a dense palladium membrane has absolute selectivity to hydrogen. At temperature of about 600K the permeation profile starts to change to the feature of activated diffusion.

Gases pair	T (K)	ΔP (bar)			
		0.5	1	1.5	2
H ₂ /N ₂ (3.741 ^a)	295	4.6	5	4.7	5.4
	485	5.6	5.1	4.1	4.9
	545	5.8	4.9	4.2	4.9
	634	5.4	4.5	3.9	4.5
	708	7.2	4.9	3.9	4.8
H ₂ /Ar (4.5 ^a)	295	5.1	5.6	5.3	6.3
	485	5.8	5.7	4.6	5.8
	545	6.2	5.6	4.7	5.5
	634	5.7	5	4.5	5
	708	7.4	5	4.2	5.3
H ₂ /C ₃ H ₈ (4.7 ^a)	295	9.3	6.6	6.6	7.3
	485	14	8.8	6.8	9
	545	21.8	11	7.2	8.7
	634	33.9	10.6	7.6	8.2
	708	38.7	10.2	4.9	8.2
H ₂ /CH ₄ (2.8 ^a)	295	3.9	3.5	3.8	4.4
	485	10.6	4	3.4	4.4
	545	9.9	4.4	3.3	4.1
	634	20.4	3.8	3.4	3.7
	708	6.5	4.2	2.4	4.3

^a Knudsen separation factor.

Table 5.19: Pure gas separation factors for different pairs of gases for Pd impregnated membrane.

5.7. Silica γ -alumina membrane

5.7.1. Pore size and surface characterization

Table 5.20 and Figure 5.37 present the pore size distribution in the silica- γ membrane. Following deposition of silica on the top of support surface, the pore size of the support was reduced to a diameter range between 1.96 to 86.48 nm. In addition, the distribution of the pore size has changed so that the small pores with an average diameter between 1.96 to 8.38 nm contributed to approximately 74 % of the total pore volume. The pores with an average diameter of 8.38 nm had the highest contribution to the total pore volume at 9.1 %.

The BET surface area of the composite membrane is about 222.03 m²/g and the BJH desorption total volume is about 0.016 cm³/g.

pore diameter (nm)	BJH desorption pore volume cm ³ /g	% Contribution to total pore volume
86.48	0.00456	2.771194
44.26	0.006003	3.648131
28.98	0.005704	3.466424
21.38	0.005707	3.468247
16.86	0.005834	3.545427
13.86	0.005854	3.557581
11.76	0.005873	3.569128
10.54	0.003437	2.088727
8.38	0.015038	9.138864
6.9	0.008282	5.033121
5.86	0.011594	7.045883
4.94	0.011886	7.223336
4.26	0.010709	6.508052
3.68	0.012466	7.575813
3.2	0.011233	6.826497
2.8	0.01082	6.575509
2.46	0.010374	6.304467
2.16	0.009917	6.02674
1.96	0.009259	5.626861

Table 5.20: Pore size distribution of silica on γ - alumina membrane.

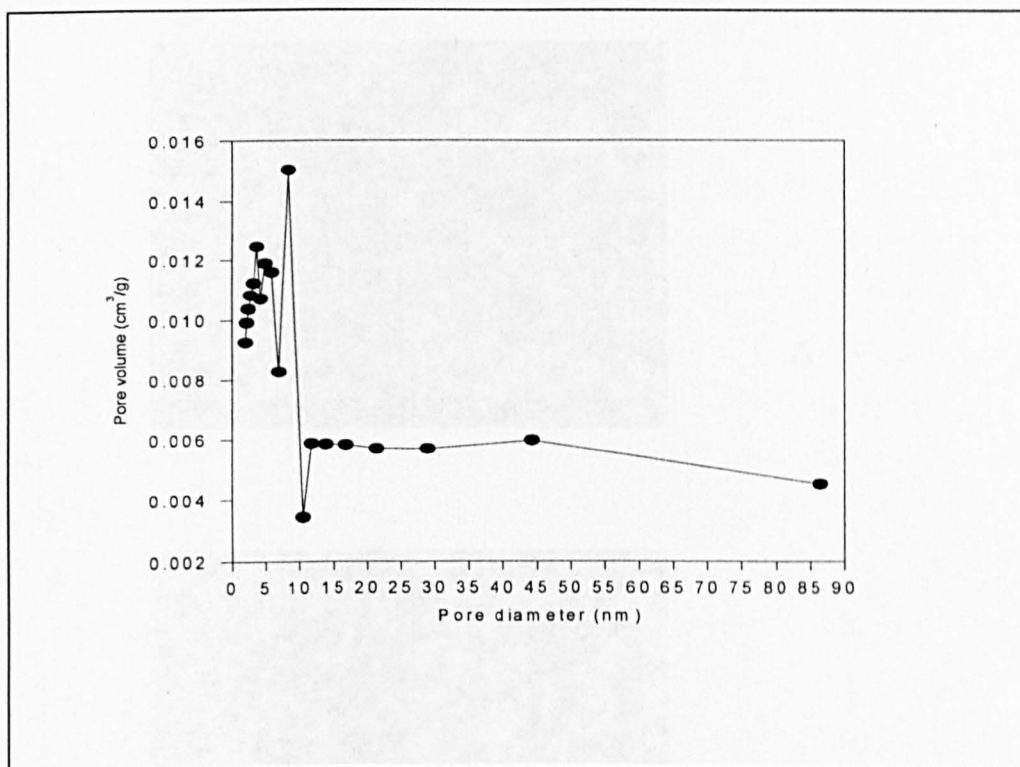
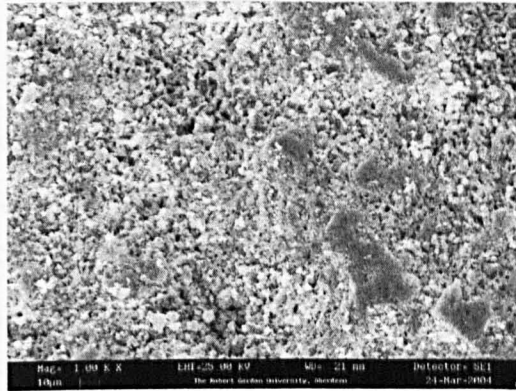
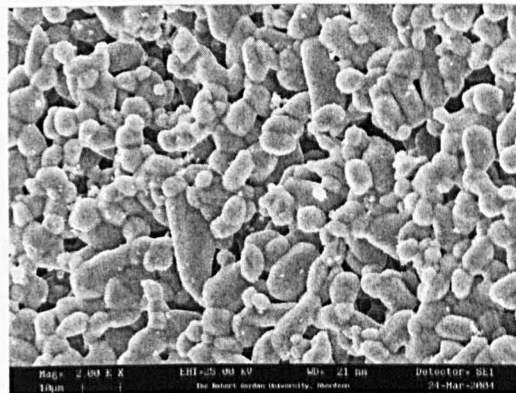


Figure 5.37: Pore size distribution of the silica on γ -alumina membrane.

A summary of the SEM micrographs obtained at various levels of dip coating is presented in Figure 5.38 for the silica γ -alumina membrane. Cross sectional SEM pictures show that the thickness of the layer is about 5 μm . The composition of the elements on the membrane surface is analysed using EDXA. The EDX analysis of the outer surface provided 37.18 % Si, 33.11% Al and 29.27 % Ti. The EDX analysis of the inner surface provided 91.67 % Ti, 5.01% Al and 2.19 % Si.



A



B



C

Figure 5.38: SEM micrographs of silica- γ -alumina membrane A) Outer surface B) Inner surface and C) Cross section.

5.7.2. Pure gas permeation

Figure 5.39 presents the hydrogen permeances of silica- γ -alumina composite membrane measured at various transmembrane pressure differentials (0.5 – 2.0 bar) and various temperatures (300 – 550 K). Since an increase in temperature corresponded to a decrease in membrane permeance. Therefore, the permeation behaviour is regarded to be dominated by either Knudsen diffusion and/or surface diffusion. In such a scenario, the pure gas separation factor shall correspond closely to the value obtained using Knudsen diffusion mechanism expressed as the inverse of the square root of the molecular weight of the diffusing gases. It is noted from the figure that an increase in transmembrane pressure differential has provided a decline in membrane permeance. Therefore, pressure differential is regarded to have influence on the hydrogen permeance only, which could be due to its size and the molecular weight which can respond easily with any change in conditions. The membrane exhibits hydrogen permeances of $5.8 - 13.5 \times 10^{-6} \text{ mol/m}^2 \cdot \text{s} \cdot \text{Pa}$ for a temperature variation from 300 – 550 K.

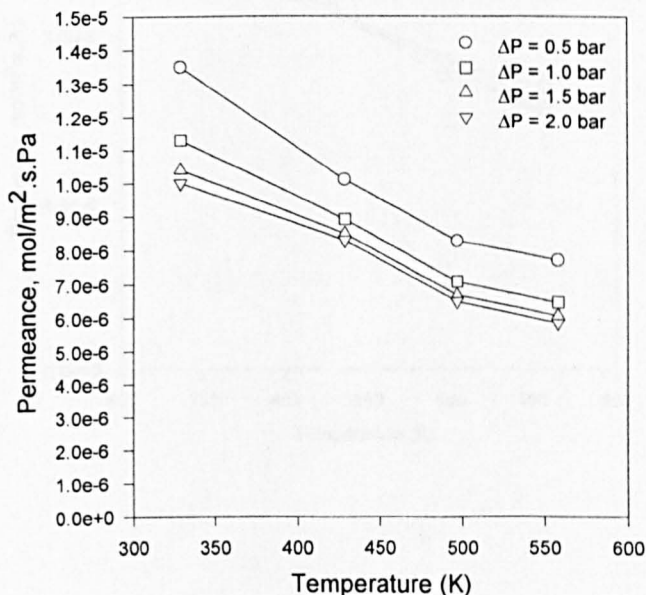


Figure 5.39: Hydrogen permeances of silica - γ -alumina composite membrane.

Figure 5.40 presents the nitrogen permeance of silica γ -alumina membrane. Compared to the permeation profiles of hydrogen which are influenced by transmembrane pressure differentials, the permeation profiles of nitrogen as can be seen from the figure to be tightly packed at different pressure differentials. Therefore, the influence of pressure differential is considered to be negligible for nitrogen species. With an increase in temperature, the permeance of nitrogen through the membrane did not change or decrease a little. This result confirms that Knudsen contribution dominates the permeance of nitrogen providing another mechanism contribution that can increase gas separation factors higher than those achieved by Knudsen diffusion such as surface diffusion. The nitrogen permeance values varied from $1.5 - 2.6 \times 10^{-6} \text{ mol/m}^2 \cdot \text{s} \cdot \text{Pa}$ which is smaller than the hydrogen permeance for a temperature variation of 300 – 550 K.

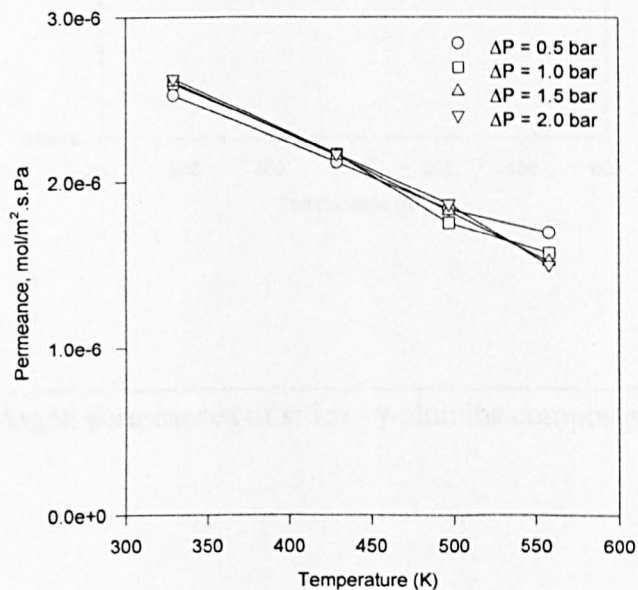


Figure 5.40: Nitrogen permeances of silica - γ -alumina composite membrane.

Figure 5.41 presents the argon permeance of silica γ -alumina membrane. The permeation profiles are closely located to one another with variation in transmembrane pressure differential, which confirms the lesser impact of pressure differentials. The membrane provides insignificant changed permeance with lower temperature (below 450 K). The argon permeances varied from a value of about $2.2 - 1.4 \times 10^{-6} \text{ mol/m}^2 \cdot \text{s} \cdot \text{Pa}$.

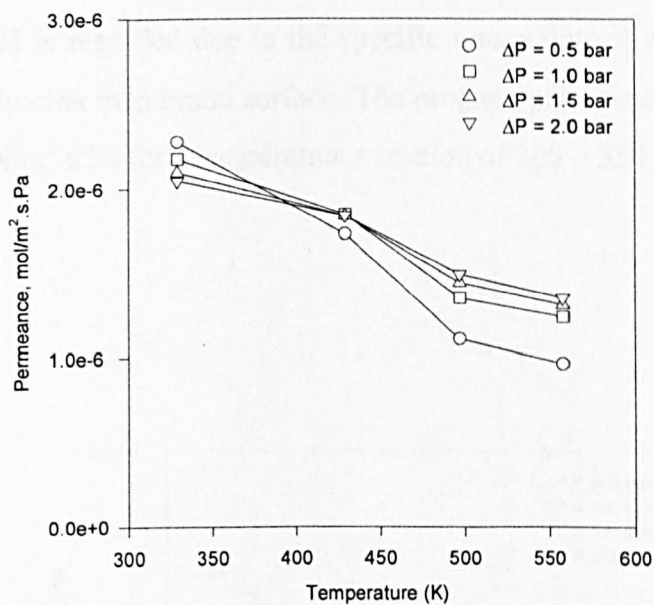


Figure 5.41: Argon permeances of silica - γ -alumina composite membrane.

Figure 5.42 presents the propane permeance of silica- γ -alumina composite membrane. It is clear from the figure that at lower pressure differentials, the propane permeance decreased with an increase with temperature. However, at higher-pressure differentials (1.0 – 2.0 bar) an increase in temperature initially increased the membrane permeance. This can be explained due to the presence of surface diffusion mechanism. However, after the intermediate temperature is achieved, the permeances followed a decline in their values with an increase in temperature, which could refer to mechanism change from surface to Knudsen. The variation of the membrane permeance behaviour with transmembrane pressure differential is regarded due to the specific interaction of propane species with the silica γ -alumina membrane surface. The propane permeances varied from $1.0 - 2.2 \times 10^{-6} \text{ mol/m}^2 \cdot \text{s} \cdot \text{Pa}$ for a temperature variation of 300 – 550 K.

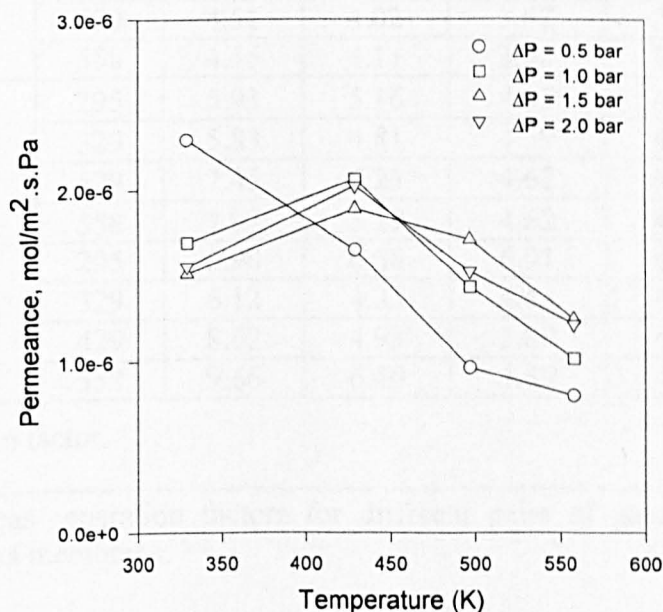


Figure 5.42: Propane permeance of silica - γ -alumina composite membrane.

5.7.3. Separation factor

Table 5.21 presents the pure gas separation factors for different gaseous pairs for silica- γ -alumina composite membrane. It is clear from the table that the separation factor for all the gaseous pairs is either lower or higher than that achieved by Knudsen diffusion mechanism at various pressure differentials. The lower separation factors of hydrogen to other gases may be due to a minute number of microcracks in the membrane layer. Small defects and cracks often appear in the membrane during the calcinations process. These defects can often be repaired by repeating the dipping process. It seems that the membranes in such a situation the gases are competitive with each other. In other words, the surface diffusion mechanism works to some extent in the permeation of these gases.

Gases pair	T (K)	ΔP			
		0.5	1	1.5	2
H ₂ /N ₂ (3.741 ^a)	295	5.37	4.35	4.01	3.82
	329	4.77	4.13	3.93	3.84
	429	4.51	4.02	3.67	3.47
	558	4.55	4.11	3.98	3.89
H ₂ /Ar (4.47 ^a)	295	5.93	5.16	4.97	4.87
	329	5.83	4.81	4.59	4.49
	429	7.45	5.23	4.62	4.34
	558	7.97	5.19	4.62	4.33
H ₂ /C ₃ H ₈ (4.69 ^a)	295	5.90	6.68	6.91	6.45
	329	6.12	4.33	4.48	4.09
	429	8.62	4.93	3.89	4.26
	558	9.66	6.40	4.89	4.80

^a Knudsen separation factor.

Table 5.21: Pure gas separation factors for different pairs of gases for silica γ -alumina membrane.

5.8. Summary

This work has demonstrated the development of five different membranes using dip coating technique with silicone elastomer as silica precursor. The silica membrane fabricated for hydrogen separation provided a lower permeance than the silica membrane for hydrogen reaction coupled with a H_2/N_2 separation factor of about 7 – 70 has been obtained for 50 – 50 H_2/N_2 mixture.

The membrane fabricated for hydrogen purification applications exhibited excellent hydrogen purification capability with a corresponding hydrogen permeance of about $4.1 \times 10^{-9} \text{ mol/m}^2 \cdot \text{s} \cdot \text{Pa}$ at 510 K with a high H_2/N_2 selectivity (> 400). It is further tested for a ternary mixture of gas consisting of H_2 , CO_2 and CH_4 to obtain excellent hydrogen purity from the permeate stream.

The last two types of membranes provide separation factors close to that achieved using Knudsen diffusion mechanism with higher membrane permeances. These membranes can be therefore used for applications in membrane reactor schemes where a selective membrane offers as a separation interface to carry out necessary performance for simultaneous reaction-separation.

For the evaluation of the membrane performance using gas permeation tests, it is insufficient to rely on the results from gas permeation with pure gases, although it was easier to perform with pure gases experimentally than with gases mixtures.

Membranes with narrow pore size that have a molecular sieving property such as membrane prepared for hydrogen purification could generate an extremely low flow rate for the gas it excluded. In this case, a significant error may be introduced for the selectivity determined by the ratio of pure gas flows. Instead mole fractions determined from feed and permeate with gas chromatograph should be used to calculate the separation factor.

Chapter 6:

MODELLING AND SIMULATION

6.1. Introduction

This chapter presents a comparative study for propane dehydrogenation in different operational schemes based on modelling and simulation for laboratory scale configurations. Operational performance of tubular reactor (where a non-selective tube holds the catalyst), annular reactor (where catalyst is placed in the annular space between the shell and tube in a non-selective membrane reactor) and other membrane reactor configurations (tubular membrane reactor and annular membrane reactor) are investigated in this work. The objective of this chapter is to simulate the performance and effectiveness of these configurations (based on conversion of propane to propylene) at different operating conditions (i.e. temperature). Three different types of membranes (i.e. silica, Pd-impregnated and silica on γ -alumina/membranes) and two different catalysts (0.5 % Pt-alumina and Pt-Sn-K on alumina) are investigated.

The length of the reactor is taken to be about 370 mm where a catalyst of size 3.4 mm diameter is hosted that corresponds to the value of L/d_p value of 100. Therefore the reactor configurations characterize a reactor with high L/d_p ratio and a size that accounts for the diameter of the reactor close to the dimensions of the catalyst. Since the simulation study is confined to configurations that suit membrane reactors in experimental, the assumptions with respect to neglecting reactor and pellet radial concentration and temperature gradients appear to be justified. Therefore, the assumptions provided similar results as obtained for the case of ethane dehydrogenation studied by Gobina et. al., (1995).

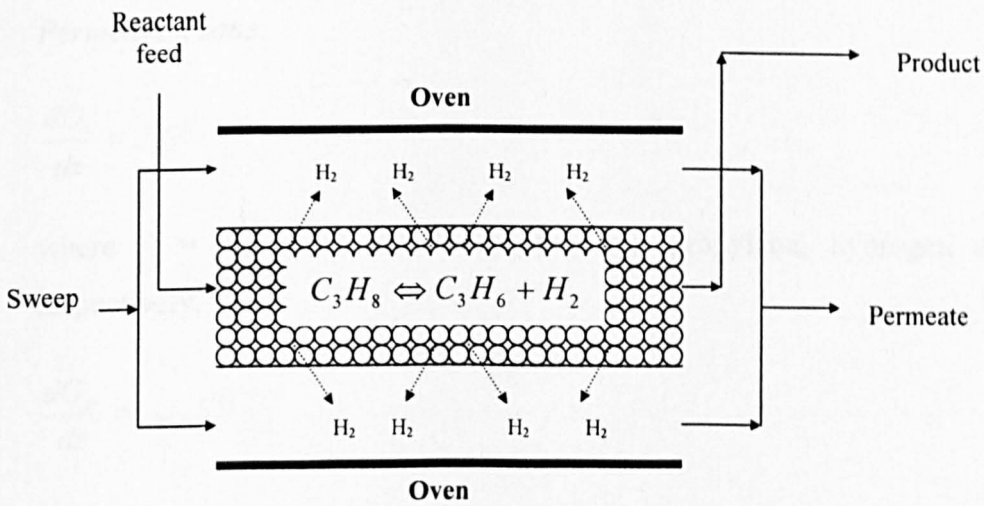
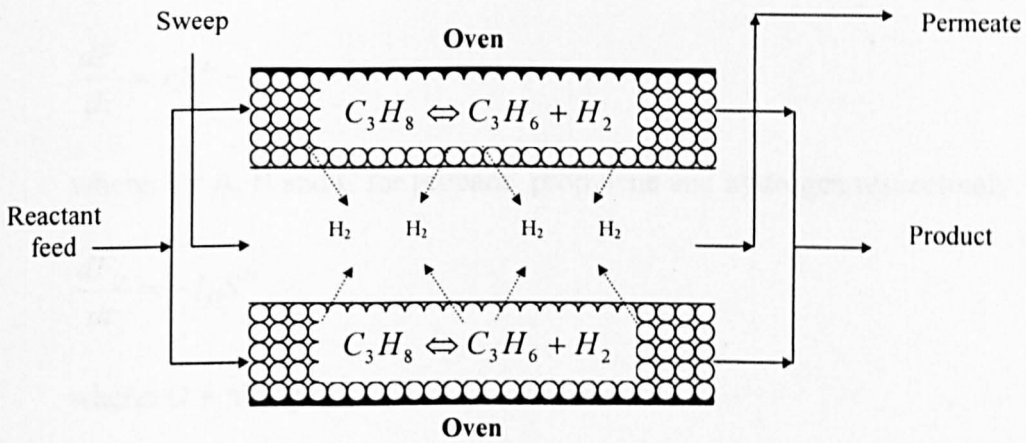
The next section presents a one dimensional axial model developed for propane dehydrogenation system for different configurations with the corresponding material performance equations (catalysts, silica and palladium impregnated membrane). The model considers energy balances in permeation and reaction zones.

6.2. Mathematical model

A one dimensional axial model is developed for the simulation of annular and tubular configurations schematically presented in Figure 6.1. The model is considering mass and energy balances (Barberi et al., 2002). The simulation model considers the following assumptions:

- 1) Steady state conditions: The flow and the properties of the flowing materials, such as temperature, pressure, composition, density and velocity at each point are constant with time.
- 2) Non-isothermal operation: the propane dehydrogenation is highly endothermic reaction.
- 3) Co-current permeation: the sweep flows in the same direction as the feed gas.
- 4) Plug flow pattern in both reaction and permeation zones: no mixing along the flow path.
- 5) Negligible effect of undesirable reactions such as coking and side reactions on conversion.
- 6) Negligible effect of radial dispersion on fluid properties. (large L/D ratio of the membrane reactor).

Sections 6.2.1 – 6.2.3 present the mathematical model comprising of mass and energy balance equations in reaction and permeation zones for tubular and annular silica and palladium-impregnated membrane reactor configurations. The model considers the presence of nitrogen as an inert in the reaction zone and argon as the sweep gas.



6.2.1. Mass balances

Reaction zone:

$$\frac{dF_i}{dz} = r_i S^R - J_i S^M \quad (6.1)$$

where: i = A, B and C for propane, propylene and hydrogen respectively.

$$\frac{dF_D}{dz} = -J_D S^M \quad (6.2)$$

where: D = nitrogen

$$\frac{dF_E}{dz} = J_E S^M \quad (6.3)$$

where: E = argon (i.e. sweep gas)

Permeation zone:

$$\frac{dG_i}{dz} = J_i S^M \quad (6.4)$$

where: i = A, B, C and D for propane, propylene, hydrogen and nitrogen respectively.

$$\frac{dG_E}{dz} = -J_E S^M \quad (6.5)$$

where: E = argon (i.e. sweep gas)

The derivation of the above mass balance expressions is presented in Appendix 6A.

Propane dehydrogenation reaction is expressed as:



Where: A refer to Propane, B refer to Propylene and C refer to Hydrogen.

The rate of disappearance of A for propane dehydrogenation is defined as:

$$r_A = k \left[P_A - \frac{P_B P_C}{K} \right] \quad (6.7)$$

Where k refers to reaction rate constant and K refer to equilibrium constant and defined as:

$$k = k_o * \exp\left(\frac{-E}{RT}\right) \quad (6.8)$$

$$K = K_o * \exp\left(\frac{-E_{eq}}{RT}\right) \quad (6.9)$$

The reaction rate for non-reacting species is taken as zero. Empirical values of different coefficients presented in equations 6.8 and 6.9 have been obtained from experimental reactor data for Pt (Yildirim et al.,1997)) and Pt-Sn-K catalysts (Assambungrat et al., 2000). The data is summarized in Table 6.1. Appendix 6B presents details with respect to the empirical values.

Parameter	Values for Pt-Sn-K catalyst	Values for Pt catalyst
k_0	127.62 kmol/(m ³ .bar.s)	1.46e7 kmol/(m ³ .bar.s)
K_0	1.73e6 bar	13.66e6 bar
E	62.7e3 kJ/mol	134.3e3 kJ/mol
E_{eq}	129 kJ/mol	127.69 kJ/mol

Table 6.1: Kinetics parameters for Pt-Sn-K catalysts (Assambungrat et al., 2000) and Pt (Yildirim et al., 1997).

The component membrane flux J_i for all the membranes are defined using the following equations:

$$J_i = Per_i \left(P^R \frac{F_i}{\sum_{i=A}^D F_i} - P^P \frac{G_i}{\sum_{i=A}^D G_i} \right) \quad (6.10)$$

$i = A, B, C$ and D for C_3H_8 , C_3H_6 , H_2 , and N_2 respectively

With partial pressures being defined as

$$P_i = \frac{F_i}{\sum_{i=A}^E F_i} P^R \quad (6.11)$$

$i = A, B, C, D$ and E for C_3H_8 , C_3H_6 , H_2 , N_2 and Ar respectively

$$J_E = Per_E (P^P G_E - P^R F_E) \quad (6.12)$$

$E = Ar$ (sweep gas)

The following section presents expressions for membrane permeances for Pd-impregnated, silica and silica on γ -alumina membranes based on the experimental investigations performed in this work. These permeance expressions are taken from the corresponding single gas permeances. It can be also noted that the silica membrane permeances are measured experimentally to a maximum temperature of about 300 °C and are therefore extrapolated to provide similar permeances at higher temperatures where the simulation study is carried out for propane dehydrogenation (400 – 600 °C).

For Pd-impregnated membrane, the corresponding component permeances (expressed as $kmol/m^2 \cdot s \cdot bar$) are presented as:

$$Per_A = Per_B = 9.01E - 06 \exp^{\frac{3.28e3}{8.314T}} \quad (6.13)$$

$$Per_C = 1.09E - 04 \exp^{\frac{2.19e3}{8.314T}} \quad (6.14)$$

$$Per_D = 2.79E - 05 \exp^{\frac{1.2e3}{8.314T}} \quad (6.15)$$

$$Per_E = 2.72E - 05 \exp^{\frac{0.97e3}{8.314T}} \quad (6.16)$$

For silica membrane, the corresponding component permeances (expressed as kmol/m².bar) are presented as:

$$Per_A = Per_B = 2.08E - 08 \exp^{\frac{6607.5}{8.314T}} \quad (6.17)$$

$$Per_C = 1.43E - 06 \exp^{\frac{-5725.94}{8.314T}} \quad (6.18)$$

$$Per_D = 1.63E - 07 \exp^{\frac{-3413.15}{8.314T}} \quad (6.19)$$

$$Per_E = 2.55E - 07 \exp^{\frac{-2754.678}{8.314T}} \quad (6.20)$$

For silica γ -alumina membrane, the corresponding component permeances (expressed as kmol/m².bar) are presented as:

$$Per_A = Per_B = 1E - 05 \exp^{\frac{10946}{8.314T}} \quad (6.21)$$

$$Per_C = 3.52E - 04 \exp^{\frac{3777}{8.314T}} \quad (6.22)$$

$$Per_D = 6.65 - 07 \exp^{\frac{4111}{8.314T}} \quad (6.23)$$

$$Per_E = 5.41E - 07 \exp^{\frac{4169}{8.314T}} \quad (6.24)$$

With respect to Pd impregnated and silica γ -alumina membrane permeances, it has to be inferred here that these membrane permeances decreased with an increase in temperature. Further, the obtained separation factors are higher and do not correspond to those predictable with Knudsen mechanism. The definable mechanism for the membrane is surface flow that could henceforth account for the membrane

performance. Since surface flow mechanism does not have any correlation that involves temperature terms, the modelling effort is directed to restrict considering membrane permeances as functions of temperature defined by suitable correlations. For this purpose, exponential fit happened to provide good fitness. The same procedure is applicable and valid for silica- γ -alumina composite membranes.

6.2.2. Energy balances

Annular configuration:

Reaction zone:

$$\frac{dT'}{dz} = \frac{U' S' (T^o - T') - U' S^M (T' - T') + r_A S^R \Delta H + J_E S^M (H'_E - H''_E)}{\sum F_i C_{ps_i}} \quad (6.25)$$

Permeation zone:

$$\frac{dT'}{dz} = \frac{U' S^M (T^s - T') + \sum_{i=A}^D J_i S^M (H_i^s - H_i')}{\sum_{i=A}^E G_i C_{pt_i}} \quad (6.26)$$

In the above expressions, oven and enthalpy of argon are considered as heat sources for the shell (reaction zone). The shell and enthalpy of permeating species are considered as the heat sources for the tube (permeation zone). Similarly, heat of reaction and membrane tube are considered as heat sinks for the shell.

Tubular configuration: Reaction zone:

$$\frac{dT'}{dz} = \frac{U' S^M (T^s - T') + r_A S^R \Delta H + J_E S^M (H''_E - H'_E)}{\sum F_i C_{pt_i}} \quad (6.27)$$

Permeation zone:

$$\frac{dT^s}{dz} = \frac{U' S^s (T^o - T^s) - U' S^M (T^s - T') + \sum_{i=A}^D J_i S^M (H_i' - H_i^s)}{\sum G_i C_{ps_i}} \quad (6.28)$$

In the above expressions, shell and argon enthalpy are considered as the heat sources for the tube (reaction zone). Oven and enthalpy of permeating species are considered as the heat sources for the shell (permeation zone). Similarly, tube is considered as the only heat sink for the shell (permeation zone) and heat of reaction is considered as the only sink for the tube (reaction zone). Appendix 6C summarises details with respect to the derivation of the expressions 6.12 – 6.15.

6.3. Outline of the study

6.3.1. Models

Six configurations consisting of silica composite and palladium-impregnated annular and tubular membrane configurations, tubular and annular reactor configurations are evaluated using the simulation model described in the previous section using two types of catalysts. Annular and tubular reactor configurations are hypothetical configurations developed for membrane reactor configurations. These configurations are developing targeted by equating the membrane flux expressions to zero. For all the configurations, similar values of reaction zone volume (S^R) and permeation area (S^M) are used. The objective for comparison is the percent conversion of propane to propylene.

The propane conversion is calculated from the molar flow rate of propane as follows:

$$C_3H_8 \text{ conversion } (\%) = \frac{(nC_3H_{8,IN} + nC_3H_{8,OUT})}{nC_3H_{8,IN}} \times 100 \quad (6.29)$$

Simple models considering mass (M) and mass and energy (ME) balances in the reaction and permeation zone are also developed from the mass, energy and pressure balance expressions by equating the right hand side of different applicable equations to zero. The temperature of the reaction zone is presented as the average reaction temperature.

6.3.2. Solution strategy

The simulation model comprising of equations 6.1 – 6.28 coupled with other physical property correlations analytical expressions are solved as an initial value problem using Runge Kutta Fehlberg (RKF 45) method. Initial conditions and other parameters used in the study are presented in Table 6.2. The total feed rate to the reaction zone is taken about 30 ml/min comprising of equimolar mixture of N_2 and C_3H_8 . The total feed rate of argon is taken as 150 ml/min. The dimensions of the membrane and shell are chosen in such a way that the reaction zone and permeation zone cross sectional area are of similar values for both annular and tubular configurations. During simulation, the model has been observed to be non-stiff. A maximum central process unit (CPU) time of about 15 s is taken for the model on a 128 MHz 366 Pentium processor.

Parameter	Value	Parameter	Value
F_A	1.166e-8 kmol/s	T^o	673 – 873 K
F_B	0	P^R	1.013 bar
F_C	0	P^P	1.013 bar
F_D	1.166e-8 kmol/s	d^{it}	1.5e-2 m
G_E	1.116e-7 kmol/s	d^{ot}	1.8e-2 m
T^s	645 K	d^{is}	2.34307e-2 m
T^t	645 K	d^{os}	2.5 e-2 m

Table 6.2: Parameters set for the comparative study.

6.3.3. Model comparison

Table 6.3 presents results obtained from the simulation model for tubular (TR) and silica tubular (SiTR) configurations. The experimental data for comparison has been taken from Yildirim et al., (1997) as the authors have only provided sets of data for both TR and SiTR configurations. This actual data indicates the membrane reactor dimensions (length, reactor diameter, tube inner and outer diameter etc.). For membrane reactor configuration, the silica permeances are also taken from Yildirim et al., (1997) and provided to the model with relevant conversion factors for adjusting the units. Since TR configuration does not have any sweep gas, it is impossible to simulate the model without any flow rate of the sweep gas.

Hence, a very low value of sweep gas (0.15 ml/min) is used to simulate the system of equations, which were observed to be stiff at that flow rate. The initial temperature of the reactants is fixed to a value of 350 K as the authors have provided the information that pre-heaters exist to heat the entering gas into the membrane reactor assembly. The flow rate of equimolar mixture of propane and nitrogen is taken as 30 ml/min and the argon flow rate is taken as 150 ml/min in exact agreement with the values taken by Yildirim et al., (1997).

Oven Temperature (°C)	TR		Silica TMR	
	Experimental data	Simulated data	Experimental data	Simulated data
436	3.80	4.19	6.7	6.89
452.5	6.25	6.015	9.7	9.53
463	7.70	7.65	13.30	13.14

Table 6.3: Results for model comparison.

In Table 6.3, the summary of results (conversions) obtained from simulation and those reported from experimental investigation. The authors have studied at a reaction (oven) temperature of about 436 – 463 °C for both TR and silica TR configurations. It can be observed from the table that the model has been in excellent agreement with the experimental data.

6.4. Results and discussion

6.4.1. Catalyst performance

Table 6.4 presents the performance of various catalysts (Pt-Sn-K) and Pt catalysts for different reactor (AR and TR) and membrane reactor (AMR and TMR) configurations. The different membranes studied include Pd impregnated γ -alumina membrane, silica composite membrane and silica on γ -alumina membrane. Corresponding membrane permeances have been taken from the experimental investigations in this work and extrapolated to higher temperatures for silica membranes. However, for Pd-impregnated membrane, high temperature experimental data has been used as the membrane studied in the temperature of about 550 °C. The following conclusions can be deduced from the table:

1. For all the configurations, Pt-Sn-K catalyst provided higher conversions than corresponding conversion obtained using Pt catalyst. The reason is expressed in appropriate literature (Assambungrat et al., 2000) who has argued that the Pt-Sn-K catalyst is capable of handling coking problems effectively and provides higher conversion than Pt catalyst. For example, for Pd-impregnated membrane reactor the conversion at 600 °C is 81.9 % using Pt-Sn-K catalyst opposed to a value of about 81.1% using Pt catalyst. It is clear that both are higher than the equilibrium conversion, which is about 50 % at 600 °C.
2. The performance of silica on γ -alumina membrane has been outstanding when compared to those simulated using other types of membranes including silica composite and Pd-impregnated membrane. It can be observed that the range of conversions using these membranes varied to a maximum conversion value of about 83.24 % at 600 °C where as the maximum conversion value of about 64.5 % using silica membrane which deposited directly on 6000 nm support and 81.9 % using Pd-impregnated membrane in AMR configuration. The difference in conversion is attributed to the membrane properties (permeance and selectivity)
3. In general, the order of conversion variation is presented as Silica on γ -alumina AMR > Silica on γ -alumina TMR > Pd impregnated AMR > Pd impregnated TMR > Silica AMR > Silica TMR > AR > TR at higher temperatures of operation.

T (Oven)	Conversion	Conversion	Conversion	Conversion
	Pt-Sn-K catalyst	Pt Catalyst	Pt-Sn-K catalyst	Pt Catalyst
	Annular reactor (AR)		Tubular reactor (TR)	
400	5.6642	5.5291	5.6642	5.5279
450	12.3168	11.9541	12.3168	11.9540
500	23.6222	22.8430	23.6220	22.8427
550	39.9331	38.6054	39.9321	38.6054
600	58.8909	57.1849	58.8890	57.1834
	Pd impregnated AMR		Pd impregnated TMR	
400	13.0874	5.9320	12.9622	5.4235
450	26.7102	21.2720	26.1660	19.0519
500	45.9293	43.0373	44.5022	39.9377
550	66.3097	64.6500	63.8016	61.3395
600	81.9113	81.1485	78.6802	77.6843
	Silica AMR		Silica TMR	
400	6.898	6.470	6.846	6.399
450	14.956	14.329	14.749	14.078
500	28.225	27.226	27.714	26.655
550	46.263	44.839	45.404	43.912
600	65.471	63.884	64.518	62.848
	Silica on γ -alumina AMR		Silica on γ -alumina TMR	
400	13.19	5.247	13.17	4.93
450	26.99	20.913	26.886	19.20
500	46.566	44.215	46.24	42.296
550	67.39	65.928	66.888	65.09
600	83.24	82.196	82.78	81.90

Table 6.4: Performance of Pt-Sn-K catalyst and Pt catalytic reactor (AR, TR) and membrane reactors (AMR, TMR) for different membranes.

Despite higher theoretical conversions, Pd-impregnated membrane is chosen for subsequent modelling study due to one basic reason i.e. its ability to offer high temperature operation (which is required for a model reaction like propane dehydrogenation). The same cannot be applicable for silica membrane due to the poor stability of silica at an elevated temperature, and the fact that silica decomposition is observed in experimental work for temperatures above 350 °C. The membrane however, offers very high H₂ and C₃H₈ flux with good selectivity.

6.4.2. Feed flow rate

Several simulations were performed to understand how the conversion changes with the feed flow rate. Figure 6.2 summarises the impact of feed flow rate for different configurations. For all these cases, feed flow rate is varied from 30 ml/min to 400 ml/min, keeping the sweep gas flow rate to be constant at 150 ml/min.

It is obvious that as the feed rate decrease, i.e., increasing contact time (defined as the catalyst weight over the propane feed flow rate) of the feed, the conversion increases and the other factor that could be related to the feed flow rate is the reactant loss. For both annular membrane reactor (AMR) and tubular membrane reactor (TMR), the conversions are decreased as the feed flow rates increases. The conversion decrease is more pronounced in the case of tubular membrane reactor. This happens because the reactant permeate through the membrane (reactant loss) and the heat demand by gas in the tube (for reaction and/or sweep gas flow) and the subsequent heat load on heat transfer from the oven to the tube via the shell. It is possible to see from this figure that the critical feed flow rate for annular membrane reactor and tubular membrane reactor is about 200 ml/min and a critical feed flow rate of about 100 ml/min for tubular reactor, above these flow rates the conversions fall below those available for annular reactor.

The conversion of AR configuration remains independent on this feed flow rate range (30-400 ml/min). This could be due to the low heat lost by the gases at high flow rate which indicates that this feed flow rate range is still acceptable for the appropriate reactor dimensions and the heat transfer coefficient in the shell (reaction

zone) is very high. Therefore, the critical reactant flow rate for the operation of AR in this case can be presented to be 400 ml/min above which the conversions decrease. In the case of TR the conversion is start to decrease above 100 ml/min feed flow rates. This is attributed to the lower heat transfer coefficient in the tube (reaction zone) that reduces reaction zone temperature. Therefore, operation of the membrane reactor configurations and TR cannot be recommended at higher feed flow rates due to decrease in conversion. This is because usually a membrane reactor is suggested for an increase in conversion and achieving lower conversions close to those acceptable for annular reactor case is not the objective.

The impact of temperature on the conversion of annular and tubular Pd-impregnated membrane reactor configurations is also presented in the figure. Usually, increasing gas feed flow rates reduce the residence time of the gas in the reactor that implies a decrease in reactor conversion. As it has been identified that the reaction zone temperature are usually higher for the case of annular membrane reactors opposed to the low reaction zone temperatures achievable in tubular membrane reactors. Coupled to this effect, the analytical expressions corresponding to Pd impregnated membrane permeances in equations 6.13 - 6.16 signify that membrane permeances decrease with increasing temperature. Therefore, the case for annular membrane reactor with Pd- impregnated membranes correspond to the characteristics of higher reaction rates and reactor conversion (due to achievement of higher temperature) and lower membrane flux for both hydrogen and propane (reactant) due to presence of higher temperatures. On the other hand, the case for tubular membrane reactors with Pd-impregnated membranes correspond to the characteristics of lower reaction rates, and reaction conversion (due to achievement of lower reaction zone temperature) and higher membrane flux for both hydrogen and propane (reactant) due to the presence of relatively lower temperatures than those present in annular membrane reactor. The net effect of these features that characterize imbalances in both reaction rate and flux tend to play a stronger role at higher feed flow rate due to reduction in residence time. Therefore, significant deviations were observed in reactor conversion especially for higher feed flow rates rather than at lower values of feed flow rate.

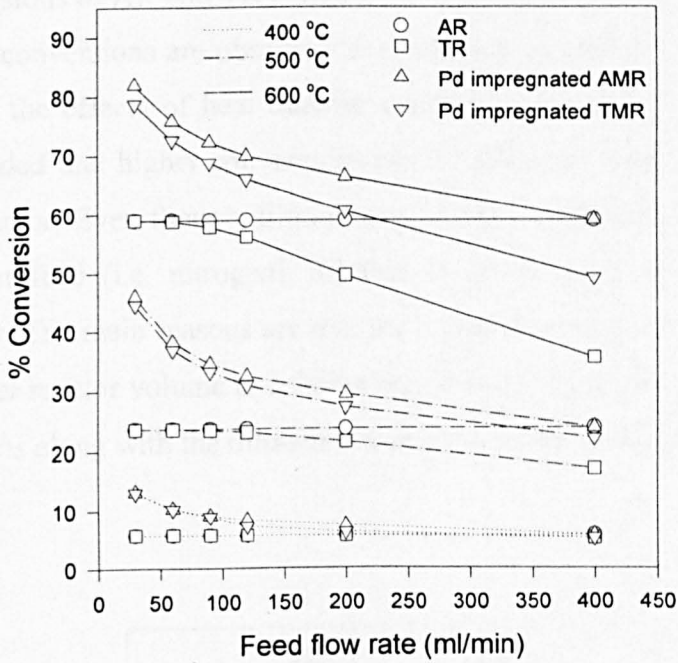


Figure 6.2: Impact of feed flow rate on different configurations.

6.4.3. Feed composition

Figure 6.3 summarises the impact of feed composition on the performance of different configurations. The feed composition is varied from 25 % propane (75 % nitrogen) to 100 % propane (0% nitrogen). During these composition variations, the total feed flow rate to the system is kept fixed at 30 ml/min. As seen in the graph, the conversion of all the configurations decreases as the propane percentage in the feed increases. In other words, the conversion decreases due to the effect of the absence of inert in the reaction zone. This can be analytically explained as follows. The presence of inert reduces partial pressure of the reactant and therefore the reaction rate decreases. The higher inert composition also reduces the hydrogen concentration and hence membrane flux. The net effect of lower partial pressure of reactant and membrane flux results in the reduction of conversion despite using a membrane reactor.

It can be seen from figure 6.3 that the conversion of annular membrane reactor is higher than the conversion of tubular membrane reactor and the equilibrium conversions of AR and TR match with one another at different reaction temperatures. These conversions are observed to match due to very low feed flow rate, which can negate the effects of heat transfer coefficient on conversion. Henceforth, it can be concluded that higher conversions can be achieved with high dilution of propane in the reactor. Even though dilution can provide additional heat in terms of the heated dilutant feed (i.e. nitrogen), dilution is not a major advantages in operating the reactor. The main reasons are that the higher flow rates of the reactor would demand a higher reactor volume to achieve equilibrium conversion. Further, the separation of products along with the dilutant is a major limitation for the utilisation of dilutant.

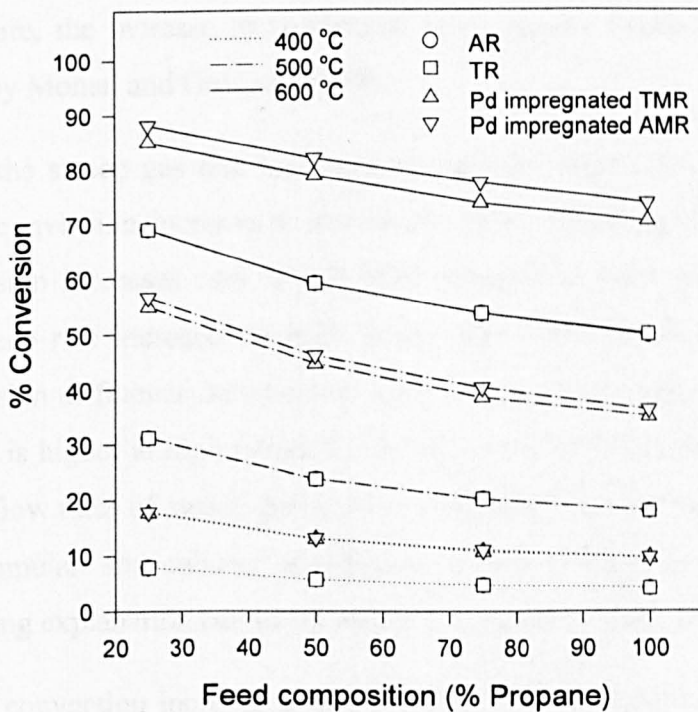


Figure 6.3: Impact of feed composition on the performance of different configurations.

6.4.4. Sweep gas flow

The effect of sweep gas flow rate on propane conversion for both tubular and annular membrane reactor configurations using palladium impregnated membrane is given in figure 6.4. The simulation results indicated an increase in conversion with sweep gas flow rate up to a point, followed by constant or possible a decrease. The conversion increase is due to the impact of the sweep gas flow on the hydrogen fluxes through the membrane. An increase in sweep gas flow removes the product faster and thus partial pressure decrease. The resulting partial pressure difference will work as a driving force for the separation through the membrane, and increasing conversion due to the lower levels of product in the reactor. The possibility of increasing conversion due to permeates of sweep gas to the reaction side giving a dilution of the reaction zone is present. Faster permeation of unconverted propane increases the loss and reduced conversion. These two effects counteract each other. Therefore, the increase in conversion is eventually limited by loss of reactant, as noted by Mohan and Govind, (1988).

When the sweep gas rate increases, the annular membrane reactor predicts a steep initial conversion increase at low sweep rates, following the initial steep increase, conversion increases very slowly after sweep flow rates of about 200-250 ml/min. As sweep rate increases to high values, the effect becomes less pronounced. The conversion difference between the tubular membrane reactor and annular membrane reactor is higher at high temperature as the sweep rate increases. On the contrary, at lower flow rates of sweep gas and lower temperatures the conversions differences of both annular and tubular membrane reactor configurations are negligible. The following explanation can be drawn from the case studies performed.

1. The conversion increase at 600 °C has been observed to be significantly high at flow rates 150-300 ml/min for Pd-AMR and the conversions achieved using tubular membrane reactor configurations are lower than those achieved using annular membrane reactor configurations in particular at high temperatures (above 500 °C) and high sweep gas flow rates. On the contrary, at lower flow rates of sweep gas and lower temperatures (400 °C) the conversions of both annular and tubular membrane reactor configurations close with each other.

2. The conversion achieved with the TMR configuration have decreased after a sweep gas flow rate of about 150 ml/min at 600 °C and 300 ml/min at 500°C. The conversion differences between tubular membrane reactor and annular membrane reactor are high at a higher temperature and a higher sweep gas flow rate. Once again the temperature system in the TMR case is regarded to be the reason for the decline in conversion at higher sweep flow rate due to back diffusion of argon from separation zone to reaction zone. Furthermore, the tube temperatures do not come close to the temperature of the oven which offers further reduction in the conversion. These two effects therefore offer the conversion of tubular membrane reactor to be lower than the corresponding values for annular membrane reactor configurations.

3. The critical flow rate (a value above which the conversion of the configuration decreases) for both annular and tubular configurations can be observed to be strongly dependent on reaction temperature and type of configuration. For example, at a temperature of about 400 °C, the critical flow rate is above 600 ml/min for both annular and tubular configurations where as at 600 °C, the critical flow rate is about 300 ml/min for annular configuration and 150 ml/min for tubular configuration.

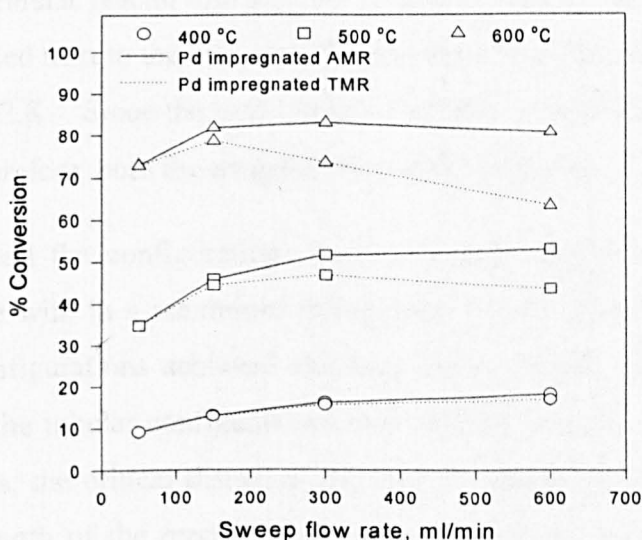


Figure 6.4: Impact of sweep gas flow on propane conversion.

6.4.5. Temperature Profiles

The variation of reaction zone temperature profiles for different configurations is presented in Figure 5.7. For all the cases, the initial reactant temperature is about 645 K and the oven temperature is about 873 K. The following analysis is derived from the temperature profiles obtained from the simulation:

1. The temperature profiles of annular reactor (AR) and Pd impregnated annular membrane reactor (Pd AMR) palladium configurations are identical and there has been insignificant difference between the final temperature of the gas in the reaction zone (872 K) and the oven temperature (873 K). This identification between the reaction zone temperature and oven temperature profiles is due to the fact that a very low flow rate of feed (30 ml/min) is used. When the feed flow rate is increased to a value of about 100 ml/min, these temperature profiles have been observed to be varying significantly with one another.
2. The temperature profile of Pd impregnated tubular membrane reactor is initially higher and later become identical with that of tubular reactor configuration. This variation is due to the observed heat transfer coefficients of the shell and the tube in both configurations.

For both annular reactor and annular membrane reactor configurations, the reaction zone is placed next to the oven and the heat transfer coefficient values varied from 57 – 174 W/m².K. Since the heat transfer coefficients are high and the feed flow rates are low, therefore, both the temperature profiles identical.

3. Almost all the configurations have achieved a temperature close to the oven temperature with in a maximum dimensionless axial distance value of 0.4. While annular configurations achieved the temperature of the oven at a critical value of about 0.2, the tubular configurations achieved the same at a value of about 0.4. In other words, the critical distances required for heating the configurations is lower than the length of the reactor which suggests that the operating conditions for all configurations are optimal. This is attributed to lower heat transfer coefficients in the reaction zone for tubular configurations opposed to higher heat transfer coefficients in the reaction zone for annular configurations.

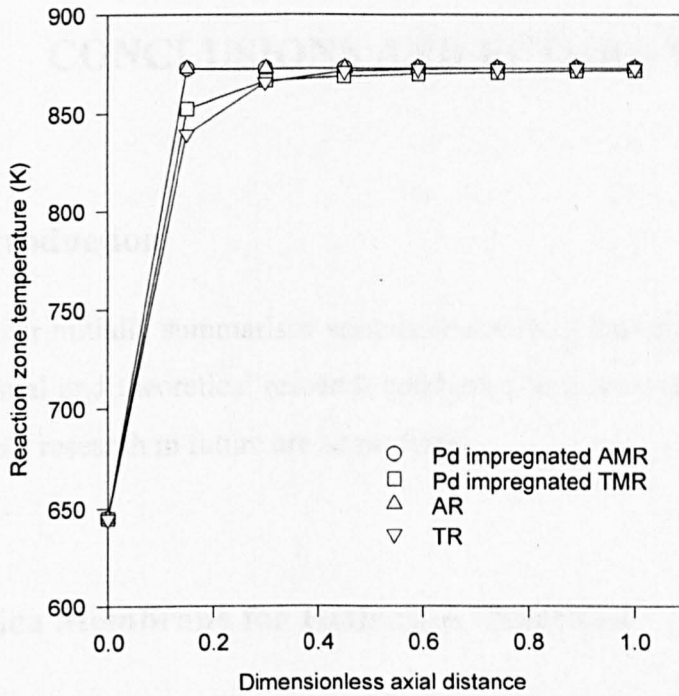


Figure 6.5: Reaction zone temperature profiles.

Chapter 7:

CONCLUSIONS AND FUTURE WORK

7.1. Introduction

This chapter initially summarises various conclusions that can be deduced from the experimental and theoretical research conducted in this work. Later, opportunities for possible research in future are summarised.

7.2. Silica Membrane for Hydrogen Reactions

A hydrogen reaction silica composite membrane has been fabricated using conventional dip-coating method with silicone elastomer as the silica precursor. The membrane proposed for reaction applications offer higher permeances for hydrogen and lower selectivity with respect to other components. The separation factor has been evaluated and is close to the value achieved by ideal Knudsen mechanism.

The developed membrane offered relatively lower permeance for hydrogen and other gases than those presented in literature with multilayer support and using TEOS as a silica source. The reason for that can be explained by the lack of a diffusion barrier between silica and the composite support which can reduce the thickness of the silica membrane. While the membrane offers lower hydrogen permeances, the cost of the membrane expected to be significantly lower than those presented in literature due to the following reasons:

- a) The composite support offers lower resistance and hence shall be cheaper.
- b) The raw materials and the equipment required for the fabrication are much cheaper than the raw materials and equipment presented in literature for the preparation of silica polymeric sols from TEOS, which involve significant investment in the experimental set up.

7.3. Silica Membrane for Hydrogen Separation

The silica membrane prepared for hydrogen separation presented single gas separation factors higher than Knudsen separation values for a hydrogen/nitrogen pair, but for hydrogen/propane pair the membrane provides a high separation factor only at higher temperatures. Lower permeances are obtained as compared with those available in literature. These lower permeances are due to the fact that the silica layer thickness deposited (30-40 μm) is higher than those fabricated using different support (30 – 100nm), with lower pore size produced by intermediate layer(s) such as γ -alumina. The higher thick membranes produce a hydrogen permeance value of $5 \times 10^{-9} \text{ mol/m}^2 \cdot \text{s} \cdot \text{Pa}$ as opposed to 10^{-6} - $10^{-7} \text{ mol/m}^2 \cdot \text{s} \cdot \text{Pa}$ for the thin layers.

The thin silica selective layers are fabricated only with the possibility of depositing a thin layer on the composite membrane whose pore size is small (5nm). Generally γ - alumina is used to obtain a layer that is about 5nm in order to function as a diffusion barrier of silica membrane. However, in this work it has not been possible to deposit γ - alumina on the support possess a high pore size of about 6000 nm and hence a thin silica layer could not be obtained which can provide higher flux.

The binary gas separation factor has been observed to be significantly higher than the single gas separation factors for hydrogen and nitrogen system. Nitrogen permeance is noted to be significantly altered and restricted due to the presence of hydrogen. From an experimental point of view, the above results are very encouraging. For example, if propane and nitrogen mixture is used as a feed to increase propane conversion, hydrogen selectivity with respect to nitrogen is particularly advantageous when compared to the value of the separation factor which is higher than the Knudsen separation factor.

With a moderate combination of hydrogen permeance and H_2/N_2 selectivity (7 – 70) at different pressure differentials, the silica composite membrane can be suggested to be applicable for hydrogen separation systems where higher product purity is not desired coupled with a moderate hydrogen permeance.

7.4. Silica Membrane for Hydrogen Purification

This work has demonstrated the fabrication of hydrogen purification silica composite membrane using modified dip-coating (suction process). The advantage of suction process over conventional dip coating is that the number of dip coating was reduced and the defects during the membrane preparation are eliminated. The other advantage is that, the repeating of coating, drying, and calcinations process is reduced therefore the period needed to prepare a membrane is less.

The experimental set up for the modified dip-coating coupled with a vacuum is relatively easy compared with the CVD process for the development of silica membrane. The vacuum application in the membrane tube has successfully blocked the macropores on the membrane surface. The silica is effectively drawn in to the macropores by cross flow plugging using the application of vacuum. Furthermore, the composite support used in this work is of higher pore size than those described in the literature and has no γ -alumina as a diffusion barrier between the silica layer and the composite support layer.

The performance of hydrogen purification silica membrane is identical to that presented by Sea et. al. (1996). Single gas hydrogen and nitrogen separation factor is observed to be about 62 at lower pressure (i.e. 1.0bar) which is much higher than the single gas separation factor evaluated using Knudsen mechanism (3.74). Binary separation factors are observed to be higher than the corresponding single gas separation factors for hydrogen and nitrogen. The observed hydrogen purity on the gas chromatograph is about 99.6 – 99.9 %. However, moderate flow rates are observed even at higher temperatures (7 ml/min at 300 °C for hydrogen) for a membrane area of 87.36 cm² and a pressure drop of 2 bars. These flow rates however can be overcome by using higher membrane surface area or developing a design that suits the use of more membrane tubes packed in a shell and tube hardware assembly or can be improved by using different support tubes with lower pore size (i.e 1000-2000 nm), which needs more investigations.

With respect to the durability of the composite membrane, it has been tested for at least five to six months. The membrane has been observed to be consistent with

respect to single gas permeation data and binary gas separation factor for the time the membrane is studied. Furthermore, the tests have demonstrated that this silica composite membrane has the capability to separate hydrogen from gas mixtures with complete hydrogen selectivity and can be used to produce pure hydrogen for applications in energetic fields in membrane reactors (i.e. isotopic hydrogen separation, fuel cell, etc.).

The application of the membrane for hydrogen purification and recovery using palladium membrane is recommended above 300 °C. This is due to the hydrogen embrittlement caused below this temperature which causes transformations in the crystal lattice. While palladium membranes are expensive and limiting due to the above reason, hydrogen purification silica membrane can be successfully applied for hydrogen purification applications in moderate temperatures (up to 300 °C) such as ammonia decomposition. With regards to the increase in flow rates, future research shall propose the introduction of diffusion barrier in order to decrease the silica thickness. Alternatively, different asymmetric supports with lower pore size may also drive membrane permeances to acceptable values.

7.5. Palladium Impregnated Silica Membrane

The Pd impregnated γ -alumina membrane exhibited very high permeances (to the order of 1×10^{-6} mol/m².s.Pa) with a range of selectivities (H₂/N₂: 3.9 – 7.2). Further the membrane can be operated at high temperatures (>300 °C). Referring to Table 1.2 presented in chapter 1, the probable applications of this membrane can be towards membrane reactor applications where high temperatures are desired. These reaction schemes refer to ethane and propane dehydrogenation. It is worth mentioning here that the silica composites have been observed to be unable to withstand higher temperatures of operation for propane dehydrogenation schemes.

One of the possible limitations of the application of this type of membrane is the higher permeances offered even for other gaseous species such as propane, nitrogen etc which can involve loss of these gaseous species towards the permeate stream.

However, a careful selection of operating conditions (temperature, pressure etc) can allow the manipulation of these losses to a minimal value. Furthermore, if there is loss towards the permeate stream, the down stream processing can be engineered to handle both permeate and retentate streams if equally important amount of gas is produced and enters the permeate stream. Alternatively, new separation schemes can be targeted that can allow extraction of these gaseous species from lower compositions. Nonetheless, if the loss of the components needs to be kept low, the membrane can undergo further pore size modification to obtain a separation layer with narrow pores, which can reduce the permeances further with an increase in selectivity.

7.6. Silica γ -Alumina Membrane

The silica γ -alumina membrane has also offered good combination of hydrogen permeances and selectivities ($6 - 13 \times 10^{-6}$ mol/m².s.Pa with a separation factor higher than to that achievable using Knudsen diffusion mechanism at temperature range 325 – 525K). Further, the set of permeances is higher than those obtained using Pd impregnated γ -alumina membrane. The membrane permeances are observed to decrease with an increase in temperature thus signifying surface diffusion mechanism. The membrane is operated to a maximum temperature of 300 °C due to inherent temperature stability problems associated with silica. The possible application of this membrane would include situations where higher permeances are necessary for reaction schemes at lower temperatures. These reaction schemes as summarised in Table 1.2 include water gas shift and toluene dehydrogenation where the reaction temperatures vary between 100 – 300 °C. Under these conditions the performance of silica membrane is stable and does not undergo degradation.

7.7. General Conclusion

The silica membranes fabricated for hydrogen separation and purification offered acceptable combination of hydrogen permeance and selectivity that can be achieved using alumina 6000nm supports. Both silica membranes for hydrogen separation and purification offered good and consistent H_2/N_2 separation factors varying from 70 – 1000. The permeation behaviour of the composite membrane is based on activated diffusion that allows higher permeances at higher temperatures. Therefore, it can be generally concluded that the membranes fabricated can be competent with those available in the literature due to their cost effective features such as cheap support, use of silicone elastomer etc.

The modified procedure of dip-coating deposition coupled with suction process has been highly successful to obtain high purities using silica composites whose macropores are completely plugged. Very high purities are achieved that reveal the separation potential of the membrane fabricated for hydrogen purification. These features allow the utilisation of hydrogen purification silica membrane for hydrogen extraction to stream temperatures of about 300 °C from various types of hydrogen rich impure streams. Furthermore, utilisation for the development of a membrane reactor for ammonia decomposition and water gas shift reaction is proposed due to inherent characteristics of the silica membrane and reaction scheme.

The hydrogen reaction membrane fabricated using a conventional dip-coating provides a good permeance but low selectivity. The impact of Pd impregnated in the surface pores of γ -alumina is evident from the separation factors observed which are higher than those achievable with Knudsen diffusion mechanism. The Pd impregnated membrane offers best combination of membrane permeances and separation factors to operate at higher temperature and lower pressure. Such a combination is suitable for a reaction scheme like propane dehydrogenation that requires operation at higher temperatures (>300 °C) and lower pressure (0.5 – 1.0 bar).

7.8. Modelling and simulation

The modelling effort constituted a mass energy and pressure balances model for membrane reactor investigation using silica composite membranes. The model has been compared using the kinetics and membrane permeances data presented by Yildirim et. al. (1997). The model has been tested for three different membranes namely silica membrane for reaction application, Pd impregnated γ -alumina membrane and silica modified γ -alumina membrane all fabricated in this work. Two different types of catalyst have been tested that refer to Pt-Sn-K and Pt catalysts. It has been observed that the performance of silica modified γ -alumina membrane is the best providing a theoretical conversion of about 83 % opposed to an equilibrium conversion value of about 50 % at 600 °C. However, since the silica membrane cannot withstand higher temperatures, the Pd impregnated γ -alumina membrane is chosen for theoretical studies. Pt-Sn-K catalyst has been selected for these studies due to providing slightly higher conversion values.

The performance of annular membrane reactor (AMR) has been observed to be strongly dependent on the feed flow rate and temperature of the oven in comparison with the tubular membrane reactor (TMR). At lower feed flow rates, AMR provided similar performance to TMR signifying both AMR and TMR operation are close to isothermal operation. However, as feed flow rate is increased, AMR operation is observed to be better than TMR due to inherent mechanisms explained in the relevant sections of chapter 6. The following conclusions hold for the performance of annular and tubular reactor configurations based on the case study:

Catalyst:

The conversion obtained using Pt-Sn-K catalyst has been about 1-2 % higher than the conversion obtained using Pt catalyst at high temperatures (600 °C).

Temperature of the oven:

The temperature of the oven significantly affects the conversion of both tubular and annular reactors. This is evident with the variation of conversion with oven temperature for various simulations.

Feed flow rate:

An increase in feed flow rate that relates to a decrease in reactant contact time usually decreases the conversion. The conversion decreases for all membrane reactor configurations and tubular configuration. The reactant flow rate is observed to not affect the performance of AR.

Feed composition:

For all configurations, an increase in feed composition leads to a decline in conversion.

Sweep gas flow:

An increase in sweep gas flow provided mixed response in the system. Up to a certain value, the sweep gas provided higher conversion at higher temperature. However, after a particular critical value, the conversion decreased. This is attributed to the heat reduction of H₂ mole fraction in the permeation zone due to high Argon gas concentration that reduces H₂ flux and conversion. Coupled to this effect, reactant loss also reduces conversion.

In conclusion, the annular reactor configurations perform better than tubular reactor configurations at lower temperatures and very well at high temperatures. The theoretical study in this work related to the operation of membrane reactors (TMR and AMR) at different features. These features include feed flow rate sweep gas flow rate, membrane permeance. It is very important to conclude that the Pd impregnated membranes offer very high conversions (about 82 %) at 600 °C with operation at 1.013 bars on both retentate and permeate sections. While a lower value of about 60 % is obtained using corresponding AR configuration, the very high value of membrane reactor conversion coupled with the ability to use a Pd impregnated membrane at higher temperature suggests the applicability of these type of membranes for industrial operation.

7.9. Summary of Conclusions

In summary, this work has been able to target certain key issues associated with silica composite membranes for hydrogen reaction, separation and purification.

The original contribution of this work is presented as follows:

- The replacement of conventional fine sized support with commercially available porous α -alumina tube with an average pore size of 6000nm. This is cheaper and eliminates the need for an extra intermediate layer deposition which requires a highly complex, tedious and time consuming process.
- The utilisation of silicone elastomer which is not widely used in membrane technology was selected as the precursor to prepare composite membranes. This eliminates the complexity involved to prepare silica polymeric sols using other silica sources such as TEOS.
- A modified dip-coating procedure to prepare composite membrane for hydrogen purification has been developed using a vacuum pump to assist suction of silicon inside the pores of the support. The membrane produced shows high hydrogen selectivity compared to that prepared using conventional dip-coating. The modified method resulted in a reduction in the number of repeated coating, drying and calcinations cycles and hence an overall reduction in the preparation time that is needed in conventional dip-coating.
- A theoretical model for the assessment of annular and tubular membrane reactor configurations for propane dehydrogenation as the model reaction is developed. This model is applied on three different membranes namely: silica-alumina membrane, silica- γ -alumina membrane and palladium impregnated membrane. Results indicated that Pd impregnated membrane provided very high theoretical conversions (82 %) at 600 °C compared with silica composite membrane.

7.10. Future work

The only limitation that can be referred to in this work is the inability of the silica composite membrane for hydrogen purification to withstand temperatures higher than 300 °C coupled with the high selectivity that is required for pure hydrogen production. Contemporary research in composite membranes and membrane reactors for hydrogen reaction, separation and purification can be successfully extended to new areas of research. These areas are confined to the improvement in membrane preparation procedures for stable and selective composite membranes that are cost effective.

The following objectives have to be considered for the development of membrane reactor technology for industrial implementation:

- Further research shall look forward to the development of suitable silica precursors that can withstand a high temperature (i.e. > 300 °C) using sol-gel method for the composite preparation. If successful, this area of research will drive the materials research to a level where the industrial implementation for high temperature reactions will be definitely feasible.
- In membrane reactor applications at high temperature, the development of excellent quality sealing materials and techniques is needed by more research conducted towards this area.
- The performance of silica membranes prepared from silicone elastomer needs to be tested experimentally in different reactions and conditions. Since the temperature limitation exists, the membrane is recommended for utilisation in membrane reactor schemes such as water gas shift, toluene dehydrogenation whose temperature of operation is up to 300 °C.

Further, if the proposed future work is successful, the implementation of silica composites for large scale processing in industry is feasible to meet the requirements of gas processing in the twenty first century.

REFERENCES

- 1) Armor, J. N., (1989). Catalysis with Permselective Inorganic Membranes, *Appl. Catal.*, 49, 1.
- 2) Armor, N. J., (1998). Application of Catalytic Inorganic Membrane Reactors to Refinery Products, *J. Memb. Sci.*, 147, 217.
- 3) Asaeda M. and Yamasaki S., (2001). Separation of Inorganic / Organic Gas Mixtures by Porous Silica Membranes, *Separation and Purification Technology*, 25, 151.
- 4) Assabumrungrat, S., White D. A., (1996). Modelling Endothermic Reactions in a Compound Membrane Reactor, *Gas. Sep. Purif.* 10 (1), 47.
- 5) Assabumrungrat S., Jhoraleecharnchai W., Praserttham P and Goto S., (2000). Kinetics for Dehydrogenation of Propane on Pt-Sn-K/ γ -Al₂O₃ Catalyst., *J. Chem. Engg., Japan*, 33 (3), 529.
- 6) Athayde, A. L., Baker R. W. and Nguyen P., (1994). Metal Composite Membranes for Hydrogen Separation, *J. Membr. Sc.*, 94, 299.
- 7) Baker, R. W., (2000). *Membrane Technology and Applications*, McGraw - Hill.
- 8) Barbieri G., Marigliano G., Golemme G. and Drioli E., (2002). Simulation of CO₂ Hydrogenation with CH₃OH Removal in a Zeolite Membrane Reactor, *Chemical Engineering Journal*, 85, 53.
- 9) Becker Y.L., Dixon A.G., Moser W.R. and Ma Y.H., (1993). Modelling of Ethylbenzene Dehydrogenation in a Catalytic Membrane Reactor, *Journal of Membrane Science*, 77, 233.
- 10) Bennett, C. O. and Myers, J. E., (1962). *Momentum, Heat, and Mass Transfer*, McGraw-Hill.

- 11) Bernstein L. A. and Lund C. R. F., (1993). Membrane Reactors for Catalytic Series and Series Parallel Reactions, *Journal of Material Science*, 77, 155.
- 12) Beuscher U. and Gooding C. H., (1998). The Permeation of Binary Gas Mixtures Through Support Structures of Composite Membranes, *Journal of Membrane Science*, 150, 57.
- 13) Bhavé R.R., (1991). *Inorganic Membranes: Synthesis, Characteristics and Applications*, Van Nostrand Reinhold, New York.
- 14) Bitter, J.G.A. (1988). Processes and Apparatus for the Dehydrogenation of Organic Compounds, U.K. Pat. Appl., GB 2201159A.
- 15) Brinker C. J. and Scherer, G. W., (1990). *Sol-gel Science: The Physics and Chemistry of sol-gel processing*, Academic press, San Diego.
- 16) Brinker, C. J., Ward, T. L., Sehgal, R., Raman, N. K., Hietala, S. L., Smith, D. M., Hua, D. W. and Headley, T. J., (1993). Ultra-microporous Silica-Based Supported Inorganic Membranes, *J. Memb. Sci.*, 77, 165.
- 17) Burggraaf, A. G. and Cot, L., (1996). *Fundamentals of Inorganic Membrane Science and Technology*, Elsevier, Amsterdam.
- 18) Champagnie A. M., Tsotsis T. T., Minet, R. G. and Wagner E., (1992). The Study of Ethane Dehydrogenation in a Catalytic Membrane Reactor, *Journal of Catalysts*, 134, 713.
- 19) Chan P.P.Y., Vanidjee K., Adesina A.A. and Rogers P.L., (2000). Modeling and Simulation of Non-Isothermal Catalytic Packed Bed Membrane Reactor for H₂S Decomposition, *Catalysis Today*, 63, 379.
- 20) Chang J. S. Roh, H. S. Park, M. S. and Park S. E., (2002). Propane Dehydrogenation over a Hydrogen Permselective Membrane Reactor, *Bull. Korean Chem. Soc.* 23 (5), 67.

- 21) Cicero, D. C., Jarr, L. A., (1985). Application of Ceramic Membranes in Advanced Coal-Based Power Generation Systems, *Sep. Sci. Technol.* 25, 1455.
- 22) Collins J.P, Schwartz R.W., Sehgal R., Ward T.L., Brinker C. J., Hagen G.P., and Udovich C.A., (1996). Catalytic Dehydrogenation of Propane in Hydrogen Permselective Membrane Reactors, *Ind. Eng. Chem. Res.*, 35, 4398.
- 23) Collins, J. P. and Way, J. D., (1993). Preparation and Characterization of a Composite Palladium-Ceramic Membranes, *Int. Eng. Chem. Res.*, 32, 3006.
- 24) Collins, R. E., (1961). Flow of Fluid through Porous Materials, Academic Press.
- 25) Connor, H., (1962). Palladium Alloy Diffusion Cells – Commercial Units for Production of Ultrapure Hydrogen, *Plat. Met. Rev.*, 4, 130.
- 26) Cowper C. J. and De Rose A. J., (1983). The Analysis of Gases by Chromatography, Pergamon Press.
- 27) De Lang, R. S. A., Keizer, A. J., Burggraaf, A. J., (1995). Characterization of Microporous Non-supported Membrane Top-layer using Physisorption Techniques, *J. Porous Mater.*, 1, 139.
- 28) De Lange R.S.A., Hekkink J.H.A., Keizer K. and Burggraaf A.J., (1995^c). Permeation and separation studies on microporous sol-gel modified ceramic membranes, *Microporous materials*, 4, 169.
- 29) De Lange R.S.A., Hekkink J.H.A., Keizer K., Burggraaf A.J., (1995^a). Formation and characterization of supported microporous ceramic membranes prepared by sol-gel modification techniques, *Journal of Membrane Science*, 99, 57.
- 30) De Lange R.S.A., Keizer K., Burggraaf A.J., (1995^b). Analysis and theory of gas transport in microporous sol-gel derived ceramic membranes. *Journal of Membrane Science*, 104, 81.

- 31) De Vos R.M., and Verweij H., (1998). Improved Performance of Silica Membranes for Gas Separation, *Journal of Membrane Science*, 143, 37.
- 32) De Vos R.M., Maier W.F., Verweij H., (1999). Hydrophobic Silica Membranes for Gas Separation. *Journal of Membrane Science*, 158, 277.
- 33) De Wiest, R. J. M., (1969). *Flow through Porous Media*, Academic Press.
- 34) Diniz da Costa J.C., Lu G.Q. and Rudolph V., (2000). Transport Mechanism in Weakly Branched Silica Films. *Adsorption Science and Technology*. World Scientific, Singapore, 381.
- 35) Diniz da Costa J.C., Lu G.Q., Rudolph V. and Lin Y.S., (2002). Novel Molecular Sieve Silica (MSS) Membranes: Characterisation and Permeation of Single-Step and Two Step Sol-Gel Membranes. *Journal of Membrane Science*, 198, 9.
- 36) Dittmeyer R., Höllein V. and Daub, K., (2001). Membrane Reactors for Hydrogenation and Dehydrogenation Processes Based on Supported Palladium, *J. of Molecular Catalysis A: Chemical*, 173, 135.
- 37) Dullien, F. A. L., (1992). *Porous Media: Fluid Transport and Pore Structure*, 2nd ed., Academic Press, New York.
- 38) Everett, D. H. and Ottewill, R. H., (1969). *Surface Area Determination*, International Union of Pure and Applied Chemistry, London, Butter Worths.
- 39) Farris, T. S., Armor, N. J., (1993). Liquid Phase-Hydrogenation Using Palladium Alloy Membranes, *Appl. Catal. A* 96, 25.
- 40) Garside, J. (1988). *Separation Technology: The Next Ten Years*, Press.
- 41) Gavalas G.R. and Ioannides T., (1993). Catalytic Isobutane Dehydrogenation in a Dense Silica Membrane Reactor, *Journal of Membrane Science*, 77, 207.

-
- 42) Gavalas G.R. and Tsapatsis M., (1992). A Kinetic Model of Membrane Formation by CVD of SiO_2 and Al_2O_3 . *AIChE Journal*, 38, 847.
 - 43) Gavalas G.R., Tsapatsis M., Kim S., Nam S.W., (1991). Synthesis of Hydrogen Permselective SiO_2 , TiO_2 , Al_2O_3 and B_2O_3 Membranes from the Chloride Precursors, *Industrial Engineering Chemistry Research*, 30, 2152.
 - 44) Gavalas, G.R., Megiris C.E., and Nam S.W., (1989). Deposition of H_2 Permselective SiO_2 Thin Films, *Chemical Engineering Science*, 44, 1829.
 - 45) Giessler S., Jordan L., Costa J., Lu G.Q., (2003). Performance of Hydrophobic and Hydrophilic Silica Membrane Reactors for the Water Gas Shift Reaction, *Separation and Purification Technology*, 32, 1-3, 255.
 - 46) Gilliland E., Baddour R.F. and Perkinson G.P., (1974). Diffusion on Surfaces. Effect on Concentration on the Diffusivity of Physically Adsorbed Gases, *Industrial Engineering Fundamentals*, 13, 95.
 - 47) Gobina E., Hou K. and Hughes R., (1995^a). Ethane Dehydrogenation in a Catalytic Membrane Reactor Coupled with a Reactive Sweep Gas, *Chemical Engineering Science*, 50, 14, 2311.
 - 48) Gobina E., Hou K. and Hughes R., (1995^b). Equilibrium – Shift in Alkane Dehydrogenation Using a High Temperature Catalytic Membrane Reactor, *Catalysis Today*, 25, 365.
 - 49) Gokhale Y.V., Noble R.D., Falconer J.L., (1995). Effects of Reactant Loss and Membrane Selectivity on a Dehydrogenation Reaction in a Membrane-Enclosed Catalytic Reactor, *Journal of Membrane Science*, 105, 63.
 - 50) Gorriz, O. F., Corberan, V. C., and Fierro, L.G., (1992). Propane Dehydrogenation and Coke Formation on Chromia-Alumina Catalysts: Effect of Reductive Pretreatments, *Ind. Eng. Chem. Res.* 31, 2670.

-
- 51) Govind, R. and Atnoor, D., (1991). Development of a Composite Palladium Membrane for Selective Hydrogen Separation at High Temperature, *Ind. Eng. Chem. Res.*, 30, 391.
 - 52) Gryaznov, V. H., Serebryannikova, O. S., Serov, Y. M., Ermilova, M. M., Karavanov, A. N., Mischenko, A. P., Orekhova, N. V., (1993). Preparation and Catalysis over Palladium Composite Membranes, *Appl. Catal. A* 96, 15.
 - 53) Hakuta T. (1988). *Advancement in Membrane Separation Technology*, Kagaku Kogaku, 52, 112.
 - 54) Hara S., Sakaki, K., Itoh N.B., Kimura, H. M., Asami K. and Inoue A., (2000). An Amorphous Alloy Membrane without Noble Metals for Gaseous Hydrogen Separation, *J. Membr. Sci.*, 164, 289.
 - 55) Hassan M.H., Way J.D., Thoen P.M., Dillon A.C., (1995). Single Component and Mixed Gas Transport in a Silica Hollow Fiber Membrane, *Journal of Membrane Science*, 104, 27.
 - 56) Hermann C.h., Quicker P. and Dittmeyer R., (1997). Mathematical Simulation of Catalytic Dehydrogenation of Ethylbenzene to Styrene in a Composite Palladium Membrane Reactor. *Journal of Membrane Science*, 136, 161.
 - 57) Hsieh H. P., (1991). Inorganic Membrane Reactors, *Catal. Rev. Sci. Engng* 33, (1&2).
 - 58) Hsieh, H. P., (1996). *Inorganic Membranes for Separation and Reaction*, Elsevier.
 - 59) Hwang G., Kim J., Choi H. and Onuki K., (2003). Stability of a silica membrane prepared by CVD using γ - and α -alumina tube as the support tube in the HI-H₂O gaseous mixture, *Journal of Membrane Science*, (2003), 293.

-
- 60) Hwang G., Onuki K., Shimizu S., Ohya H., (1999). Hydrogen Separation in H₂-H₂O-HI Gaseous Mixture using the Silica Membrane Prepared by Chemical Vapor Deposition, *Journal of Membrane Science*, 162, 83.
- 61) Hwang, G.-J. and Onuki, K., (2001). Simulation Study on the Catalytic Decomposition of Hydrogen Iodide in a Membrane Reactor with a Silica Membrane for the Thermochemical Water-Splitting IS Process, *Journal of Membrane Science*, 194, 207.
- 62) Internet website reference 1: http://www.chemical-engineering-design.com/design%20thesis/Hydrogen/Hydrogen_Properties&uses..pdf
- 63) Internet website reference 2: <http://www.the-innovationroup.com/ChemProfiles/Hydrogen.htm>
- 64) Internet website reference 3: <http://www.airliquide.com/en/business/industry/oilgas/applications/purification.asp>
- 65) Internet website reference 4: <http://www.mtrinc.com/Pages/Refinery/refinery.html>
- 66) Ioannides T. and Gavalas G. R. (1993). Catalytic Isobutane Dehydrogenation in a Dense Silica Membrane Reactor, *Applied Catalysis A: General*, 96 (1), 106.
- 67) Itoh N., Shindo, Y., Hakuta, T. and Yoshitome, H., (1984). Enhanced Catalytic Decomposition of HI by using a Microporous Membrane, *Int. J. Hydrogen Energy*, 9 (10), 825.
- 68) Itoh, N. (1987). A Membrane Reactor using Palladium, *AIChE J.* 33, 1576.
- 69) Itoh, N., (1990). Simulation of Bifunctional Palladium Membrane Reactor, *J. of Chem. Eng. of Japan*, 23(1), 81.

-
- 70) Itoh, N., Shindo, Y., Haraya, K., Obata, K., Hakuta, T. and Yoshitome, H., (1985). Simulation of a Reaction Accompanied by Separation, *Int. Chem. Eng.*, 25, 138.
 - 71) Itoh, N., Tomura, T., Tsuji T. and Hongo M., (2000). Deposition of Palladium Inside Straight Mesopores of Anodic Alumina Tube and Its Hydrogen Permeability, *Microporous and Mesoporous Materials*, 39, 103.
 - 72) Jayaraman, V., Lin, Y. S., Pakala, M. and Lin, R. Y., (1995). Fabrication of Ultrathin Metallic Membranes on Ceramic Supports by Sputter Deposition, *J. Memb. Sci.*, 99, 89.
 - 73) Jiang S., Yan Y., Gavalas G.R., (1995). Temporary Carbon Barriers in the Preparation of H₂ Permselective Silica Membranes, *Journal of Membrane Science*, 96, 275.
 - 74) Keizer, K., Uhlhorn, R. J. R., Van Vuren, R. J. and Burggraaf, A. J., (1988). Gas Separation Mechanisms in Microporous Modified g-Al₂O₃ Membranes, *Journal of Membrane Science*, 39, 285.
 - 75) Kikuchi, E. and Uemiya, S. (1991). Preparation of Supported Thin Palladium - Silver Alloy Membranes and their Characteristics for Hydrogen Separation, *Gas Sep. Purif.* 5, 261.
 - 76) Kikuchi, E., (1995). Palladium / Ceramic Membranes for Selective Hydrogen Permeation and Their Application to Membrane Reactor, *Catal. Today*, 25, 333.
 - 77) Kitao S., Kameda H., and Asaeda M., (1990). Gas Separation by Thin Porous Silica Membrane of Ultra Fine Pores at High Temperature, *Membrane*, 15, 222.
 - 78) Koukou M.K., Chaloulou G., Papayannakos N., Markatos N.C., (1997). Mathematical Modelling of the Performance of Non-Isothermal Membrane Reactors, *International Journal of Heat and Mass Transfer*, 10, 2407.

-
- 79) Kuraoka K., N. Kubo, T. Yazawa, (2000). Microporous Silica Xerogel Membrane with High Selectivity and High Permeance for Carbon Dioxide Separation, *Journal of Sol-Gel Science and Technology*, 19, 515.
- 80) Kusakabe K., Sakamoto S., Saie T. and Morooka S., (1999). Pore Structure of Silica Membranes Formed by a Sol-Gel Technique Using Tetraethoxysilane and Alkyltriethoxysilanes, *Separation and Purification Technology*, 16, 139.
- 81) Larbot, A., alary, j. A., Guizard, C. and Cot L., (1987). New inorganic ultrafiltration membranes: preparation and characterization, *Int. J. High technology Ceramics* 3, 143.
- 82) Lee D. and Oyama S. (2002). Gas Permeation Characteristics of a Hydrogen Selective Supported Silica Membrane, *Journal of Membrane Science*, 210, 291.
- 83) Lee D., Lee Y., Nam S., Sea B. and Lee K., (2003). Preparation and Characterization of SiO₂ Composite Membrane for Purification of Hydrogen from Methanol Steam Reforming as an Energy Source System for PEMFC, *Separation and Purification Technology*, 32, 45 – 50.
- 84) Lee S-Y., Lee S-J, Kwon S-J, Yang S-M and Park S. B., (1995). Preparation of Sol - Gel Driven Alumina Membrane Modified by Soaking and Vapor – Deposition Method, *Journal of Membrane Science*, 108, 97.
- 85) Li A, Xiong G., Gu J., Zheng L., (1996). Preparation of Pd / Ceramic Composite Membrane 1. Improvement of the Conventional Preparation technique, *J. Membr. Sc.*, 110, 257.
- 86) Marigliano G., Barbieri G. and Drioli E., 2001. Effect of Energy Transport on a Palladium-Based Membrane Reactor for Methane Steam Reforming Process, *C. Today.*, 67 (1-3), 85.
- 87) Meunier G. and Manaud J. P., (1992). Thin Film Permeation Membranes for Hydrogen Purification, *International J. of Hydrogen Energy*, 17, 599.

-
- 88) Moaddeb M. and Koros, W. J., (1995). Silica – Treated Ceramic Substrates for Formation of Polymer-Ceramic Composite Membranes, *Ind. Eng. Chem. Res.*, 34, 236.
- 89) Mohan K. and Govind, R., (1988). Analysis of a Cocurrent Membrane Reactor, *AIChE J.*, 32, 2083.
- 90) Mordkovich, V. Z., Baichtoch, Yu. K., and Sosna, M. H., (1992). The Large – Scale production of Hydrogen from Gas Mixtures: A use for Ultra–Thin Palladium Alloy Membranes, *International J. of Hydrogen Energy*, 18, 539.
- 91) Morooka S., Kim S.S., Yan S., Kusakabe K. and Watanabe M., (1996). Separation of hydrogen from an H₂-H₂O-HBr system with an SiO₂ membrane formed in macropores of an α -alumina support tube. *International Journal of Hydrogen Energy*, 21 (3), 183.
- 92) Morooka S., Yan S., Kusakabe K., Akiyama Y., (1995). Formation of hydrogen permselective SiO₂ membrane in macropores of α -alumina support by thermal decomposition of TEOS. *Journal of Membrane Science*, 101, 89.
- 93) Mulder, M. (1996). *Basic Principles of Membrane Technology*, Kluwer Academic Publishers, London.
- 94) Munoz-Aguado, M. J., and Gregorkiewitz, M., (1996). Preparation of Silica-Based Microporous Inorganic Gas Separation Membranes. *Journal of Membrane Science*, 111, 7.
- 95) Munro L. A., (1964). *Chemistry in Engineering*, Prentice – Hall, INC., Englewood Cliffs, N. J., 256.
- 96) Nair B.N., Keizer K., Elferink W.J., Gilde M.J., Verweij H., Burggraaf A.J., (1996). Synthesis, Characterisation and Gas Permeation Studies on Microporous Silica and Alumina-Silica Membranes for Separation of Propane and Propylene, *Journal of Membrane Science*, 116, 161.

-
- 97) Nair B.N., Yamaguchi T., Okubo T., Suematsu H., Keizer K., Nakao S., (1997). Sol-Gel Synthesis of Molecular Sieving Silica Membranes, , J. Membr. Sci. , 135, 237
- 98) Nakao S., Suzuki T., Sugawara T., Tsuru T., Kimura S., (2000). Preparation of Microporous Membranes by TEOS/O₃ CVD in the Opposing Reactants Geometry, Mesoporous and microporous materials, 37, 145.
- 99) Nijmeijer A., Bladergroen B.J., Verweij H., (1998). Low-Temperature CVI Modification of γ -alumina Membranes, Mesoporous and Microporous Materials, 25, 179.
- 100) Nishiyama, N., Park, D. H. and Egashira, Y. (2003). Pore Size Distributions of Silylated Mesoporous Silica MCM-48 Membranes, Separation and Purification Technology, 32, 127.
- 101) Nobel, R. D., Stern, S. A., (1995). Polarization Phenomena and Membrane Fouling, Membrane Separations Technology: Principles and Applications, chapter 2, 53.
- 102) Osada Y., Nakagawa, T., (1992). Membrane Science and Technology, Marcel Dekker, INC.
- 103) Osipow, L. I., (1962). Surface Chemistry Theory and Industrial Applications, Chapman & Hall, Ltd., London.
- 104) Pandey P., Chauhan, R. S., (2001). Prog. Polym. Science, 26, 853.
- 105) Philpott, J. E., (1985). Hydrogen Diffusion Technology. Commercial Applications of Palladium Membrane, Plat. Met. Rev., 29, 12.
- 106) Prabhu A., Oyama S.T., (2000). Highly Hydrogen Selective Ceramic Membranes: Application to the Transformation of Greenhouse Gases, Journal of Membrane Science, 176, 233.

-
- 107) Prabhu A.K., A. Liu, L. G. Lovell and S. T. Oyama (2000). Modeling of the Methane Reforming Reaction in Hydrogen Selective Membrane Reactors, *Journal of Membrane Science*, 177, 83.
- 108) Quicker P., Höllein V. and Dittmeyer R. (2000). Catalytic Dehydrogenation of Hydrocarbons in Palladium Composite Membrane Reactors, *Catalysis Today*, 56, 1.
- 109) Raman, N. K., and Brinker, C. J., (1995). Organic Template Approach to Molecular Sieving Silica Membranes, *J. Membr. Sci.*, 105, 273.
- 110) Rao, M. B. and Sircar, S, (1993). Nanoporous Carbon Membranes for Separation of Gas Mixtures by Selective Surface Flow, *Journal of Membrane Science*, 85, 253.
- 111) Richard V., Favre E., Tondeur D., Nijmeijer A., (2001). Experimental Study of Hydrogen, Carbon Dioxide and Nitrogen Permeation through Microporous Silica Membrane, *Chemical Engineering Journal*, 84, 593.
- 112) Rouessac V., Ferreira P. and Durand J. (2003). Preparation of Silica Membranes Inside Macroporous Alumina Tubes by PECVD for Hydrogen Selectivity, *Separation and Purification Technology*, 32, 1-3, 37.
- 113) Rouquerol, J., Avnir, D., Fairbridge, C. W., Everett D. H., Haynes, J. H., Pernicone, N., Ramsay, J. D. F., Sing, K. S. W., Unger, K. K., (1994). Recommendations for the Characterization of Porous Solids, *Pure & Appli. Chem.* 66, 1739.
- 114) Ruthven, D. M., (1984). Principles of Adsorption and Adsorption Processes, John Wiley & Sons, 1.
- 115) Saracco, G. and Specchia, V., (1994). Catalytic Inorganic Membrane Reactors: Present Experience and Future Opportunities, *Catal. Rev. Sci. Engng*, 36, 305.

-
- 116) Saracoo, G., Neomagus, H. W. J. P., Versteeg, G. F., Van Swaaij, W. P. M., (1999). High-Temperature Membrane Reactors: Potential and Problems, *Chem. Eng. Sci.*, 54, 1997.
- 117) Satterfiels, C. N., (1991). *Heterogeneous Catalysis in industrial Practice*, 2 nd ed. McGraw-Hill, New York, 131.
- 118) Schafer R., Noack M., Kolsch P., Stohr M. and Caro J., (2003). Comparison of Different Catalysts in the Membrane Supported Dehydrogenation of Propane, *Catalysis Today*, 82 , 1-4, 15.
- 119) Schafer R., Noack M., Kolsch P., Thomas S., Seidel-Morgenstern A., Caro J. (2001). Development of a H₂-selective SiO₂-Membrane for the Catalytic Dehydrogenation of Propane, *Separation and Purification Technology*, 25, 3 - 9.
- 120) Schroeder, H. (1969. In *Physics of Thin Films*; Hass, B.; Thus, R. E., Eds.; *Advances in Research and Development*; Academic Press: New York, Vol. 5, 87.
- 121) Scriven, L. E., (1988). *Better Ceramics through Chemistry III*. Eds. Brinker, C. J., Clark, D. E. and Ulrich, D. R., (Mat. Res. Soc., Pittsburgh, Pa.), 717-722.
- 122) Sea B., Ando K., Kusakabe K., Morooka S., (1998). Separation of Hydrogen from Steam using a SiC-Based Membranes Formed by Chemical Vapor Deposition of Triisopropylsilane, *Journal of Membrane Science*, 146, 73.
- 123) Sea B., Kusakabe K., Morooka S., (1997). Pore Size Control and Gas Permeation Kinetics of Silica Membranes by Pyrolysis of Pheny-Substituted Ethoxysilanes with Cross-Flow through a Porous Support Wall. *Journal of Membrane Science*, 1, 30, 41.
- 124) Sea B., Watanabe M., Kusakabe K., Morooka S., Kim S., (1996). Formation of Hydrogen Permselective Silica Membrane for Elevated Temperature Hydrogen Recovery from a Mixture Containing Steam. *Gas Separation and Purification*, 10, 3, 187.

-
- 125) Sheintuch M and Dessau R. M., (1996). Observations, Modeling and Optimization of Yield, Selectivity and Activity During Dehydrogenation of Isobutane and Propane in a Pd Membrane Reactor, *Chemical Engineering Science*, 51, (4), 535.
- 126) Shelekhin, A. B., Pien, S. and Ma Y. H., (1995). Permeability, Surface Area, Pore Volume and Pore Size of Vycor Glass Membrane Heat-Treated at High Temperature. *Journal of Membrane Science*, 103, 39.
- 127) Shouxiang, Ma, Jiang, Ming-Xuan and Morrow,(1991). Correlation of Capillary Pressure Relationship and Calculations of Permeability, SPE No. 22685.
- 128) Shu, J., Grandjean, B. P. A. and Kaliaguine, S., (1993). Simultaneous Deposition of Pd and Ag on Porous Stainless Steel by Electroless Plating, *J. Membr. Sc.*, 77, 181.
- 129) Shu, J., Grandjean, B. P. A., van Neste, A. and Kaliaguine, S., (1991). Catalytic Palladium – Based Membrane Reactors: A Review, *Can. J. Chem. Eng.*, 69, 1036.
- 130) So J., Yang S. and Park S.B., (1998). Preparation of Silica-Alumina Composite Membranes for Hydrogen Separation by Multi-Step Pore Modifications. *Journal of Membrane Science*, 147, 147.
- 131) Soria, R., (1993). Overview on Industrial Membranes, *Catal. Today*, 25, 285.
- 132) Sotowa K., Hasegawa Y., Kusakabe K., Morooka S., (2002). Enhancement of CO Oxidation by use of H₂ Selective Membranes Impregnated with Noble Metal Catalysts, *International Journal of Hydrogen Energy*, 27, 339.
- 133) Sperling, L. H., (1992). Introduction to Physical Polymer Science, John Wiley and Sons.

-
- 134) Stitt E. H., Jackson S. D., Shipley D. G. and King F., (2001). Modelling Propane Dehydrogenation in a Rotating Monolith Reactor , *Catalysis Today*, 69, 217.
- 135) Sturchio M., Nechamkin H. and Dorfman H., (1966). *Chemistry Principles and Concepts*, Prentice-Hall, Inc., Englewood Cliffs, N. J., 103.
- 136) Tough, I. (2001). *An Introduction to the Scanning Electron Microscope*, Class Notes, Department of Applied Science, The Robert Gordon University.
- 137) Tough, I. (2002). *Quantitative X-Ray Analysis using Scanning Electron Microscope*, Class Notes, Department of Applied Science, The Robert Gordon University.
- 138) Tsai C., Tam S., Lu Y. and Brinker C.J., (2000). Dual Layer Asymmetric Microporous Silica Membranes, *J. Membr. Sci.* , 169, 255.
- 139) Tsapatsis M., and Gavalas, G., (1994). Structure and Aging Characteristics of H₂ Permselective SiO₂ Vycor Membranes, *J. Memb. Sci.*, 87, 281.
- 140) Tsapatsis, M., Kim, S., Nam, S. W. and Gavalas, G., (1991). Synthesis of Hydrogen Perselective SiO₂, TiO₂, Al₂O₃ and B₂O₃ Membranes from the Chloride Precursors, *Ind. Eng. Chem. Res.*, 30, 2152.
- 141) Tsuru, T., Sudou, T., Kawahara, S., Yoshioka, T. and Asaeda M, (2000). Permeation of Liquids Through Inorganic Nanofiltration Membranes, *J. of Colloid and Interface Sci.*, 228, 292.
- 142) Uemiya S., Sato N., Ando, H., Kude, Y., Sugino, K., Sato, N., Matsuda, T., and Kikuchi, E. (1988). A Palladium / Porous Glass Composite Membrane for Hydrogen Separation, *Chem. Lett.*, 1687.
- 143) Uemiya, S., Matsuda T., and Kikuchi E. (1990). Aromatization of Propane Assisted by Palladium Membrane Reactor, *Chem. Lett.*, 1335.

-
- 144) Uemiya, S., Matsuda, T., Kikuchi, E., (1991). Hydrogen Permeable Palladium-Silver Alloy Membrane Supported on Porous Ceramics, *Journal of Membrane Science*, 56, 315.
- 145) Uemiya, S., Sato, N., Ando, H., Kikuchi, E. (1991^a). The Water Gas Shift Reaction Assisted by a Palladium Membrane Reactor, *Ind. Eng. Chem. Res.*, 30, 585.
- 146) Uemiya, S., Sato, N., Ando, H., Matsuda, T., and Kikuchi, E. (1991^b). Steam Reforming of Methane in a Hydrogen – Permeable Membrane Reactor, *Appl. Catal.*, 67, 223.
- 147) Uhlhorn R.J.R., Keizer K., Burggraaf A.J., (1989). Gas and Surface Diffusion in Modified γ -alumina Systems. *Journal of Membrane Science*, 46, 225.
- 148) Uhlhorn R.J.R., Keizer K., Burggraaf A.J., (1992). Gas Transport and Separation with Ceramic Membrane. Part I, *Journal of Membrane Science*, 66, 259.
- 149) Uhlhorn, R. J. R., Keizer, K. and Burggraaf, A. J., (1992). Gas Transport and Separation with Ceramic Membranes. Part II: Synthesis and Separation Properties of Microporous Membranes, *J. Membr. Sci.*, 15 (4), 222.
- 150) Vitulli G., Pitzalis E., Salvadori P., Capannelli G., Monticelli O., Servida A. and Julbe A., (1995). Porous Pt/SiO₂ Catalytic Membranes Prepared Using Mesitylene Solvated Pt Atoms as a Source of Pt Particles, *Catalysis Today*, 25 (3-4), 249.
- 151) Weyten H., Keizer K., Kinoo A., Luyten J and Leysen R (1997). Dehydrogenation of Propane Using a Packed-Bed Catalytic Membrane Reactor, *AIChE Journal*, 43, 1819.
- 152) Weyten H., Luyten J., Keizer K., Willems L. and Roger Leysen (2000). Membrane Performance: The Key Issues for Dehydrogenation Reactions in a Catalytic Membrane Reactor, *Catalysis Today*, 56 (1-3), 3.

-
- 153) Wu J.C.S., Flowers D.F. and Liu P.K.T. (1993). High Temperature Separation of Binary Gas Mixtures Using Microporous Ceramic Membranes, *Journal of Membrane Science*, 77, 85.
- 154) Wu J.C.S., Sabol H., Smith G.W., Flowers D. F. and Liu P.K.T. (1994). Characterization of Hydrogen Permselective Microporous Ceramic Membranes, *Journal of Membrane Science*, 96, 275.
- 155) Xomeritakis G. and Lin Y. S., (1996). Fabrication of a Thin Palladium Membrane Supported in a Porous Ceramic Substrate by Chemical Vapor Deposition, *J. Membr. Sc.*, 120, 261.
- 156) Yan, S., Maeda, K., Kusakabe, K., Morooka, S., and Makiyama, Y., (1994). Hydrogen-Permselective SiO_2 Membrane Formed in Pores of Alumina Support Tube by CVD with TEOS, *Ind. Eng. Chem. Res.*, 33, 2096.
- 157) Ye J., Dan G., and Yuan Q., (1991). The Preparation of Ultra Thin Palladium Membrane, *Engineering Materials*, 61&62, 437.
- 158) Yeung, K. L. and Varma, A., (1995). Novel Preparation Techniques for Thin Metal – Ceramic Composite Membranes, *AIChE J.* 41, 2131.
- 159) Yildirim Y., Gobina E. and Hughes R., (1997). An Experimental Evaluation of High Temperature Composite Membrane Systems for Propane Ddehydrogenation. *J. Mem. Sci.*, 135, 107.
- 160) Yoldas, B. E., (1975). Alumina Sol Preparation from Alkoxides, *Am. Ceram. Soc. Bull.*, 54 (3), 289.
- 161) Young D. M. and Crowell A. D., (1962). *Physical Adsorption of Gases*, London, Butter Worths.
- 162) Zaman J. and Chakma A., (1994). Inorganic membrane reactors – review, *Journal of Membrane Science*, 92, 1.

- 163) Zaspalis, V. T., van Praag, W., Keizer, K., van Ommen, J. G., Ross, J. R. H. and Burggraaf, A. J., (1991). Reactor Studies Using Alumina Separation Membranes for the Dehydrogenation of Methanol and n-Butane, *Applied Catalysis*, 74, 223.
- 164) Zhao, R., Itoh, N., Govind, R., (1990). Novel Oxidative Membrane Reactor for Dehydrogenation Reaction – Experimental Investigation, *ACS Symp. Ser.*, 437, 216.
- 165) Ziaka Z.D., Minet R.G., Tsotsis T.T. (1993), A High Temperature Catalytic Membrane Reactor for Propane Dehydrogenation, *Journal of Membrane Science*, 77, 221.

Appendix 5: Support surface area

Single point	BET	BJH adsorption	BJH desorption
99.5406 m ² /g	257.5623 m ² /g	181.0905 m ² /g	168.9011 m ² /g

Appendix 6A: Derivation of mole balance expressions

a) Balances in the reaction zone

Component mole balances can be presented according to the following equation in the membrane reactor

$$\text{Feed in} = \text{Feed out} + \text{Feed lost in reaction} + \text{Feed lost in permeation} \quad (\text{Eq. 6A.1})$$

For component A (propane) the feed into a differential element dl in the plug flow membrane reactor can be presented as

$$\text{Feed in} = (F_A)_{in} \quad (\text{Eq. 6A.2})$$

The total stream leaving out can be presented as

$$\text{Feed out} = (F_A)_{out} \quad (\text{Eq. 6A.3})$$

The amount of reactant feed lost in the reaction is given as the rate of the reaction multiplied by the volume of the reaction zone

$$\text{Feed lost in reaction} = -r_A \cdot V \quad (\text{Eq. 6A.4})$$

where r_A is the rate of A lost in the reaction and is a positive term.

The amount of component A lost in the permeation is given according to the equation

$$\text{Feed lost in permeation} = J_A \cdot A \quad (\text{Eq. 6A.5})$$

The volume and area element of the differential element dl for the membrane reactor are presented as

$$V = S^R \cdot dz \quad (\text{Eq. 6A.6})$$

$$A = S^M \cdot dz \quad (\text{Eq. 6A.7})$$

where S^R and S^M are cross sectional area of the reaction zone and circumference of the tube (based on outer diameter) respectively.

Substituting the above expressions in the first equation provides the following expression

$$(F_A)_{in} = (F_A)_{out} - r_A \cdot S^R \cdot dz + J_A \cdot S^M \cdot dz \quad (\text{Eq. 6A.8})$$

Rearranging the terms in the above expression yields

$$\frac{(F_A)_{out} - (F_A)_{in}}{dz} = r_A \cdot S^R - J_A \cdot S^M \quad (\text{Eq. 6A.9})$$

In other words, a differential equation results from the above and is presented as

$$\frac{dF_A}{dz} = r_A \cdot S^R - J_A \cdot S^M \quad (\text{Eq. 6A.10})$$

For components B and C, similar equations can be obtained as

$$\frac{dF_B}{dz} = r_B \cdot S^R - J_B \cdot S^M \quad (\text{Eq. 6A.11})$$

$$\frac{dF_C}{dz} = r_C \cdot S^R - J_C \cdot S^M \quad (\text{Eq. 6A.12})$$

For component D (nitrogen) which does not participate in the reaction, the expression would be

$$\frac{dF_D}{dz} = -J_D \cdot S^M \quad (\text{Eq. 6A.13})$$

Component E permeates from permeation zone to reaction zone and hence the expression would be

$$\frac{dF_E}{dz} = J_E \cdot S^M \quad (\text{Eq. 6A.14})$$

b) Balances in the permeation zone

A mass balance expression in the permeation zone can be presented for component A as

$$\text{Feed out} = \text{Feed in} + \text{Flux} \cdot \text{area} \quad (\text{Eq. 6A.15})$$

for components A - D (due to permeation from reaction zone to permeation zone)

and

$$\text{Feed out} = \text{Feed in} - \text{Flux} \cdot \text{area} \quad (\text{Eq. 6A.16})$$

for component E (due to permeation from permeation zone to reaction zone) i.e.,

$$(G_A)_{out} = (G_A)_{in} + J_A \cdot S^M \cdot dz \quad (\text{Eq. 6A.17})$$

$$(G_E)_{out} = (G_E)_{in} - J_E \cdot S^M \cdot dz \quad (\text{Eq. 6A.18})$$

The above expression can be formulated as a differential equation as

$$\frac{(G_A)_{out} - (G_A)_{in}}{dz} = \frac{dG_A}{dz} = J_A \cdot S^M \quad (\text{Eq. 6A.19})$$

$$\frac{(G_E)_{out} - (G_E)_{in}}{dz} = \frac{dG_E}{dz} = -J_E \cdot S^M \quad (\text{Eq. 6A.20})$$

Similar expressions can be also obtained for components B -D as

$$\frac{dG_B}{dz} = J_B \cdot S^M \quad (\text{Eq. 6A.21})$$

$$\frac{dG_C}{dz} = J_C \cdot S^M \quad (\text{Eq. 6A.22})$$

$$\frac{dG_D}{dz} = J_D \cdot S^M \quad (\text{Eq. 6A.23})$$

Appendix 6B: Derivation of kinetic parameters

a) Pt-Al₂O₃ catalyst

Yildirim and Gobina (1997) provided the following plot in their work on propane dehydrogenation using 0.5 wt % Pt on Al₂O₃ catalyst pellets. The authors have described that the y-intercept in Figure 5A refers to the initial rate of the reaction.

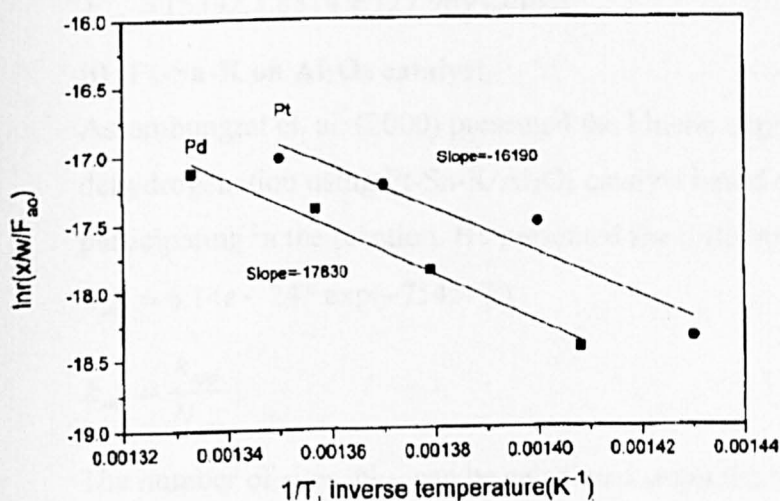


Figure 6A: Catalytic reactor studies by Yildirim and Gobina (1997).

In other words, the y-intercept of the Pd catalyst plot refers to the forward rate constant. Therefore the forward reaction rate constant can be given as

$$k_0 = \exp(16.5) = 1.46e7 \frac{\text{kmol}}{\text{m}^3 \cdot \text{atm} \cdot \text{s}} \quad (\text{Eq. 6B.1})$$

The activation energy of the forward reaction rate is given as the slope of the Pt based catalyst plot i.e., 16190.

Therefore activation energy is given as

$$E = 16190 * 8.314 = 134.6e3 \text{ kJ/mol} \quad (\text{Eq. 6B.2})$$

It is to be noted that the rate constant is given with respect to the volume of the catalyst rather than the weight of the catalyst.

The equilibrium constant values can be calculated by using the following equation:

$$\ln K = \ln K_0 - \frac{E_{eq}}{RT} \quad (\text{Eq. 6B.3})$$

The constants in the above equation were obtained from the literature (Stull et. al. (1960)) and the final equilibrium constant expression can be presented as

$$\ln K = -\frac{15392.1}{T} + 16.43 \quad (\text{Eq. 6B.4})$$

In other words, the constants in the equilibrium constant expression can be given as

$$K_o = \exp(16.43) = 13360240.3bar \quad (\text{Eq. 6B.5})$$

$$E_{eq} = 15392.1.8314 = 127.969 \text{ kJ/mol} \quad (\text{Eq. 6B.6})$$

b) Pt-Sn-K on Al₂O₃ catalyst

Assambungrat et. al. (2000) presented the kinetic expression for propane dehydrogenation using Pt-Sn-K/Al₂O₃ catalyst based on the number of sites participating in the reaction. He presented the following equations

$$k_{site} = 6.14e - 24 * \exp(-7545/T) \quad (\text{Eq. 6B.7})$$

$$k_{site} = \frac{k_{app}}{N_{site}} \quad (\text{Eq. 6B.8})$$

The number of sites, N_{site} can be calculated using the information given by the authors as

$$N_{site} = \frac{1.9e - 7}{2.86e - 28} = 6.63e20 \quad (\text{Eq. 6B.9})$$

Therefore the kinetic expression for apparent kinetic constant is given as

$$k_{app} = 6.14e - 24 * 6.63e20 * \exp(-7545/T) \quad (\text{Eq. 6B.10})$$

or

$$k_{app} = 4.079e - 3 * \exp(-7545/T) \quad (\text{Eq. 6B.11})$$

The unit of k_{app} is given as mol/kg.s.Pa. Converting the unit to kmol/(kg.s.bar) one would get the expression for kinetic constant as

$$k = 4.079e - 3 * 1e - 3 * 1.013e5 * \exp(-7545/T) \quad (\text{Eq. 6B.12})$$

or

$$k = 0.41325 * \exp(-7545/T) \quad (\text{Eq. 6B.13})$$

The above expression is for kg of catalyst. In order to determine the density of the catalyst bed, data is taken from Yildirim and Gobina (1993). The authors suggest that 2.55 g of catalyst is being packed into a tube of about 0.7 cm inner diameter to give a membrane area of about 18.5 cm²/gcat. Therefore the length of the membrane is estimated as

$$L = \frac{18.5 * 2.55}{3.14 * 0.7} = 21.4 \text{ cm} \quad (\text{Eq. 6B.14})$$

Therefore the density of the catalyst in the membrane is calculated as

$$\rho_{\text{cat}} = \frac{2.55}{\frac{3.14}{4} * 0.7^2 * 21.4} = 0.309 \frac{\text{g}}{\text{cm}^3} \quad (\text{Eq. 6B.15})$$

In other words, the density of the catalyst bed is 309 kg/m³.

Therefore the kinetic expression with respect to the reactor volume is expressed as

$$k = 0.41325 * 309 * \exp(-7545/T) \quad (\text{Eq. 6B.16})$$

or

$$k = 127.876 * \exp(-7545/T) \quad (\text{Eq. 6B.17})$$

where

$$k_0 = 127.876 \frac{\text{kmol}}{\text{m}^3 \cdot \text{s} \cdot \text{bar}} \quad (\text{Eq. 6B.18})$$

and

$$E = 7545 * 8314 = 627.3 \text{kJ} / \text{kmol} \quad (\text{Eq. 6B.19})$$

The equilibrium constant has been presented by the authors as

$$K = 1.76e12 * \exp(-15521/T)$$

Thereby, the equilibrium constant and equilibrium activation energy can be given as

$$K = \frac{1.76e12}{1.013e5} = 1737416 \text{bar} \quad (\text{Eq. 6B.20})$$

and

$$E_{eq} = 15521 * 8314 = 129 \text{kJ} / \text{mol} \quad (\text{Eq. 6B.21})$$

Appendix 6C: Derivation of energy balance expressions

a) Annular membrane reactor

i) Reaction zone

The general energy balance expression for the membrane reactor can be expressed as

$$\text{Energy input} = \text{Energy output} + \text{Energy lost in reaction} + \text{Energy lost to tube}$$

$$(\text{Eq. 6C.1})$$

The total energy input is due to three heat sources namely the fluid, oven and the enthalpy gain due to permeation of component E from permeation zone to reaction zone.

The energy input through fluid is expressed as a function of the fluid flow, heat capacity and temperature of the fluid

$$\text{Energy input through fluid} = \sum_{i=A}^E F_i \cdot C_{ps_i} \cdot (T^s)_m \quad (\text{Eq. 6C.2})$$

Energy input through the oven is given as

$$\text{Energy input through oven} = U^s \cdot S^s \cdot dz \cdot (T^o - T^s) \quad (\text{Eq. 6C.3})$$

Energy input through the permeation of component E is given as

$$\text{Energy input through enthalpy of E} = (H_E^t - H_E^s) J_E \cdot S^M \cdot dz \quad (\text{Eq. 6C.4})$$

Therefore total energy input is given as

$$\text{Total Energy input} = \sum_{i=A}^E F_i \cdot C_{ps_i} \cdot (T^s)_m + U^s \cdot S^s \cdot dz \cdot (T^o - T^s) + (H_E^t - H_E^s) J_E \cdot S^M \cdot dz \quad (\text{Eq. 6C.5})$$

Total energy output is the energy the fluid would carry while leaving the reactor i.e.,

$$\text{Energy output} = \sum_{i=A}^E F_i \cdot C_{ps_i} \cdot (T^s)_{out} \quad (\text{Eq. 6C.6})$$

Total energy lost in the reaction is a function of the rate of reaction multiplied by the volume of the reaction zone multiplied by the heat of reaction i.e.,

$$\text{Energy lost in reaction} = -r_A \cdot S^R \cdot dz \cdot \Delta H \quad (\text{Eq. 6C.7})$$

The energy lost to the tube is a function of tube heat transfer coefficient and is expressed as

$$\text{Energy lost to tube} = U^t S^M dz (T^s - T^t) \quad (\text{Eq. 6C.8})$$

Substituting the above expressions in energy balance equation gives the following equation

$$\begin{aligned}
& U^s \cdot S^s \cdot dz \cdot (T^o - T^s) + (H_E^i - H_E^s) J_E \cdot S^M \cdot dz \\
& + \sum_{i=A}^E F_i \cdot Cps_i \cdot (T^s)_{in} = \sum_{i=A}^E F_i \cdot Cps_i \cdot (T^s)_{out} - r_A \cdot S^R \cdot dz \cdot \Delta H + U^i \cdot S^M \cdot (T^s - T^i) \cdot dz
\end{aligned}$$

(Eq. 6C.9)

Re arranging terms, one would get the following expression

$$\begin{aligned}
\sum_{i=A}^E F_i \cdot Cps_i \cdot \frac{(T^s)_{out} - (T^s)_{in}}{dz} &= U^s \cdot S^s (T^o - T^s) - U^i \cdot S^M \cdot (T^s - T^i) \\
&+ (H_E^i - H_E^s) J_E \cdot S^M + r_A \cdot S^R \cdot \Delta H
\end{aligned}$$

(Eq. 6C.10)

i.e,

$$\frac{dT^s}{dz} = \frac{U^s S^s (T^o - T^s) - U^i S^M (T^s - T^i) + r_A S^R \Delta H + J_E S^M (H_E^i - H_E^s)}{\sum F_i Cps_i}$$

(Eq. 6C.10)

ii) Permeation zone

The general energy balance expression for the membrane reactor can be expressed as

Energy input = Energy output

The total energy input is due to three heat sources namely the fluid, the shell and the enthalpy gain due to permeation of components A-D from reaction zone to permeation zone.

The energy input through fluid is expressed as a function of the fluid flow, heat capacity and temperature of the fluid

$$\text{Energy input through fluid} = \sum_{i=A}^E G_i \cdot Cpt_i \cdot (T^i)_{in}$$

(Eq. 6C.11)

Energy input through the shell is given as

$$\text{Energy input through the shell} = U^i \cdot S^M \cdot dz \cdot (T^s - T^i)$$

(Eq. 6C.12)

Energy input through the permeation of components A - D is given as

$$\text{Energy input through enthalpy of components A - D} = \sum_{i=A}^D (H_i^s - H_i^t) J_i \cdot S^M \cdot dz$$

(Eq. 6C.13)

Therefore total energy input is given as

$$\begin{aligned} \text{Total Energy input} &= U^t \cdot S^M \cdot dz \cdot (T^s - T^t) + \sum_{i=A}^D (H_i^s - H_i^t) J_i \cdot S^M \cdot dz \\ &+ \sum_{i=A}^E G_i \cdot C_{pt,i} \cdot (T^t)_{in} \end{aligned}$$

(Eq. 6C.14)

Total energy output is the energy the fluid would carry while leaving the permeation zone i.e.,

$$\text{Energy output} = \sum_{i=A}^E G_i \cdot C_{pt,i} \cdot (T^t)_{out}$$

(Eq. 6C.15)

Substituting the above expressions in energy balance equation gives the following equation

$$\begin{aligned} U^t \cdot S^M \cdot dz \cdot (T^s - T^t) + \sum_{i=A}^D (H_i^s - H_i^t) J_i \cdot S^M \cdot dz \\ + \sum_{i=A}^E G_i \cdot C_{pt,i} \cdot (T^t)_{in} = \sum_{i=A}^E G_i \cdot C_{pt,i} \cdot (T^t)_{out} \end{aligned}$$

(Eq. 6C.16)

Rearranging terms, one would get the following expression

$$\sum_{i=A}^E G_i \cdot C_{pt,i} \cdot \frac{(T^t)_{out} - (T^t)_{in}}{dz} = U^t \cdot S^M \cdot (T^s - T^t) + \sum_{i=A}^D (H_i^s - H_i^t) J_i \cdot S^M$$

(Eq. 6C.17)

i.e.,

$$\frac{dT^t}{dz} = \frac{U^t \cdot S^M (T^s - T^t) + \sum_{i=A}^D J_i \cdot S^M (H_i^s - H_i^t)}{\sum_{i=A}^E G_i \cdot C_{pt,i}}$$

(Eq. 6C.18)

b) Tubular membrane reactor

Similar expressions for energy balances can be obtained for tubular reactors and can be expressed as

$$\frac{dT'}{dz} = \frac{U' S^M (T^s - T') + r_A S^R \Delta H + J_E S^M (H_E^s - H_E^t)}{\sum F_i C_{p,i}} \quad (\text{Eq. 6C.19})$$

for reaction zone

and

$$\frac{dT^s}{dz} = \frac{U^s S^s (T^o - T^s) - U' S^M (T^s - T') + \sum_{i=A}^D J_i S^M (H_i^t - H_i^s)}{\sum G_i C_{p,i}} \quad (\text{Eq. 6C.20})$$

for permeation zone.

Appendix 6D: Physical properties of component gases

Physical properties of various pure gases are either estimated or taken from subsequent non-linear correlations developed or available in literature (Perry (1997), McCabe, Smith and Harriott (1993)).

The component enthalpies in the shell and the tube are expressed as:

$$C_{p,s_A} = [acpa + acpb.T^s + acpc.(T^s)^2 + acpd.(T^s)^3] 4184 \quad (\text{Eq. 6D.1})$$

$$C_{p,s_B} = [bcpa + bcpb.(T^s) + bcpc.(T^s)^2 + bcpd.(T^s)^3] 4184 \quad (\text{Eq. 6D.2})$$

$$C_{p,s_C} = [ccpa + ccpb.(T^s) + ccpc.(T^s)^2 + ccpd.(T^s)^3] 4184 \quad (\text{Eq. 6D.3})$$

$$C_{p,s_D} = [dcpa + dcpb.(T^s) + dcpc.(T^s)^2 + dcpd.(T^s)^3] 4184 \quad (\text{Eq. 6D.4})$$

$$C_{p,s_E} = [ecpa + ecpb.(T^s) + ecpc.(T^s)^2 + ecpd.(T^s)^3] 4184 \quad (\text{Eq. 6D.5})$$

$$C_{p,t_A} = [acpa + acpb.T^t + acpc.(T^t)^2 + acpd.(T^t)^3] 4184 \quad (\text{Eq. 6D.6})$$

$$C_{p,t_B} = [bcpa + bcpb.(T^t) + bcpc.(T^t)^2 + bcpd.(T^t)^3] 4184 \quad (\text{Eq. 6D.7})$$

$$C_{p,t_C} = [ccpa + ccpb.(T^t) + ccpc.(T^t)^2 + ccpd.(T^t)^3] 4184 \quad (\text{Eq. 6D.8})$$

$$C_{p,t_D} = [dcpa + dcpb.(T^t) + dcpc.(T^t)^2 + dcpd.(T^t)^3] 4184 \quad (\text{Eq. 6D.9})$$

$$C_{p,t_E} = [ecpa + ecpb.(T^t) + ecpc.(T^t)^2 + ecpd.(T^t)^3] 4184 \quad (\text{Eq. 6D.10})$$

The relations for component enthalpies in the shell and the tube are calculated using the following expressions:

$$H_A^s = \left[acpa.T^s + acpb.\frac{(T^s)^2}{2} + acpc.\frac{(T^s)^3}{3} + acpd.\frac{(T^s)^4}{4} \right].4184 \quad (\text{Eq. 6D.11})$$

$$H_B^s = \left[bcpa.T^s + bcpb.\frac{(T^s)^2}{2} + bcpc.\frac{(T^s)^3}{3} + bcpd.\frac{(T^s)^4}{4} \right].4184 \quad (\text{Eq. 6D.12})$$

$$H_C^s = \left[ccpa.T^s + ccpb.\frac{(T^s)^2}{2} + ccpc.\frac{(T^s)^3}{3} + ccpd.\frac{(T^s)^4}{4} \right].4184 \quad (\text{Eq. 6D.13})$$

$$H_D^s = \left[dcpa.T^s + dcpb.\frac{(T^s)^2}{2} + dcpc.\frac{(T^s)^3}{3} + dcpd.\frac{(T^s)^4}{4} \right].4184 \quad (\text{Eq. 6D.14})$$

$$H_E^s = \left[ecpa.T^s + ecpb.\frac{(T^s)^2}{2} + ecpc.\frac{(T^s)^3}{3} + ecpd.\frac{(T^s)^4}{4} \right].4184 \quad (\text{Eq. 6D.15})$$

$$H_A^t = \left[acpa.T^t + acpb.\frac{(T^t)^2}{2} + acpc.\frac{(T^t)^3}{3} + acpd.\frac{(T^t)^4}{4} \right].4184 \quad (\text{Eq. 6D.16})$$

$$H_B^t = \left[bcpa.T^t + bcpb.\frac{(T^t)^2}{2} + bcpc.\frac{(T^t)^3}{3} + bcpd.\frac{(T^t)^4}{4} \right].4184 \quad (\text{Eq. 6D.17})$$

$$H_C^t = \left[ccpa.T^t + ccpb.\frac{(T^t)^2}{2} + ccpc.\frac{(T^t)^3}{3} + ccpd.\frac{(T^t)^4}{4} \right].4184 \quad (\text{Eq. 6D.18})$$

$$H_D^t = \left[dcpa.T^t + dcpb.\frac{(T^t)^2}{2} + dcpc.\frac{(T^t)^3}{3} + dcpd.\frac{(T^t)^4}{4} \right].4184 \quad (\text{Eq. 6D.19})$$

$$H_E^t = \left[ecpa.T^t + ecpb.\frac{(T^t)^2}{2} + ecpc.\frac{(T^t)^3}{3} + ecpd.\frac{(T^t)^4}{4} \right].4184 \quad (\text{Eq. 6D.20})$$

Similar expressions for viscosities and thermal conductivities can be presented as

$$\mu_A = Va_A + Vb_A T + Vc_A T^2 \quad (\text{Eq. 6D.21})$$

Heat capacity constants		Viscosity constants		Thermal conductivity constants	
acpa	-0.966	Va _A	0.0014	La _A	0.03004
acpb	7.279e-2	Vb _A	1e-7	Lb _A	0
acpc	-3.755e-5	Vc _A	9e-9	Lc _A	0
acpd	758e-9				
bpc _A	0.753	Va _B	0.0025	La _B	0.03004
bpc _B	5.691e-2	Vb _B	2e-5	Lb _B	0
bpc _C	-2.91e-5	Vc _B	0	Lc _B	0
bpc _D	5.88e-9				
ccp _A	6.952	Va _C	0.0078	La _C	0.0502
ccp _B	4.576e-4	Vb _C	5e-6	Lb _C	0.0005
ccp _C	9.563e-7	Vc _C	1e-8	Lc _C	-8e-8
ccp _D	-0.2079e-9				
dcp _A	6.903	Va _D	0.0073	La _D	0.0104
dcp _B	0.0753e-2	Vb _D	4e-5	Lb _D	6e-5
dcp _C	0.193e-5	Vc _D	-6e-9	Lc _D	-8e-9
dcp _D	0.6816e-9				
ecp _A	4.97	Va _E	-0.0101	La _E	0.0082
ecp _B	0	Vb _E	9e-5	Lb _E	4e-5
ecp _C	0	Vc _E	-3e-8	Lc _E	-5e-9
ecp _D	0				

Table 6D: Parameters for heat capacities, thermal conductivities and viscosities.

$$\mu_B = Va_B + Vb_B T + Vc_A T^2 \quad (\text{Eq. 6D.22})$$

$$\mu_C = Va_C + Vb_C T + Vc_C T^2 \quad (\text{Eq. 6D.23})$$

$$\mu_D = Va_D + Vb_D T + Vc_D T^2 \quad (\text{Eq. 6D.24})$$

$$\mu_E = Va_E + Vb_E T + Vc_E T^2 \quad (\text{Eq. 6D.25})$$

$$\lambda_A = La_A + Lb_A T + Lc_A T^2 \quad (\text{Eq. 6D.26})$$

$$\lambda_B = La_B + Lb_B T + Lc_B T^2 \quad (\text{Eq. 6D.27})$$

$$\lambda_C = La_C + Lb_C T + Lc_C T^2 \quad (\text{Eq. 6D.28})$$

$$\lambda_D = La_D + Lb_D T + Lc_D T^2 \quad (\text{Eq. 6D.29})$$

$$\lambda_E = La_E + Lb_E T + Lc_E T^2 \quad (\text{Eq. 6D.30})$$

Parameters related to the expressions 6D 1 – 30 are presented in Table 6D.